STRUCTURAL AND FUNCTIONAL INVESTIGATION OF NA^+, K^+-ATPASE REGULATORS: FXYD PROTEINS AND CARDIAC GLYCOSIDES

Thesis submitted in accordance with the requirements of the University of Liverpool for the degree of Doctor in Philosophy

by

Christopher Andrew Paul Whittaker

September 2011

ABSTRACT

The Na^+, K^+-ATPase is an integral membrane protein that is essential for maintaining the ionic gradient in eukaryotes which is required for many important cellular processes including maintaining cell volume and the secondary transport of solutes. This project investigates the structure, function and physical properties of two classes of inhibitors of the Na^+, K^+-ATPase, FXYD proteins and the cardiac glycosides. This was achieved with a range of biophysical methods including solid-state NMR.

The FXYD proteins are a family of seven physiological inhibitors of the Na^+, K^+-ATPase named after a shared PFXYD domain. They are transmembrane proteins of 64-178 amino acids which share sequence homology in their transmembrane domains but are sequentially diverse in their cytoplasmic domains. As the members of the FXYD family are tissue specifically expressed and they affect the activity of the Na^+, K^+-ATPase in different ways it is thought that the variable cytoplasmic domains of these proteins are responsible for the unique functional features of each FXYD protein. This work focuses on two FXYD proteins: phospholemman (PLM) which has been linked to cardiac arrhythmia and Mat-8, a marker for several forms of cancer which has two isoforms varying in the lengths of their cytoplasmic domains (short form and long form). The initial hypothesis is that the cytoplasmic region of PLM interacts with the Na^+, K^+-ATPase at one or more specific sites which causes a reduction of ATPase activity. This interaction is likely regulated by Ser 68 and/or Ser 63 phosphorylation and occurs in close proximity of the cell membrane surface due to the affinity of the cytoplasmic region of PLM for negatively charged lipid bilayers. This feature is unlikely shared with short form Mat-8 as it does not have any identified phosphorylation sites but due to lack of data on long form Mat-8 it is not clear whether or not its cytoplasmic region interacts with the Na^+, K^+-ATPase in a similar way to PLM.

Initially, work was undertaken to develop a system to express and purify PLM and Mat-8. An existing method based on the expression of inclusion bodies was first investigated but was found to be inefficient. A new system was therefore developed which successfully enabled the expression and purification of the short form of Mat-8. Further optimisation of this procedure will allow the expression and purification of isotopically labelled Mat-8 suitable for analysis by NMR.

Synthetic peptides corresponding to the cytoplasmic domains of PLM and Mat-8 were studied in isolation of the transmembrane domains in order to investigate their interactions with Na+,K+-ATPase and with phospholipid membrane surfaces. The cytoplasmic domain of PLM has been found to interact with negatively charged phospholipid membrane surfaces and inhibit the Na^+, K^+-ATPase. These effects are reduced upon phosphorylation of Ser 68 suggesting phosphorylation has a role in regulating inhibition of the Na^+, K^+-ATPase by PLM. It was found here that the short isoform of Mat-8 neither interacts with membrane surfaces nor inhibits Na^+,K^+-ATPase whereas the long isoform of Mat-8, which has an additional 26 amino acids in the cytoplasmic region, also binds to negatively charged cell membranes and inhibits the Na^+, K^+-ATPase albeit to a smaller extent. Motivated by these results, bioinformatic analysis identified a potential small linear Na^+, K^+-ATPase binding motif; SxxRxS, which is present in PLM, long form Mat-8, several other binding partners of the Na^+, K^+-ATPase but not any other FXYD proteins. This motif in PLM was modelled onto a binding site predicted by Anchorsmap, showing both electrostatic and steric compatibility and favouring a site of interaction of the PLM cytoplasmic domain situated close to the membrane surface where interactions with lipid headgroups are possible.

The cardiac glycosides are drugs used in heart failure and cardiac arrhythmia which are potent inhibitors of the Na^+, K^+-ATPase. Solid-state NMR methods were developed to investigate the position of cardiac glycosides in the high-affinity site within native membranes, by exploiting ouabain derivatised in the steroid moiety with a ^{13}C-labelled acetonide bridge. By using the solid-state NMR technique of cross-polarisation, the natural abundance ^{13}C nuclei from lipid headgroups and protein side chains can be observed together with a signature peak from the bound ouabain derivative. The paramagnetic broadening agent manganese was titrated into the membranes to probe the depth of the ouabain binding site. Paramagnetic broadening agents shorten the T2 times of local nuclei causing peak broadening with a distance-dependent relationship, thereby having greater effects on more accessible nuclei. The reduction of the ligand peak intensity was compared to the natural abundance ^{13}C signals to estimate the depth of the acetonide bridge. The results suggest that the acetonide group attached to the steroid moiety is close to the surface of the protein. This methodology can now be used with double ^{13}C-labelled ouabain to determine the orientation of the ligand in the binding site. The work presented here provides a range of insights into the structure function relationship of FXYD proteins and reveals a novel method for probing the depths of ligands within transmembrane proteins which can be applied to other systems.

CONTENTS

Contents

LIST OF FIGURES

LIST OF TABLES

ACKNOWLEDGMENTS

I would like to thank my supervisors Dr. David Middleton and Dr. Dan Rigden for their time and input. I would also like to thank Dan's postdoc Dr. Jaclyn Bibby particularly for her help in the GOLD studies.

Thanks also must go to Prof. Mikael Esmann who has given me a huge amount of help and advice and was very accommodating in both of my trips to the University of Aarhus where he taught me so much. His technician Anja was also particularly helpful and I am extremely grateful for her all of her hard work even with an injured hand.

I also don't think I could have got this thing finished without Dr. Eleri Hughes who has constantly pushed me and looked out for me. Sure I exploit the motherly side in her but its only because I like her. I'd like to thank the rest of the lab especially for enduring my small bouts of crazy during writing up.

Thank you to Dena who has been had to deal with me coming home ridiculously late for months on end but she still has my tea waiting on the table. A thesis, you may have gathered, is rather stressful to produce. Dena has been the perfect distraction from that stress. When all I've wanted to do is scream, Dena somehow makes me laugh.

Finally I have to thank my mum and my brother John. Without sounding melodramatic John has saved my life twice which makes him a pretty good brother. My mum has encouraged me my whole life and worked incredibly hard to put me through University, I just don't know how to break it to her that there is not as much money in Science as she thinks and I can't buy her that holiday home in the Bahamas she deserves.

ABBREVIATIONS

Ank - Ankyrin

ATP – Adenosine Triphosphate

BCL-XL - B-cell Lymphoma-Extra Large

CD – Circular Dichroism

CHIF - Corticosteroid-Induced Factor

CMC – Critical Micelle Concentration

COSY – Correlation Spectroscopy

CP – Cross Polarisation

DiLiMOT – Discovery of Linear Motifs

DMPC - Dimyristoylphosphatidylcholine

DOPC - Dioleoylphosphatidylcholine

DOPE - Discrete optimized protein energy

DOPG - Dioleoylphosphatidylglycerol

DOPS - Dioleoylphosphatidylserine

DPPE - Dipalmitoylphosphoethanolamine

DPPC - Dipalmitoylphosphatidylcholine

DQF - Double-Quantum Filtered

FA - Formic Acid

EB – Elution Buffer

EDTA - Ethylenediaminetetraacetic Acid

FXYD - Phe-X-Tyr-Asp motif

GA – Genetic Algorithm

GOLD - Genetic Optimisation for Ligand Docking

HPLC – High Performance Liquid Chromatography

HSQC - Heteronuclear single-quantum correlation spectroscopy

IPTG - Isopropyl β-D-1-thiogalactopyranoside

ITC – Isothermal Titration Calorimetry

KSI - Ketosteroid Isomerase

LB – Lysogeny Broth

LMV – Large Multilamellar Vesicles

MAS – Magic Angle Spinning

Mat-8 – Mammary Tumour 8 KDa

mBCL-XL – mutated B-cell Lymphoma-Extra Large

MBP – Maltose Binding Protein

metaPrDOS - meta Protein DisOrder prediction System

MOPS - 3-(N-morpholino)propanesulfonic acid

MUSCLE - Multiple Sequence Comparison by Log- Expectation

N3 – Neutralisation Buffer

NCX1 - Sodium-Calcium exchanger 1

NMR – Nuclear Magnetic Resonance

NOESY - Nuclear Overhauser effect spectroscopy

ODA - Ouabain Diacetonide

OFDA - Ouabain Fluorodiacetonide

OMA - Ouabain Monoacetonide

O/N - Overnight

OPM – Orientations of Proteins in Membranes

P1 – Resuspension Buffer

P2 – Lysis Buffer

PDB – Protein Data Bank

PE – Wash Buffer

PI3K - Phosphoinositide 3-kinase

PKA – Protein Kinase A

PKC – Protein Kinase C

PLB - Phospholamban

PLM – Phospholemman

PMSF - Phenylmethanesulfonylfluoride

ppm - Parts Per Million

PSI – Pound per Square Inch

RIC - Related to Ion Channel

SDS - Sodium Dodecyl Sulfate

SDS-PAGE - Sodium Dodecyl Sulfate Polyacrylamide Gel Electrophoresis

SERCA - Sarco/Endoplasmic Reticulum Ca^{2+}-ATPase,

SRC - Sarcoma

STP - Surface Triplet Propensities

SUV – Small Unilamellar Vesicles

T_3 - Triiodothyronine

TBST - Tris-Buffered Saline and Tween 20

TEMED - Tetramethylethylenediamine

TEVP - Tobacco Etch Virus Protease

TFE - Trifluoroethanol

TLC - Thin Layer Chromatography

TLE - Transducin-Like Enhancer of split

TPPM – Two-Pulse Phase Modulation

Chapter 1

1.1. Introduction

The Na^+, K^+-ATPase is a membrane embedded ion pump. The importance of the Na^+, K^+-ATPase is highlighted by the fact that it consumes 20-30% of ATP production at rest in all mammalian cells (Jorgensen *et al.*, 2003). The electrochemical gradient induced by the Na^+, K^+-ATPase is vital for many important cellular processes. These include maintaining membrane potentials, maintaining cell volume and the secondary transport of other solutes in all eukaryotes.

1.1.2. History – Sodium Pump

In the 1930s it was generally accepted that the cell membrane could actively transport nutrients such as sugar but it was not widely accepted that small ions like Na^+ could enter or leave the cell in a similar manner. This all changed when techniques were developed to produce radioactive isotopes of hydrogen, nitrogen, carbon and oxygen (Hevesy, 1938). Dean noted (Dean, 1941) from his own experiments and the work of others (Heppel and Schmidt, 1938; Heppel, 1939; Steinbach, 1940) that Na^+ was found in high concentrations in muscle cells and this Na^+ was rapidly replaced by K^+ ions when they were made available. He theorised that as the muscle can actively move potassium and sodium ions against concentration gradients there must be some sort of an energy requiring

pump, possibly located in the fibre membrane, which can pump out the sodium or, conversely, pump in the potassium. As the notion of such a system was so radical there was no significant response to the work of Dean until 1957 when Skou discovered the biochemical mechanism responsible for the exchange of Na^+ and K^+ ions across the cell membrane (Skou, 1957). It was described as a membrane embedded ATPase with catalytic properties. This work followed the discovery of an ATPase in the sheath part of the giant axon in crab nerves (Libet, 1948). ATP hydrolysis is used frequently in nature to provide energy for non-passive processes so it was hypothesised this ATPase must provide an active function. Skou analysed these crab nerves further in order to discover what this function was. He observed that the membranes have a small Mg^{2+} induced ATPase activity. When Mg^{2+} was added with Na^+ it generated a small increase in activity, which was not observed when Mg^{2+} was added with K^+. However upon addition of both Na^+ and K^+ in the presence of Mg^{2+} there was a significant combined positive effect on activity. This result and those of later experiments from other laboratories lead to the identification and characterisation of Na^+, K^+-ATPase (Skou, 1965) and as a result in 1997 Skou received share of the Nobel prize for chemistry for "the first discovery of an ion-transporting enzyme, Na^+, K^+ -ATPase".

1.1.2. Mechanism

The Na^+, K^+-ATPase has two major subunits. The α-subunit is the catalytic subunit where all the ions are bound and exchanged whereas the β-subunit alters the α-subunit to give it affinity for Na^+ and K^+. The Na^+, K^+-ATPase operates in a cyclic mechanism, exchanging three Na^+ ions from inside the cell with two K^+ ions from the extracellular matrix. The cytoplasm has a very high concentration of proteins which have a negative charge neutralised by the K^+ pumped into the cell. This electrogenic translocation generates an ionic gradient as the extracellular matrix is more positively charged than the cytoplasm. Under equilibrium conditions intracellular concentrations of Na^+ and K^+ are 10-20 mM and about 150 mM respectively. Na^+ activation of the Na^+, K^+-ATPase occurs when intracellular Na^+ ion concentration goes beyond the threshold at 15-20% above the maximum. Extracellular concentrations are typically around 4 mM K^+ and 140 mM Na^+. K^+ activation of the Na^+, K^+-ATPase occurring when going beyond the threshold at approximately 85% above the typical extracellular K^+ ion concentration. Ionic translocation by the Na^+, K^+-ATPase induces many conformational transitions of the protein that are dependent on the energy released from ATP hydrolysis. The Na^+, K^+-ATPase is a P-type ATPase and like other P-type ATPases the Na^+, K^+-ATPase has two major conformations known as E_1 and E_2 which have different affinities for Na^+ and K^+ and changes between these two conformations are induced by phosphorylation and dephosphorylation.

Figure 1.1 shows a schematic representation of the how these conformational changes occur and their implications. At rest (when Na^+ and K^+ are below activation thresholds) the Na^+, K^+-ATPase appears to be in the phosphorylated E_2 conformation (E_2P) as it has been shown to be in the absence of Na^+ and K^+ ions (Skou and Esmann, 1983). E_2P will bind two K^+ ions with low affinity (giving $E_2P.2K^+$) and this in turn induces a change into a K^+ occluded form ($E_2P(2K^+)$) (Glynn and Richards, 1982). The equilibrium between $E_2P.2K^+$ and $E_2P(2K^+)$ is shifted far towards the latter and thus the apparent E_2P affinity for K^+ is in fact very high with $K_{0.5}$ just a few μM. The transformation from high K^+ affinity ($E_2P(2K^+)$) to high Na^+ affinity ($E_1.3Na^+$) is very slow in the absence of ATP but upon ATP binding the rate of this transition is increased to form $E_1.3Na^+.ATP$; the conformation where both 3 sodium ions and 1 ATP molecule is bound to the Na^+, K^+-ATPase. This causes a loss of affinity for K^+ ions and they are released into the cytoplasm. It is important to note that ATP is not hydrolysed at this point so this increase in transitional rate is passive, i.e. down the free energy gradient. The hydrolysis of ATP is induced after the binding of the Na^+ ions where Na^+ bestows catalytic activity to the system. The released phosphate transfers to Asp 369 of the α-subunit which leads to Na^+ occlusion ($E_1.P$ ($3Na^+$)). De-occlusion of these Na^+ ions has only recently been fully understood. This is because much of the knowledge for the mechanism of the Na^+, K^+-ATPase has been obtained from the sarcoplasmic reticulum Ca^{2+}-ATPase (SERCA), which has 65% similarity

to the α-subunit of the Na^+, K^+-ATPase (Sweadner and Donnet, 2001). SERCA has two cation (Ca^{2+}) binding sites with the corresponding sites in Na^+, K^+-ATPase alternatively occupied by Na^+ and K^+. The third Na^+ binding site is unique to the Na^+, K^+-ATPase so there is no corresponding data from SERCA to compare to. As a result of this the third Na^+ binding site is not very well understood. The simplest explanation would be that all three Na^+ ions are released at once; however, there is no significant corresponding binding event unlike the de-occlusion of K^+ ions induced by the binding of ATP. This suggests de-occlusion of Na^+ could happen in a very different manner to de-occlusion of K^+. A more refined model is shown in Figure 1.2. This is based on observations using high-time-resolution measurements (Hilgemann, 1994; Holmgren *et al.*, 2000). Initially all three Na^+ ions are occluded (E_1P3Na^+). The third binding site likely releases its Na^+ ion first (E_2P3Na^+) which would explain the quick large charge movement (around 100 μs). This observation is much like what is observed in an ion channel. This, in turn causes the remaining two Na^+ binding sites to reorganise thus causing a relatively slow de-occlusion (4 ms) of the remaining Na^+ ions (E_2P2Na^+). This returns the Na^+, K^+-ATPase to E_2P conformation and thus a cycle is completed.

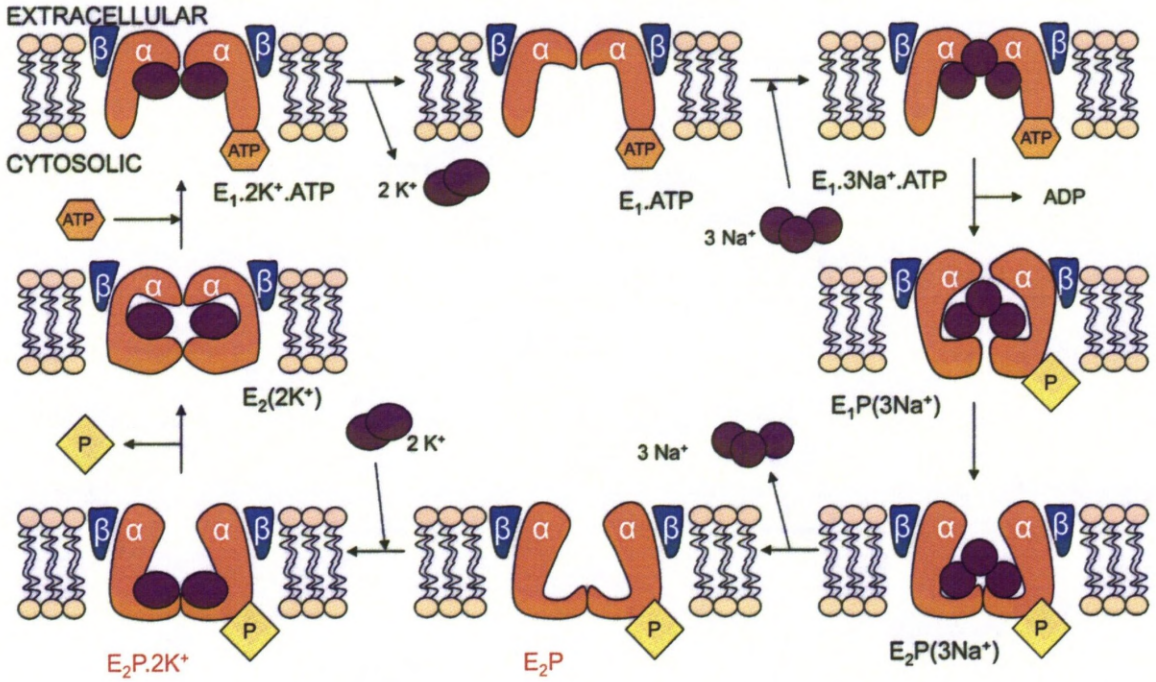

Figure 1.1. A schematic mechanism of the Na^+, K^+ ATPase. Details of this mechanism are given in text. Image adapted from Skou and Esmann (1992). The conformations (E_1 and E_2) are shown in each step with conformations for which structures are solved shown in red.

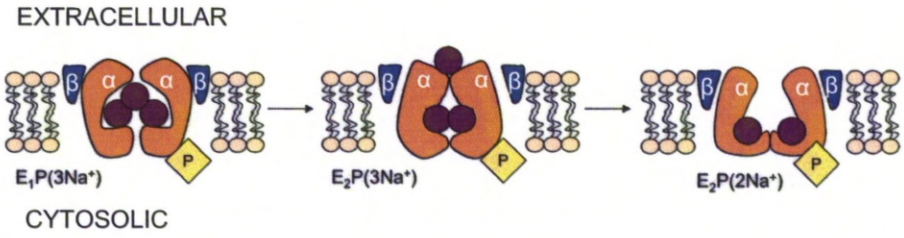

Figure 1.2. Refined mechanism of the Na^+, K^+-ATPase. The de-occlusion of Na^+ remains unclear; it appears to be a two step process where one specialised Na^+ site unique to the Na^+, K^+-ATPase releases its ion first causing a rearrangement of the enzyme allowing the remaining two cation binding sites to release their Na^+ ions, allowing subsequent binding of K^+ ions (Hilgemann, 1994).

Further insight into the third Na^+ binding site was gained upon solving the structure of the Na^+, K^+-ATPase (Morth *et al.*, 2007) which is discussed later.

1.1.3. Structure

The minimal functional enzyme unit of the Na^+, K^+-ATPase is made up of a large α-subunit of around 1012 amino acids and a smaller β-subunit of around 300 amino acids both primary sequences of which were first determined in sheep (Shull *et al.*, 1985). There are four α-subunit (α1-α4) and three β-subunit (β1-β3) isoforms in mammalian cells potentially giving twelve different isozymes with different functional properties (Blanco and Mercer, 1998). Until recently much of the structural information about the α-subunit was obtained from modelling it to the x-ray crystal structure of SERCA (Toyoshima *et al.*, 2000). However subsequently x-ray structures have been solved in the $E_2P.(2K^+)$ conformation of Na^+, K^+-ATPase from

pig kidney published in 2007 (Morth *et al.*, 2007) and then shark rectal gland published in 2009 (Shinoda *et al.*, 2009). SERCA and the α-subunit of the Na^+, K^+-ATPase are sequentially and structurally very similar as shown in the sequence alignment (Appendix A) and the structural alignment (Figure 1.3.). Both are P-Type ATPases (type II) which means they both undergo conformational changes between E1 and E2 forms which are dependent on phosphorylation and dephosphorylation. (Chan *et al.*, 2010). Both proteins contain ten transmembrane helices (M1-M10) which make up the cation transport path. They also have three cytoplasmic domains; the A-domain (actuator), P-domain (phosphorylation) and N-domain (nucleotide-binding) (Toyoshima *et al.*, 2000; Morth *et al.*, 2007). The P-domain is the central part of the protein and contains the phosphorylation site (Asp 351 in the Na^+, K^+-ATPase) in a negatively charged pocket, key in the mechanism described earlier. It is made up of two segments vastly separated in the amino-acid sequence. The N-terminal part (ranging approximately between Asn 330 and Asn 359 in the Na^+, K^+-ATPase) is connected to helix M4 and the C-terminal part (approximately from Lys 605 to Asp 737 in the Na^+, K^+-ATPase) to helix M5. The N-domain is the largest domain and contains the ATP binding pocket which is positively charged (surrounds Phe 487 in the Na^+, K^+-ATPase). It is made up of the amino acids that are inserted in-between the two P-domain parts. The A-domain is the smallest and is made up of the cytoplasmic N-terminus (two short α-helices) and an insertion

between M2 and M3 (these helices in the Na^+, K^+-ATPase can be seen in Figure 1.4.) It is connected to the transmembrane region by long loops leaving it virtually isolated. These 3 large regions are able to move in a concerted fashion which is vital in the conformational changes described in the earlier mechanism. The N-domain is particularly mobile in the presence of ions (Toyoshima *et al.*, 2000; Morth *et al.*, 2007) a property conferred by a hinge region, the presence of which is indicated by the ease of isolating the N domain with several proteases (Champeil *et al.*, 1998). Phosphorylation of the P-domain by hydrolysis of the bound ATP brings the N-domain closer to the P-domain (Nakamoto and Inesi, 1984) allowing the phosphorylation signal to be passed on.

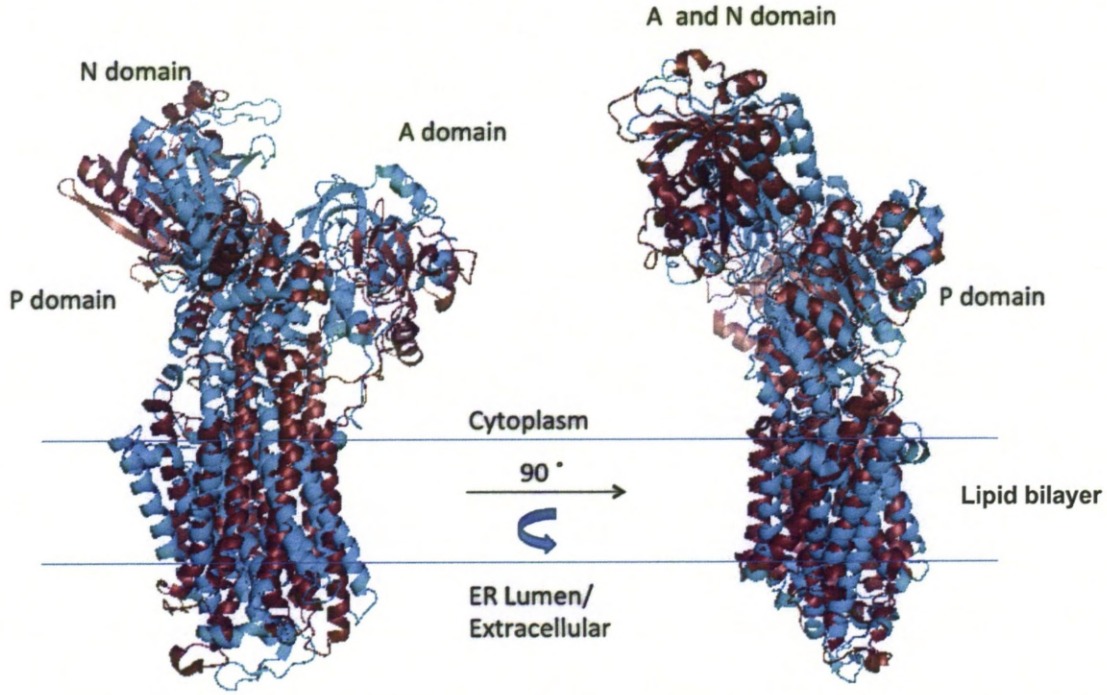

Figure 1.3. Alignment of SERCA and the α-subunit of the Na^+, K^+-ATPase. SERCA in red aligned with the Na^+, K^+-ATPase in cyan. The approximate site of the lipid bilayer is shown. To make the A, N and P domains clear the complexes are shown at two different angles. Produced in PyMol from published structures (Toyoshima *et al.*, 2000; Morth *et al.*, 2007) which are in comparable conformations in the enzymatic cycle (E2P (2K+) and $E_2P(2Ca^{2+})$.

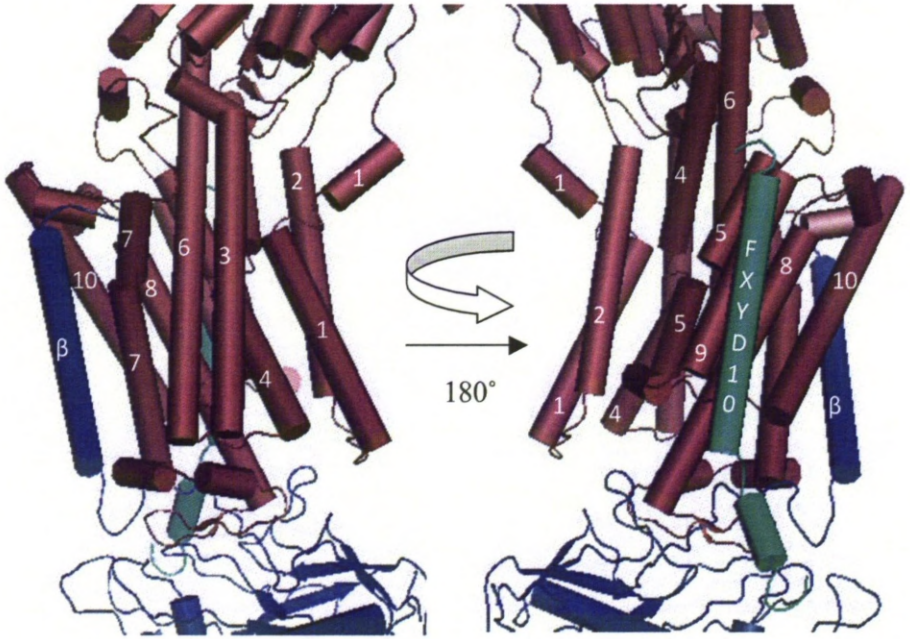

Figure 1.4. Transmembrane helices of the Na+, K+-ATPase. Movements and interactions of the 10 transmembrane helices appear vital to the function of the Na^+, K^+-ATPase. However both structures solved of the Na^+, K^+-ATPase are in the E_2P ($2K^+$) conformation so this is yet to be confirmed. The α-subunit is indicated in red with all transmembrane helices labelled. The complex is shown from two angles to make all helices clear. β-subunit is in blue and FXYD10 (as this is from shark rectal gland) is in green. Produced in PyMol from published data (Shinoda *et al.*, 2009).

As stated earlier the structure of the Na^+, K^+-ATPase gave further insight into the third Na^+ binding site (Morth *et al.*, 2007). It was noted the helix M10 ends with three arginine residues (Arg 1003-1005 which are highly electropositive), a PGG motif and an eight-residue extension relative to the C-terminus of SERCA. A five-residue truncation of the C-terminus of the Na^+, K^+-ATPase results in a 26-fold reduction in Na^+ affinity compared to wild type, yet the truncation had no effect on K^+ affinity. This is similar to what was observed when Tyr 771 (helix M5 (Vilsen *et al.*, 1997) and Thr 807 (helix M6 (Vilsen, 1995)) were mutated. These two residues along with Glu 954 (helix M9) have been suggested to make up the third Na^+ binding site (Li *et al.*, 2005) and the structure has since revealed these three residues cluster and bridge to the second Na^+/K^+ binding site. Due to the effects of the C-terminal truncation it was proposed the direct contact the C-terminus has with alpha M5 optimises Na^+ binding at the third site.

The arginine cluster at the C-terminus of helix M10 could act as a voltage sensor as observed in voltage-dependant ion channels (ref) that move in response to membrane depolarisation. This would activate a C-terminus switch that alters the relationship of the C-terminus with the third Na^+ binding site during depolarisation/repolarisation with consequences on Na^+ affinity.

When the shark rectal gland Na^+, K^+-ATPase structure was solved at a higher resolution (2.4 Å) in the E_2P ($2K^+$) conformation (Shinoda *et al.*, 2009) it validated the assumption that its tertiary structure is very similar to SERCA. In fact four out of five residue positions were virtually identical even down to side chain conformations. Many key differences between the two structures were found, however, helping understand how subtle changes can give very different functions. Firstly the N-domain of the Na^+, K^+-ATPase is ~20° further from the P-domain than that of SERCA in the equivalent E_2P ($2Ca^{2+}$). This could well explain the much faster ATPase turnover (the Na^+, K^+-ATPase is nearly seven times faster than SERCA). The transmembrane helices M5 and M7 (Figure 1.4.) have unwound regions in the Na^+, K^+-ATPase which are not present in SERCA. In M7 this gives a distinct kink of ~18° which has a distinct role in K^+ binding. The M5 helix straightens in the E_2P>E_2>$E_1.2Ca^{2+}$ transition in SERCA (Toyoshima *et al.*, 2000). If a similar event happened in the Na^+, K^+-ATPase it would cause M7 to push towards M10 inducing large scale structural changes in the P-domain, M3 and the carboxy-terminal segment of the α and β subunits. This gives M7-M10 a much bigger role in the Na^+, K^+-ATPase than SERCA and might change the position of the β-subunit (which does not associate with SERCA) cytoplasmic domain.

Indeed, the β-subunit is only found in two P-type ATPases the Na^+, K^+-ATPase and the gastric H^+, K^+-ATPase. It has long been strongly

suggested that the β-subunit plays a key role in altering the α-subunit allowing it to transport K^+ (Geering, 2001). By completely solving the structure of the β-subunit insights into how this may occur have been proposed (Shinoda *et al.*, 2009). Although the single transmembrane helix of the β-subunit is quite detached from the transmembrane helices of the α-subunit in this solved structure it does form key interactions with M7 and M10. Two aromatic clusters involving these helices and aromatics in the β-subunit form complex hydrogen bonds and salt bridges. These intricate interactions could well explain how the β-subunit alters the Na^+, K^+-ATPase to have an affinity for K^+.

1.1.4. Regulation

The Na^+, K^+-ATPase is clearly a critical and complex system so understandably requires strict regulatory control. There are several different ways this is achieved. These either affect the regulation of gene expression of the Na^+, K^+-ATPase or affect the rate of reaction. The simplest of the latter type is already clear from the mechanism; increased intracellular Na^+ or extracellular K^+ increase Na^+, K^+-ATPase activity. More complex mechanisms of regulation are discussed below.

Thyroid hormones induce an increase in Na^+, K^+-ATPase expression and thus its concentration in the cell membrane. Studies on rat thyroidectomies (Asano *et al.*, 1976), showed a 35% decrease in Na^+, K^+-ATPase activity

after thyroidectomy and a 54% increase when pre treated with the thyroid hormone triiodothyronine (T_3). Further studies with the radioactive labelled [^{3}H]ouabain could quantify this effect of thyroid hormones via liquid scintillation counting. Ouabain is a highly specific and high affinity inhibitor of the Na^+, K^+-ATPase (discussed later), binding at 1:1 stoichiometry allowing Na^+, K^+-ATPase concentration to be determined by bound [^{3}H]ouabain. [^{3}H]ouabain reveals Na^+, K^+-ATPase concentration to be largest in the brain, intermediate in the skeletal muscle, lower in the kidney, and at its lowest in the liver (Lin and Akera, 1978). T_3 treated rats had a largely increased Na^+, K^+-ATPase concentration in skeletal muscle, kidney and liver but not in brain. This has been confirmed with increased Na^+, K^+-ATPase mRNA upon addition of T_3 in rats (Yalcin *et al.*, 1999).

Insulin appears to have a role in altering rate of reaction of the Na^+, K^+-ATPase. Diabetes is a condition where either insulin is no longer produced (type 1) or no longer recognised by receptors (type 2). Diabetes patients often suffer from a condition known as diabetic retinopathy. This is due to abnormalities such as reduced endothelial cell density and increased endothelial pleomorphism (Olsen and Busted, 1981; Roszkowska *et al.*, 1999; Inoue *et al.*, 2002). It is caused by decreased Na^+, K^+-ATPase activity in the corneal endothelium (Herse, 1990; Herse and Adams, 1995) which is in turn caused by the reduced insulin levels in the condition (Hatou *et al.*, 2010).

These systems are both very general as they affect so many other processes in the cell. There are also specific regulatory molecules of the Na^+, K^+-ATPase which alter the rate of ATP hydrolysis and ionic transport. Two such mechanisms are the focus of this project. A family of proteins called FXYD proteins are physiological regulators of the Na^+, K^+-ATPase and form part of the complex whereas cardiac glycosides are pharmacological regulators and bind to a specific region in the α-subunit. Both are discussed in detail below.

1.2. FXYD Proteins

The FXYD proteins are a family of short polypeptides each having a single helical transmembrane domain localised in the plasma membrane (Garty and Karlish, 2005). They were classified as a single family after the Na^+, K^+-ATPase γ-subunit and the proteins phospholemman (PLM), Mat-8, and corticosteroid-induced factor (CHIF) showed sequence similarity following analysis despite no clear related function. (Sweadner and Rael, 2000). These proteins have a signature sequence (Figure 1.5.) of 35 amino acids where sequence similarity is high. Contained within the signature sequence is the Phe-X-Tyr-Asp (FXYD) motif in the extracellular region after which the family was named. The function of this motif remains unclear as it has been shown to be important for a stable interaction with the α- subunit of the Na^+, K^+-ATPase in CHIF and Na^+, K^+-ATPase γ-subunit (Beguin *et al.*, 2001) but not in a later identified FXYD7 (Crambert *et al.*, 2004).

Sequence similarity between members is generally poor outside the signature sequence. With this information the protein "related to ion channel" (RIC) was identified as a fifth member of the family (previously not identified due to it having a much longer N-terminal segment) and further bioinformatics revealed two more un-named proteins (Sweadner and Rael, 2000). Since this paper FXYD proteins have been named in order of discovery; FXYD1 (PLM), FXYD2 (γ-subunit), FXYD3 (Mat-8), FXYD4 (CHIF), FXYD5 (RIC) and FXYD6/FXYD7 (the two unnamed members although FXYD6 has since been given the alternative name phosphohippolin). In this thesis all proteins will be referred to by their original names (e.g. PLM and Mat-8). No subsequent FXYD proteins have been discovered in mammals since this study. However additional members FXYD8-12 (Tipsmark, 2008) have been discovered in fish. FXYD10 is noteworthy as it has its structure solved in complex with the Na^+, K^+-ATPase (Figure 1.4.). All 7 mammalian members have been shown to interact with and regulate the Na^+, K^+-ATPase. PLM (Crambert *et al.*, 2002), γ-subunit (Beguin *et al.*, 1997; Pu *et al.*, 2001), Mat-8. (Crambert *et al.*, 2005; Arimochi *et al.*, 2007), CHIF (Garty *et al.*, 2002) and FXYD7 (Beguin *et al.*, 2002) all reduce the affinity of the Na^+, K^+-ATPase for Na^+ and/or K^+ ions although their effect can depend on which Na^+, K^+-ATPase α-subunit isoform it interacts with. For example, RIC increases affinity for Na^+ and/or K^+ ions in an α1β1 complex (Lubarski *et al.*, 2005) whereas FXYD6 slightly decreases apparent K^+

affinity and significantly decreases the apparent Na^+ affinity of the Na^+, K^+-ATPase α1-β1 isozymes. In contrast when FXYD6 associates with α1-β2 isozymes it in fact increases apparent K^+ and Na^+ affinity (Delprat *et al.*, 2007). What is interesting is that not only do the FXYD proteins have different regulatory effects on the Na^+, K^+-ATPase, they are also tissue specifically expressed. Table 1.1 shows the tissues in which each member is expressed. This suggests that FXYD proteins alter the activity of the Na^+, K^+-ATPase to match the specific needs of individual tissue types. The specificity of expression suggests they are specifically designed to meet the needs of specific tissues. The signature sequence (highlighted in Figure 1.5.) suggests they may share some kind of function(s) or membrane targeting.

1.2.1. Comparing FXYD Proteins

As mentioned the FXYD proteins have homology in the 35 amino acid signature sequence but poor homology outside of this. Fig 1.5 shows a comparison of the human FXYD proteins. The alignment (Figure 1.5a) shows sequence similarity is poor outside the signature sequence between all seven members. However certain pairs of FXYD proteins have high sequence similarity outside the signature sequence that is related to their evolutionary path highlighted by the phylogenetic tree (Figure 1.5b). Table 1.1. shows where FXYD proteins are expressed in humans.

Table 1.1: The FXYD family. The table below shows the FXYD proteins, where they are expressed in mammals, and also FXYD10 from shark the structural information available

Protein	*Common name(s)*	*Expressed in*	**Structural information**
FXYD1	Phospholemman	Heart, liver, skeletal muscle	Solution state NMR (Teriete *et al.*, 2007)[a]
FXYD2	The γ subunit of Na^+,K^+-ATPase	Kidney, heart, stomach	Structure as part of Na^+, K^+-ATPase in pig kidney[b]
FXYD3	Mat-8	Colon, stomach, uterus	Limited structure known (human)(Franzin *et al.*, 2007a)[b]
FXYD4	CHIF	Kidney collecting duct, distal colon	Solution state NMR (rat) (Franzin *et al.*, 2007d)[b]
FXYD5	RIC, dysadherin	Heart, brain, spleen, lung, liver, skeletal muscle, kidney, testis	None
FXYD6	Phosphohippolin	Brain and kidney	None
FXYD7		Brain (cerebellum, cerebrum, hippocampus and stem)	None
FXYD10		Shark rectal gland	Structure as part of Na^+, K^+-ATPase in shark rectal gland (Shinoda *et al.*, 2009)[a]

[a]Solution state NMR (in micelles)

[b]X-Ray crystallography

1.2.3. The Na^+, K^+-ATPase is regulated by FXYD proteins

As stated earlier, it appears the FXYD proteins have a major role in regulating the Na^+, K^+-ATPase in a specific way to dependent on tissue type. There are methods which have confirmed that all seven FXYD proteins regulate the Na^+, K^+-ATPase. These include co-immunoprecipitation (Bibert *et al.*, 2006; Fuller *et al.*, 2009) and distinct modulation of Na^+, K^+-ATPase activity by different FXYD proteins and FXYD protein silencing (Han *et al.*, 2006; Bibert *et al.*, 2009) (discussed for PLM and Mat-8 later). The region of interaction appears to be the transmembrane region (very common for two interacting membrane proteins) but it is speculated the non-conserved regions of FXYD proteins which are largely in the cytoplasmic region confer the tissue specific effects of FXYD proteins on Na^+, K^+-ATPase. Indeed in PLM there is evidence for the cytoplasmic region having an inhibitory effect on the Na^+, K^+-ATPase (discussed later).

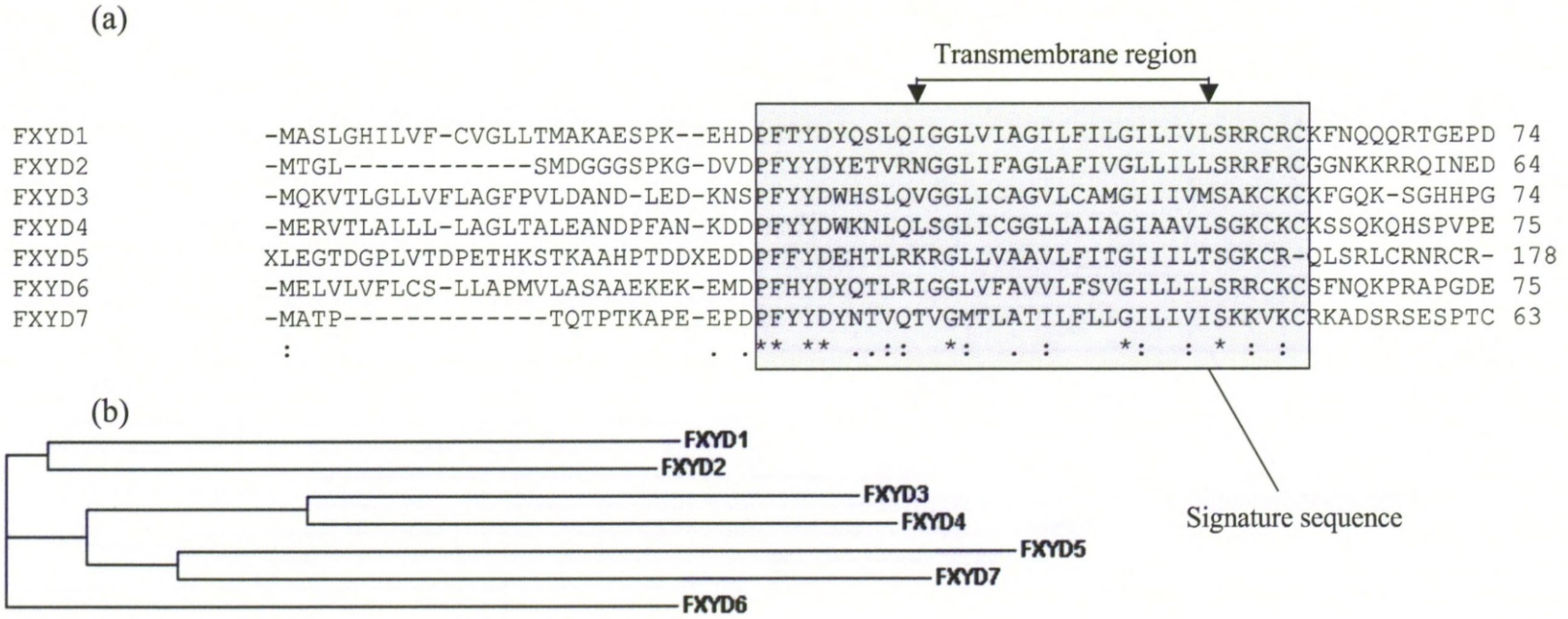

Figure 1.5. Comparison of FXYD Proteins. (a) an alignment of the seven human FXYD proteins with the 35 amino acid signature sequence shown in the grey box. ("*": identical. ":": conserved substitutions (amino acids with similar properties). ".": semi-conserved substitution (similar shaped amino acids). FXYD5 is unusually long for a FXYD protein so two large portions of its sequence have been replaced by an X to allow alignment. (b) phylogentic tree to show evolutionary relationship between human FXYD proteins. Both images produced in ClustalW2.

1.2.4. Phospholemman (FXYD1)

PLM was originally referred to as simply "15-kDa protein" when first discovered but was renamed phospholemman (Palmer *et al.*, 1991) as it is located on the plasma membrane and its two phosphorylation sites in the cytoplasmic region that may regulate its function. Immunoprecipitation experiments (Crambert *et al.*, 2002) have shown PLM interacts with the Na^+, K^+-ATPase and decreases the apparent Na^+ affinity and also the apparent K^+ affinity (to a smaller degree). It also interacts with the Na^+-Ca^{2+} exchanger (NCX1) in muscle cells (Dostanic *et al.*, 2004). Experiments with PLM-knockout mice (Jia *et al.*, 2005) contradict other data as ATPase assays of Na^+, K^+-ATPase purified from wild type and PLM knock out mice showed a 50% decrease in activity when PLM is knocked out, despite no change in Na^+, K^+-ATPase expression levels revealed by immunoprecipitation. This suggests PLM in fact stimulates the Na^+, K^+-ATPase. However these contradictions may in fact be evidence that PLM has two conformations, and in some way whilst interacting with the Na^+, K^+-ATPase, its functional effect can change from a positive to a negative effect.

1.2.5. Mat-8 (FXYD3)

Mat-8 was discovered in 1994 in murine breast tumours (Morrison and Leder, 1994) as a novel gene induced by Ras and Neu oncogenes. It has

since been linked to many other cancers including human breast tumour cell lines (Morrison *et al.*, 1995), colorectal cancer cell lines (Arimochi *et al.*, 2007) and pancreatic cancer cell lines (Kayed *et al.*, 2006). The first real evidence for an interaction between Mat-8 and the Na^+, K^+-ATPase was discovered as recently as 2005 (Crambert *et al.*, 2005). Several proteins including rat Mat-8, Na^+, K^+-ATPase, colonic H^+,K^+-ATPase and SERCA were variously co-expressed in *Xenopus* oocytes. Immunoprecipitation experiments performed on these proteins showed that Mat-8's strongest co-immunoprecipitation was Na^+, K^+-ATPase. Mat-8 also associated with colonic H^+, K^+-ATPase (although to a lesser extent) but showed no interaction with SERCA. These experiments also revealed that Mat-8 induces a small yet significant reduction in the affinity of Na^+, K^+-ATPase for external K^+ (15-40% depending on membrane potential) and also an approximately 20% reduction of affinity for Na^+ (as opposed to sequentially similar CHIF, which increases affinity). More recently it has been discovered these affinity changes were actually only caused by one isoform of Mat-8. There is in fact a longer isoform with a 26-amino acid insertion after the transmembrane domain (Figure 1.6.) (Bibert *et al.*, 2006).

```
>Mat-8 Short Form cytoplasmic region
S-------------------------AKCKCKFGQKSGHHPGETPPLITPGSAQS
>Mat-8 Long Form cytoplasmic region
SEWRSSGEQAGRGWGSPPLTTQLSPTGAKCKCKFGQKSGHHPGETPPLITPGSAQS
```

Figure 1.6. Comparison of cytoplasmic regions of Mat-8 isoforms. Both isoforms are identical in the transmembrane and extracellular region (not shown) but the long isoform has an extra 26 amino acids in the cytoplasmic region.

Functional information on the long isoform is limited but unlike the short form Na^+, K^+-ATPase affinity for external K^+ decreases to a larger extent (up to 50%) but affinity for Na^+ actually increases (~15%) Differences in expression levels of the Mat-8 isoforms have been difficult to analyse due to their high similarity and small size but the short form does seem to have much higher levels of expression in cancer than long form (Yamamoto *et al.*, 2009). The Na^+, K^+-ATPase interaction with Mat-8 was then further studied with fluorescence tags in colorectal cancer cells (Arimochi *et al.*, 2005), which showed the distribution of Mat-8 in cells. Using GFP and Myc tags it was revealed that Mat-8 was found to co-localise with the Na^+, K^+-ATPase on intracellular membranes. These membranes were then prepared and immunoprecipitation confirmed that the Na^+, K^+-ATPase α-subunit and Mat-8 co precipitate, further suggesting an important interaction between the two. Recently, Mat-8 silencing experiments in human colon adenocarcinoma cells have shown an increased affinity of the Na^+, K^+-ATPase for Na^+ and K^+ ions strengthening the argument that Mat-8 decreases the affinity of the Na^+, K^+-ATPase for ions (Bibert *et al.*,

2009). Despite this increase of ion affinity the rate of reaction of the Na^+, K^+-ATPase actually decreases whilst total α-subunit levels expressed and present at the membrane are unchanged. This could be explained by differential isoform expression as in Mat-8 deficient cells there is a reduction of the Na^+, K^+-ATPase α1-subunit and an increase in α3-subunit (Mat-8 associates with α1-subunit). Difficulties arose in detecting β-subunit isoforms by western blot, however it was observed that β1-subunit expression was downregulated in Mat-8 deficient cells which causes the cell to be poorly differentiated. Aside from this, mechanistic information details on the Mat-8/Na^+, K^+-ATPase are scarce.

A large amount of the experimental work presented in this thesis shows the results of experiments to analyse the effects of FXYD proteins on the Na^+, K^+-ATPase. The source of the Na^+, K^+-ATPase used is pig kidney (Jørgensen, 1974) and spiny dogfish rectal gland (Esmann *et al.*, 1979) as they are the most effective known methods of obtaining the enzyme. The isoforms purified by these methods are α1β1 from pig kidney and α3β1 from spiny dogfish rectal gland. These are physiologically relevant isoforms to use as PLM interacts with all α1-3/β1-2 and both isoforms of Mat-8 associate stably with all α1-4/β1 complexes (Bibert *et al.*, 2006)

1.2.6. Structures of FXYD proteins

The structures of FXYD proteins, PLM and CHIF have been solved by NMR (Franzin *et al.*, 2007c; Teriete *et al.*, 2007). There is also limited structural information for Mat-8 which shows locations of secondary structure on the sequence, as determined by heteronuclear single quantum coherence (HSQC) experiments (Franzin *et al.*, 2007b). Figure 1.7. shows these two solved structures. These structures were solved using solution state NMR in detergent micelles and not bilayers. Micelles are a relatively poor model for a cell membrane as they do not consist of a bilayer unlike native membranes. It appears structural similarity is good inside and poor

Fig 1.7. Structures of FXYD proteins. 3D structures of PLM and CHIF so far the only mammalian FXYD proteins that have structures solved.. Regions are labelled as follows: orange; cytoplasmic, green; transmembrane, blue; extracellular. Structures obtained from the Protein Data Bank (PDB) from (Franzin *et al.*, 2007d; Teriete *et al.*, 2007) Both PLM and CHIF had 100 conformers calculated however only 20 PLM conformers and 1 CHIF conformer were submitted which are represented here.

outside of the transmembrane domain which is supported by the sequence as outside of the signature sequence (predominantly comprising the transmembrane domain), sequence similarity is very poor. This further suggests that the unique functions of FXYD proteins are regulated by the extracellular and cytoplasmic regions of the FXYD proteins. These unique features are either unknown or poorly understood but usefully these regions are soluble so when produced as small peptide fragments can be used in solution in assays (Pavlovic *et al.*, 2007). A large focus of this project will be to attempt to find possible roles for these fragments and to see if differences in structure could be could be related to function.

1.2.7. Roles of Mat-8 and PLM in disease

In order to improve treatments of diseases it is important to understand the proteins involved in them. This can lead to targeted drug design. Mat-8 appears to have a role in many cancers. It was discovered to be overexpressed in murine breast tumours (Morrison and Leder, 1994) and has since been discovered to be a marker for other cancers including prostate (Grzmil *et al.*, 2004), pancreatic (Kayed *et al.*, 2006) and colorectal (Arimochi *et al.*, 2007). It is unclear if the upregulation of Mat-8 has an effect on cancer or is just a consequence although evidence for the former is increasing. For example Mat-8 has been shown to be linked to tumour protein 53 (p53) as it is upregulated by 5-Fluorouracil treatment of

breast cancer cells in a manner dependent on p53 (Jorgensen *et al.*, 2003). Inhibition of Mat-8 expression reduces cell proliferation (Grzmil *et al.*, 2004), so it could be that, again like p53, the role of Mat-8 is in cell proliferation and not antiproliferation. Perhaps p53 induces genes including Mat-8 that are involved in cell proliferation as part of a negative feedback loop. Recently, Mat-8 silencing in human colon adenocarcinoma cells showed impeded cell differentiation and a small increase in cell apoptosis, which in contrast to the previous work does not translate into decreased cell proliferation (Bibert *et al.*, 2009). However, Mat-8 was actually shown to be down-regulated in colon and kidney cancer (Kayed *et al.*, 2006), which would support results that Mat-8 perhaps does not have an effect on Caco-2 cell proliferation. It is possible that Mat-8 has two different roles in cancer. In cancer cells that are unable to differentiate, Mat-8 could encourage cell proliferation, whereas in differentiation-competent cells like human colon adenocarcinoma cells, Mat-8 may have no effect on cell proliferation but in fact decreases cell apoptosis and promotes cell differentiation. This is all still quite speculative but it seems increasingly likely that Mat-8 is more than a mere marker for cancers and has its own distinct role.

PLM has a role in cardiac disease although it is also poorly understood. However there is increasing evidence that the Na^+, K^+-ATPase -PLM

interaction could be a valid drug target. When PLM is knocked out in mouse hearts there is depression of contractile function which was associated with mild hypertrophy (Chan *et al.*, 2010). Intracellular Na^+ ion concentration is up to 3 mM higher during heart failure, which can greatly affect Na^+/Ca^+ exchange and effect cardiac contractile function. As mentioned earlier, the Na^+, K^+-ATPase exports three Na^+ ions per cycle and is in fact the main method of Na^+ extrusion. Importantly cardiac Na^+, K^+-ATPase activity decreases after a myocardial infarction (Zhang *et al.*, 2006) and in heart failure (Dixon *et al.*, 1992). FXYD proteins are expressed tissue specifically and the predominant FXYD protein in heart tissue is PLM. Overexpression of PLM appears to cause both reduced Na^+, K^+-ATPase function and a reduced Na^+, K^+-ATPase expression(Zhang *et al.*, 2006). It was recently highlighted (Shattock, 2009), that drugs that decrease Na^+ influx protect against ischaemic injury and arrhythmias in animal models. This suggests that drugs that increase Na^+ efflux by stimulating the Na^+, K^+-ATPase could provide a novel method of clearing intracellular Na^+ in heart failure. PLM has been shown to inhibit the Na^+, K^+-ATPase so altering its activity via drug targeting could stimulate the Na^+, K^+-ATPase to give the desired treatment.

1.3. Cardiac Glycosides

Cardiac glycosides were first used as drugs over 200 years ago (Withering, 1785), with extracts of digitalis purpurea (foxglove) used to treat heart disorders. As this was a long time before modern biology there was no understanding of how this drug worked. In fact the mechanism of cardiac glycosides did not begin to be understood until 1965 when another cardiac glycoside known as ouabain was shown to specifically inhibit the Na^+, K^+-ATPase (Schatzmann HJ, 1965).

1.3.1. Characteristics and structure of Cardiac Glycosides

The cardiac glycosides all have a characteristic structural motif comprised of a steroid nucleus, a sugar moiety and a lactone moiety (Figure 1.8). The steroid nucleus only varies in its side chains between members. The lactone moiety is what defines the subclass of cardiac glycoside. A cardenolide has a five-membered unsaturated butyrolactone ring in this position whereas a bufadienolide has a six-membered unsaturated pyrone ring. Finally, the sugar moiety can be any of a range of sugars such as glucose, galactose, mannose, rhamnose and digitalose. The sugar itself has no active role but they do affect the pharmacodynamics and pharmacokinetics of the cardiac glycosides (Prassas and Diamandis, 2008). These effects include the speed of absorption and potency. This variation has allowed over one hundred cardiac glycosides to be extracted from vegetal sources (Melero *et al.*, 2000).

Due to a very specific site for plant derived cardiac glycosides being present in the animal protein complex of the Na^+, K^+-ATPase, it seemed likely that animal produced equivalent cardiac glycosides must also exist. This would give cardiac glycosides both a pharmacological and a physiological role. Many cardiac glycosides have been extracted from animals, most of which have been from frogs (Pieter and Fanie, 1998). Endogenous ouabain has been extracted from mammal sources including human plasma (Hamlyn *et al.*, 1991; Mathews *et al.*, 1991), bovine adrenal cortex (Schneider *et al.*, 1998) and bovine hypothalamus (Kawamura *et al.*, 1999). Differences between endogenous and exogenous ouabain are very discreet and have made it difficult to prove that animals naturally produce ouabain. However increased levels of ouabain in conditions like hypertension and detection of a marinobufagenin-like cardiac glycoside in urine after acute myocardial infarction (Bagrov *et al.*, 1998) suggest cardiac glycosides are produced by the animals themselves.

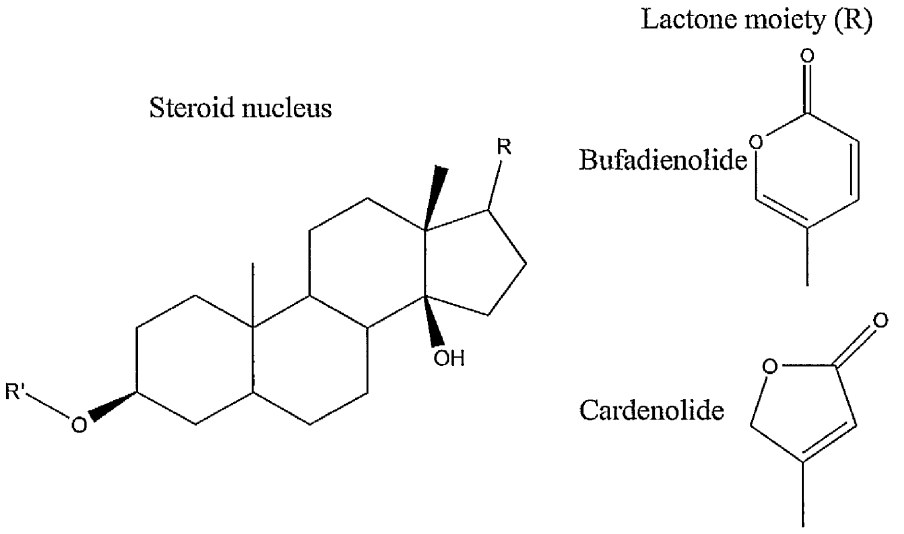

Figure 1.8. Signature cardiac glycoside motif. The backbone of the cardiac glycosides is the steroid nucleus common to all members. R represents the lactone moiety which defines its subtype. R' represents the sugar moiety (e.g. rhamnose), which may control the pharmacodynamic and pharmacokinetic properties.

1.3.2. Mechanism

As described earlier the Na^+, K^+-ATPase goes through a dephosphorylation step which changes the cation affinity from K^+ to Na^+. Cardiac glycosides block this event from occurring stopping the cycle from completing and completely inactivating the enzyme (Godfraind, 1984). It appears that this occurs primarily in the E_2P conformation (as opposed to the $E_2P.2K^+$ conformation) as ouabain affinity for the Na^+, K^+-ATPase decreases in the presence of K^+ (Sachs, 1974; Hobbs and Dunham, 1978). The site at which

this occurs is not fully clear. Mutagenesis studies have revealed that when Cys^{104}, Tyr^{108} (Canessa *et al.*, 1992), Gln^{111} (Price and Lingrel, 1988), Pro^{118} (Schultheis and Lingrel, 1993), Asp^{121} (Price *et al.*, 1989), Asn^{122} (Lingrel *et al.*, 1991), Tyr^{308} (Canessa *et al.*, 1993), Leu^{330}, Ala^{331}, Thr^{338} (Croyle *et al.*, 1997b), Phe^{786}, Leu^{793}, Phe^{863} (Palasis *et al.*, 1996), Thr^{797} (Burns and Price, 1993), Arg^{880} (Schultheis *et al.*, 1993) and Phe^{982} (Croyle *et al.*, 1997a; Sweadner and Donnet, 2001) are substituted there were negative effects on the binding of ouabain to the Na^+, K^+-ATPase. As seen in Figure 1.9. most of these are found in the transmembrane region in close proximity of the FXYD protein.

Figure 1.9. Residues that affect ouabain binding. In this structure (Morth *et al.*, 2007) of the Na^+, K^+-ATPase the α-subunit is shown in green, the β-subunit is show in cyan and the γ-subunit is shown in pink. The red spheres indicate locations of residues that reduce ouabain binding when replaced with other amino acids by mutagenesis.

To understand this interaction better, NMR and modelling studies were performed (Middleton *et al.*, 2000). By studying isotopically labelled ouabain derivatives bound to unlabelled Na^+, K^+-ATPase it was shown that

the majority of the interactions between ouabain and the Na^+, K^+-ATPase appeared to be due to the steroid nucleus lying across the surface of the α-subunit secured most likely by hydrogen bonds. In this conformation the sugar moiety faces away from the surface of the membrane and is free to move into contact with one or more aromatic residues. Recent full Na^+, K^+-ATPase structures have disputed this. Two x-ray crystallography structures of the Na^+, K^+-ATPase with bound ouabain have been solved, the first structure is from shark rectal fin Na^+, K^+-ATPase with ouabain soaked into the protein crystals (Ogawa *et al.*, 2009), whilst the second structure is from pig kidney Na^+, K^+-ATPase incubated with ouabain, pre-crystallisation (Yatime *et al.*, 2011). The former paper was performed in the low affinity $E_2P.(2K^+)$ conformation and shows ouabain bound at a similar site to that previously shown (Middleton *et al.*, 2000) but it is intercalated into the transmembrane helices perpendicular to the membrane surface. The more recent paper in the high affinity ouabain binding state is in a similar conformation but is shifted laterally by about 2 Å towards the αM1–2 transmembrane helices. It is unclear if this change is due to the difference in affinity states of Na^+, K^+-ATPase, the method of applying ouabain to the Na^+, K^+-ATPase, or the organism from which Na^+, K^+-ATPase was extracted.

1.4. Aims of this work

The aims of this project focus on gaining further understanding of the structural and functional interaction of FXYD proteins and cardiac glycosides with the Na^+, K^+-ATPase. The initial hypothesis of this study is that the cytoplasmic region of PLM interacts with one or more specific sites on the surface of the Na^+, K^+-ATPase which alters ATPase activity. This interaction is likely regulated by phosphorylation of Ser 68 and/or Ser 63 both located in the cytoplasmic region of PLM. Short form Mat-8 and CHIF should not share this feature as they do not have similar phosphorylation sites. It is unclear if long form Mat-8 would also not share this feature as it has only recently been discovered and it is not known if it contains phosphorylation sites within its cytoplasmic region like PLM. Any interaction of the cytoplasmic region of PLM and the Na^+, K^+-ATPase would have to compliment the affinity the cytoplasmic region of PLM has for negatively charged lipid bilayers. It is therefore hypothesised the interaction of the cytoplasmic region of PLM and the Na^+, K^+-ATPase is in close proximity of the cell membrane surface to allow this to happen.

The work performed to test this hypothesis and gain further understanding of cardiac glycosides four main headings:

1.4.1. The association of the cytoplasmic region of FXYD proteins with phospholipid bilayers

The cytoplasmic region of PLM is known to interact with negatively charged phospholipid bilayers (Clayton *et al.*, 2005). In this project the cytoplasmic regions of other FXYD proteins including both isoforms of Mat-8 and CHIF will be tested to see if they too interact with negatively charged membranes in a similar fashion. The interaction of the PLM cytoplasmic domain with phospholipid bilayers will be investigated further by developing a system for determining peptide/lipid interactions in the presence of the Na^+, K^+-ATPase. This will help determine if the observed interaction of the cytoplasmic region of PLM with negatively charged phospholipid bilayers is physiologically relevant.

1.4.2. The function of the cytoplasmic region of FXYD proteins

This section of the work involved testing the effect of the cytoplasmic regions of PLM, both isoforms of Mat-8 and CHIF on Na^+, K^+-ATPase activity. The effect of PLM phosphorylation on the potency of its functional effects on the Na^+, K^+-ATPase was also investigated. The final aim of this section was to further analyse the interaction between the cytoplasmic region of PLM and the Na^+, K^+-ATPase using bioinformatics

techniques. The interaction could be modelled and provide insight as to how this could affect ion affinity of the Na^+, K^+-ATPase.

1.4.3. The development of an expression system for FXYD proteins

Work was undertaken to develop a system in the pMAL vector for the expression and purification of FXYD proteins as an alternative to a current protocol (Thai *et al.*, 2005) which could not be reliably replicated. With the new expression system in place, further refinements had to be carried out to allow the expression and purification of fully labelled fusion proteins in quantities suitable for NMR.

1.4.4. The development of a new method to determine the orientation of cardiac glycosides in the Na^+, K^+-ATPase

The final section of work aimed to develop a novel method for probing the depths that ligands penetrate the transmembrane region of a protein, which would allow the orientation of ouabain within the Na^+, K^+-ATPase to be determined. The initial aim of this section was to produce a ouabain derivative containing ^{13}C acetonide bridges. This would produce a signature peak when analysed by solid-state NMR. The second aim using solid-state NMR was to observe the ouabain derivative whilst bound to the Na^+, K^+-ATPase. By using cross-polarisation techniques the natural abundance ^{13}C peaks in Na^+, K^+-ATPase can be observed. The final aim

was to observe the effect of the paramagnetic broadening agent manganese on both the natural abundance ^{13}C and the ouabain derivative signature peak to probe the depth of ouabain penetration within the Na^+, K^+-ATPase.

Chapter 2

2.1. Nuclear Magnetic Resonance

Nuclear magnetic resonance (NMR) spectroscopy, particularly in the solid state, is the principal technique used in this project. The theory of NMR is described in detail in several textbooks (Evans, 1995; Duer, 2004) and websites (Reusch, 2000; Hornack, 2011). This chapter briefly describes the main theoretical aspects that are relevant to the work presented in this thesis.

2.2. Nuclear Spin and the Larmor Frequency

For nuclei to be NMR active they must have the quantum mechanical property known as spin given the symbol *I* to represent total angular momentum. Nuclei with an odd atomic mass number have fractional spins (e.g. ^{1}H, ^{13}C, ^{31}P have a spin of 1/2, ^{11}B has a spin of 3/2 and ^{17}O has a spin of 5/2). Even mass nuclei with odd atomic numbers have integral spins (e.g. ^{2}H, ^{14}N have a spin of 1). Both of these nuclei types are therefore suitable for NMR as they have at least one unpaired proton. Even mass nuclei with even atomic numbers have a spin of 0 making them NMR silent (e.g. ^{12}C and ^{16}O). The movement of the unpaired positively charged protons in nuclei with spin produces a magnetic field with nuclear magnetic moment, which is defined by the following equation:

$$\mu = \frac{\gamma I h}{2\pi} \tag{2.1}$$

Where γ is the gyromagnetic ratio (the proportionality constant) and h is Planck's constant (6.26×10^{-34} J s^{-1}).

When an external magnetic field (B_0) is applied to a sample, each nuclear magnetic moment will either align with the magnetic field (α spin) or against it (β spin) (Figure 2.1).

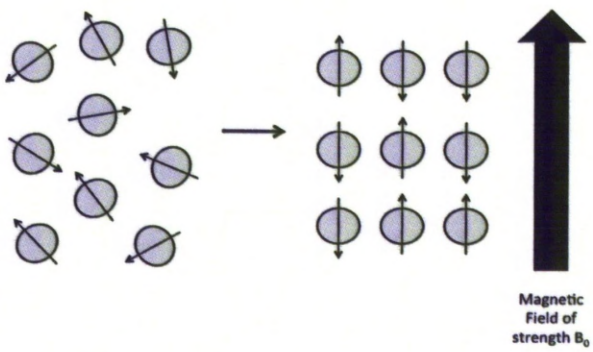

Figure 2.1. Effect of external magnetic field on the orientation of the magnetic moments of nuclei with spin properties.

When $I \neq 0$ a nucleus cannot align exactly with or against the applied magnetic field. The nucleus will in fact precess at an angle around the applied magnetic field at an angular frequency specific to each nucleus known as the Larmor frequency (v) (Figure 2.2). Larmor frequency is defined by the following equation:

$$\nu = \frac{\gamma B_0}{2\pi} \tag{2.2.}$$

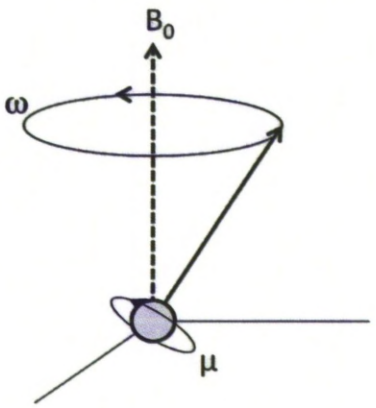

Figure 2.2. Representation of the spin and precession of a nucleus within an applied magnetic field.

Larmor frequency is also related to angular velocity ω (rad s^{-1}) and is given by the following equation:

$$\omega = 2\pi\nu \tag{2.3.}$$

The number of possible orientations a nuclei has with respect to the magnetic field is $2I + 1$ so for common NMR experiments on biomolecules observing ^{13}C, ^{1}H or ^{15}N which all have spin values of ½ there are two possible orientations. These two orientations either align against the field (antiparallel) and are said to be in a high-energy state whereas the ones that align with it are in a low energy state (parallel). This splitting of energy

levels is known as the Zeeman effect. The population of each state is determined by the difference in energy (ΔE) between these two states in an applied magnetic field, according to the Boltzmann equation:

$$\frac{N_\beta}{N_\alpha} = e^{-\Delta E/k_B T} \qquad (2.4.)$$

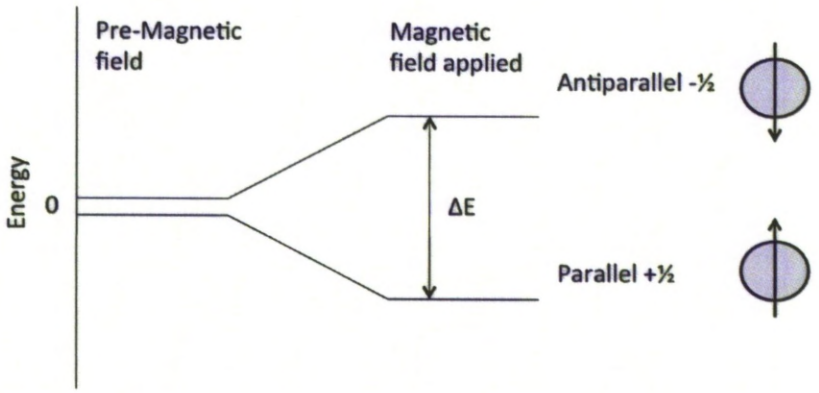

Figure 2.3. Effect of external magnetic field on energy levels. As magnetic moments are usually distributed randomly there is no net energy in the absence of an external magnetic field. In this sample on nuclei where I = ½ all nuclei either adopt a +½ (low) or a -½ (high) energy state in the presence of an external magnetic field.

The change in energy is proportional to gyromagnetic ratio and B_0 due to Planck's law according to the following equation:

$$\Delta E = \frac{h\gamma B_0}{2\pi} = h\nu \qquad (2.5.)$$

2.3. Radio Frequency Pulses

The Boltzmann equation indicates that at equilibrium the high energy and low energy states of nuclei are nearly equally populated, but there is a slight excess of low energy state nuclei giving a bulk magnetisation (M_0) parallel the z axis of B_0. In magnetic fields of up to 21 Tesla the Larmor frequency falls within the MHz range, i.e. radio frequency (RF). When electromagnetic radiation at the Larmor (radio) frequency is applied to the nuclei along an axis perpendicular to the z axis of the magnetic field B_0 the nuclear spins begin to precess about the oscillating magnetic field. This effect is known as nuclear magnetic resonance. The net effect of this process is to cause M_0 to flip from alignment with B_0 to alignment with the direction of the 90° pulse.

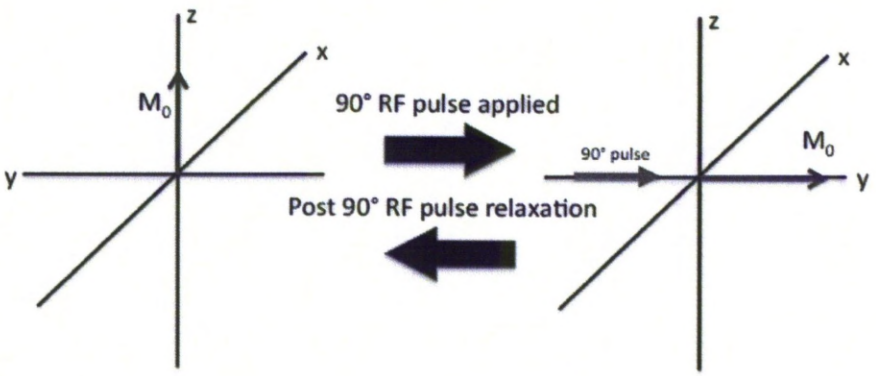

Figure 2.4. Diagram showing the flipping of magnetisation due to the effects of a 90° RF pulse.

After the RF pulse is complete the sample magnetisation is able to undergo free precession around the xy plane generating a current in the surrounding

coil of the NMR spectrophotometer which is processed as a sinusoidal signal comprising all the Larmor frequencies of all the nuclear spins in the sample. The signal is detected by the spectrometer as a dampened wave or free induction delay (FID) (Figure 2.5.). In a typical experiment many FIDs are added together because the signal detected is often very weak and noisy. By adding together scans the signal accumulates and the signal to noise ratio improves. Finally the FID is treated with a mathematical function known as a Fourier transformation (FT) which converts it into a frequency domain spectrum in which the individual nuclear frequencies are represented by peaks (Figure 2.5.).

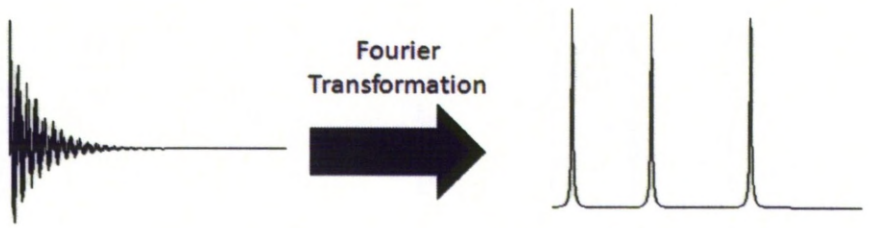

Figure 2.5. Fourier Transformation (FT) of a Free Induction Decay into a Frequency Domain Spectrum.

2.4. Relaxation

When the nuclear spins are perturbed from their equilibrium state, they become subject to processes known as relaxation, which affect the appearance of the NMR spectrum and must be taken into account when

setting up an NMR experiment. After the RF pulse is switched off the alignment of M_0 reverts from the xy axis back to B_0 by a process known as spin-lattice (or longitudinal) relaxation (Figure 2.4.). This process determines the rate at which the spin states re-establish their Boltzmann populations. The time constant for this process is called T1. Spin-lattice relaxation takes a relatively long amount of time (sometimes minutes) particularly compared to other spectroscopic techniques. T2 occurs simultaneously to T1 and it is driven by interactions of the nuclear spins and by inhomogeneities in B_0. When the RF pulse is switched off the individual nuclei experience slightly different local magnetic fields and have their own Larmor frequencies. This causes precessing spins to lose phase coherence (i.e. they diphase) with time and the result is seen in the exponential dampening of the NMR signal. The NMR signal often decays to zero long before the nuclear spins re-establish their equilibrium state.

2.5. Chemical Shift

The NMR frequency of a nuclear spin is dependent on the strength of the applied magnetic field, as shown above, and also on the very small magnetic fields generated by the circulating electron cloud around the nucleus. Hence the NMR spectrum is sensitive to the *chemical shielding* of the nuclei. The movement of electric charges of the electron cloud around a nucleus induce a local magnetic field that opposes (and sometimes

enhances) the applied field B_0. The effective magnetic field (B_{eff}) experienced by the nucleus is therefore defined by the following equation:

$$B_{eff} = B_0(1 - \sigma) \tag{2.6.}$$

where σ in equation 2.6. is the chemical shielding tensor. The actual resonance frequency ω_0 of a nucleus is therefore given by:

$$\omega_0 = \frac{\gamma}{2\pi} B_0(1 - \sigma_{ref}) \tag{2.7.}$$

The chemical shift tensor defines the extent a nucleus is "shielded". This becomes important in solid state NMR and is described later (2.6.1.1.). σ_{ref} refers to the reference material which in solid state NMR is usually adamantane. All chemical shifts in an NMR spectrum are defined as differences in chemical shift from this reference. In practice, the frequencies ω are expressed as chemical shifts relative to the frequency ω_0 of a reference molecule. Chemical shift (δ) is defined by the following equation and it is in parts per million (ppm):

$$\delta = \frac{\omega - \omega_0}{\omega_0} \times 10^6 \tag{2.8.}$$

2.6. Solid State NMR

2.6.1. Anisotropic Spin Interactions

Many of the internal magnetic interactions which affect precessional frequency of a nuclear spin are anisotropic; in other words, the magnitude of the interaction depends on the orientation of the nucleus within the applied magnetic field. In a liquid sample rapid molecular tumbling averages out the effects of these anisotropic interactions and narrow peaks are generally observed in the NMR spectrum at each resonance frequency. In a solid sample molecules are static and the nuclei have all possible orientations within the applied magnetic field, each associated with an orientationally-dependent resonance frequency. As a consequence the NMR peaks for a solid sample are very much broader than for a liquid sample unless special measures are taken. The broad spectra are called powder patterns in recognition of the orientational distribution of a powder sample.

The next sections describe the three principal anisotropic interactions that are relevant to this thesis.

2.6.1.1. Chemical Shielding Anisotropy

The chemical shielding tensor can be described by a second rank tensor σ with principal elements σ_{11}, σ_{22} and σ_{33} reflecting the anisotropy of the

interaction. The isotropic value of the shielding tensor seen in isotropic liquids is an average of the principle elements:

$$\sigma_{iso} = {}^{1}/_{3}\,(\sigma_{11} + \sigma_{22} + \sigma_{33}) \qquad (2.9.)$$

The chemical shielding tensor, which is related to the electron distribution surrounding the nucleus, can be represented by an ellipsoid drawn in a reference frame in which σ_{11}, σ_{22} and σ_{33} are aligned along the principle axes x', y' and z' (Figure 2.6.)

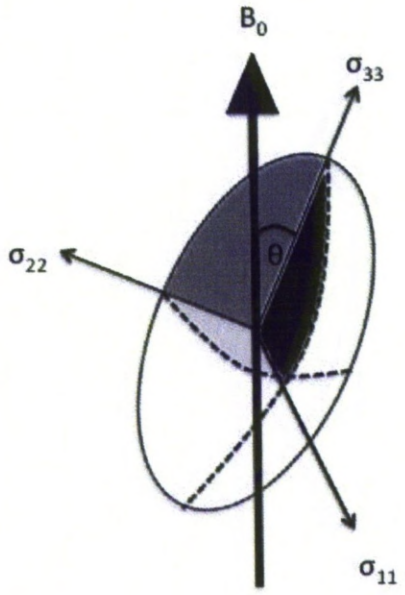

Figure 2.6. The Chemical Shielding Ellipsoid. This indicates the different orientations of the magnetic field relative to B_0 resulting in different resonance positions for the same chemical species.

In a solid sample the lack of tumbling removes the averaging effects seen in a solution sample, which means every slight deviation in orientation has its own chemical shift, causing broadening of peaks belonging to one chemical species. This is represented in Figure 2.7.

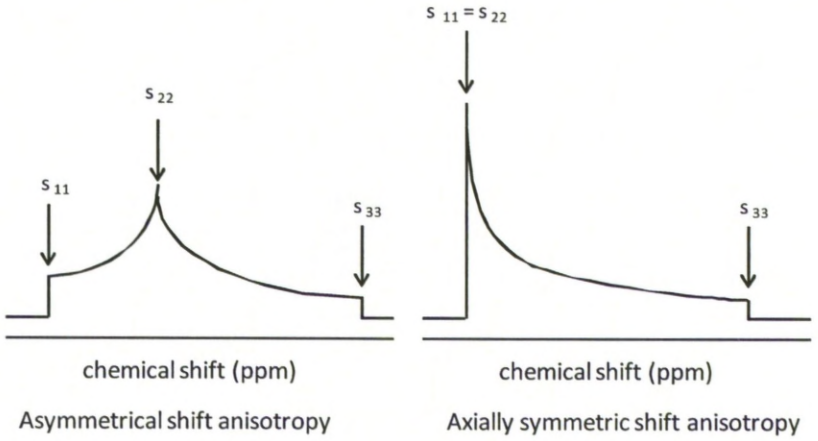

Figure 2.7. Theoretical powder line shapes for the chemical shift tensor in asymmetrical and axially symmetric nuclei.

The chemical shielding σ for a given nucleus is determined by:

$$\sigma = \sigma_{iso} + {}^{1}/_{2}\,\Delta(3cos^{2}\theta - 1) \qquad (2.9.)$$

Where θ is the angle between the z axis of the principal axis system and the magnetic field B_0 and Δ is the span of the chemical shielding anisotropy, defined as:

$$\Delta\sigma = \sigma_{33} - {}^{1}/_{2}\,(\sigma_{11} + \sigma_{22}) \qquad (2.10)$$

In a powder the shape and width of the spectrum is determined by the principle elements and by the statistical distribution of orientations (Figure 2.7).

2.6.1.2. Dipole-Dipole Coupling

As shown in equation 2.1., nuclei possess a magnetic dipole moment μ. Dipole-dipole coupling is the interaction through space of two or more magnetic moments and is analogous to the interaction of a pair of bar magnets. In essence, a single spin acts like a bar magnet with its own magnetic field and another spin in close proximity to it interacts with this magnetic field. This much like chemical shift anisotropy is averaged out in a solution sample and needs no consideration. In a solid state NMR homonuclear and heteronuclear dipolar coupling cause broadening of spectral peaks. For a pair of dipolar coupled nuclear spins $I1$ and $I2$ the NMR lines are split into a doublet separated by frequency Δν according to

$$\Delta v = D(3cos^2\theta - 1) \qquad (2.11.)$$

Where D is the dipolar coupling constant given by:

$$D = \frac{\gamma_{I1}\gamma_{I2}h}{2\pi r^3} \qquad (2.12.)$$

Here r is the linear distance separating the spins, θ is the angle of the dipolar vector relative to B_0 and γ_{I1} and γ_{I2} are the gyromagnetic ratios of the two spins used in this equation (Figure 2.8.).

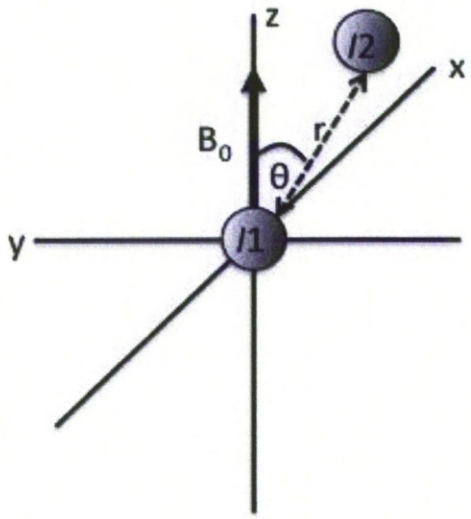

Figure 2.8. Representation of dipolar coupling between two nuclear spins *I*1 and *I*2.

A spectrum of a powder sample is a superimposition of doublets split by frequencies dependent on the statistical distribution of dipolar vector orientations. In organic and biomolecular materials the strongest dipolar couplings occur between proton spins (because of their high gyromagnetic ratio and abundance), which give rise to extremely broad and uninformative spectra. For this reason, protons are not routinely observed directly in solid-state NMR at the time of writing, although methods are being developed to improve the resolution of proton spectra.

2.6.1.3. Quadrupole Interactions

Nuclei of spin > ½ possess a quadrupolar moment Q, which interacts with the electric field gradient generated by the circulating electrons and causes rapid spin-lattice relaxation. A nucleus of spin 1 such as ^{2}H possess 3 spin states; +1, 0 and -1 which occupy 3 energy levels in an applied magnetic field. In an isotropic liquid the quadrupolar interaction is averaged to zero and the energy levels are equally spaced with transition frequency due to the Zeeman effect. In the solid-state the quadropolar interactions are non-zero and consequently the energy levels become shifted positively or negatively so that the transition frequencies, the frequencies of transitions from +1 to 0 and 0 to -1, V_A and V_B, become inequivalent. (Figure 2.9.)

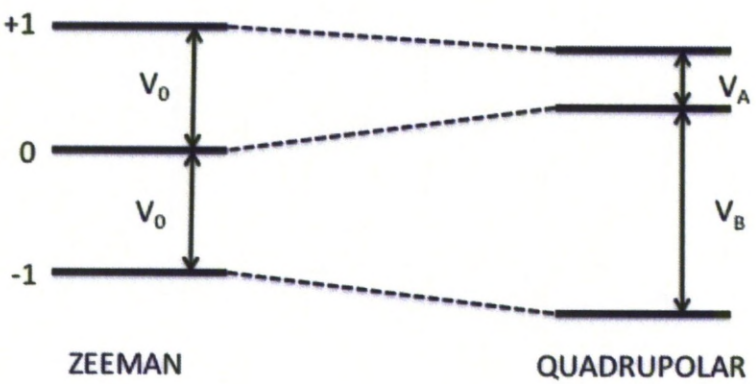

Figure 2.9. The effect on transitional frequencies due to quadropolar interactions in nuclei with a spin of 1.

The quadropular interaction is also orientation dependent as represented in the following equation:

$$\Delta\nu_Q = {}^3/_4\left(\frac{e^2qQ}{h}\right)(3cos^2\theta - 1) \qquad (2.13)$$

Where e^2qQ is the quadrupole coupling constant.

2.6.2. Solid-State NMR methods

2.6.2.1. Wide Line NMR

The shape of anisotropically broadened solid-state NMR lines can be analysed to give information on dynamics and interactions. This is particularly useful when the observed line arises from a unique nuclear site in a molecule, but line shape analysis becomes more difficult when the NMR spectrum is a superimposition of signals from many chemically inequivalent nuclei. The spin 1 nucleus ^2H is attractive for this purpose because it can be incorporated into molecules such as phospholipids at specific sites, so that the spectrum can be assigned immediately and unambiguously. The anisotropy of the quadrupolar interaction gives rise to a characteristic spectrum called *Pake patterns* (Figure 2.10.). The horns of the *Pake patterns* are split by $\Delta\nu_Q$ (which is related to the quadrupolar coupling constant shown in equation 2.13.) which is sensitive to molecular motions and to the orientation of functional groups relative to an axis of

rotation. It will be shown in Chapter 3 how this phenomenon can be exploited to probe the interactions of peptides with headgroup-deuterated phospholipid membranes.

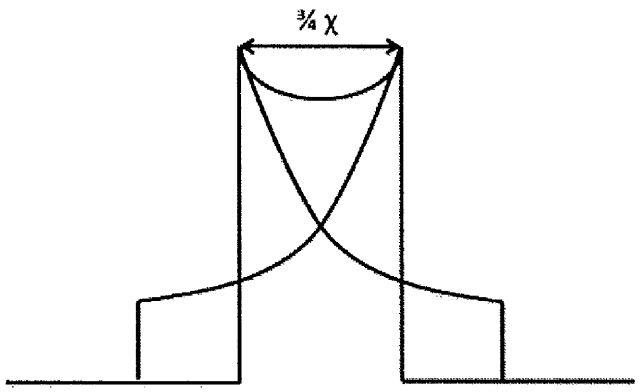

Figure 2.10. The *Pake pattern* formed in a deuterium spectra due to there being two allowed spin transitions.

2.6.2.2. Solid-State NMR methods for high resolution spectra

The majority of solid-state NMR experiments use techniques to overcome the effects of anisotropic spin to produce high-resolution spectra in which peaks from individual nuclear sites can be observed at different chemical shifts. The principal line-narrowing technique in solid-state is magic angle spinning but can also be combined with cross polarisation.

2.6.3.1 Magic Angle Spinning

The magnitude of the line broadening interactions have a $3\cos^2\theta$-1 dependency on the magnetic field (recall that θ is the angle between the magnetic field and the axis of the co-ordinate system expressing the anisotropic interaction). When θ equals 54.7°, the chemical shielding, dipolar coupling and quadrupolar interactions become zero because $3\cos^2(\theta) - 1 = 0$. The angle of 54.7° is therefore known as the magic angle. If a powder sample is rotated mechanically in the applied magnetic field about an axis inclined at the magic angle, all anisotropic interactions are averaged to zero over one cycle of rotation. If the spinning frequency approaches or exceeds the frequency range of the anisotropic interaction, then the effects of the anisotropy are eliminated from the spectrum and narrow lines are observed.

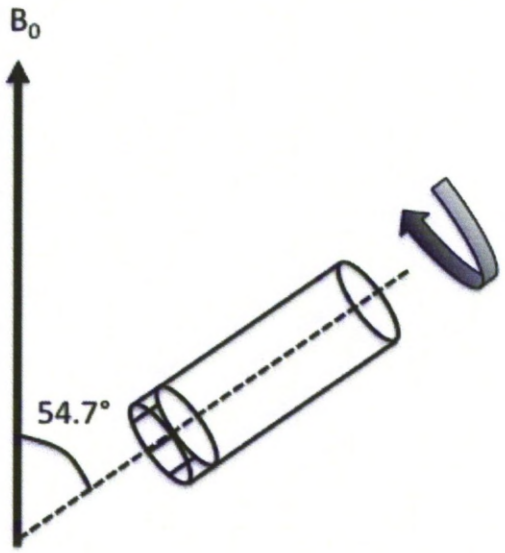

Figure 2.11. Diagram representing a sample spinning at 54.7° or the magic angle relative to the applied field B_0. A method to reduce line broadening in solid state NMR.

For a nucleus such as ^{13}C, the chemical shielding anisotropy can be 15-20 kHz and so the sample must be spun at this frequency to completely remove the effects. At slower spinning rates the MAS spectrum will consist of a series of "spinning sidebands". These are sharp lines that radiate from the central chemical shift peak set apart at a frequency equal to the spinning speed (Figure 2.12.). The spinning sidebands will effectively take signal away from the central peak reducing signal intensity i.e. the faster a sample is spun, the fewer sidebands are observed resulting in better signal to noise. If spinning sidebands appear in a region of interest in a sample, an alternative spin speed must be selected and in some cases

experiments will have to be run at different spin speeds to get a full picture. Figure 2.12. shows the creations of spinning sidebands at different spin speeds.

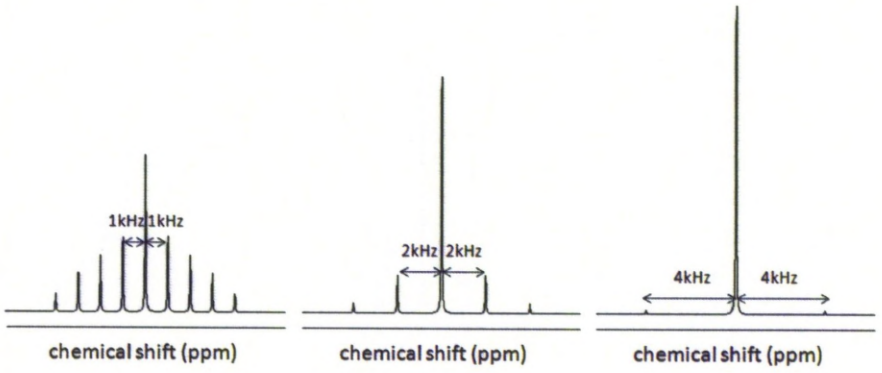

Figure 2.12. Representation of the effect of increased spin rate in solid-state NMR MAS experiments.

Dipolar couplings involving the network of protons in organic materials are normally very strong and the effects of these couplings cannot be completely eliminated from the spectrum with MAS rates that are achieved with current technology. Consequently, proton MAS spectra are rather broad even at MAS rates of 50 kHz. When less abundant nuclei such as ^{13}C or ^{31}P are observed, as in Chapter 3 and Chapter 6 of this thesis, strong heteronuclear couplings with protons must be removed by combining MAS with high-power proton decoupling, in which proton spins are irradiated with a strong radiofrequency field during sampling of the FID.

2.6.3.2 Hartmann-Hahn Cross Polarisation

Observing dilute spins like ^{13}C presents two major problems. Firstly the low abundance of nuclei means the signal to noise ratio is inevitably poor. Secondly, the spin-lattice relaxation times of dilute spins (T1) are very long due to the absence of strong homonuclear dipolar interactions. This means that large delays must be left between accumulation of successive scans and consequently experiment times to achieve a suitable signal to noise ratio can be very long. Hartmann-Hahn cross polarisation (CP) is a signal enhancement technique used in solid-state NMR to counteract these problems. CP works by transferring the magnetisation from an abundant and sensitive spin (usually ^{1}H) to a dilute spin with lower sensitivity (e.g. ^{13}C). A pulse scheme for a typical cross polarisation experiment is shown in Figure 2.13.

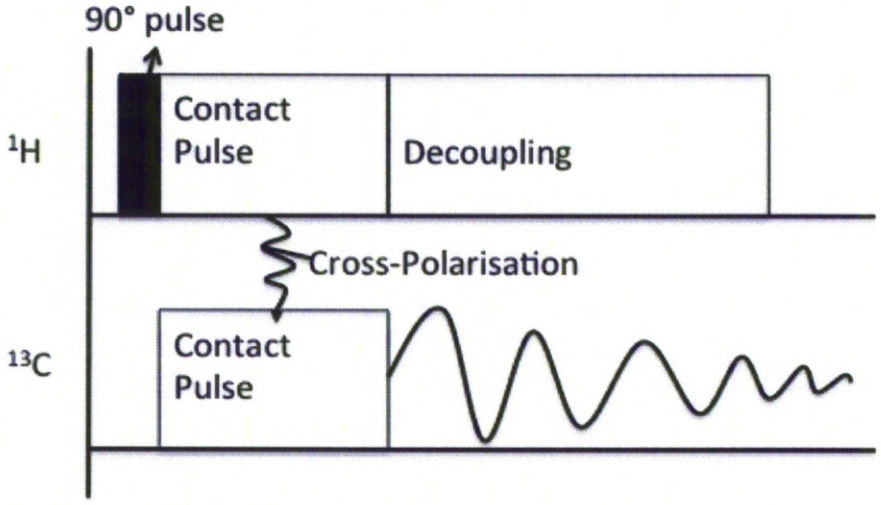

Figure 2.13. A typical cross polarisation pulse sequence. Following the 90° pulse magnetisation is transferred from ^{1}H to ^{13}C by cross polarisation. ^{13}C is then observed whilst ^{1}H is decoupled from ^{13}C.

The initial ^{1}H 90° pulse creates ^{1}H magnetisation along –y. The ^{1}H contact pulse is then applied on resonance which is continuous and maintains the magnetisation along –y in the absence of a 90° pulse. This is known as the spin-lock field ($B_1(^1H)$). The ^{13}C contact pulse is applied simultaneously to the ^{1}H contact pulse. This must be set to move ^{13}C into the same axis as ^{1}H at the same Larmor frequency to allow cross-polarisation to occur. This is known as the Hartman-Hahn matching condition, which is given by the following equation:

$$\gamma_H B_1(^1H) = \gamma_X B_1(X) \qquad (2.14.)$$

CP has been used on cell membranes to allow the observation of natural abundance ^{13}C peaks in both frozen and in a "fluid" state (Spooner *et al.*, 1994). Early CP NMR on lipid membranes was performed on frozen membranes, which allows efficient CP to occur. However, this is an inaccurate picture of real cell membranes which are in a "fluid" state. The two different states have different dynamic properties which are detectable by NMR. In either case CP can be used to detect natural abundance ^{13}C of membrane proteins and the membrane it is embedded in. A sample spectra studying GalP in native membranes is shown in Figure 2.14, showing how CP solid state NMR can detect the effects of ^{13}C labelled ligand (in this case glucose) binding to membrane embedded protein. This is possible since the nuclear spins of the ligand become restrained upon binding allowing cross-polarisation to occur. Free ligand is not restrained and will therefore not be detectable by solid-state NMR as cross-polarisation will be ineffective. This means solid-state NMR can be used to provide evidence of ligands binding to proteins.

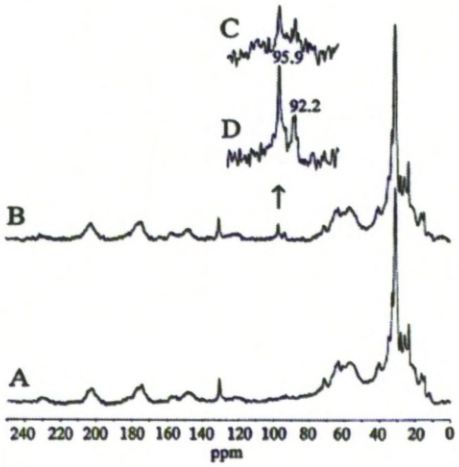

Figure 2.14. The effect of glucose on GalP in native cell membranes. All samples contain GalP in native membranes. Two full spectra containing 0.5 μmol GalP (A) then titrated D-[1-^{13}C]glucose (B) are shown. Expanded spectra (90-100 ppm) containing the minimum detectable 250 nmol of D-[1-^{13}C]glucose (C) and maximum detectable D-[1-^{13}C]glucose (D) are also shown. Figure taken from Spooner *et.al.*, 1994.

Chapter 3

3.1. Study of interactions of the cytoplasmic region of FXYD Proteins with membranes and the Na^+, K^+-ATPase

All seven FXYD proteins interact with the Na^+, K^+-ATPase (Beguin *et al.*, 1997; Pu *et al.*, 2001; Beguin *et al.*, 2002; Crambert *et al.*, 2002; Garty *et al.*, 2002; Crambert *et al.*, 2005; Arimochi *et al.*, 2007). As FXYD proteins are tissue-specifically expressed it is thought they alter activity of the Na^+, K^+-ATPase to suit the needs of the tissue (Crambert and Geering, 2003). This hypothesis has been supported by evidence showing that different FXYD proteins cause ion affinities in the Na^+, K^+-ATPase to change in different ways. For example the FXYD protein RIC (related to ion channel) increases affinity for Na^+ and/or K^+ ions in an $\alpha 1\beta 1$ complex but in the same complex FXYD6 slightly decreases apparent K^+ affinity and significantly decreases the apparent Na^+ affinity of the Na^+, K^+-ATPase (Lubarski *et al.*, 2005). The 35 amino acid signature sequence (Figure 1.5) of FXYD proteins incorporates the entire transmembrane region and a large part of the extracellular region. It is therefore unlikely the tissue specific features of FXYD proteins are found in this region. Therefore this chapter aims to look into the interaction of the Na^+, K^+-ATPase with the cytoplasmic region of FXYD proteins where there is the most variation in amino acid sequence in order to understand how FXYD proteins alter the ion affinity of the Na^+, K^+-ATPase to suit the needs of the tissue in which it is located. Two FXYD proteins were

selected for study. The first is phospholemman (PLM); its cytoplasmic region has been shown to interact with negatively charged membrane surfaces (Clayton *et al.*, 2005) and is subject to phosphorylation (discussed later) which may be crucial to the function of the cytoplasmic region. Mat-8 was also selected as it has a cytoplasmic region of a similar size but a very different sequence to PLM.

PLM has an arginine-rich cytoplasmic region giving it a net positive charge. A full length PLM structure has been solved by solution NMR in SDS micelles (Teriete *et al.*, 2007). This is shown in Figure 3.1. A micellar environment is not at all indicative of a biomembrane environment so the cytoplasmic region in this structure may not be an accurate representation of the cytoplasmic region in its natural phospholipid bilayer environment. Nevertheless, the structure shows the cytoplasmic region to consist of the continuation of the transmembrane helix connected to another helix (h4) via a relatively long linker region which would allow flexibility of h4.

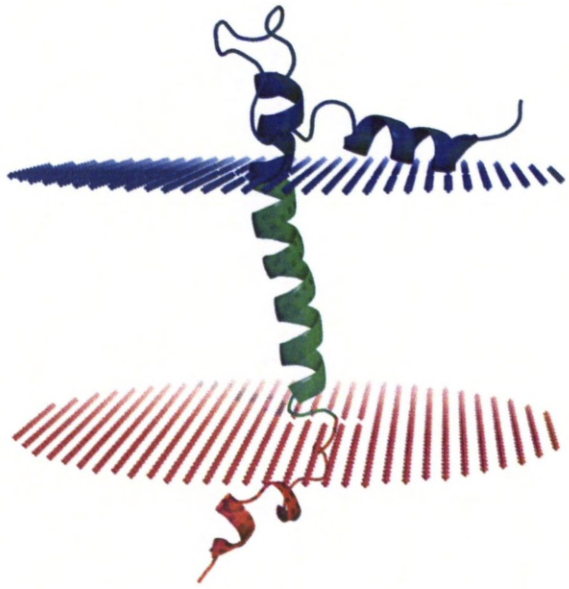

Figure 3.1. Structure of PLM solved in SDS micelles with predicted bilayer location. The structure of PLM was solved in SDS micelles (Teriete *et al.*, 2007) by solution NMR. The above structure (PDBID:2JO1) has the following colour scheme: cytoplasmic region (blue), transmembrane region (green) and extracellular region (red). The predicted membrane locations are indicated (downloaded from Orientations of Proteins in Membranes database (OPM).

The cytoplasmic region of PLM has been shown to be phosphorylated at four residues. These residues are highlighted in Figure 3.2. Protein kinase A (PKA) phosphorylates at Ser 68 whereas protein kinase C (PKC) phosphorylates at both Ser 63 and Ser 68 (Palmer *et al.*, 1991; Walaas *et al.*, 1994).

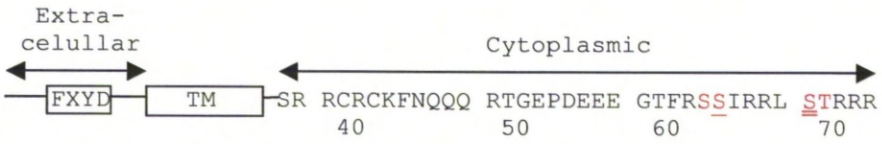

Figure 3.2. Sequence of the cytoplasmic region of Phospholemman. One letter amino acid codes of the cytoplasmic region of PLM are shown. Phosphorylation sites are highlighted in red. Both PKA and PKC phosphorylated Ser 68 (double underlined) whereas Ser 63 is only phosphorylated by PKC (single underlined). Location of the cytoplasmic region relative to the extracellar region (containing FXYD motif) and the transmembrane (TM) domain is indicated. Sequence is from human PLM.

PLM reduces V_{max} of the ATPase activity of the Na^+, K^+-ATPase, however this effect is reduced upon phosphorylation of PLM (Fuller *et al.*, 2009) by PKA. Voltage clamp experiments have revealed that phosphorylation of Ser 68 alone induces an increase of 31% in Na^+, K^+-ATPase current (Silverman *et al.*, 2005). Experiments on PLM knock out and wild type mice confirm this observation (Pavlovic *et al.*, 2007). Introduction of synthetic peptide representing the 19 C-terminal residues of PLM to these murine cells revealed unphosphorylated peptide reduced Na^+, K^+-ATPase activity whereas Ser 68 phosphorylated peptide increased Na^+, K^+-ATPase activity. As both PKA and PKC cause Ser 68 to be phosphorylated, PLM could have a role in two separate cell signalling pathways. NMR studies have shown that phosphorylation of Ser 68 causes the ^1H and ^{15}N chemical shifts in the helix of the cytoplasmic region (h4) to change, indicating a change in orientation of the cytoplasmic region independent of the rest of

the protein (Teriete *et al.*, 2009). With this observation, a model is proposed (Figure 3.3.), where the cytoplasmic region of PLM undergoes a conformational change upon phosphorylation of Ser 68. The non-phosphorylated orientation was modelled by removing the γ-subunit from the structure of the Na^+, K^+-ATPase from pig kidney ((Morth *et al.*, 2007) PDBID:3KDP) and replacing its co-ordinates with the structure of PLM solved in Na^+, K^+-ATPase-free SDS micelles (Teriete *et al.*, 2007). This allows the sidechains of h4 to interact with both the Na^+, K^+-ATPase and the cell membrane surface. The alternative conformation induced by Ser 68 phosphorylation models h4 moving to an alternative site above a negatively charged crevice in the transmembrane region which has been shown to alter ion affinity of the Na^+, K^+-ATPase when a single positive charge is added (Reyes and Gadsby, 2006). This could explain the mechanism by which phosphorylation modulates the inhibition of the Na^+, K^+-ATPase by PLM.

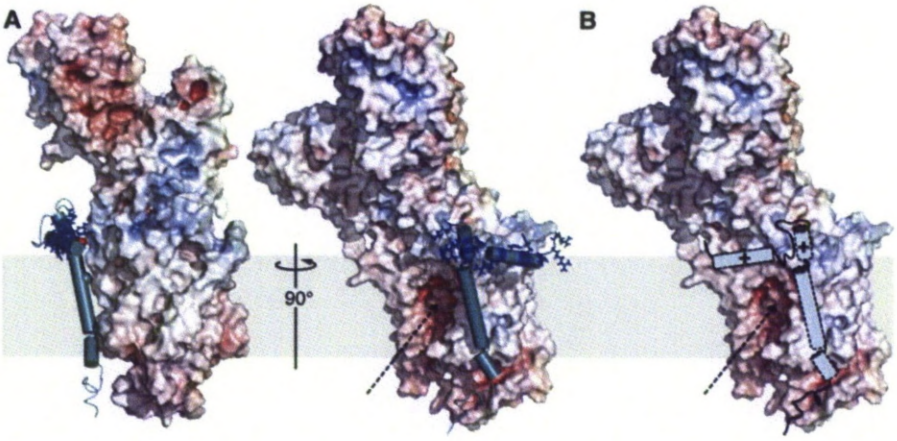

Figure 3.3. Model of PLM within the Na^+, K^+-ATPase complex showing the change in the cytoplasmic region following phosphorylation. (a) The pig kidney Na^+, K^+-ATPase structure with γ-subunit removed and replaced with PLM shown at two angles. (b) possible alternative orientation of PLM due to Ser 68 phosphorylation. Dotted arrow indicates negatively charged crevice of the Na^+, K^+-ATPase which leads to the ion binding pocket in the centre of the α-subunit. Figure taken from (Teriete *et al.*, 2009).

The cytoplasmic region of PLM not only affects Na^+, K^+-ATPase function but also binds to phospholipid bilayers with a preference for negative phospholipids (Clayton *et al.*, 2005). The same study also analysed peptides representing the cytoplasmic region of phospholamban (PLB_{1-23}), both in its phosphorylated and unphosphorylated form. Phospholamban shares similarities with PLM in that they are both small phosphoproteins with a single hydrophobic transmembrane span. Whilst PLM inhibits the Na^+, K^+-ATPase, phospholamban inhibits the related ATPase SERCA and this inhibition is relieved upon phosphorylation (Sasaki *et al.*, 1992). PLM phosphorylation may also result in the relief of inhibition of its binding

partner the Na^+, K^+-ATPase but this possibility is yet to be investigated. Residues 38-72 of PLM which encompass the cytoplasmic domain were therefore selected for study to further understand the significance of phosphorylation at Ser 68. This will be achieved by using synthetic peptides that contain the cytoplasmic sequence (Figure 3.2.) which will be referred to as PLM_{38-72} for the non-phosphorylated form and $pPLM_{38-72}$ where Ser 68 is phosphorylated. Phosphorylation of PLM is likely to play a role in the tissue specific effects of Na^+, K^+-ATPase since there is no experimental evidence demonstrating phosphorylation of any other mammalian FXYD proteins.

Mat-8 is a much less well understood member of the FXYD protein family. Although there is no evidence that it is a physiological phosphorylation substrate, it does have two isoforms unlike PLM (Bibert *et al.*, 2006). The two isoforms (called long form and short form) have identical extracellular and transmembrane regions but the long form contains an additional 26 amino acids in the cytoplasmic region (Figure 3.4.) The short form of Mat-8 decreases the apparent K^+ and Na^+ ion affinities of the Na^+, K^+-ATPase over a wide range of membrane potentials, whereas long form Mat-8 decreases the apparent K^+ affinity at slightly negative and positive membrane potentials and in complete contrast to short form Mat-8 slightly increases the apparent Na^+ affinity of the Na^+, K^+-ATPase (Bibert *et al.*, 2009). The balance of the two isoforms in the cell appears vital to

function as in human breast cancer cells the short form Mat-8 is overexpressed whereas long form Mat-8 levels remain normal (Yamamoto *et al.*, 2009).

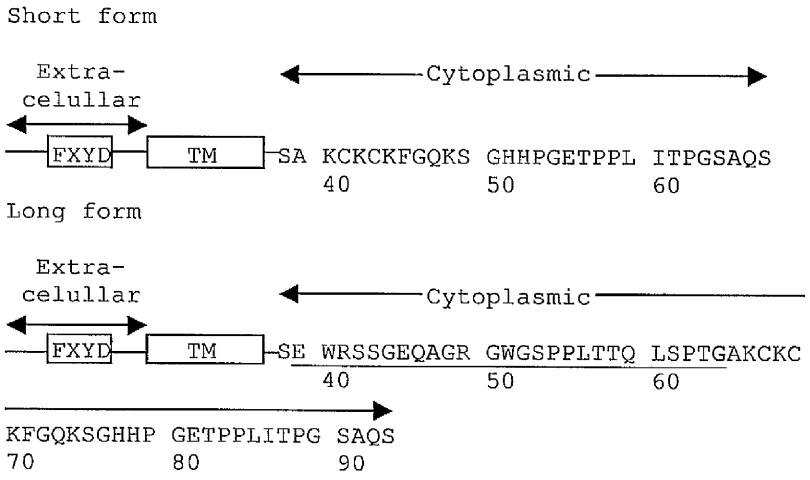

Figure 3.4. Cytoplasmic regions of both Mat-8 isoforms. Long form and short form Mat-8 have identical extracellular and transmembrane regions but the long form has an additional 26 amino acids in the cytoplasmic region (underlined). Location of the extracellular region (with FXYD domain), transmembrane region (TM) are shown.

As the cytoplasmic region contains the only difference between the two isoforms it seems likely that this region is key to their differential effects on the Na^+, K^+-ATPase. The cytoplasmic region of both isoforms of Mat-8 was therefore selected for study as to their effects on the activity of the Na^+, K^+-ATPase in order to further understand the differences between the two isoforms further. Like PLM this will be achieved using synthetic peptides designed to represent the sequence of the cytoplasmic

regions of both Mat-8 isoforms (Figure 3.4.) and will be referred to as Mat-8sf$_{38-67}$ for the short isoform and Mat-8lf$_{38-90}$ for the long isoform.

This chapter will look at how the cytoplasmic regions of PLM and both isoforms of Mat-8 interact with the Na^+, K^+-ATPase and cell membranes. There is evidence the cytoplasmic region of PLM regulates the Na^+, K^+-ATPase (Pavlovic *et al.*, 2007) and ^2H NMR has shown the cytoplasmic region of PLM also interacts with negatively charged phospholipid headgroups (Clayton *et al.*, 2005) but the two interactions are yet to be reconciled. To resolve how both of these interactions might occur *in vivo* several methods will be employed.

^2H NMR will be utilised to analyse Mat-8sf$_{38-67}$ and Mat-8lf$_{38-93}$ interacting with phospholipid bilayer surfaces. Another peptide CHIF$_{38-69}$ will also be studied; this is based on the cytoplasmic region of the FXYD protein CHIF. This was selected in order to compare results with the short isoform of Mat-8, with which it shares over 60% sequence identity (Figure 3.5.). The full structure of CHIF has also been solved in SDS micelles (Franzin *et al.*, 2007a). To confirm and quantify these interactions, isothermal titration calorimetry (ITC) will be used to measure enthalpy changes when phospholipid bilayers are titrated into the cytoplasmic peptides; PLM$_{38-72}$, p PLM$_{38-72}$, Mat-8sf$_{38-67}$, Mat-8lf$_{38-93}$ and CHIF$_{38-69}$. In all synthetic phospholipid based experiments in this

thesis either LMVs (large multilamellar vesicles) or SUVs (small unilamellar vesicles) are used. Figure 3.6. compares these two types of vesicles to detergent micelles which were used to solubilise PLM and CHIF to allow their structural determination by solution-state NMR. LMVs and SUVs are both composed of phospholipid bilayers, which mimic the phospholipid bilayer of the cell membrane whereas micelles are made of a monolayer and are therefore not representative of a cell membrane environment.

```
SG KCKCKSSQKQ-HSPVPEKAIPLITPGSATTC  CHIF
SA KCKCKFGQKSGHHP-GETP-PLITPGSAQS   Short form Mat-8
```

Figure 3.5. Alignment of the cytoplasmic regions of CHIF and short form Mat-8. Although the cytoplasmic region contains the most variation between FXYD proteins there is high similarity between Mat-8 short form and CHIF. Identical residues are highlighted in red.

Following determination of interactions of cytoplasmic peptides with membranes, evidence would need to be produced to confirm this interaction still occurs in membranes containing the Na^+, K^+-ATPase. A system would therefore need to be developed to remove the Na^+, K^+-ATPase from its native membrane and reconstitute it into synthetic membranes similar to ones used in ^2H NMR and ITC. With the Na^+, K^+-ATPase reconstituted into these membranes further studies can be

performed to confirm whether cytoplasmic peptides bind to cell membranes in the presence of the Na^+, K^+-ATPase.

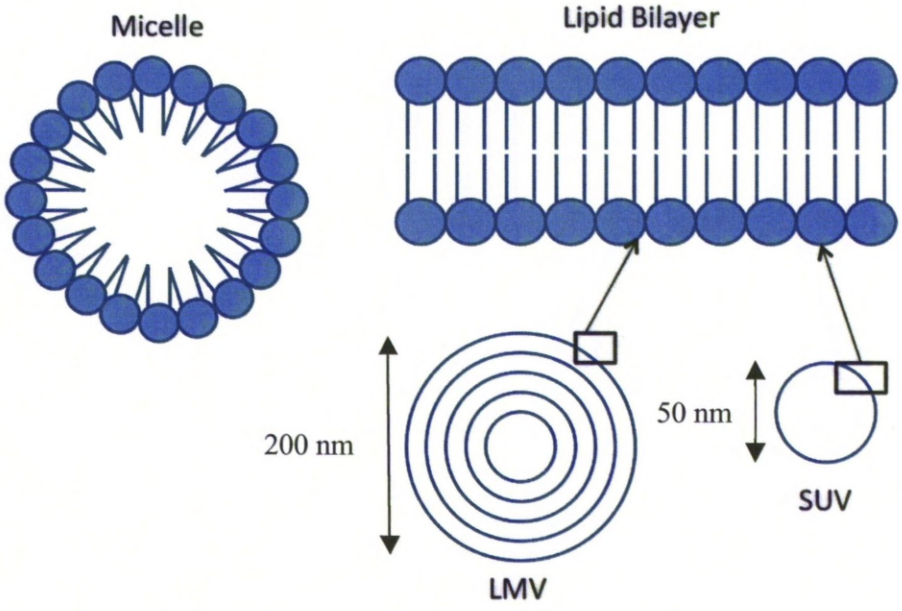

Figure 3.6. Model systems for cell membranes. When studying membrane proteins different systems are used to emulate cell membranes. Detergent micelles are often used as they can make proteins soluble however they are a monolayer unlike the phospholipid bilayer found in cell membranes. Liposomes are considered more representative of cell membranes as they consist of bilayers either single bilayers (small unilamellar vesicles (SUVs)) or multiple bilayers (large multilamellar vesicles (LMVs)).

The effect of cytoplasmic peptides on the activity of the Na^+, K^+-ATPase will also be determined using functional ATPase assays. As the cytoplasmic region of FXYD proteins is the most varied region it is possible it is responsible for the tissue-specific changes to Na^+, K^+-ATPase function. By establishing this the effect of $PLM_{38\text{-}72}$ on reconstituted Na^+,

K^+-ATPase could be analysed and compared to the effects seen in non-reconstituted Na^+, K^+-ATPase in order to explain why, and under what circumstances, PLM_{38-72} interacts with both the Na^+, K^+-ATPase and cell membranes.

3.2. Materials and Methods

3.2.1. Materials

Phospholipids were purchased from Avanti® Polar Lipids Inc. Peptides were purchased from Peptide Protein Research Ltd. and were designed to represent the cytoplasmic regions of PLM (Figure 3.1.), short form Mat-8 (Figure 3.2.) and CHIF (Figure 3.5.). Peptide designed to represent the cytoplasmic region of long form Mat-8 (Figure 3.2.) was purchased from GenicBio Biotechnology Ltd. Ascorbic acid supplied by J.T. Baker. Ammonium heptamolybdate tetrahydrate and trisodium citrate-dihydrate supplied by Merck. All other materials were supplied by Sigma.

3.2.2. Na^+, K^+-ATPase sample preparation

All Na^+, K^+-ATPase membranes were prepared from either pig kidney or spiny dogfish rectal gland by the group of Prof. Mikael Esmann at the University of Aarhus using previously described methods (Jørgensen, 1974; Esmann *et al.*, 1979). Final samples have a protein concentration of 5-6 mg ml^{-1} determined by the Lowry method (Lowry *et al.*, 1951) and a

protein to phospholipid concentration 100:1 determined by wet ashing method (Bartlett, 1959). Sample purity is revealed by SDS-PAGE to be approximately 70%.

3.2.3. Functional ATPase assays

ATP hydrolysis rates were measured using the method of Baginski (Baginski *et al.*, 1967). Reagent A was prepared on the day of experiment by dissolving 3 g of cold ascorbic acid in 100 mL of 0.5 M HCl. Cold 10% ammonium heptamolybdate solution (5 mL) was then added to this with stirring. Various NaCl concentrations were prepared in quadruplet at 10 fold desired final concentration and 50 μL of each were added to 350 μL of test solution (with final concentrations after addition of enzyme and peptide of 30 mM Histidine, 3 mM Na-ATP, 20 mM KCl, 4 mM $MgCl_2$, 0.33 mg mL^{-1} albumin). For each quadruplet, 50 μL of water or peptide was added to three samples and 50 μL of 1 mM ouabain was added to the fourth as a blank (ouabain completely inhibits Na^+, K^+-ATPase activity at this concentration). Samples were pre-heated at 37°C for 90 seconds and each reaction was initiated by addition of 50 μL of Na^+, K^+-ATPase membranes (0.5 μg ml^{-1} in 20 mM histidine and 25% glycerol. Samples were incubated at 37°C for precisely 15 minutes. Hydrolysis of ATP was halted with addition of 1 mL cold reagent A and left on ice. After at least 6 minutes 1.5 mL of 1:1 SDS: reagent AC (30 mM sodium-m-arsenite, 140

mM trisodium citrate-dihyrate, 4% acetic acid) were added and samples were returned to 37°C for 10 minutes. The absorbance of samples was read at 850 nm using water as a blank.

3.2.4. Preparation of Phospholipid Vesicles

Large multilamellar vesicles (LMVs) of DMPC-d_4/DOPG were prepared by first weighing 10 mg of total lipid composed of DMPC-d_4 and DOPG in a 2:1 molar ratio, and dissolving in the minimum volume of chloroform to give a clear solution. The chloroform solutions were dried to a film under nitrogen and high vacuum overnight. The lipid film was then resuspended in 50 μL of sample buffer containing 10 mM Tris and 1 mM EDTA at pH 7.4. The suspension was vortexed and subjected to five freeze–thaw cycles. Where appropriate, the peptide was added in 5 μL of sample buffer to attain a lipid:peptide molar ratio of 50:1 or 20:1, and the vortex, freeze-thaw process repeated.

Small unilamellar vesicles (SUVs) were prepared from 2:1 DMPC:DOPG, 2:1 DMPC/DOPC and 2:1 DMPC/DOPS (molar ratios). Lipids were prepared in chloroform and then dried under nitrogen and high vacuum, before resuspension in 10 mM Tris, pH 7, 1 mM EDTA, pH 7.4. Sonication was carried out for 2–3 min on ice, using a Dawe Ultrasonic

probe sonicator (London) at 50% duty cycle, output control 5, to promote formation of SUVs as described previously (Zhu *et al.*, 2003).

3.2.5. Wide ^{2}H NMR

Spectra were recorded on a Bruker Avance 400 MHz spectrometer operating at a frequency of 61.00 MHz for ^{2}H. Wide line ^{2}H NMR spectra of membranes containing DMPC-d_4 (1,2-dimyristoyl-*sn*-glycero-3-phosphocholine labelled with deuterium) were obtained using a double-tuned nonspinning probe head with fixed horizontal 5 mm coil. Spectra were recorded as a result of accumulating 10000–20000 transients with a 1 s recycle delay. The quadrupole echo sequence (90_x–τ–90_y–τ–acquisition) sequence (Davis *et al.*, 1976), was used with a 90° pulse length of 4 μs and delay τ of 22 μs. The experimental temperature was 30°C.

3.2.6. ^{31}P NMR

Spectra were recorded on a Bruker Avance 400 MHz spectrometer operating at a frequency of 62.12 MHz for ^{31}P. Magic-angle spinning (MAS) ^{31}P NMR spectra were recorded using a double tuned MAS probe with sample rotation rate of 4 kHz. The samples were contained within a 4 mm diameter zirconia rotor, and spectra were recorded after applying a single 4 μs 90° pulse at the frequency ^{31}P followed by 50 kHz proton decoupling during the acquisition period. Experiments were performed at maintained temperatures of 4 °C, 9 °C, 14 °C and 19 °C.

3.2.7. Isothermal Titration Calorimetry

Small unilamellar vesicles (SUVs) were produced as described in 3.2.4 at a 10 mM concentration. Heat flow resulting from peptide binding to SUVs was measured using the ultrasensitive iTC_{200} MicroCalorimeter (MicroCal LLC, Northampton, MA). Reaction cell volume and total injection volume were 200 and 40 µl. Experiments were performed at 25 °C, at a power reference setting of 6 µcal/s with stirring of 1000 rpm. Prior to use all solutions were degassed under vacuum. Data analysis was carried out using the Origin v.7 software (MicroCal). Experimental conditions were designed following established protocols (Oldenburg *et al.*, 1996; Joachim, 1997; Abraham *et al.*, 2005). The reaction cell contained a 100 µM solution of peptide (PLM_{38-72}, $pPLM_{38-72}$, Mat-$8sf_{38-67}$, Mat-$8lf_{38-93}$ or $CHIF_{38-69}$), in 10 mM Tris; 1 mM EDTA, pH 7.4. Lipid SUVs were injected via the syringe. Titrations were carried out at intervals up to 10 min in 0.5-2 µl aliquots following an initial discard aliquot of 0.3 µl. Each injection generates a heat of reaction, determined by integration of the individual peaks from the heat flow trace.

3.2.8. Reconstitution of the Na^+, K^+-ATPase in synthetic lipids

Lipid preparations of 100% DMPC, 100% DOPC and 2:1 molar ratio DMPC:DOPG were dissolved in 333 µL of reconstitution buffer (histidine 20 mM, 150 mM KCl, 4 mM $MgCl_2$, pH 7) and 667 µL $C_{12}E_8$ 150 mg/mL. This was sonicated in a water bath sonicator for 1.5 hours at 4°C. 3.6 mL

spiny dogfish enzyme (5.6 mg mL^{-1}) was added to 450 µL KCl 1.5 M/$MgCl_2$ 40 mM and 450 µL $C_{12}E_8$ 70 mg/mL. This mixture was centrifuged at 50000 rpm for 1 hour at 10 °C. 1.05 mL of the supernatant (solubilised enzyme/native membranes) was added to 0.630 mL histidine 20 mM/ KCl 150 mM/$MgCl_2$ 4 mM, pH 7 and 0.84 mL of sonicated lipid.

1106 mg of BioBeads were added to give a 12:1 ratio by weight of biobeads to $C_{12}E_8$. This mixture was incubated overnight in a cold room on a shaker. Membranes were removed from BioBeads with a pasteur pipette. Excess BioBeads were removed by passing the sample through an 8µm filter. Samples were put into ultracentrifuge bottles and topped up to 10 mL with histidine 20 mM/ KCl 150 mM/$MgCl_2$ 4mM, pH 7. The samples were centrifuged at 60,000 rpm for 1 hour at 10°C. The resulting pellets were homogenized in 0.84 mL histidine sucrose EDTA (HSE). This was performed in two 0.42 mL volumes the second being used as a rinse to minimise loss. The ATPase activity of the reconstituted Na^+, K^+-ATPase was tested with the Baginski method.

Control samples of Na^+, K^+-ATPase reconstituted into native membranes were produced by not adding any sonicated lipid after solubilising enzyme/native membranes with $C_{12}E_8$. The Na^+, K^+-ATPase was reconstituted back into the native membranes by using BioBeads as described for reconstitutions into synthetic membranes.

3.3. Results

3.3.1. The interaction of FXYD protein cytoplasmic domains with phospholipid bilayers.

3.3.1.1. Wide-Line ^{2}H NMR

The initial focus of this chapter is the interaction of the FXYD protein cytoplasmic domains with the Na^{+}, K^{+}-ATPase. The cytoplasmic regions of FXYD proteins are both water-soluble and in close proximity to phospholipid headgroups. Specific phospholipid headgroups may therefore influence the conformation of these cytoplasmic domains. Solid-state NMR is increasingly being utilised to understand the interactions of proteins with phospholipid headgroups (Franzin and Macdonald, 2001; Clayton *et al.*, 2005). Two principal methods for this are ^{2}H NMR and ^{31}P NMR. Wide-line ^{2}H NMR is a static technique which means magic angle spinning is not utilised and the anisotropic quadrupolar interactions that give rise to wide peaks are observed in the spectrum (Seelig and Macdonald, 1987). Lipid vesicles can be prepared using synthetic lipids into which ^{2}H is incorporated into sites on phospholipid headgroups. Phospholipids are carefully selected to produce an environment emulating cell membranes. This means having an overall slightly negative charge which would be contributed by negatively charged phospholipids like DOPG. Native membranes are also in a fluid state at body temperature; therefore synthetic membranes must consist of enough unsaturated phospholipids like DOPG (1,2-dioleoyl-*sn*-glycero-3-[phospho-*rac*-(1-

glycerol)), DOPC (1,2-dioleoyl-sn-glycero-3-phosphocholine) and DOPS (dioleoyl-sn-glycero-3-phospho-L-serine) so the bilayer is in a fluid state at experimental temperatures. DMPC (1,2-dimyristoyl-sn-glycero-3-phosphocholine) is zwitterionic and often mixed with negatively charged phospholipids to produce bilayers with similar features to native cell membranes. DMPC can also be labelled with deuterium at its phospholipid headgroup to produce DMPC-*d4*, which is frequently used in solid state NMR. The structure of these phospholipids and the locations of the ^{2}H labels are shown in Figure 3.7.

Glycerophospholipid general structure

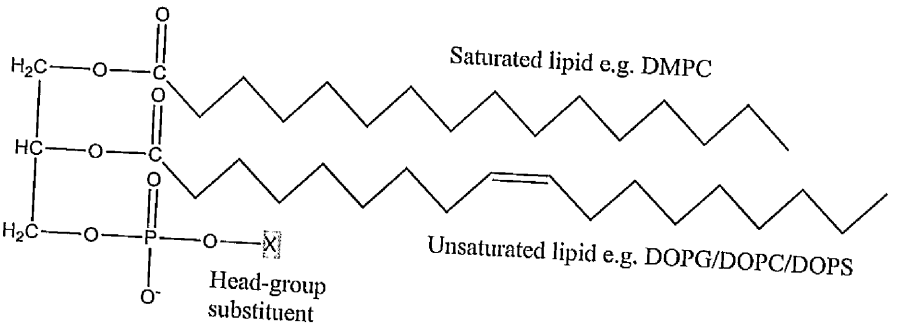

Formulae of head-group substituent (X)

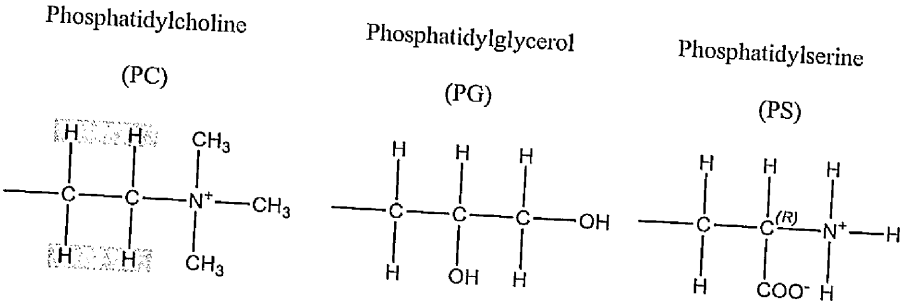

Figure 3.7. Chemical Structures of phospholipids used in this chapter. The general glycerophospholipid structure is shown highlighting the differences between the unsaturated and saturated fatty acid tails. Examples of head-group substituents (X) are also shown. Phosphatidylcholine the headgroup of DMPC and the ^{2}H sites for DMPC-*d4* which is used in ^{2}H NMR are highlighted in green.

The line shape of a DMPC-*d4* ^{2}H spectrum is particularly sensitive to changes in the orientation of the phospholipid headgroup due to perturbations caused by the interactions of proteins and peptides and is now a well established method for probing lipid/peptide interactions (Arêas *et al.*, 1997; Arêas *et al.*, 1998; Franzin and Macdonald, 2001). This

method has revealed that PLM_{38-72} associates with negatively charged phospholipid bilayers (Clayton *et al.*, 2005). These ^2H NMR experiments were repeated using peptides that represent the cytoplasmic regions of both Mat-8 isoforms; Mat-$8sf_{38-67}$ and and Mat-$8lf_{38-93}$. $pPLM_{38-72}$ was also tested to see the effect of Ser 68 phosphorylation on membrane affinity as well as $CHIF_{38-69}$ as a comparison to the homologous Mat-$8sf_{38-67}$ (Figure 3.5.)

The ^2H NMR spectra of 2:1 DMPC-*d4*:DOPG LMVs in the presence of PLM_{38-72} (Clayton *et al.*, 2005) and $pPLM_{38-72}$ (provided by personal communication with Dr. Eleri Hughes), are shown in Figure 3.8 with α and β splittings indicated. The LMVs contain a 33% negative charge which is about three times higher than those of cell membranes in nature (Akio, 1971). If the negative charge was as low as observed *in vivo* the small interaction would become undetectable. By using a higher concentration of negatively charged phospholipid the interaction can be measured. Although this is clearly not ideal, the phospholipid interaction of a cytoplasmic peptide is weaker in isolation and very different to a typical protein/protein interaction. Such interaction is made more likely due to the constant close proximity of the cytoplasmic regions and membrane surfaces *in vivo,* this helps validate the results since these residues are tethered in place by the transmembrane domain. When phospholipid headgroups are perturbed the α and β splittings will change.

Table 3.1. shows the changes in splitting values due to increased concentration of cytoplasmic peptides. Both PLM_{38-72} and $pPLM_{38-72}$ peptides appear to induce a change in splittings. There is approximately a 1 kHz decrease in α-splittings at a 50:1 ratio with a subsequent additional 0.5 kHz decrease at a 20:1 ratio. The β-splittings increase by approximately 1 kHz increase at a 50:1 ratio of lipid to PLM peptide with a further increase in β-splittings of approximately 200 Hz at 20:1 lipid to PLM peptide ratio.

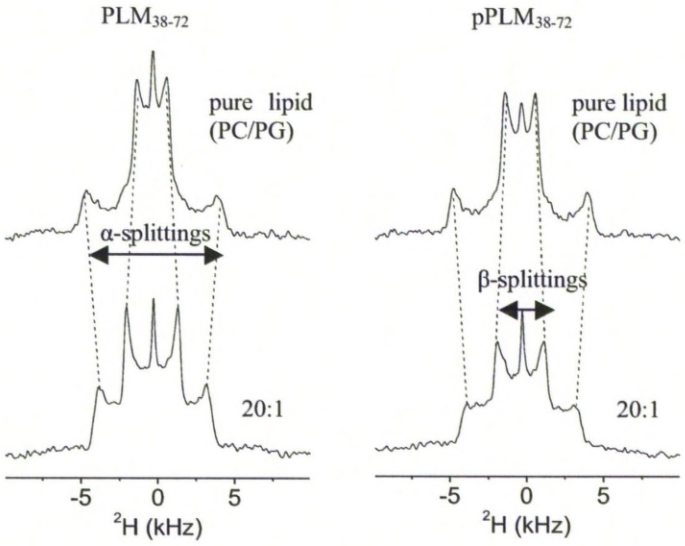

Figure 3.8. ^{2}H NMR showing the effect of PLM_{38-72} and $pPLM_{38-72}$ on phospholipid bilayers. Wide line ^{2}H NMR spectra of membranes containing DMPC-d_4 and DOPG in a 2:1 molar ratio (5 mg total lipid) alone and in the presence of PLM_{38-72} and $pPLM_{38-72}$ in a lipid to peptide molar ratio of 20:1. The quadrupole splittings for the deuterons at the α- and β-choline positions of DMPC-d_4 are denoted by the separation between the pairs of dotted lines. The spectra were obtained at 30 °C and are the result of accumulating 8000 scans. Figure taken from Clayton *et al.*, 2005.

Further ^{2}H NMR experiments were performed on DMPC-*d4*:DOPG LMVs in the presence of Mat-8sf$_{38-67}$, Mat-8lf$_{38-93}$ or CHIF$_{38-69}$ (Figure 3.9.). Mat-8sf$_{38-67}$ has a smaller effect than the PLM peptides with an approximate 1 kHz decrease in α-splittings and approximately 300 Hz increase in β-splittings at the 20:1 lipid to peptide ratio. At a 50:1 lipid to Mat-8sf$_{38-67}$ ratio there is a very small change in splittings suggesting a much larger quantity of Mat-8sf$_{38-67}$ is required to make any appreciable change to the splittings in ^{2}H NMR spectra than the PLM peptides. Both Mat-8lf$_{38-93}$ and CHIF$_{38-69}$ have only small changes in α and β splittings of approximately 100-500 Hz at the 20:1 lipid to peptide ratio. The Mat-8lf$_{38-93}$ spectra required double the number of scans to achieve the signal to noise seen in Figure 3.9. which is not as good as the spectra for other peptides. Ideally this would be repeated but as the process requires several milligrams of expensive peptide it was not possible.

In ^{2}H NMR a change in splittings indicates an interaction of peptide with the phospholipid surface by perturbation of the orientation of the choline headgroup. These data suggest that PLM$_{38-72}$ and pPLM$_{38-72}$ have the strongest interaction with negatively charged phospholipid bilayers whilst Mat-8sf$_{38-67}$ also interacts with phospholipid bilayers albeit to a smaller extent. CHIF$_{38-69}$ seems to have little effect on negatively charged phospholipid bilayers. The quality of data for Mat-8lf$_{38-93}$ is not good enough to draw any definite conclusions. These spectra may only detect

variations in the structures or orientations of the peptides at the membrane surface, which perturb the phospholipid headgroup in some way. This means ^{2}H NMR alone cannot quantify interactions between peptides and phospholipid membrane surfaces.

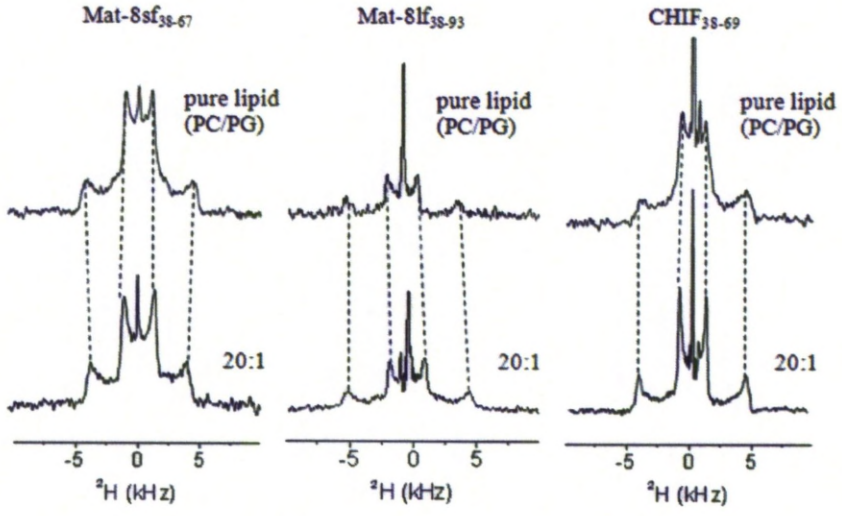

Figure 3.9. ^{2}H NMR showing the effect of Mat-8sf$_{38-67}$, Mat-8lf$_{38-93}$ and CHIF$_{38-69}$ on phospholipid bilayers. Wide line ^{2}H NMR spectra of membranes containing DMPC-d_4 and DOPG in a 2:1 molar ratio (5 mg total lipid) alone and in the presence of Mat-8sf$_{38-67}$, Mat-8lf$_{38-93}$ and CHIF$_{38-69}$ in a lipid to peptide molar ratio of 20:1. The spectra were obtained at 30 °C and are the result of accumulating 8000-16000 scans.

Table 3.1. α and β splittings in ^{2}H NMR spectra of 2:1 DMPC-*d4*:DOPG at various lipid:cytoplasmic peptide concentrations. All values given in Hz.

	$\Delta\nu_Q\alpha$ (Hz)			$\Delta\nu_Q\beta$ (Hz)		
Peptide	Lipid only	50:1	20:1	Lipid only	50:1	20:1
PLM_{38-72}	8559	7608	6951	2002	3179	3377
$pPLM_{38-72}$	8667	7674	6958	2009	2674	3073
Mat-$8sf_{38-67}$	8661	8639	7862	2121	2236	2499
Mat-$8lf_{38-93}$	9165	9000	8859	2478	2500	2536
$CHIF_{38-69}$	8690	8962	8793	2108	2178	1864

3.3.1.2. Isothermal Titration Calorimetry

As ^{2}H NMR is only indicative of an interaction between peptides and phospholipid headgroups, ITC was performed to quantify any potential binding that is occurring. ITC can measure thermodynamic properties of a biological interaction such as peptide binding to phospholipid. These thermodynamic properties include binding affinity (K_a) and enthalpy changes (ΔH). The liposomes selected were SUVs as they do not sediment unlike LMVs. Sedimentation would interfere with the recording of enthalpy changes by ITC. 2:1 molar ratio DMPC:DOPG SUVs (overall negative charge) were investigated for direct comparison to the ^{2}H NMR data. 2:1 molar ratio DMPC:DOPC SUVs (zwitterionic) were also investigated as they have identical hydrocarbon chains to 2:1 DMPC:DOPG but have a different net headgroup charge. At the outset of the project, work had already been carried out measuring binding affinities

of both PLM_{38-72} and $pPLM_{38-72}$ for 2:1 DMPC:DOPG and DMPC:DOPC SUVs by ITC by Dr. Eleri Hughes (Figure 3.10) who reported effective affinity constants (K_a) for PLM_{38-72} and $pPLM_{38-72}$ of 3.07×10^{-6} M^{-1} and 2.70×10^{-4} M^{-1} respectively (Table 3.2.), but no appreciable binding in DMPC:DOPC. Although the affinity constant is higher in PLM_{38-72} than $pPLM_{38-72}$ there is a wider spread of points in the former, making it more difficult to fit the data. That said the difference is relatively large suggesting that Ser 68 phosphorylation reduces the affinity for negatively charged membranes by reducing the electrostatic potential of the peptide as it introduces a negative charge or by altering the structure of the peptide.

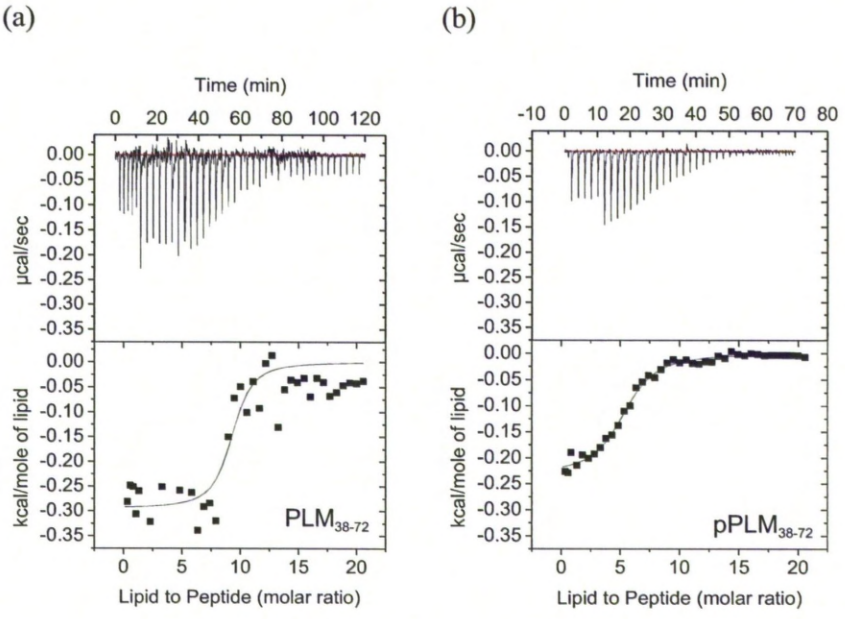

Figure 3.10. Affinity of PLM_{38-72} (a) and $pPLM_{38-72}$ (b) for 2:1 DMPC/DOPG membranes. ITC binding curve for lipid vesicles (25 to 50 µM lipid per injection) titrated into 100 µM PLM_{38-72}. Curves were generated by integrating the raw enthalpic data and fitted by the MicroCal 'one set of sites' function (black line). Experimental temperature 25°C. Data provided by personal communication with Dr. Eleri Hughes.

To compare the other peptides to PLM the same SUVs of DMPC:DOPG and DMPC:DOPC were titrated into Mat-$8sf_{38-67}$ (Figure 3.11.), Mat-$8lf_{38-93}$ (Figure 3.12.) and $CHIF_{38-69}$ (Figure 3.13.). The values for K_a and ΔH are shown in Table 3.2. Although none of these peptides had as strong binding as PLM_{38-72} in DMPC:DOPG, Mat-$8lf_{38-93}$ still had an effective affinity constant that was considerably higher than the affinity constant of Mat-$8sf_{38-67}$ suggesting the extra 26 amino acids in the long isoform of Mat-8 have a role in membrane binding. Although binding

affinity is very small in Mat-8sf$_{38-67}$ it is clearly higher than CHIF$_{38-69}$ which effectively shows no binding at all with negatively charged phospholipids. Interestingly with the exception of an additional single histidine residue in Mat-8sf$_{38-67}$ these two peptides share the same charged amino acids (Figure 3.5.). This suggests that any lipid/peptide interactions involve more than simply electrostatic potential. The observations agree with the ^{2}H NMR data for DMPC:DOPG as PLM$_{38-72}$ showed the largest changes in α and β splittings as well as the largest affinity constant. Mat-8sf$_{38-67}$ showed a relatively small change in α and β splittings and relatively small binding affinity constant whilst CHIF$_{38-69}$ had a negligible effect on α and β splittings and had no effective affinity constant. Although peptides showed varied levels of binding to the negatively charged DMPC:DOPG, binding levels were effectively zero in DMPC:DOPC. DMPC:DOPG and DMPC:DOPC have identical hydrocarbon chains but has a zwitterionic surface. This suggests that electrostatic potential plays the major role in phospholipid binding but is not the only factor.

(A) DMPC:DOPG (B) DMPC:DOPC

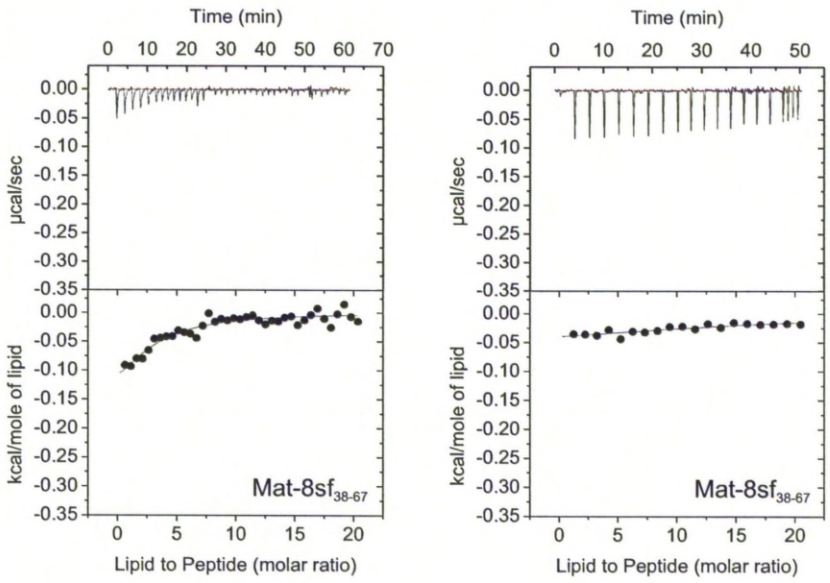

Figure 3.11. Affinity of Mat-8sf$_{38-67}$ for 2:1 DMPC:DOPG (A) and 2:1 DMPC:DOPC (B) membranes. ITC binding curve for 100 µM Mat-8sf$_{38-67}$ titrated with lipid vesicles (25 to 50 µM lipid per injection). Curves were generated by integrating the raw enthalpic data and fitted by the MicroCal 'one set of sites' function (black line). Experimental temperature 25°C.

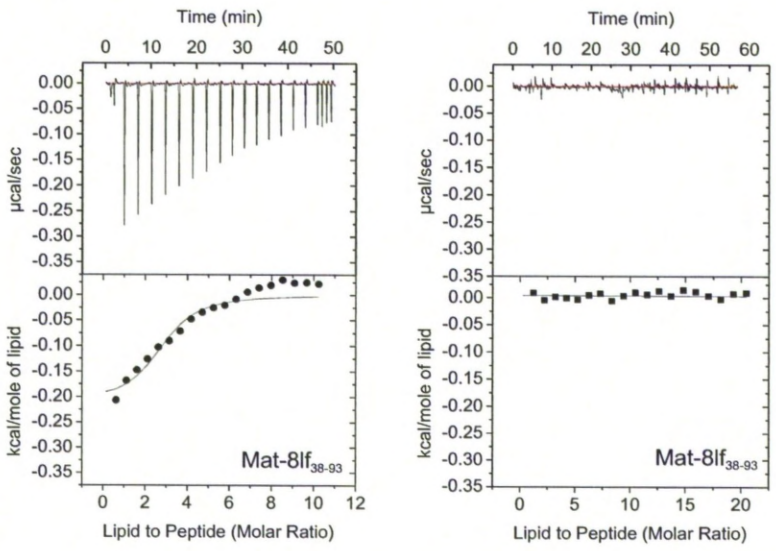

Figure 3.12. Affinity of Mat-8lf$_{38-93}$ for 2:1 DMPC:DOPG (A) and 2:1 DMPC:DOPC (B) membranes. ITC binding curve for 100 µM Mat-8lf$_{38-93}$ titrated with lipid vesicles (25 to 50 µM lipid per injection). Curves were generated by integrating the raw enthalpic data and fitted by the MicroCal 'one set of sites' function (black line). Experimental temperature 25°C.

(A) DMPC:DOPG (B) DMPC:DOPC

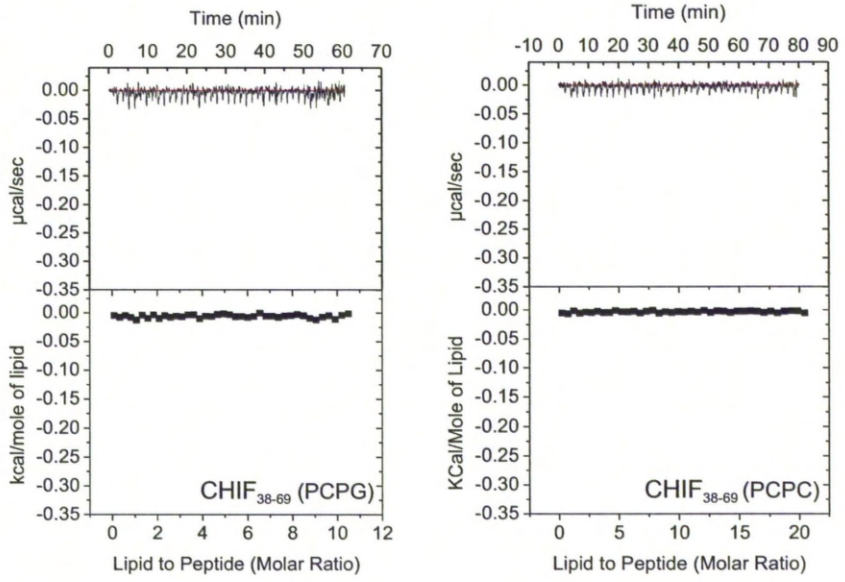

Figure 3.13. Affinity of $CHIF_{38-69}$ for 2:1 DMPC:DOPG (A) and 2:1 DMPC:DOPC (B) membranes. ITC binding curve for 100 µM $CHIF_{38-69}$ titrated with lipid vesicles (25 to 50 µM lipid per injection). Curves were generated by integrating the raw enthalpic data and fitted by the MicroCal 'one set of sites' function (black line). Experimental temperature 25˚C.

Table 3.2. Thermodynamic data for DMPC:DOPG and DMPC:DOPC titrated into cytoplasmic peptides. Standard errors are given in brackets. The values for both PLM_{38-72} and $pPLM_{38-72}$ were provided by personal communication with Dr. Eleri Hughes. The data for PLM_{38-72} and $pPLM_{38-72}$ in DMPC:DOPC membranes is not shown but showed no binding.

	K_a (M^{-1})		ΔH (cal/mol)	
Peptide	PC:PG	PC:PC	PC:PG	PC:PC
PLM_{38-72}	3.07×10^{-6} (1.26×10^{-5})	--	-211.9 (29.05)	--
$pPLM_{38-72}$	2.70×10^{-4} (3.55×10^{-3})	--	-232.4 (4.924)	--
Mat-$8sf_{38-67}$	3.07×10^{-3} (1.37×10^{-3})	3.43×10^{-3} 2.22×10^{-3}	-243.4 (143.5)	-107.8 (40.67)
Mat-$8lf_{38-93}$	3.276×10^{-4} (1.92×10^{-4})	0.0357 (4.93)	-211.9 (29.05)	1.771×10^{-5} (7.720×10^{-9})
$CHIF_{38-69}$	0.0147 (39.4)	0.930 (4.53×10^{-3})	-7.292×10^{-4} (1.304×10^{-9})	-7.811×10^{-4} (5.452×10^{-9})

In the ITC experiments presented so far DOPG was used as the negatively charged phospholipid. DOPG is a bacterial phospholipid and the peptides used are representing mammalian (human) proteins. Further experiments were performed using the negatively charged mammalian phospholipid DOPS in place of DOPG (i.e. 2:1 molar ratio DMPC:DOPS SUVs) to confirm the relatively strong interactions observed in PLM_{38-72} and Mat-$8lf_{38-93}$ with negatively charged phospholipids. Results are indicative

of an interaction between the cytoplasmic region of PLM and long form Mat-8 with cell membranes as shown in Figure 3.14. The binding affinities (shown in Table 3.3.) are actually stronger than those observed for both peptides in DMPC:DOPG which suggests PLM_{38-72} and Mat-$8lf_{39-93}$ are sensitive to the chemical structure of the phospholipid head-groups and the acyl chains as well as surface charge.

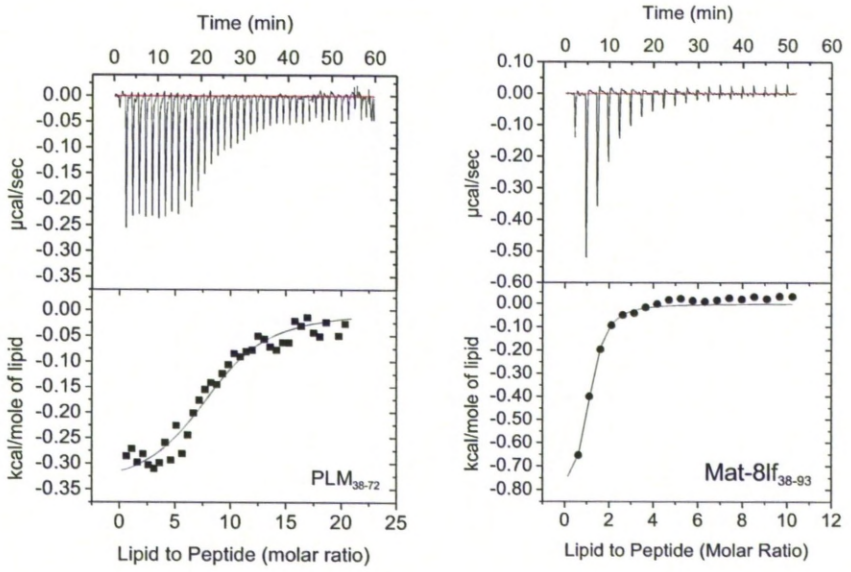

Figure 3.14 Affinity of PLM_{38-72} and of Mat-$8lf_{38-90}$ for 2:1 DMPC/DOPS membranes. ITC binding curves for both 100 µM PLM_{38-72} and 100µM Mat-$8lf_{38-93}$. titrated with lipid vesicles (25 to 50 µM lipid per injection). Curves were generated by integrating the raw enthalpic data and fitted by the MicroCal 'one set of sites' function (black line). Experimental temperature 25°C. PLM_{38-72} data provided by personal communication with Dr. Eleri Hughes.

Table 3.3. Thermodynamic data of DMPC:DOPS titrated into PLM_{38-72} and Mat-$8lf_{38-93}$. Standard errors are given in brackets. The values for PLM_{38-72} were provided by personal communication with Dr. Eleri Hughes.

Peptide	K_a (M^{-1})	ΔH (cal/mol)
PLM_{38-72}	3.67×10^{-6}	-350.3 (18.25)
	(2.13×10^{-6})	
Mat-$8lf_{38-93}$	6.62×10^{-4}	-874.8 (88.98)
	2.07×10^{-4}	

The overall charge in all peptides is actually relatively similar, when taking into account positive arginine, histidine and lysine residues compared to negatively charged glutamate and aspartate residues. The net charges of PLM_{38-72}, Mat-$8sf_{38-67}$, Mat-$8lf_{38-93}$ and $CHIF_{38-69}$ are +6, +5, +5 and +4 respectively. This suggests that charge likely plays a significant role in lipid binding but structure is also important. For example PLM_{38-72} has an arginine rich C-terminus which contains the Ser 68 phosphorylation site. This could suggest that this region rather than the rest of the cytoplasmic region is crucial for binding negatively charged phospholipids. The 26 amino acids present in long form Mat-8 but not short form Mat-8 have no net change in charge but do contain two arginine residues near the N-terminus which would be predicted to be close to the cell membrane. This proximity could explain why it has a much higher affinity for cell

membranes, than the short isoform. It is important to note that although the ^{2}H NMR has shown different degrees of interactions between cytoplasmic FXYD peptides and negatively charged but not zwitterionic phospholipids, this is determined in pure lipid, in the absence of the Na^{+}, K^{+}-ATPase. This means it is unclear if these peptides are capable of similar phospholipid interactions in the presence of their physiological target.

3.3.1.3. ^{31}P MAS NMR

To analyse the effects of peptides on phospholipid membranes in the presence of the Na^{+}, K^{+}-ATPase, the protein needed to be incorporated into well defined phospholipid bilayers. Ideally this would be carried out in the same membrane types as the ^{2}H NMR and ITC experiments for direct comparison. The Na^{+}, K^{+}-ATPase was reconstituted into 2:1 DMPC DOPG at 50:1, 100:1 and 200:1 lipid to protein ratios. 100:1 is the native lipid to protein ratio. All three reconstituted samples were analysed by ^{31}P MAS solid-state NMR and titrated with PLM_{38-72} at 50:1 and 20:1 lipid to peptide molar ratios. At a 50:1 lipid to protein ratio a 33:1 lipid to peptide ratio titration was also performed. This method was selected in preference to ^{2}H NMR as it is more sensitive to PLM_{38-72} (Clayton *et al.*, 2005) and therefore requires smaller samples. ITC is unsuitable as the Na^{+}, K^{+}-ATPase is insoluble. Each experiment was run at temperatures of 4°C, 9°C, 14°C and 19°C. By using MAS, the chemical shift of DMPC and DOPG

can be assigned separately. For each spectra the peaks for DMPC and DOPG were analysed using Origin 8.5 using a Lorentzian peak function (Figure 3.15.). This allowed the chemical shift change and broadening of each peak after addition of peptide to be determined. Figures 3.16-3.18. show the change in chemical shift frequency following addition of PLM_{38-72} and the relative peak intensity after each titration of peptide compared to lipid alone. All of the data presented are for measurements made at 19°C and 4°C but findings at other temperatures are very similar. At 19°C DMPC, DOPG and DOPC are all in their liquid phase whereas at 4°C, DMPC is in a gel phase and DOPC and DOPG are in a liquid phase. In the previous ^{31}P MAS solid state NMR on Na^+, K^+-ATPase-free lipid vesicles the DOPG peak remains relatively narrow whilst the peak for DMPC broadens markedly, which suggests PLM_{38-72} impairs mobility of DMPC (Clayton *et al.*, 2005). If similar results are observed here the mobility of DMPC will be impaired by PLM_{38-72} at 19°C but will have no effect at 4°C as it is in its gel phase and already restrained. At all three lipid to protein ratios there is no significant change in chemical shift frequency. However there is a broadening effect due to peptide observed on both DMPC and DOPG. This is likely due to the different phospholipid environments as the nature of the membranes presented here is unclear whereas in the published data peptide is titrated into LMVs. LMVs are comprised of multiple bilayers which means a high local concentration of peptide could occur in the interbilayer space resulting in a larger effect than would be seen on a

single bilayer. In the ^{31}P data presented here, PLM_{38-72} impairs the mobility of both DMPC and DOPG to a small extent as there is a small non-selective peak broadening for both phospholipids suggesting a slight interaction with the membrane surface. Importantly, this effect is reduced with increased Na^+, K^+-ATPase levels. This is the first evidence of PLM_{38-72} binding to phospholipid bilayers in the presence of the Na^+, K^+-ATPase.

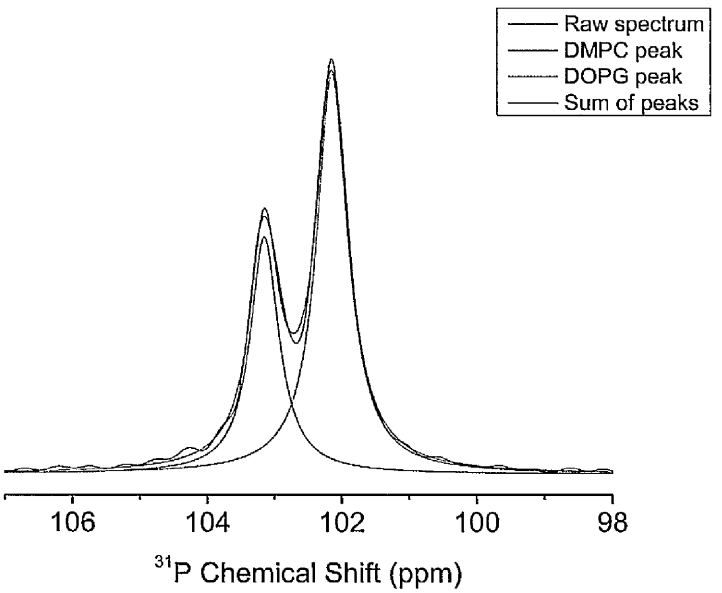

Figure 3.15. Example of ^{31}P NMR spectra. DMPC and DOPG give separate chemical shifts at approximately 102 and 103 ppm respectively. Data have been analysed using a Lorentz function and the calculated overlapping peaks are shown. This example spectrum was performed at 19°C in the absence of PLM peptide.

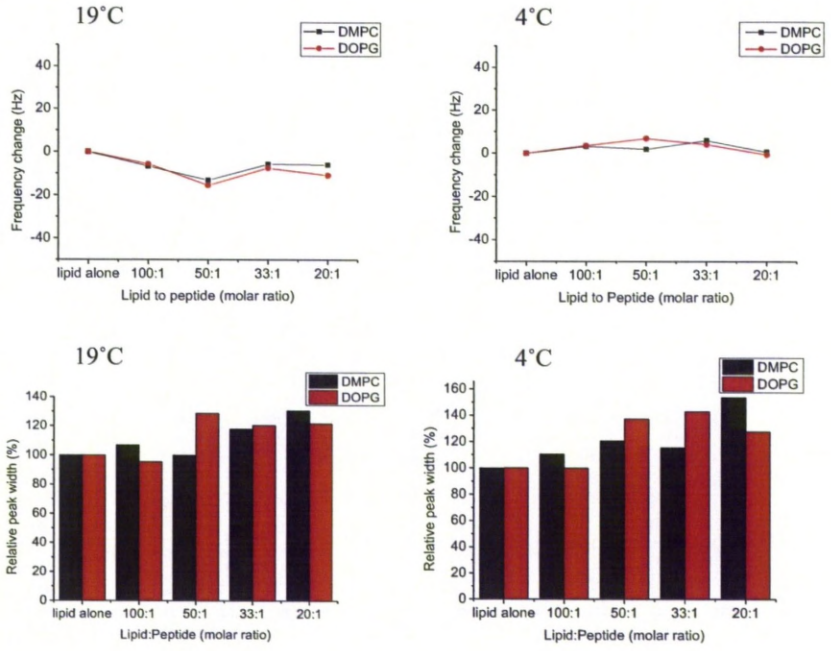

Figure 3.16. Effect of PLM_{38-72} on chemical shift and peak width of DMPC and DOPG. Chemical shift calculated as a frequency change from the peptide-free chemical shift. Peak width relative to peptide-free reconstituted Na^+, K^+-ATPase protein. Lipid to protein ratio is 50:1 and experimental temperature is 19°C and 4°C as indicated.

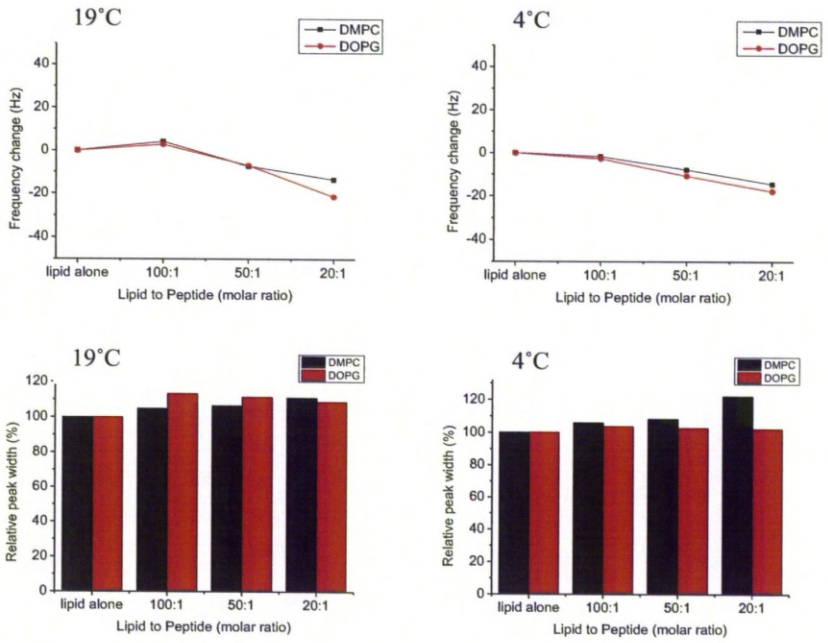

Figure 3.17. Effect of PLM_{38-72} on chemical shift and peak width of DMPC and DOPG in absence of peptide. Lipid to protein ratio is 100:1 and experimental temperature is 19°C and 4°C as indicated. Experimental parameters described in Figure 3.16.

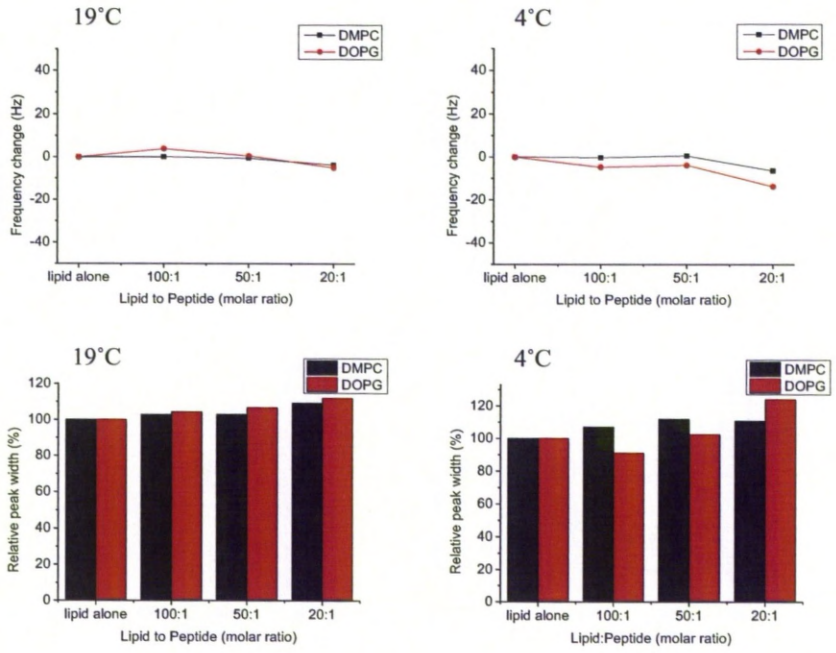

Figure 3.18. Effect of PLM_{38-72} on chemical shift and peak width of DMPC and DOPG in absence of peptide. Lipid to protein ratio is 200:1 and experimental temperature is 19°C and 4°C as indicated. Experimental parameters described in Figure 3.16.

3.3.1.4. Interaction of FXYD protein cytoplasmic domains with the Na^+, K^+-ATPase.

FXYD proteins have different effects on ion affinities of the Na^+, K^+-ATPase as discussed earlier. It is hypothesised that the specific effect of each FXYD protein is largely due to the actions of the cytoplasmic region as this is where the FXYD proteins are most sequentially diverse. The functional effect of the cytoplasmic peptides; PLM_{38-72}, $pPLM_{38-72}$, Mat-$8sf_{38-67}$, Mat-$8lf_{38-93}$ and $CHIF_{38-69}$ was determined by following the Na^+ activation of ATP hydrolysis with and without peptide. This ATPase assay was selected as it is a well established system for determining kinetic data like V_{max} and $K_{0.5}$ for the Na^+, K^+-ATPase (Esmann, 1988). Figures 3.19-20. show the Na^+ activation curves of pig kidney Na^+, K^+-ATPase with and without 100 μM cytoplasmic peptide. It is important to note that the Na^+, K^+-ATPase samples used were from pig kidney membranes and therefore contain the FXYD protein γ-subunit in the protein complex. As the γ-subunit has no predicted cytoplasmic region the peptides representing the cytoplasmic domains of other FXYD proteins used in these assays are free to interact with the entire cytoplasmic region of the Na^+, K^+-ATPase.

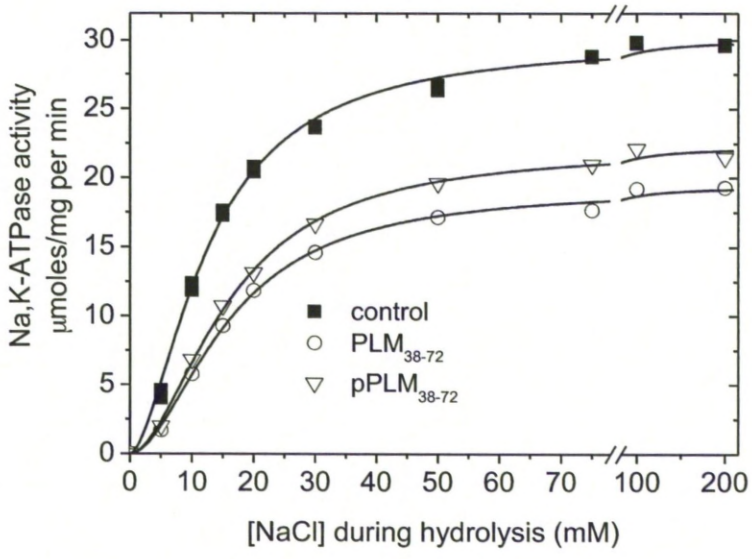

Figure 3.19. Na^+ activation curve of Na^+, K^+-ATPase in pig kidney membranes with and without $PLM_{38-72}$and $pPLM_{38-72}$. Kidney Na^+, K^+-ATPase activity was determined at the indicated concentrations of Na^+ with and without 100 µM PLM_{38-72} and $pPLM_{38-72}$ and data fit with a Hill function. Experiments performed in triplicate at 37°C. This assay was performed by Angelina Damgaard at the University of Aarhus.

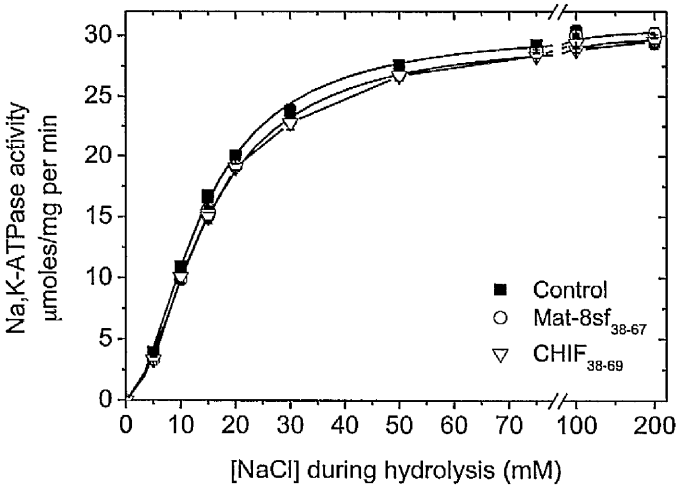

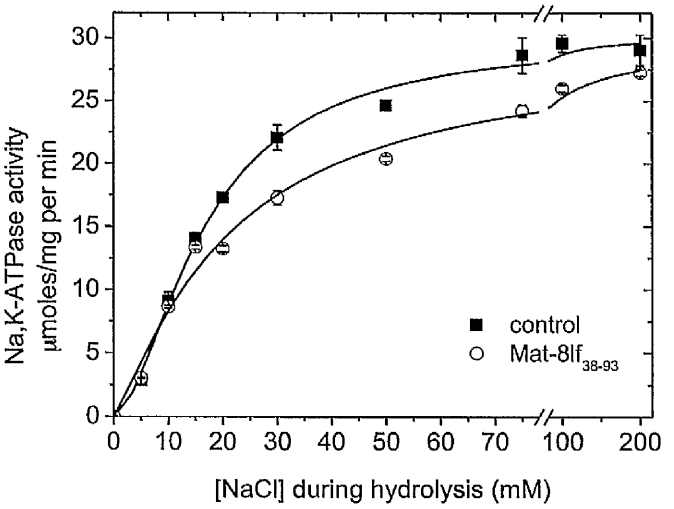

Figure 3.20. Na^+ activation curves of Na^+, K^+-ATPase with and without Mat-8sf$_{38-67}$, CHIF$_{38-69}$ and Mat-8lf$_{38-93}$ in pig kidney membranes. Kidney Na^+, K^+-ATPase activity was determined at the indicated concentrations of Na^+ with and without 100 µM Mat-8sf$_{38-67}$and CHIF$_{38-69}$ (top graph) and Mat-8lf$_{38-93}$ (bottom graph) and data fit with a Hill function. Error bars indicate standard error. Experiments performed in triplicate at 37°C. These assays were performed by Angelina Damgaard at the University of Aarhus.

Table 3.4. shows the apparent V_{max} and $K_{0.5}$ values calculated from these activation curves using the following Hill equation:

$$V = V_{max} \times \frac{[Na^+]^n}{K_{0.5}n + [Na^+]^n} \quad (4.1.)$$

The Mat-8sf$_{38-67}$ and CHIF$_{38-69}$ peptides appear to have no effect on either V_{max} or $K_{0.5}$ which suggests that the inhibitory effects of full length short form Mat-8 and CHIF are due to the transmembrane region (Garty *et al.*, 2002; Crambert *et al.*, 2005). PLM$_{38-72}$ has the largest effect on the activity of the Na^+, K^+-ATPase as it reduces apparent V_{max} by approximately 40% and increases $K_{0.5}$ by approximately 15%. This effect is reduced by phosphorylation as pPLM$_{38-72}$ only reduces apparent V_{max} by 20% and increases $K_{0.5}$ by the same factor as PLM$_{38-72}$. This suggests phosphorylation of PLM partially relieves the inhibition of the Na^+, K^+-ATPase by the cytoplasmic region of PLM. Mat-8lf$_{38-93}$ has no effect on V_{max} but causes an approximate 40% increase in $K_{0.5}$.This highlights a significant difference between the Mat-8 isoforms with the long isoform of Mat-8 having a larger inhibitory effect on the Na^+, K^+-ATPase than the short form. These data suggest that the functional differences between the two isoforms are due specifically to the differences in their cytoplasmic domains.

Table 3.4. Apparent V_{max} and $K_{0.5}$ values for pig kidney Na^+, K^+-ATPase with and without 100 μM cytoplasmic peptide. Standard errors are indicated in brackets.

Parameter	*Treatment*					
	Control	PLM_{38-72}	$pPLM_{38-72}$	Mat-$8sf_{38-67}$	Mat-$8lf_{38-93}$	$CHIF_{38-69}$
V_{max}	30.0 (1.8)	17.7 (3.0)	23.7(1.2)	30.2 (1.5)	29.3 (1.8)	29.6 (1.2)
$K_{0.5}$	13.5 (0.41)	15.9 (0.47)	16.0(0.46)	13.3 (0.32)	21.7 (3.1)	13.4 (0.36)

As the ^{31}P NMR experiments revealed that the cytoplasmic peptide of PLM can bind phospholipids in the presence Na^+, K^+-ATPase, further insight on how this might affect the ATPase activity was investigated by performing further ATPase assays in Na^+, K^+-ATPase reconstituted into different phospholipids.

Reconstitution of the Na^+, K^+-ATPase into synthetic membranes is well known to result in partial loss of function. For example, Na^+, K^+-ATPase reconstituted into DOPC membranes results in just 40-60% of original pump activity (Alpes *et al.*, 1988). The best reported recovery of activity is 80%, achieved in 1:1 molar ratio of dipalmitoylphosphatidylcholine: dipalmitoylphosphatidylethnnolamine (DPPC:DPPE), improved further to 86% in the presence of 55% cholesterol (Santos *et al.*, 2005). DPPC and DPPE are both zwitterionic so despite being the best known system for Na^+, K^+-ATPase activity recovery, no interaction with any of the FXYD protein cytoplasmic peptides would be expected. An alternative composition of reconstitution phospholipids therefore had to be

determined. Pig kidney Na^+, K^+-ATPase was reconstituted into DOPC alone (as had been performed recently (Hansen *et al.*, 2011)), 2:1 molar ratio DMPC:DOPG (for direct comparison to the experiments so far) and DMPC alone (as a control as Na^+, K^+-ATPase should lose activity as it is a saturated phospholipid). As a further control, solubilised pig kidney Na^+, K^+-ATPase was reconstituted into the native membrane it was originally extracted from (referred to as "native" membranes). This was achieved by solubilising the Na^+, K^+-ATPase in with its native membranes before reforming the Na^+, K^+-ATPase membranes using BioBeads. Initially ATPase activity was measured by the Baginski method at a Na^+ concentration of 100 mM. This was to test if any phospholipid systems caused a near total loss in activity. Activity remained in all phospholipid compositions with the exception of 100% DMPC. Activity in Na^+, K^+-ATPase reconstituted into 2:1 molar ratio DMPC:DOPG was comparable to Na^+, K^+-ATPase reconstituted into native membranes and was approximately 70% of original Na^+, K^+-ATPase activity. Na^+, K^+-ATPase reconstituted in DOPC alone had approximately 30% of original activity and Na^+, K^+-ATPase reconstituted in DMPC alone resulted in a virtual complete loss of activity. This suggests that the Na^+, K^+-ATPase requires the presence of negatively charged phospholipids for activity as well as compatible phospholipid chain lengths. Full Na^+ activation curves were therefore produced with Na^+, K^+-ATPase reconstituted into 2:1 molar ratio DMPC:DOPG and DOPC alone (Figure 3.22.). Control Na^+ activation

curves of native pig kidney Na^+, K^+-ATPase membranes and solubilised pig kidney Na^+, K^+-ATPase reconstituted native membranes (Figure 3.21.) were also performed. This reveals that solubilisation of Na^+, K^+-ATPase with $C_{12}E_8$ does not irreversibly kill ATPase activity. Figure 3.23 shows V_{max} and $K_{0.5}$ for all reconstitutions.

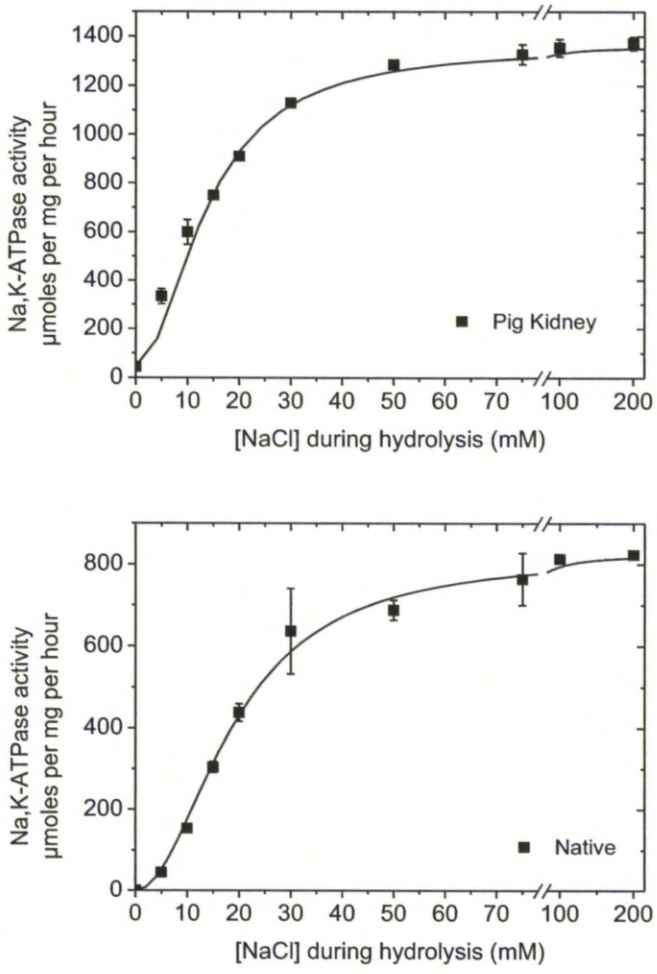

Figure 3.21. Na^+ activation curve of pig kidney Na^+, K^+-ATPase before and after reconstitution into native membranes. Kidney Na^+, K^+-ATPase activity was determined at the indicated concentrations of Na^+ and data fit with a Hill function. Experiments performed at 37°C. Native membrane assays performed by Angelina Damgaard of the University of Aarhus.

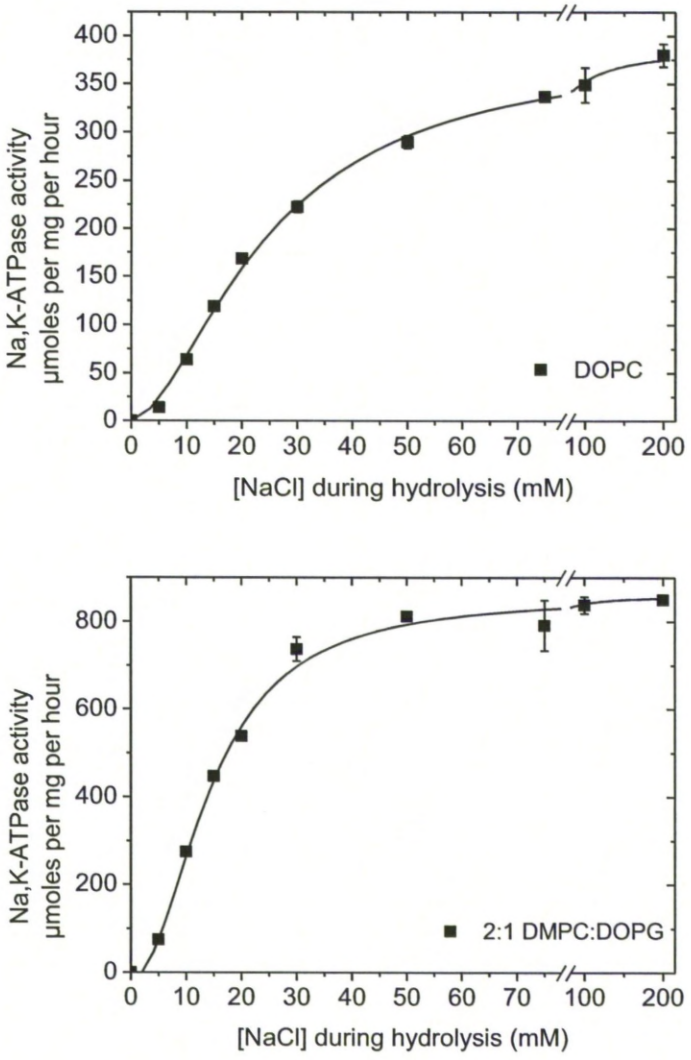

Figure 3.22. Na^+ activation curve of pig kidney Na^+, K^+-ATPase reconstituted into DOPC and 2:1 DMPC:DOPG. Kidney Na^+, K^+-ATPase activity was determined at the indicated concentrations of Na^+ and data fit with a Hill function. Experiments performed at 37°C.

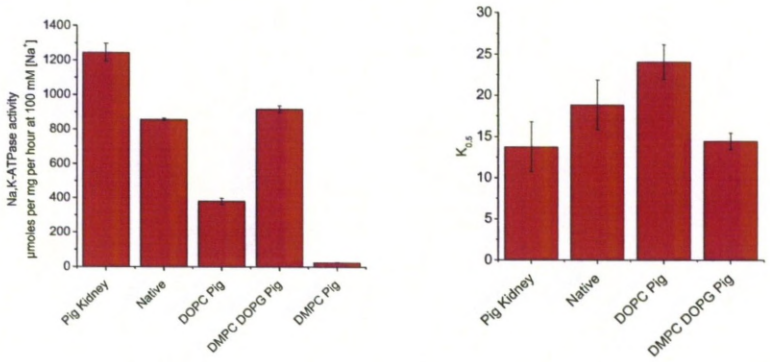

Figure 3.23. Functional analysis of the Na^+, K^+-ATPase in different phospholipid membranes. Pig kidney Na^+, K^+-ATPase activity was determined at 100 mM Na^+ in the presence of 20 mM KCl, 3 mM ATP, 4 mM $MgCl_2$ (pH 7.4 at 37 °C). This was repeated after reconstituting in various phospholipid preparations.

As activity remains in DMPC:DOPG and DOPC the activities of Na^+, K^+-ATPase reconstituted in these two systems was measured at 15 mM and 100 mM Na^+ with and without PLM_{38-72} (Figure 3.24.). Full activation curves would have been ideal but the quantity of PLM_{38-72} peptide was limited. In DMPC:DOPG membranes a similar reduction of activity due to PLM_{38-72} at 15 mM Na^+ is observed to that previously observed in pre-reconstitution native Na^+, K^+-ATPase (Figure 3.19.). However the reduction of activity due to PLM_{38-72} at 100 mM in DMPC:DOPG membranes is much smaller than in native Na^+, K^+-ATPase. In DOPC alone the reduction of activity due to PLM_{38-72} is smaller at both 100 mM Na^+ and 15 mM Na^+ than in pre-reconstitution native Na^+, K^+-ATPase. This suggests that PLM_{38-72} is not sequestering and immobilising DOPG as

if this was the case, the concentration of DMPC around the Na^+, K^+-ATPase would increase, which would not support activity (Figure 3.24.). These results would suggest that the effect of PLM_{38-72} on V_{max} and $K_{0.5}$ is reduced when the Na^+, K^+-ATPase is reconstituted into DMPC:DOPG than observed in native Na^+, K^+-ATPase membranes. This is most likely due to a larger proportion of PLM_{38-72} binding to phospholipids than the Na^+, K^+-ATPase in the reconstituted sample due to the increased negative membrane surface charge. This would suggest that *in vivo* any interaction between PLM_{38-72} and membrane surfaces is not solely driven by electrostatic interactions but also indicates weak non-selective interactions. This could allow PLM_{38-72} to potentially switch more easily between a membrane associated and an enzyme bound form. As the reconstituted sample has a 33% negative surface charge, which is around three times higher than native membranes, it would seem likely that PLM_{38-72} is associating more preferably to the synthetic phospholipids over the Na^+, K^+-ATPase than it would to native cell membranes.

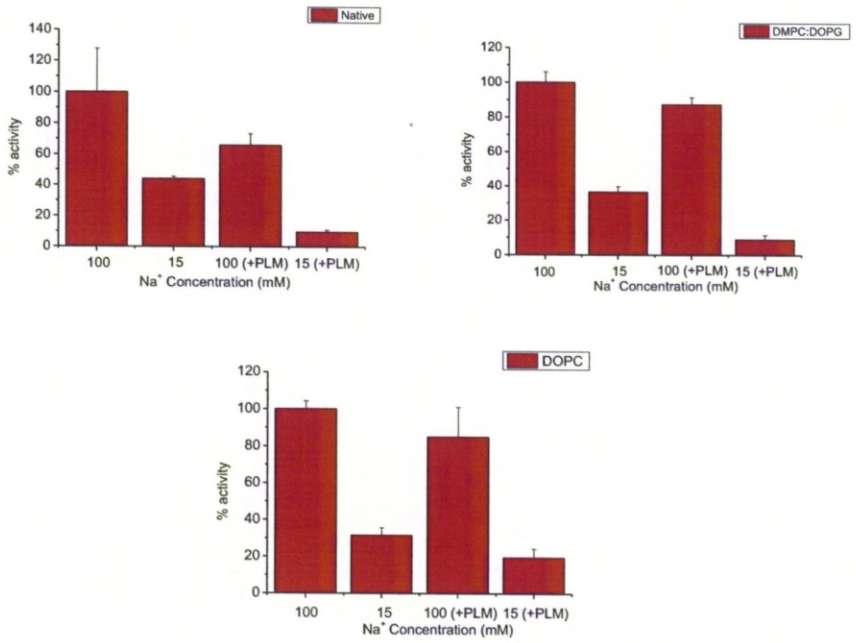

Figure 3.24. ATPase activities of the Na^+, K^+-ATPase in different membrane environments. Activities measured at 100 and 15 mM Na^+ with and without 100 μM PLM_{38-72}. Control (Native) shows Na^+, K^+-ATPase activity before reconstitution and DMPC:DOPG and DOPC show activities of the Na^+, K^+-ATPase reconstituted into the relevant phospholipid environments.

3.4. Discussion

The cytoplasmic domain of FXYD proteins is the most varied region between members of the family. It would therefore seem likely that the specific functions observed for each FXYD protein are a direct result of this region. PLM was the first FXYD protein to be discovered (Palmer *et al.*, 1991) and as a result is the best understood member of the family. Interestingly its cytoplasmic region has been observed to bind to both

negatively charged phospholipid membranes (Clayton *et al.*, 2005) and inhibit the Na^+, K^+-ATPase (Pavlovic *et al.*, 2007). This chapter has shed some light into how these two interactions can be reconciled. PLM has two physiological phosphorylation sites in the cytoplasmic domain (Palmer *et al.*, 1991; Mounsey *et al.*, 2000) that appear to alter the effect of the region on both cell membranes and the Na^+, K^+-ATPase. Both ^2H NMR and ITC have revealed that PLM_{38-72}, a peptide representing the cytoplasmic domain of PLM, binds to negatively charged membranes whilst having no affinity for zwitterionic membranes (Figure 3.8 and Figure 3.10). This is likely because PLM_{38-72} has a net positive charge. However, it would appear that this interaction relies on more than electrostatic potential as PLM_{38-72} also has a preference for eukaryotic phospholipids over prokaryotic phospholipids (Figure 3.10 and Figure 3.14). This suggests that the affinity of PLM_{38-72} for phospholipid membranes is determined by specific phospholipid headgroup sidechains. ^{31}P NMR experiments revealed that PLM_{38-72} can bind to phospholipid headgroups in the presence of the Na^+, K^+-ATPase. However, this effect is much smaller than that seen previously in the absence of the Na^+, K^+-ATPase (Clayton *et al.*, 2005). This previous study also showed that PLM_{38-72} had a preference for DOPG over DMPC whereas in the data measured here in the presence of enzyme it would seem that PLM_{38-72} has a similar effect on both phospholipid types. This suggests the Na^+, K^+-ATPase reduces the binding of PLM_{38-72} to the cell membrane. Ser 68 phosphorylation also reduces the

potency of PLM_{38-72} as an inhibitor of the Na^+, K^+-ATPase (Figure 3.19.). Phosphorylation introduces an extra a negative charge to PLM_{38-72} making its net charge less positive, which could explain the reduced affinity for both cell membranes and the Na^+, K^+-ATPase. This supports NMR data which reveals a conformational change of the cytoplasmic region after phosphorylation (Teriete *et al.*, 2009), which could be indicative of PLM_{38-72} moving away from the cell membrane whilst either also moving away from the Na^+, K^+-ATPase or re-orientating onto an alternative site on the protein surface. Additionally, by reconstituting the Na^+, K^+-ATPase into DMPC:DOPG membranes the effect of PLM_{38-72} inhibition was reduced. DMPC:DOPG is 33% negatively charged which is about three times as much as observed in native membranes (Akio, 1971). This means the synthetic membranes could exaggerate the PLM/phospholipid interaction, so reducing its interaction with enzyme leads to reduced ATPase activity inhibition. It does confirm that PLM_{37-72} appears to interact with the membrane surface rather than sequestering and immobilising DOPG as observed previously (Clayton *et al.*, 2005). If DOPG was indeed immobilised by PLM_{38-72} a much larger loss of function would be expected in reconstituted membranes as by removing DOPG from the Na^+, K^+-ATPase the local concentration of DMPC would increase, conditions that do not support ATPase activity (Figure 3.24.). The fact that the interaction of PLM_{38-72} with cell membranes is small suggests that the slight difference in phospholipid binding affinities of PLM_{38-72} and

$pPLM_{38-72}$ is insignificant when compared to the effect on the Na^+, K^+-ATPase.

The fact that CHIF and short form Mat-8 have no significant effect on negatively charged phospholipid bilayers (Figure 3.9, 3.11 and 3.13) or activity of the Na^+, K^+-ATPase (Figure 3.20.) highlights the importance of phosphorylation in the regulation of PLM and thus the Na^+, K^+-ATPase. There is no evidence supporting either CHIF or short form Mat-8 as phosphorylation targets *in vivo* and are therefore more likely to be functionally inert anchoring domains. Figure 3.25 illustrates a possible dynamic equilibrium of multiple conformations of the cytoplasmic region of PLM conferred by a flexible linker region present between the transmembrane domain and the cytoplasmic helix (Teriete *et al.*, 2007). The precise conformation adopted may be controlled by phosphorylation.

CYTOPLASM

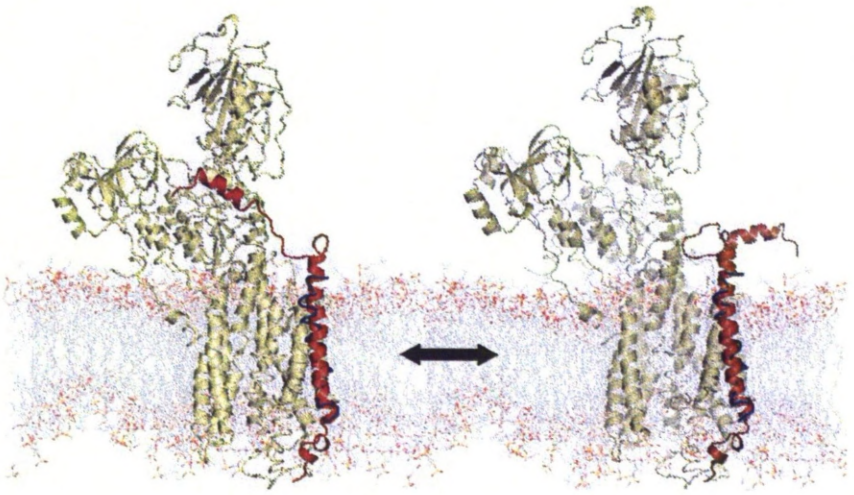

EXTRACELLULAR

Figure 3.25. Proposed equilibrium between two conformations of PLM controlled by phosphorylation. The cytoplasmic region of PLM could occupy several orientations in dynamic equilibrium, the most extreme of which are shown above. This may be controlled by phosphorylation of Ser 63 and Ser 68 located on the cytoplasmic helix. Figure from published paper (Hughes *et al.*, 2011).

The work in this chapter also revealed that the cytoplasmic region of the long isoform of Mat-8 can act as an inhibitor of the Na^+, K^+-ATPase (Figure 3.20.). The only difference from the short isoform of Mat-8 is an additional 26 amino acids at the start of the cytoplasmic region (Bibert *et al.*, 2006). As the short form has no effect on function the 26 amino acids are clearly significant. It is unclear if they have a direct role in Na^+, K^+-ATPase binding or if they instead allow the C-terminal residues to occupy

alternative sites on the Na^+, K^+-ATPase surface that are out of reach in the short Mat-8 isoform. As the long isoform of Mat-8 is a recent discovery and is not very well understood it is feasible that it does have physiological phosphorylation sites that have not yet been discovered. NetPhos (Blom *et al.*, 1999), was therefore used, which uses neural network predictions for serine, threonine and tyrosine phosphorylation sites in eukaryotes. It predicts four possible sites (Figure 3.26.), three of which are notably in the 26 amino acids not present in short form Mat-8. It is therefore possible that the inhibition of the Na^+, K^+-ATPase by long form Mat-8 is regulated by phosphorylation much like PLM.

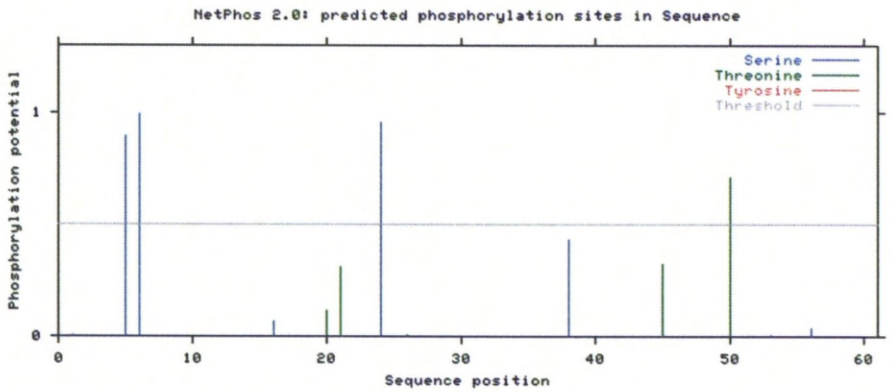

Figure 3.26. NetPhos prediction of phosphorylation sites in the cytoplasmic region of long form Mat-8. The sequence of the cytoplasmic region of long form Mat-8 is indicated with the three predicted serine sites shown in blue (with scores of 0.898 0.995 0.956) and the threonine site shown in green (with a score of 0.710)

Chapter 4

4.1. Expression and Purification of FXYD Proteins

An initial aim of this project was to develop an expression system for one or more FXYD proteins to enable structural studies to be performed. The procedure had to be reproducible and suitable for producing labelled protein samples to be analysed by NMR. All NMR experiments require over 99% purity of target protein and proteins must be uniformly labelled with NMR suitable isotopes ^{13}C and ^{15}N to achieve the required sensitivity. As FXYD proteins are membrane proteins their expression and purification can be very difficult largely due to solubility issues. Membrane proteins are also difficult to overexpress. This chapter discusses the development of the methods to create FXYD protein samples for use in NMR experiments. Previously the Marassi group have attempted to express FXYD proteins as fusion proteins with a tag that promotes the formation of inclusion bodies. The fusion partners attempted include ketosteroid isomerise (KSI) (Thai *et al.*, 2005), a portion of the Trp ΔLE 1413 polypeptide (TLE) (Crowell *et al.*, 2003), and two mutated forms of B-cell lymphoma-extra large (BCL-XL) vector (Thai *et al.*, 2005). The first mutated BCL-XL fusion partner is BCL173 where the C-terminal domain (residues 213–233) and the flexible loop (residues 44–84) of BCL-XL are removed, and the two methionine residues (Met159 and Met170) are mutated to leucine to facilitate CNBr cleavage of FXYD protein from the fusion partner as CNBr cleaves at

methionine residues. The second mutated BCL-XL is BCL99, which has further deletions based on the structure of the soluble form of BCL-XL (Muchmore *et al.*, 1996). In addition to the deletions in BCL173, the residues 1–116 (which form a flexible loop) as well as helices 1–4 in the structure of the soluble form of BCL-XL are also deleted. The expression levels for these systems is compared in the SDS-PAGE gel shown in Figure 4.1. where the BCL-XL mutants clearly produce more fusion protein than either KSI or TLE fusion partners. This chapter describes the efforts to produce FXYD protein using one of these mutated vectors and the development of new methods of FXYD protein production in the pMAL vector.

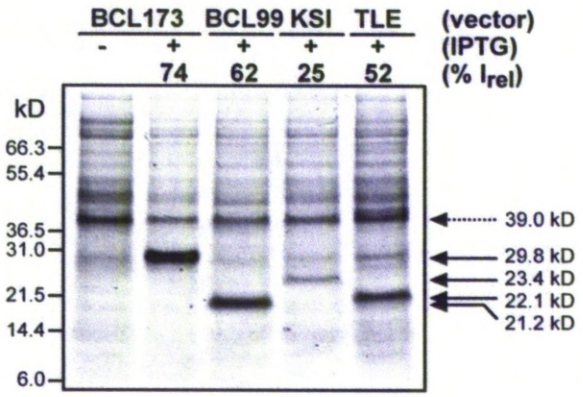

Figure 4.1. Comparison of overexpressed fusion protein levels of PLM with different fusion protein tags. Overexpressed protein shown for a BCL173 tag (29.8 kDa), BCL99 (21.2 kDa), KSI (23.4 kDa) and TLE (22.1 kDa). Pre-induction cells are shown (-IPTG) and the intensities (% I_{rel}) of each overexpressed band relative to the band at 39 kDa (dashed arrow) are indicated. Figure taken from (Thai *et al.*, 2005).

All proteins were expressed in *Escherichia coli* (*E.coli*) as this is the preferred system for protein expression for many reasons. These include low cost, fast growth times, fast rate of expression and high plasmid copy number. Expression in *E. coli* is generally easier to perform than other systems like yeast. There are many strains widely available with different properties and the cells can be stored long term. This method of protein expression can be achieved in low cost growth media making it a very economical way to produce the milligram quantities of proteins required for NMR.

As the proteins of interest are membrane proteins they will be particularly insoluble in aqueous media. Most purification procedures rely on methods that require the production of soluble protein or that targets the protein to inclusion bodies. The methods employed in this chapter use constructs that express the protein fused to another protein partner to promote either the formation of inclusion bodies or improve solubility. The first method generates a fusion protein with a mutated form of B-cell leukaemia/lymphoma extra long (mBCL-XL) as the fusion partner repeating previous methods (Thai *et al.*, 2005). This protein forms inclusion bodies when expressed alone and has been shown to do the same in an mBCL-XL/FXYD fusion. These inclusion bodies can be lysed then solubilised to give liquid samples suitable for cleavage and purification. In the second method, incorporation of the FXYD gene into the pMAL vector

expresses a fusion construct with maltose binding protein (MBP). MBP is a very soluble protein so theoretically an MBP/FXYD fusion protein would express at least partially in a soluble form. A protease site engineered between the two proteins would allow the fusion protein to be cleaved following purification on an amylose resin columns to which the MBP would bind.

4.2. Materials and Methods

4.2.1. Materials

The primary Mat-8 anti-mouse monoclonal antibody (product name FXYD3 (M-20)) was purchased from Santa Cruz Biotechnology. The Novex® WesternBreeze™ Chromogenic Immunodetection Kit for dot-drop experiments was purchased from Roche. Chloroform and methanol were provided by Fisher Chemicals. All other chemicals were supplied by Sigma-Aldrich and were of molecular biology grade.

The pBCL99 plasmid was provided by Francesca Marassi of the Burnham Institute, California (Figure 4.3.). This plasmid is based on the pET vector (Figure 4.2. (Thai *et al.*, 2005)) and produces a fusion protein of target (e.g. phospholemman (PLM)) and modified B-cell lymphoma-extra large (BCL-XL) protein that expresses as inclusion bodies.

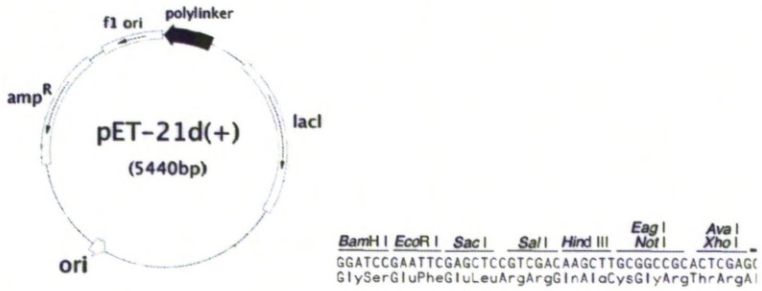

Figure 4.2. Plasmid map of the pET-21d(+). The pBCL vector is based on the pET-21d(+) vector (shown). The polylinker region contains several restriction sites (shown) and is the location into which the desired sequence is cloned. The vector is ampicillin resistant (Amp^R). Expression is induced by Isopropyl β-D-1-thiogalactopyranoside (IPTG), which inactivates the lacI gene which codes for the LacL protein which represses promoter Ptac. Origins of plasmid replication (ori) is also shown. F1 ori is for producing single stranded plasmids when co infected with M13 helper phage (not used in this project). Figure adapted from pET-21a-d(+) literature on the Novagen website.

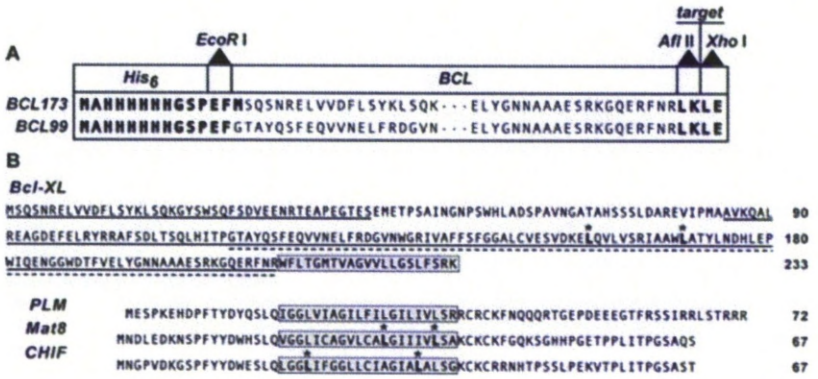

Figure 4.3. Plasmid map of pBCL vector. The sequence (A) contains a His tag and a modified Bcl-XL sequence separated by an EcoRI restriction site. Downstream of the modified Bcl-XL is an AflI and an XhoI restriction site. Sequence A is subcloned into the pET vector at the polylinker region (pLink) and the target protein of interest (e.g. PLM) is subcloned into the AflI/XhoI sites in sequence A. Where required the target protein has an N-terminal Met added for CNBr cleavage. (B) shows the different BCL sequences used by the Marassi group; BCL173 and BCL99 with the cloned FXYD protein sequences shown above. Both vectors lack the hydrophobic C terminus (grey box). BCL99 is used in this thesis and is highlighted by the dotted line and therefore lacks the first 116 residues of BCL. Figure taken from Marassi group (Thai *et al.*, 2005)

The pMAL-c2X plasmid was purchased from New England Biolabs. The plasmid map is shown in Figure 4.4. This system was selected as it successfully expressed and purified the small transmembrane proteins phospholamban (PLB) and sarcolipin (SLN) (Buck *et al.*, 2003) which are regulators of the sarcoplasmic reticulum Ca^{2+}-ATPase (SERCA) with a single transmembrane region much like FXYD proteins are in respect to the Na^{+}, K^{+}-ATPase. This system expresses a fusion protein of maltose binding protein (MBP) and the selected target protein sub-cloned into the construct. The Mat-8 DNA sequence was altered to include a Tobacco etch virus protease (TEVP) cleavage site preceding the Mat-8 coding sequence. The recognition site for TEVP is Glu-Asn-Leu-Tyr-Phe-Gln-Gly (with the cleavage occurring between Gln and Gly) (Kapust *et al.*, 2002). Therefore, a fusion protein was designed with a TEVP cleaveage site located between MBP and Mat-8 sequences. Codons were also optimised for the preference of the bacteria. This sequence was engineered into the pMAL-c2X plasmid by Yorkshire Bioscience Ltd (York) (Figure 4.4.).

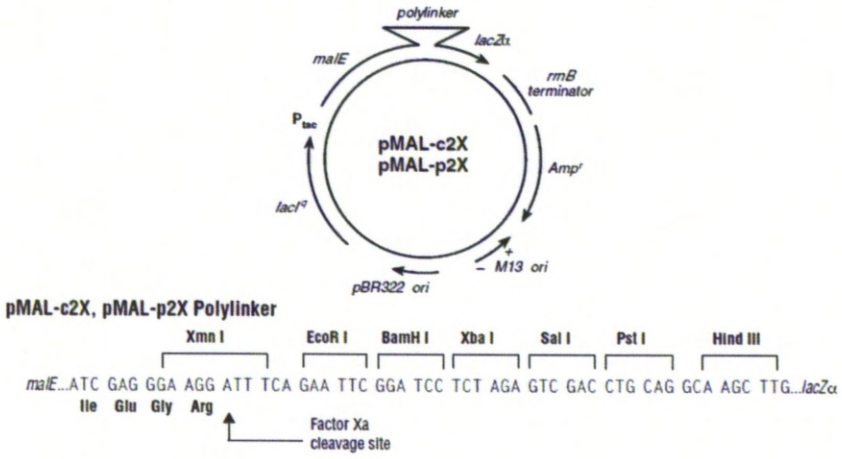

Figure 4.4. Plasmid map of pMal-c2X vector. Polylinker region contains several restriction sites (shown) and is the location into which the desired sequence is cloned. Upstream of the polylinker is the gene malE which transcribes maltose binding protein (MBP) thus the vector produces an MBP fusion protein. The vector is ampicillin resistant (Amp^r), has a LacZ gene for use as a reporter gene (not required in this project). Expression is induced by Isopropyl β-D-1-thiogalactopyranoside (IPTG) which inactivates the lacI gene which codes for the LacL protein which represses promoter Ptac. The terminator where translation is halted and origins of plasmid replication (ori) are also shown. Figure taken from New England BioLabs.

The *E.Coli* cell lines investigated were: XL1-Blue for plasmid maintenance and BL21 (DE3), Rosetta, Origami DE3 and C41 (DE3) for protein expression.

All cells were purchased from Novagen with the exception of C41 (DE3) cells which were purchased from Lucigen. Unless otherwise stated all methods were taken from Molecular Cloning: A Laboratory Manual (Orkin, 1990).

4.2.2. Preparation of competent E. coli

Different cell lines were made competent for either protein expression or plasmid maintenance. Lysogeny Broth (LB) (250 mL) was inoculated with 1% (v/v) overnight *E. coli* culture and supplemented with 20 mM $MgSO_4$ and grown to mid-log phase (OD_{600} 0.4-0.6). OD_{600} measurements were taken using a Cary 300 Bio U.V. visible spectrophotometer. The cell suspension was spun down for 5 min. at 10,000 x g at 4 °C. The cells were harvested and resuspended in 100 ml TFB1 (30 mM KAc, 10 mM $CaCl_2$, 50 mM $MnCl_2$, 100 mM RbCl, 15% glycerol; pH 5.8) and incubated on ice for 5 min. The cell suspension was spun down for 5 min. at 10,000 x g at 4 °C, resuspended in 10 ml TFB2 (10 mM MOPS, 75 mM $CaCl_2$, 10 mM RbCl, 15% glycerol; pH 6.5) and incubated on ice for an hour. Cells were then frozen at -80 °C in 200 µl aliquots.

4.2.3. Transformation of competent E. coli

The appropriate plasmid (2 µl) was added to competent cells (50 µl) and the cells were incubated on ice for 30 min. The cells were then heat shocked at 42 °C for 90 s, replaced on ice for 2 min. then 800 µl of LB was added before incubating with shaking (200 rpm 37 °C) for an hour. The cell suspension was concentrated by centrifugation, removing 800 µl of the supernatant and resuspending the pelleted cells in the remaining volume. 25 µl of the resuspended cells was spread onto an agar plate containing ampicillin (50 µg/mL). Both vectors contain ampicillin resistance genes

permitting growth of transformed cells only. Agar plates were incubated overnight at 37 °C. Controls were also set up: a negative without plasmid added in the initial step and a positive control where plates contained no ampicillin. The plasmid free-plate should have no colonies as none of the cells are ampicillin resistant and the ampicillin-free, plate should have high growth as cells will grow whether or not they have been successfully transformed. The transformed plate will have a number of colonies dependent on transformation efficiency which would range from one or two colonies to a few hundred. Each colony originates from one individual transformed bacterial cell. The control plates help confirm whether all colonies on the transformed plate have indeed taken up the plasmid and are suitable to use for expression.

4.2.4. Preparation of glycerol cell stocks

A transformed colony (produced as described in 4.2.3.) was removed from a plate with a sterile pipette tip and placed into LB (50 mL) and ampicillin (200 μg/mL) and incubated with shaking overnight at 37°C. The overnight culture was aliquoted into 800 μL fractions and 200 μL of sterile glycerol was added to each before storage at -80°C.

4.2.5. Plasmid preparation

To produce additional plasmid when required plasmid preparation from *E. Coli* culture was carried out. Plasmid preparation was performed with a QIAGEN® QIAprep spin miniprep kit. This kit contains spin columns to purify the DNA and several buffers the contents of which are undisclosed. These include resuspension buffer (P1), lysis buffer (P2), wash buffer (PE), neutralisation buffer (N3) and elution buffer (EB). LB broth (1 mL) with ampicillin (200 μg/mL) was inoculated with a single colony picked from a transformed plate using non expressing cells (XL1-blue) before incubating with shaking (200 rpm, 37 °C) overnight. This was pelleted and resuspended in Buffer P1 (250 μl) before adding Buffer P2 (250 μl) to lyse the cells and was immediately mixed by inverting 6 times. Buffer N3 (350 μl) was added to neutralise and again was inverted 6 times. The mixture was spun down for 10 min. at 17,900 x g to remove cell debris and the supernatant containing plasmid was added to a spin column. This spin column was centrifuged for 1 min. then washed by adding Buffer PE (750 μl) to remove impurities and centrifuged again for 1 min. Flow through was removed and centrifuged again for 1 min to ensure all buffer was spun through the column. DNA bound to the column (plasmid) was eluted by adding Buffer EB (50 μl), allowing to stand for 1 min. and centrifuging into a 1.5 mL microcentrifuge tube for 1 min. Eluted DNA was stored in elution buffer at -20°C.

4.2.6. Expression of PLM in pBCL plasmid

The methods for pBCL expression are based on the work by the Marassi group (Thai *et al.*, 2005). LB broth (50 mL) with ampicillin (100 μg/mL) was inoculated with a single colony picked from a pBCL99 (containing PLM) transformed plate (as described in 4.2.4.) before incubating with shaking (200 rpm 37 °C) for 5 hours. 1 mL of this culture was added to 100 mL of minimal M9 media with ampicillin (100 μg/mL) and grown overnight. The cells was spun down and harvested for 10 min. at 8,000 x g at 4 °C. The pellet was resuspended in minimal M9 media with ampicillin and used to inoculate 1 L of minimal M9 media with ampicillin and glucose to an OD_{600} of 0.05-0.1 and was allowed to grow to OD_{600} of 0.7-0.9 by incubating with shaking (200 rpm 37°C). Cells were induced with 1 mM IPTG for 4 hr after which cells were spun down in a Sorvall refrigerated centrifuge for 10 min. at 8000 x g at 4 °C and resuspended in 30 mL buffer A (50mM Tris–HCl, pH 8.0, 15% glycerol) and frozen ovennight at -20°C. Thawed cells were lysed by French press and the soluble fraction was removed by centrifugation at 48,000g, 4°C for 30 minutes. The remaining pellet was washed twice by homogenising with fresh buffer A and repeating centrifugation. The final pellet was solubilised in 6M guanidium chloride (30 mL) and centrifuged at 48,000g, 4°C for 2 hours.

4.2.7. CNBr Cleavage

Methodology for this procedure was adapted from (Thai *et al.*, 2005). Particular safety care had to be adhered to due to the potential dangers of CNBr. Experiments were performed with face mask, lab coat and two pairs of nitrile gloves. All experiments were performed in fume hood. 10 mL of 70 % formic acid (FA) was prepared in a 15 mL falcon tube and added at 4-fold excess by volume to solubilised inclusion bodies.

5M CNBr in acetonitrile was added slowly to solubilised inclusion bodies at various ratios to establish ideal cleavage conditions. Samples were wrapped in foil and left overnight at room temperature. Outer gloves, pipette tips, eppendorfs were added to 5M KOH before being neutralised with bleach and washed into the sink with copious amounts of water. Samples were lyophilised three times, with water being added between runs. The freeze drier was allowed to defrost before emptying the thawed liquid into a beaker of 5M KOH and neutralised with bleach. Contents of beaker were washed into the sink with copious amounts of water. The freeze dryer condenser was cleaned with 5M KOH followed by bleach.

4.2.8. Expression of PLM in pMAL vector

Attempts were made to express PLM in the pMAL vector in a variety of cell strains, including BL21 (DE3), Rosetta, Origami (DE3) and C41. Each cell strain was transformed as in 4.2.4. LB (50 mL) with ampicillin (200

μg/mL) and glucose (2 mg/mL) was inoculated with a single colony containing pMAL (PLM) picked from a transformed plate before incubating with shaking (200 rpm 37 °C) overnight. The cells were centrifuged and harvested for 10 min. at 8,000 x g at 4 °C. The pellet was resuspended in LB with ampicillin and glucose and used to inoculate 50 mL of LB with ampicillin and glucose to an OD_{600} of 0.05-0.1 and allowed to grow to OD_{600} of 0.7-0.9 by incubating with shaking (200 rpm 37°C). The culture was induced with 1 mM Isopropyl β-D-1-thiogalactopyranoside (IPTG) and one flask was returned to 37 °C with shaking (200 rpm) overnight then centrifuged (8000g, 10 min, 4°C). The pelleted cells were resuspended in 3 mL column buffer (20 mM Tris-HCl, 200 mM NaCl, 1 mM EDTA). These 3 mL samples were lysed using pulsed sonication for three 10 s runs with 30 s intervals using a Dawe Ultrasonic probe sonicator at 50% duty cycle, output control 7. Lysed cells were centrifuged (19, 000g, 10 min, 4°C) and insoluble protein (pellet) was compared with soluble protein (supernatant) by SDS-PAGE.

4.2.9. Expression tests of MBP/Mat-8 fusion protein

Optimal expression conditions for MBP/Mat-8 fusion protein were determined by expression tests. LB (50 mL) with ampicillin (200 μg/mL) and glucose (2 mg/mL) was inoculated with a single colony and grown overnight at 37°C. The overnight culture was centrifuged and harvested for

10 min. at 8,000 x g at 4 °C. The pellet was resuspended in LB containing ampicillin and glucose and used to inoculate three flasks with 150 mL of LB with ampicillin and glucose to an OD_{600} of 0.05-0.1 and allowed to grow to OD_{600} of 0.7-0.9 by incubating with shaking (200 rpm 37°C). All flasks were induced with 1 mM IPTG and one flask was returned to 37 °C with shaking (200 rpm) whereas the other two flasks were incubated with shaking (200 rpm) at different temperatures (18°C and 25°C). This determined an optimal expression temperature. 50 mL samples from each flask were taken at 3 hr, 5 hr and 7 hr intervals and a final sample of the remaining 50 mL was taken after incubating overnight, in order to determine optimal induction time. All samples were centrifuged (8000g, 10 min, 4°C) and cells were resuspended in 3 mL column buffer (20 mM Tris-HCl, 200 mM NaCl, 1 mM EDTA). These 3 mL samples were lysed using pulsed sonication for three 10 s runs with 30 s intervals using a Dawe Ultrasonic probe sonicator at 50% duty cycle, output control 7. Lysed cells were centrifuged (19, 000g, 10 min, 4°C) and insoluble protein (pellet) was compared with soluble protein (supernatant) by SDS-PAGE. Other potential variables such as optimal IPTG concentration and optimal detergent (Triton® X-100 for improved solubility) concentration were determined in the same way.

4.2.10. Expression of MBP/Mat-8 fusion protein in LB

LB (50 mL) with ampicillin (200 μg/mL) and glucose (2 mg/mL) was inoculated with a single colony picked from a pMal (containing Mat-8) transformed plate before incubating with shaking (200 rpm 37 °C) overnight. The cells were centrifuged and harvested for 10 min. at 8,000 x g at 4 °C. The pellet was resuspended in LB with ampicillin and glucose and used to inoculate 1 L of LB with ampicillin and glucose to an OD_{600} of 0.05-0.1 and was allowed to grow to OD_{600} of 0.7-0.9 by incubating with shaking (200 rpm 37°C). Cells were induced with 0.25 mM (IPTG) for 3 hr after which cells were spun down in a Sorvall refrigerated centrifuge for 10 min. at 8000 x g at 4 °C and resuspended in 30 mL column buffer (20 mM Tris-HCl, 200 mM NaCl, 1 mM EDTA, 0.5% Triton® X-100) and frozen overnight at -20 °C. The freeze thaw cycle aids cell lysis. The column buffer contained Triton® X-100 detergent to aid solubility.

4.2.11. Expression of pMAL/Mat-8 fusion protein in minimal media

Mat-8 was expressed in M9 minimal media made up of 990 mL solution A (12.5 mg/ml Na_2HPO_4, 7.5 mg/ml KH_2PO_4) and 10 mL of solution B (400 mg/mL glucose, 100 mg/mL NH_4Cl, 24 mg/mL $MgSO_4.7H_2O$, 2 mg/mL $CaCl_2.2H_2O$, 1 mg/mL ampicillin and 1 mg/mL Thiamine HCl). This was further supplemented with vitamins and minerals to increase expression (Buck *et al.*, 2003) (Minerals: 6 mg/L $CaCl_2$, 6 mg/L $FeSO_4$, 1 mg/L $MnCl_2$, 0.8 mg/L $CoCl_2$, 0.7 mg/L $ZnSO_4$, 0.3 mg/L $CuCl_2$,

0.02 mg/L H_3BO_3, 0.25 mg/L $(NH_4)_6MO_7O_{24}$, and 5 mg/L EDTA; Vitamins: 1 mg/L calcium pentothenate, 1 mg/L biotin, and 1 mg/L folic acid, 1 mg/L niacinamide, and 1 mg/L pyridoxal phosphate). Minimal media usually compromises yield compared to LB but by using ^{13}C labelled glucose the expressing cells will use the isotopically labelled glucose as its sole carbon source thus producing uniformly ^{13}C labelled proteins suitable for study by NMR. ^{15}N labelled NH_4Cl can be used in a similar way separately for ^{15}N NMR or in parallel for multi dimensional experiments observing both ^{13}C and ^{15}N (Lian and Middleton, 2001). Cells were grown in LB (to OD_{600} of 0.7-0.9) as in 3.2.6. but were resuspended in minimal media following centrifugation prior to induction with IPTG.

4.2.12. Purification of pMAL/Mat-8 fusion protein

Phenylmethanesulphonylfluoride (PMSF) (0.5 mM) and DNase I (25 μg/mL) were added to cells defrosted from the previous step to inhibit proteases and break down DNA. The cells were then lysed using the Sim Aminco French Pressure Cell at 1000 PSI and the lysate was spun down for 30 min. at 19,000 x g at 4 °C. The supernatant was filtered with a 0.2 μm filter before purification on an amylose resin column.

4.2.12.1. Amylose resin affinity chromatography

The fusion protein was purified on an amylose resin column. The protocol was adapted from the pMAL™ Protein System and Purification manual from New England BioLabs®. 10 mL of resin was added to a 50mL Falcon tube and centrifuged with 50 mL of column buffer (20 mM Tris-HCl, 200 mM NaCl, 1 mM EDTA, 0.5% Triton® X-100) x 2 at 6000 x g for 10 min at 4 °C. The supernatant was removed and 10 mL of column buffer was added to the equilibrated resin before adding the supernatant from the cell lysis step (3.2.8.). The lysate/resin mixture was left on a shaker in a cold room overnight to allow protein binding before being transferred to the column where flow through was collected. 50 mL of column buffer was passed through the column three times and retained. This was repeated twice with fresh column buffer to wash away impurities that do not bind to the column. The amylose resin was transferred to a 50 mL Falcon tube with elution buffer (30 mL column buffer with 10 mM maltose) to remove the maltose binding protein (MBP)/Mat-8 fusion protein from the resin and left shaking overnight at 4°C. The amylose resin was then transferred to the column and the eluent was collected.

4.2.12.2. Cleavage of fusion protein

The 30 mL of eluted fusion protein was cleaved by addition of TEVP (1 mL, 1 mg/mL) and incubated at room temperature overnight. A typical preparation produces approximately 20 mg of fusion protein (plus impurities) present according to a Bradford assay. TEVP is highly specific so should only cleave at the TEVP site Glu-Asn-Leu-Tyr-Phe-Gln-(Gly/Ser) engineered into the plasmid in-between MBP and Mat-8. The cleaved fusion protein was flash frozen with liquid nitrogen and stored at -80°C.

4.2.12.3. Chloroform/Methanol Precipitation of cleaved MBP/Mat-8 fusion protein

Chloroform/methanol precipitation (Wessel and Flügge, 1984) was used to remove detergent from the samples in order to prevent interference with subsequent purification steps. 1 part of TEVP-cleaved fusion protein was added to 4 parts methanol and 1 part chloroform, vortex mixing in-between each addition. Three parts of MilliQ water was then added to this mixture which causes a phase separation in which protein is precipitated in the chloroform/methanol/water interphase. This mixture was centrifuged at 14,000g for 1 min to collect the precipitated protein at the top of the bottom organic layer. The top aqueous layer was removed (not disturbing protein between layers) and the same volume of methanol originally added was vortex

mixed with the sample again and the mixture was centrifuged at 14,000g for a further 2 min to pellet the sample at the base of the tube. As much methanol was removed as possible without disturbing the pellet and the samples were then dried under a stream of nitrogen and then under high vacuum. These solid samples contain MBP, Mat-8, TEVP and other impurities.

4.2.12.4. High Performance Liquid Chromatography

The solid samples obtained after chloroform methanol precipitation that contain Mat-8 and impurities were dissolved in 7M guanidium chloride and made up to a final volume of 600 µl. Mat-8 was purified by high performance liquid chromatography (HPLC) using a C5 analytical column (Supelco Discovery® Bio Wide Pore) and carried out on a Gilson 322 instrument. Columns were equilibrated with 95% solvent A (H_2O + 0.1% TFA): 5% solvent B (Acetonitrile + 0.1% TFA) for 5 minutes. The sample was injected onto the column and the gradient was ramped from 5 to 95% Solvent B at a flow rate of 1 ml/min. Mat-8 was eluted with a linear gradient over 95 minutes and 1.5 ml samples were collected from 30 minutes until the end. Elution of protein is indicated by a large peak and theoretically there should be an equal molar concentration of MBP and Mat-8 eluted in different

fractions as they were co-expressed as a fusion protein. Samples were then lyophilised for further experiments.

4.2.13. Analysis of protein products

4.2.13.1. SDS-PAGE

0.75 mm thick gels of either 10% or 15% polyacrylamide were prepared using the BIORAD Protean II kit as follows: For 10% polyacrylamide resolving gels 3.3 mL 30% acrylamide, 2.5 mL 1.5 M Tris buffer; pH 8.8, 4.1 mL RO (reverse osmosis) water and 100 µL 10 % SDS and for 15% polyacrylamide resolving gels 5 mL 30% acrylamide, 2.5 mL 1.5 M Tris buffer; pH 8.8, 2.4 mL RO water and 100 µL 10 % SDS. Stacking gels were made up of 1.3 mL 30% acrylamide, 2.5 mL 0.5 M Tris buffer; pH 6.8, 6.1 mL RO (reverse osmosis) water and 100 µL 10 % SDS. 15% polyacrylamide resolving gels have a wider protein size range but poorer band separation than 10% polyacrylamide resolving gels. The appropriate resolving gel had 75 µL of ammonium persulphate (APS) (100 mg/mL) and 7.5 µL of tetramethylethylenediamine (TEMED) added immediately before casting and allowing to set, with a thin layer of saturated butanol on top to ensure a flat surface. The stacking gel also had 75 µL of APS (100 mg/mL) and 7.5 µL of TEMED added to it before casting on top of the set resolving gel. Well combs were added to the unset stacking gel to make wells for protein samples. SDS-PAGE samples were made up as follows:

10 µl protein sample, 10 µl RO water, 20 µl SDS-PAGE sample buffer (0.5 M Tris (Melford); pH 6.8, 50% glycerol, 10% (w/v) SDS, 5% (v/v) β-mercaptoethanol, 0.1% (w/v) bromophenol blue made up to necessary volume with RO water). SDS-PAGE samples were then heated at 100 °C for 5 min. and 7.5 µl loaded onto the gel. 5 µl of Sigma markers were also loaded onto each gel. Gels were run at 200 V for around 1 hour until the dye from the samples had run off the gel. Gels were stained for an hour in Coomassie G250 (0.1% Coomassie G250, 45% methanol, 45% RO water, 10% acetic acid) with shaking at room temperature. Gels were de-stained with water overnight.

4.2.13.2. Western Blot (Dot-Blot)

The protocol from the Novex® WesternBreeze™ kit was followed with Polyvinylidene fluoride (PVDF) membranes submerged in methanol for 5 seconds before equilibration in RO water. These were placed on damp filter paper before adding 1 µL of sample and allowing it to absorb before incubating with shaking at room temperature in 1 mL of 1% blocking solution (diluted in maleic acid solution (100 mM maleic acid, 150 mM NaCl; pH 7.5) for 30 min. Blocking solution (prevents non-specific binding of antibody to the membrane) was discarded then Mat-8 monoclonal antibody was diluted 1:5000 in 1% blocking solution and 1 mL added to the PVDF membrane and incubated with shaking at room

temperature for 30 min. Antibody was discarded and 4 wash steps of 2 mL of TSBT (50 mM Tris, 150 mM NaCl, 0.1% (v/v) Tween 20; pH 7.5) for 10 min with shaking at room temperature were performed. Anti-mouse horseradish peroxidase-conjugated secondary antibody (provided in the Novex® WesternBreeze™ kit) was diluted to 800 mU/ml in maleic acid solution and 1 mL added to the PVDF membrane and incubated with shaking at room temperature for 30 min. A further 4 x 15 min washes were performed then membranes were stained for 30 minutes with ready to use stain (5-Bromo-4-chloro-3-indolyl phosphate/Nitro blue tetrazolium chloride) which detects the alkaline phosphatase activity of secondary antibody.

4.3. Results

4.3.1. Expression of PLM in the pBCL plasmid

The pBCL plasmid containing the PLM sequence (Thai *et al.*, 2005) was provided by Francesca Marassi in order to express and purify PLM. This expression system involves expressing PLM as a fusion protein with an altered B-cell lymphoma protein (BCL) sequence. Small membrane proteins are often expressed as fusion proteins as they are difficult to overexpress alone. BCL was selected in this case as it expresses as inclusion bodies. Inclusion bodies occur when bacteria form aggregates of misfolded protein. The proteins are often relatively pure and can be

refolded using urea. In this expression system the inclusion bodies are solubilised using guanidium chloride and followed by CNBr cleavage at the Met-X linkage between mBCL-XL and PLM. This method has high safety risks that must be taken into account. Transformed cells were grown overnight then used to inoculate 1 litre of LB to an OD_{600} of 0.05-0.1. This was grown to an OD_{600} of 0.7-1.0 and induced with 1 mM IPTG. These cells were expressed at a variety of temperatures and induction times. Inclusion bodies containing insoluble protein were later solubilised and Figure 4.5 shows whole cell samples in these various conditions. Overexpressed fusion protein is present to varying degrees in all conditions although seemingly to a lesser extent than previously (Thai *et al.*, 2005).

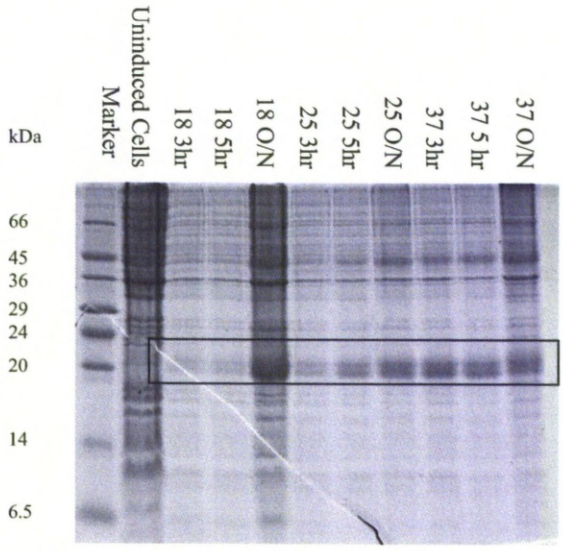

Figure 4.5. Successful PLM fusion expression in pBCL construct. Lanes show protein present in whole cells after induction with IPTG for various times and temperatures. The fusion protein is ~22 kDa and the corresponding band is indicated by the box Low range markers (Sigma) are used as shown.

CNBr cleavage was performed on samples after solubilising in guanidium chloride. As guanidium chloride interferes with the Bradford reagent, protein levels could not be accurately determined to calculate CNBr molar excesses. Therefore 100 mg of protein was used as a guideline and different molar excesses were calculated and used on a small scale. Bovine serum albumin (BSA) was also cleaved by CNBr as a positive control to confirm the effectiveness of CNBr cleavage. Figure 4.6. shows the results of these experiments. In the positive control the starting material (66.8 kDa BSA) is partially cleaved giving some remaining starting material and two

other clear bands. From the methionine residues present in BSA fragments of 29.6 kDa, 10.5 kDa, 3.9 kDa and two fragments of 11.4 kDa are expected. The 29.6 kDa fragment is clearly apparent. The two 11.4 kDa fragments and the 10.4 kDa fragment appear to have travelled the same distance along the gel which is entirely possible given their similarity in size. The 3.9 kDa fragment is too small to be seen on this gel and has most likely run off the end. The markers suggest some deviations in size however as this technique separates proteins by shape and there is a lot of overlap of bands this is to be expected. It is clear CNBr also has an effect on the expressed and solubilised pBCL proteins but it is not clear if PLM is present.

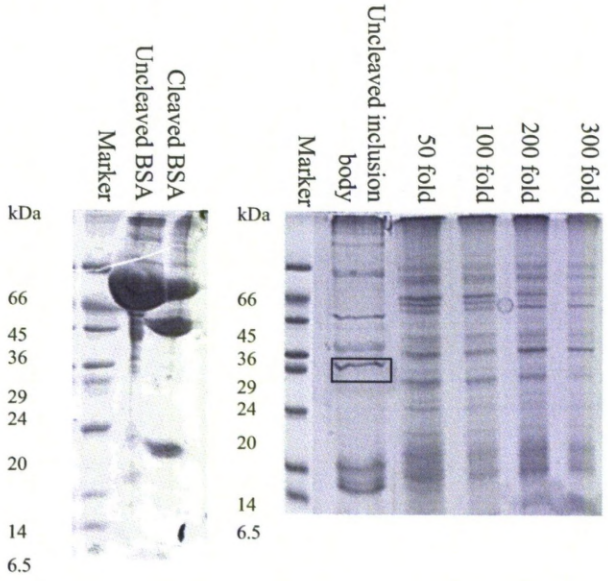

Figure 4.6. CNBr cleavage of BSA and expressed protein from pBCL plasmid. As a positive control BSA was cleaved with CNBr as shown on the left gel. Fragments are expected to be 29.6, 11.4 (x2), 10.5 and 3.9 kDa with BSA starting material expected at 66.8 kDa. The gel on the right shows the proteins expressed and solubilised from the pBCL plasmid (with the BCL/PLM fusion protein indicated by the box) and the results of CNBr cleavage at different molar excesses. Low range markers (Sigma) are used as shown.

The overexpressed band (indicated by the box in Figure 4.6.) was cut from the gel and digested with trypsin. The resulting protein fractions were analysed by mass spectrometry. The resulting spectra did not correlate with the expected fractions of a trypsin digest of an mBCL/PLM fusion protein. This meant there was no way of proving the CNBr cleavage was working. Unfortunately the published data for this system did not show any gels of

either the CNBr cleavage or the purification procedure which meant there was no point of reference. Due to the safety implications of CNBr cleavage this expression system was not pursued further to allow development of a safer method of the expression and purification of FXYD proteins.

4.3.2. Expression of PLM in the pMAL plasmid

The pMAL construct was selected as an alternative system to express and purify PLM. This vector has, as a starting point, been used successfully to express and purify other similar small transmembrane proteins (Buck *et al.*, 2003). The target protein is expressed as a fusion protein with maltose binding protein (MBP) which aids solubility and allows purification via an amylose affinity column. After purification fusion proteins can be cleaved with TEVP providing a TEVP site has been engineered in-between the MBP and target protein sequences. In pBCL solubility is achieved with guanidium chloride and urea which would inhibit proteases like TEVP and thus requires the use of highly volatile CNBr as a cleaving agent. pMAL is therefore a much safer system than pBCL. PLM was subcloned into the pMAL vector with the TEVP site by Yorkshire Bioscience Ltd. This was transformed into several cell types; BL21 (DE3), Origami, Rosetta and C41 (DE3) and were induced overnight at 37°C. Each cell type was lysed by French Press and spun down to give soluble (supernatant) and insoluble protein (pellet). Results are shown in in Figure 4.7. PLM is approximately

8 kDa whilst MBP is approximately 42 kDa making the fusion protein around 50 kDa. No overexpressed protein appears at this size in any cell type. This is consistent with the difficulties encountered in PLM expression described previously (Thai *et al.*, 2005).

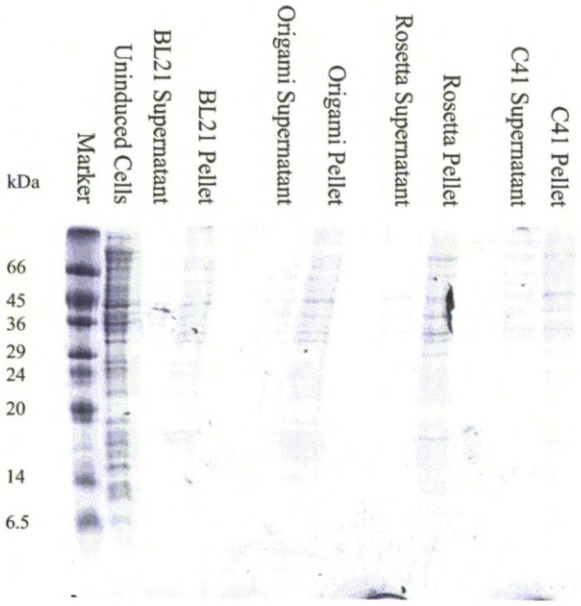

Figure 4.7. Attempted expression of MBP/PLM fusion protein. Lanes show soluble (supernatant) and insoluble (pellet) protein present after inducing with IPTG for 3 hours. No cell type yields any significant level of overexpressed protein (expected ~50 kDa). Low range markers (Sigma) are used as shown.

4.3.3. Transforming pMal/Mat-8 plasmid into *E. Coli*

As PLM proved difficult to express, focus was transferred to another FXYD protein; Mat-8. Although Mat-8 has been expressed by the Marassi group in the pBCL plasmid (Franzin *et al.*, 2007b) the structural data

acquired from it is limited. It also required the mutation of two methionine residues to leucine residues in the transmembrane region to facilitate CNBr cleavage. This is not necessary in the pMAL plasmid when using TEVP cleavage at a highly specific site. Mat-8 expression was therefore attempted in the pMal plasmid after the difficulties of PLM in the same construct.

In standard transformation protocols after transformation occurs there is a growth step in which LB is added to the transformed cells before incubating for an hour at 37°C. These cells in LB are then plated out and grown overnight. After several attempts with this method using the pMal plasmid containing Mat-8 and making fresh competent cells no colonies formed despite the control plates with no ampicillin showing high growth. An extra centrifugation step was thus added after the growth step. The pelleted the cells were resuspended in a small volume and plated out, effectively increasing the concentration of cells spread onto the agar plate. This proved a successful step as suitable colonies formed. These colonies were selected for expression. Cell stocks of these colonies were produced. However these cell stocks failed to grow when added to fresh LB with ampicillin. The difficulty of transformation and the unreliability of cell stocks suggest bacterial cells reject the pMal plasmid containing Mat-8. Nevertheless by transforming directly prior to each expression, MBP/Mat-8 fusion protein can be successfully overexpressed as will be shown later.

4.3.4. Expression and purification tests of MBP/Mat-8 fusion protein

The ideal expression conditions depend on many factors, one of which is the sequence of the protein itself. This means that to overexpress a given protein, an ideal set of expression conditions will need to be determined that will optimise protein expression in the system selected. This is achieved by first trying different expression conditions on a small scale, determining which conditions are best then scaling up to larger volumes capable of producing milligram quantities of protein. The Mat-8/MBP fusion protein transformed into BL21 (DE3) cells underwent several of these expression tests to optimise yield. Tests were initially performed in LB, which is much richer than minimal media and usually yields more protein. The first tests covered temperature of expression and time of induction. Cells were all grown at 37°C until they reached an OD of 0.7-1.0. This is the point at which cells were induced with IPTG. At this point cells will have just begun their stationary phase (Figure 4.8.). Inducing earlier would have the cells in exponential growth phase so media and energy of the cells would be wasted. Inducing cells too late will put them in death phase where cell numbers will start to reduce, thus reducing potential levels of protein. Upon induction bacterial cells were split into three incubators operating at different temperatures; 18°C, 25°C and 37°C. The optimal temperature for bacterial growth is 37°C although reducing temperature is, in some cases, favourable as this slows down expression

and increases protein solubility. Samples were taken from the bacterial cultures at each temperature at three different time points: 3 hours, 5 hours

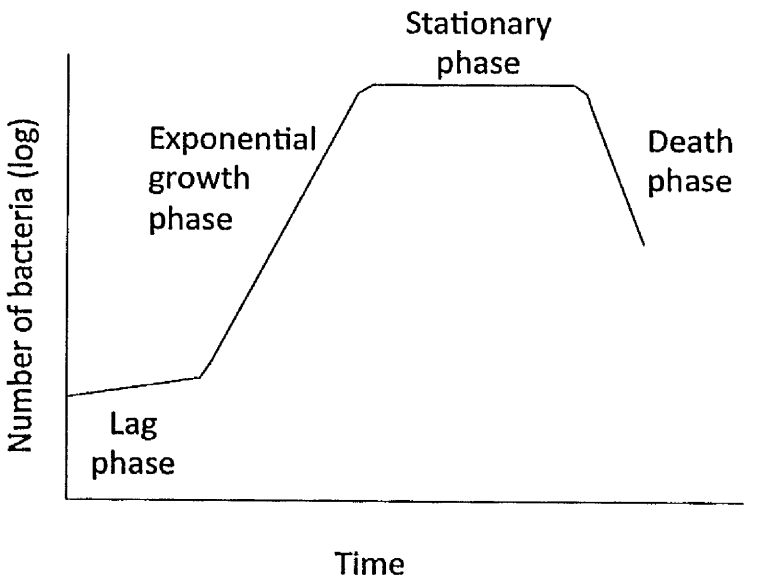

Figure 4.8. Growth phases of bacteria. In a bacterial culture, cells undergo four phases. Initially at the lag phase growth is slow, while cells adjust to the new conditions. This is followed by an exponential growth phase where bacteria rapidly multiply. At a saturation point cells then enter stationary phase where no growth occurs. When nutrients begin to be exhausted cells enter death phase in which cells begin to die allowing their nutrients to be used by the remaining living cells.

and overnight. Certain proteins can begin to degrade or become insoluble at higher concentrations so allowing expression overnight is not always desirable. The cell samples were lysed by sonication and centrifuged to separate soluble and insoluble protein. The 15% SDS-PAGE gels of each

of the three induction temperatures (18°C, 25°C and 37°C) at the four time points (3 hours, 5 hours, 7 hours and overnight) are shown in Figure 4.9. At each time point the soluble (supernatant) and insoluble (pellet) protein is shown and the intact pre-lysis cells (whole cells) and pre-induction cells (uninduced) are included for comparison. A box indicates the location of the MBP/Mat-8 fusion protein on the SDS-PAGE gel. This is around 50 kDa, a combination of MBP (42 kDa) and Mat-8 (8 kDa). Each whole cell sample contains overexpressed MBP/Mat-8 fusion protein but when cells are lysed the majority of protein is insoluble as it is found in the pellet. Cooler temperatures (i.e. 18°C and 25°C) yield less protein as expected but the potential gain of improved fusion protein solubility is not observed. Therefore, 37°C was selected as the optimal expression temperature. At 37°C, longer induction times simply result in increased insoluble protein as each soluble sample (supernatant) at this temperature looks very similar whilst the insoluble samples (pellet) show increased fusion protein over time. A 3-hour induction time was selected as a result.

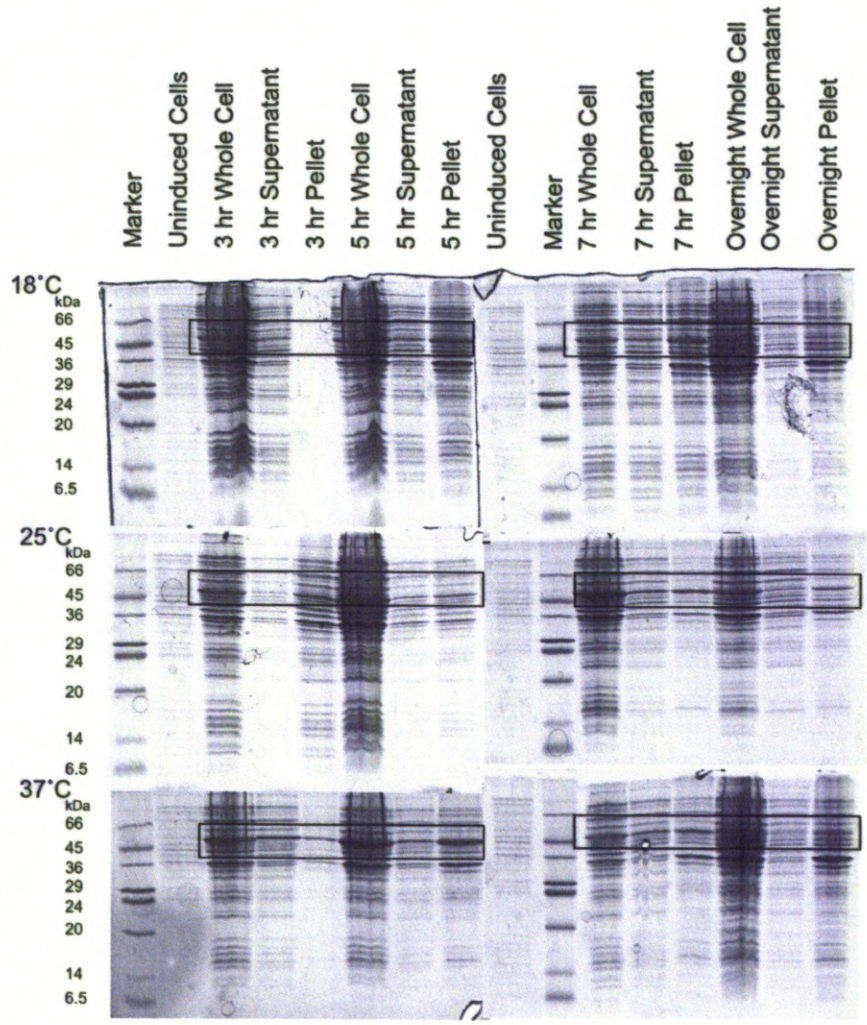

Figure 4.9. Expression tests to determine ideal time and temperature conditions for expression of Mat-8/MBP fusion protein. Expression was carried out at 18°, 25° and 37°C in LB. with samples taken at different induction times. The fusion protein of interest is ~50 kDa and is indicated by the boxes. Supernatants contain soluble protein and pellets contain insoluble protein. Whole cells are all proteins produced post induction and uninduced all proteins pre-induction. Low range markers (Sigma) are used in all gels as shown.

IPTG concentration can also affect the solubility of expressed protein by reducing the rate of expression. Therefore further expression tests altering IPTG concentration at time of induction were carried out. Four different IPTG concentrations were tested (0.25 mM, 0.50 mM, 0.75 mM and 1.0 mM), inducing at 37°C for 3 hours. The 15% SDS-PAGE gels of each of these IPTG concentrations are shown in Figure 4.10. At each concentration of IPTG the soluble (supernatant) and insoluble (pellet) protein is shown with intact pre-lysis cells (whole cells) and pre-induction cells (uninduced) included for comparison. A box indicates the location of the MBP/Mat-8 fusion protein on the SDS-PAGE gel. Total fusion protein (whole cell) increases with higher IPTG concentrations. However when these cells are lysed more soluble fusion protein (supernatant) is expressed at lower IPTG concentrations. 0.25 mM IPTG was therefore selected for induction.

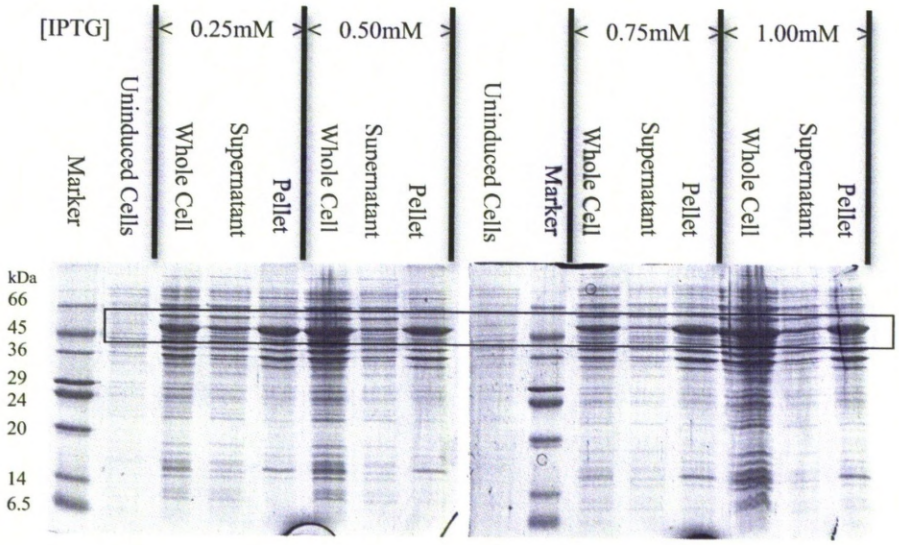

Figure 4.10. Expression tests to determine ideal IPTG concentration. IPTG concentrations of 0.25, 0.50, 0.75 and 1 mM were tested inducing at 37°C for 3 hours. The fusion protein of interest is ~50 kDa and is indicated by the box. Supernatants contain soluble protein and pellets contain insoluble protein. Whole cells are all proteins produced post induction and uninduced all proteins pre-induction. Low range markers (Sigma) are used in all gels as shown.

Although selecting the best induction time, induction temperature and IPTG concentration appeared to improve fusion protein solubility, it was clear that there was still a lot of protein expressed in an insoluble form. Therefore the detergent Triton X-100 ® (TX-100) was incorporated into the lysis buffer to see if it could improve fusion protein solubility. Purification tests were performed with and without TX-100 (0.5%) in the column buffer used to resuspend the cells before lysis and throughout the amylose column purification procedure. Fusion protein was expressed at

the determined optimal conditions (3 hour expression time 37°C, 0.25 mM IPTG) both with and without TX-100 at 0.5% (v/v). The soluble protein (supernatant) was added to a small amount of amylose resin, to which the MBP fusion protein would be expected to bind, and washed with buffer. The washed resin and expression samples were observed on a 15% gel (Figure 4.11). There is a more intense fusion protein band (indicated by box) present in the supernatant (soluble protein) when TX-100 is used in the column buffer in which cells are resuspended which suggests TX-100 aids solubility. Importantly, when supernatants are added to amylose resin there is more fusion protein bound in the presence of TX-100 than in a TX-100-free environment (amylose resin lanes) which suggests TX-100 could improve yield of purified protein when scaled up to a full amylose column as it increases solubility without affecting binding to amylose resin.

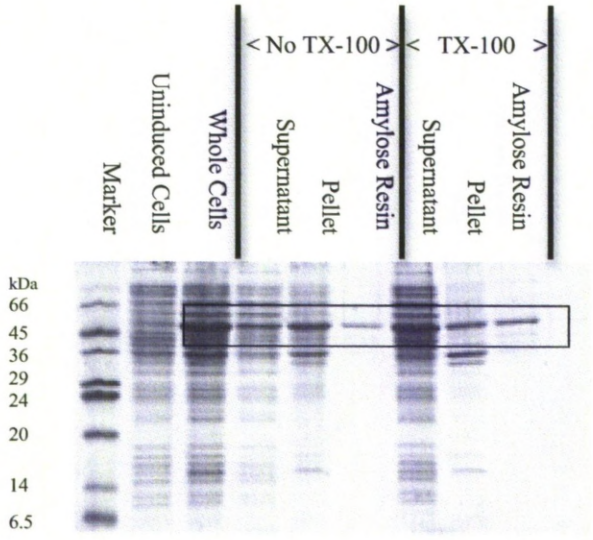

Figure 4.11. Purification tests with and without TX-100. Purification tests with and without TX-100 (0.5% v/v) were performed in order to determine if it would aid protein solubility. The fusion protein of interest is ~50 kDa and is indicated by the box. These expression tests were taken further by adding soluble protein to amylose resin to determine whether the fusion protein would bind to the amylose column. Low range markers (Sigma) are used as shown.

To determine the optimal TX-100 concentration required to extract soluble fusion protein from the cells, further small-scale experiments were performed. The optimal conditions were used again and four TX-100 concentrations were tested: 0.25%, 0.5%, 0.75% and 1% (v/v). Soluble protein produced in these conditions was observed on a 15% gel (Figure 4.12.). The box highlights the position of the fusion protein and this indicates 0.5% (v/v) gave improved solubility over 0.25% TX-100 and

comparable solubility to 0.75% and 1.0% TX-100, therefore 0.5% TX-100 was selected for full scale expression.

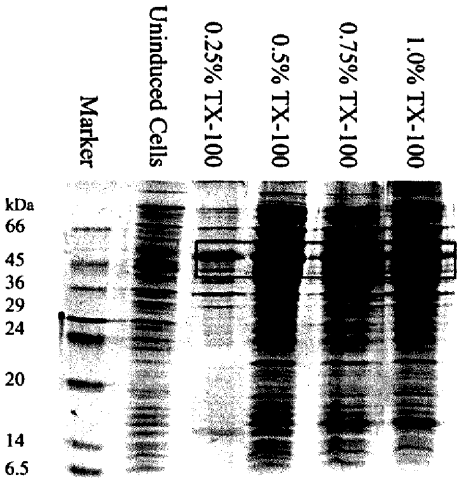

Figure 4.12. Purification tests with various TX-100 concentrations.. The samples shown here are soluble protein samples with TX-100 concentrations 0.25%, 0.5%, 0.75% and 1.0% (v/v) in the buffer. The fusion protein of interest is ~50 kDa and is indicated by the box Low range markers (Sigma) are used as shown.

4.3.5. Full scale expression/purification of MBP/Mat-8 fusion protein in LB

With expression conditions determined on a small scale these same conditions were scaled up to a full 1-litre preparation. Samples were collected at key stages of expression and purification and were analysed in a 15% SDS-PAGE gel (Figure 4.13.) The box indicates the location of the fusion protein. Good levels of expressed soluble protein are observed as indicated by the intense fusion protein band in the supernatant sample. This

soluble protein was allowed to bind to resin overnight before the eluent was collected (flow through). There is a fusion protein band in the eluent which suggests not all fusion protein binds to the resin possibly because of denaturation by the detergent. Buffer washes contain very little fusion protein but several other bands indicate the removal of protein impurities. After these wash steps, a sample of the amylose resin was taken which indicates a large amount of fusion protein has successfully bound to the column. This fusion protein was eluted with elution buffer and can be seen in the eluted protein lane. A sample of the resin after elution revealed protein was still bound to the amylose column so the elution was repeated with fresh elution buffer (as indicated by 2^{nd} eluted protein) and another post elution resin sample reveals virtually no protein was left bound to the column.

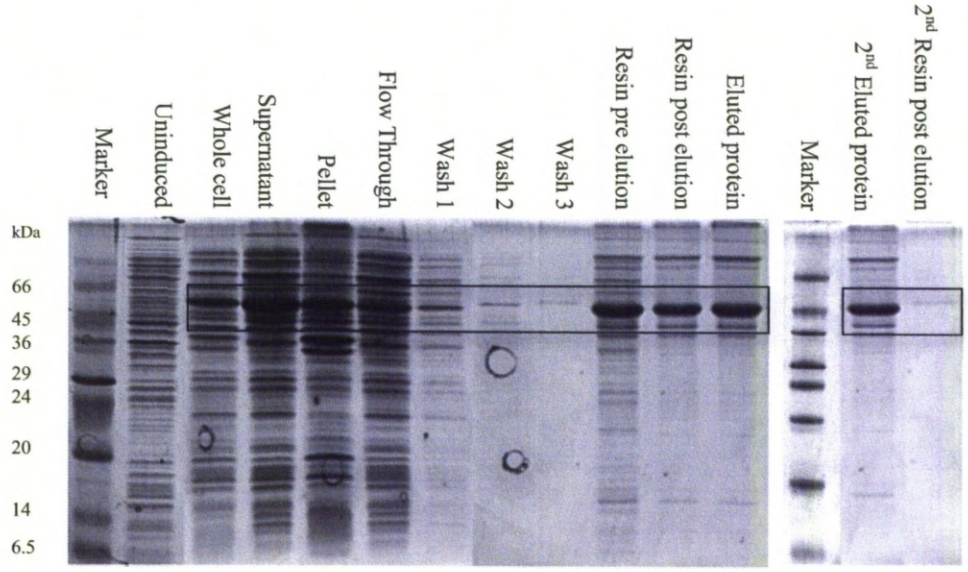

Fig 4.13. Full scale expression and purification of MBP/Mat-8 fusion protein. The fusion protein was expressed in 1 L of LB and run through an amylose column before being eluted with elution buffer. The fusion protein of interest is ~50 kDa and is indicated by the boxes. Supernatants contain soluble protein and pellets contain insoluble protein. Whole cells are all proteins produced post induction and uninduced all proteins pre-induction. Samples of flow through and wash steps are shown as well as protein bound to the resin before and after adding elution buffer. The elution step was repeated as not all fusion protein was eluted (indicated as 2nd eluted protein) Low range markers (Sigma) are used in both as shown.

With successful expression and part purification established, Mat-8 needed to be cleaved from MBP in the fusion protein. This was done with TEVP which recognised the specific sequence in between MBP and Mat-8 in the fusion protein. To determine an optimal TEVP concentration for maximal fusion protein cleavage, small scale cleavage experiments were performed

on amylose column purified fusion protein. Figure 4.14 shows a 10% SDS-PAGE gel (for improved separation to make the difference between fusion protein and MBP clear), of various concentrations of TEVP added to the purified fusion protein and incubated overnight at room temperature. At this percentage gel Mat-8 is expected to run off the gel. Cleavage appears to be successful as the intensity of the fusion protein band reduces whilst the intensity of the MBP band (42 kDa) increases with increased TEVP concentration. Maximal cleavage is achieved at 250 μg/mL as the ratio of the intensity of MBP:fusion protein does not improve beyond this point. The extent of cleavage is monitored by the MBP band as the Mat-8 band is not clearly visible on the gel as it does not stain particularly well due to its small size.

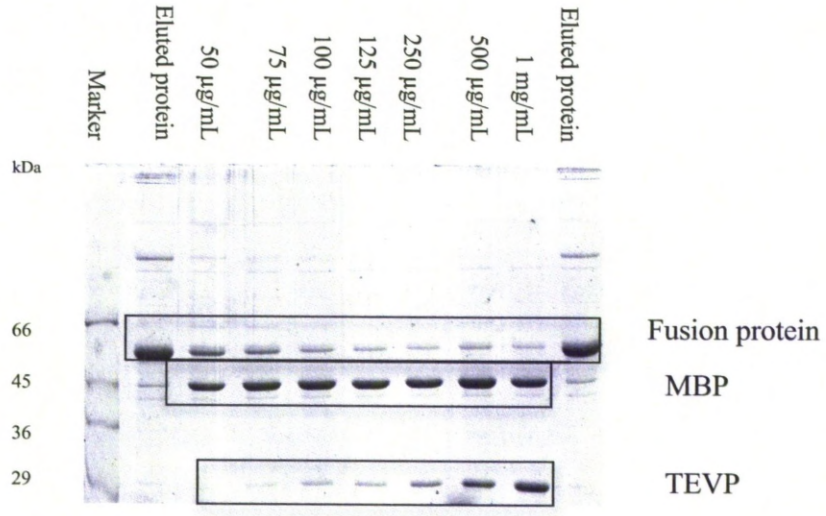

Fig 4.14. Determination of optimal TEVP concentration for maximal MBP/Mat-8 fusion protein cleavage. Pilot cleavage tests were performed on the amylose column purified fusion protein, varying concentration of TEV protease which can be seen at the bottom of the gel. The concentration of TEV is shown above the gel and eluted protein is treated with no TEV. Cleavage was carried out overnight at 4 °C. Separation was carried out on a 10% acrylamide gel. The fusion protein, MBP and TEVP are indicated by boxes. Low range markers (Sigma) are used as shown.

Following cleavage, Mat-8 needed to be purified from MBP, TEVP and other impurities. This was first approached by attempting to cleave the fusion protein when it was still bound to the amylose column. The principle behind this was to omit the elution step following resin binding and buffer washes and instead resuspend the amylose resin in column buffer containing 250 µg/mL TEV protease and incubate at room

temperature overnight before returning the resin back to the gravity column. Cleaved MBP and other impurities should remain bound to the resin whilst TEVP and Mat-8 should now be eluted. The 15% SDS-PAGE in Figure 4.15 shows that although the elution appears to contain Mat-8 it also contains a large quantity of MBP and fusion protein suggesting at some point in this process MBP and fusion protein lost affinity for the amylose column and therefore co-eluted with Mat-8. The eluted protein was therefore applied to a packed column with fresh amylose resin. Figure 4.15. also shows the elution from the rebuilt column and shows the process reduces the quantity of MBP and fusion protein but only to a small extent.

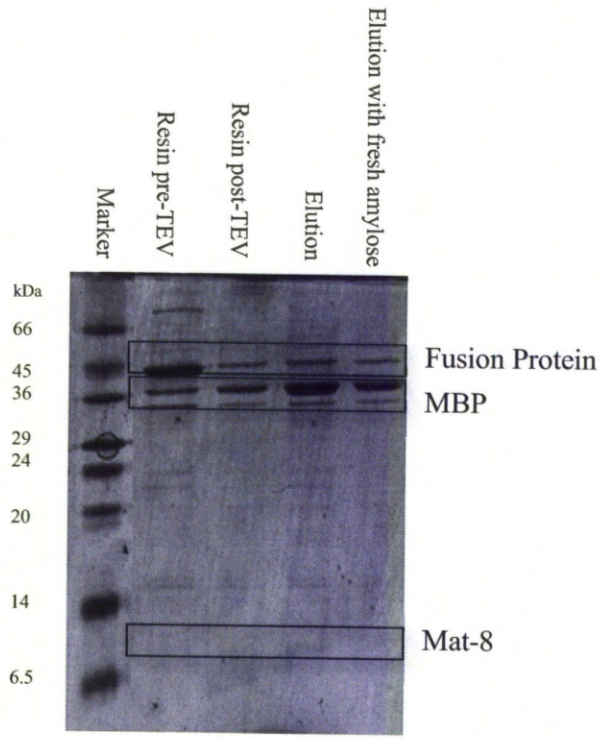

Fig 4.15. Cleavage of MBP/Mat-8 fusion protein in presence of amylose resin. Following fusion protein resin binding and buffer washes, amylose was resuspended in column buffer containing TEVP to attempt an on column cleavage . A faint band at around 8 kDa (the size of Mat-8) is visible in the cleaved elution. Also present is MBP and fusion protein Low range markers (Sigma) are used as shown.

The second approach to separating MBP and fusion protein after cleavage was by using dialysis to remove TX-100. MBP is a water soluble protein whilst Mat-8 requires detergent for solubility. By removing the TX-100 by dialysis it was hoped that MBP would remain in solution whilst Mat-8 would precipitate allowing removal by centrifugation. Dialysis tubing with

a 3 kDa cut off was used in order to retain Mat-8 in the tubing. The amylose column purification was performed and the eluted protein was cleaved with TEVP then dialysed into column buffer containing no TX-100. The buffer was replaced after four hours with fresh buffer twice to promote movement of TX-100 out of the dialysis sample. The contents of the dialysis tubing were centrifuged (19,000 rpm, 4°C, 30 mins) and the supernatant and pellet were run on an SDS-PAGE gel (Figure 4.16). The pellet was very small and contained Mat-8 and all impurities with most protein remaining in the supernatant including Mat-8. This suggests that only some TX-100 was removed by dialysis which caused some protein to precipitate. Not only is this method inefficient for detergent removal but the precipitated protein still contains large quantities of impurities, although the purity of Mat-8 is enhanced as seen from the increased relative intensity of the Mat-8 band compared to the supernatant after dialysis.

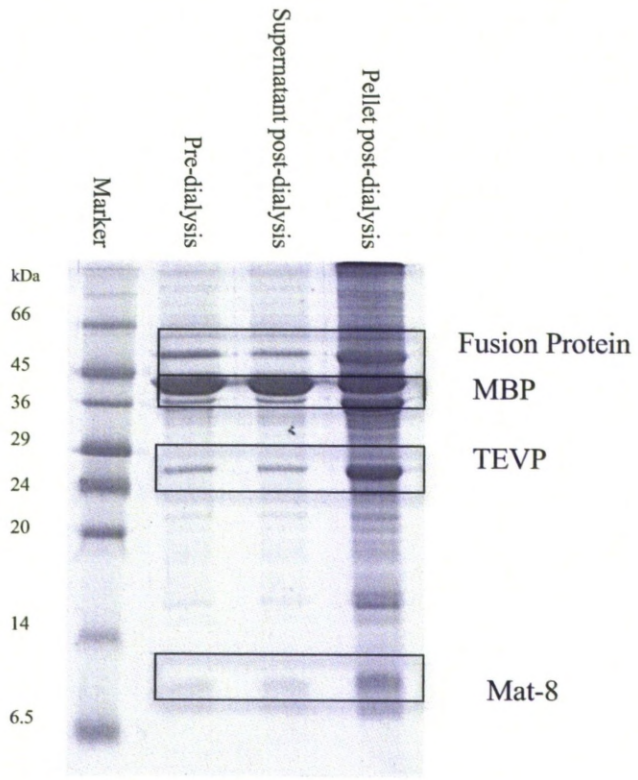

Fig 4.16. Dialysis of cleaved MBP/ Mat-8 fusion protein to remove TX-100. Eluted fusion protein contained 0.5% TX-100 in column buffer and was cleaved with TEVP. This was dialysed into column buffer with no TX-100. Fusion protein, MBP, TEVP and Mat-8 are indicated by boxes. The pellet was very small and both supernatant and pellet contained Mat-8 and all impurities Low range markers (Sigma) are used as shown.

A third approach for purifying Mat-8 involved an alternative method of removing detergent by chloroform/methanol precipitation (CMP). CMP is a method for protein precipitation that has proved particularly effective at removing TX-100 (Wessel and Flügge, 1984). Methanol, protein sample (30 mL) and chloroform are mixed at a 4:1:1 ratio. At this point the

solvents, TX-100 and protein can all associate with each other. By addition of water, a phase separation is induced as methanol is able to associate with water in the aqueous phase whilst the density of chloroform means it forms an organic phase below this. TX-100 is particularly soluble in chloroform so is pulled down into the organic phase whilst water molecules associated with protein are displaced by methanol causing them to precipitate in the aqueous phase. Centrifugation causes the precipitated proteins to pellet in the interphase between the aqueous phase and organic phase. Small membrane proteins are soluble in methanol and not water so it was hypothesised that Mat-8 would remain in the aqueous phase whilst impurities would precipitate in the interphase. The 15% SDS-PAGE gel Figure 4.17. shows both the organic phase and aqueous phase and the precipitated protein in the interphase. It appears that all proteins are precipitated in the interphase suggesting Mat-8 requires a higher percentage of methanol than is present in the aqueous phase for solubility.

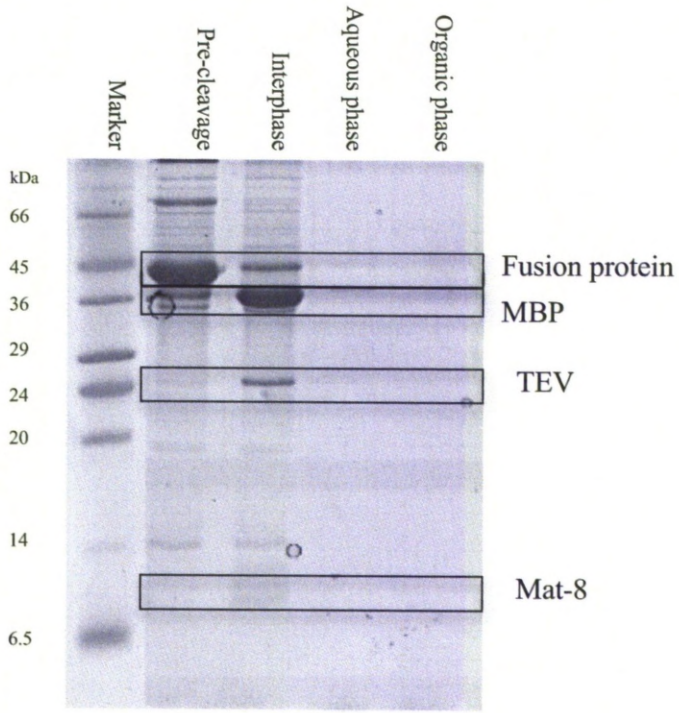

Fig 4.17. Chloroform Methanol Precipitation of TEVP cleaved MBP/Mat-8 fusion protein. Eluted fusion protein underwent chloroform methanol precipitation. Virtually all protein is present in the interphase. Fusion protein, MPB and Mat-8 are indicated by arrows. Low range markers (Sigma) are used as shown.

Although chloroform methanol precipitation did not give the desired result it did precipitate all the protein which suggests that the majority of TX-100 had been removed. The precipitated Mat-8 protein with impurities from chloroform-methanol precipitation was dissolved in aqueous 7M guanidium chloride and run on reverse-phase HPLC with an acetonitrile gradient which separates proteins by hydrophobicity. The HPLC trace can

be seen in Figure 4.18. which reveals two clear peaks (a and b) after the guanidium hydrochloride peak.

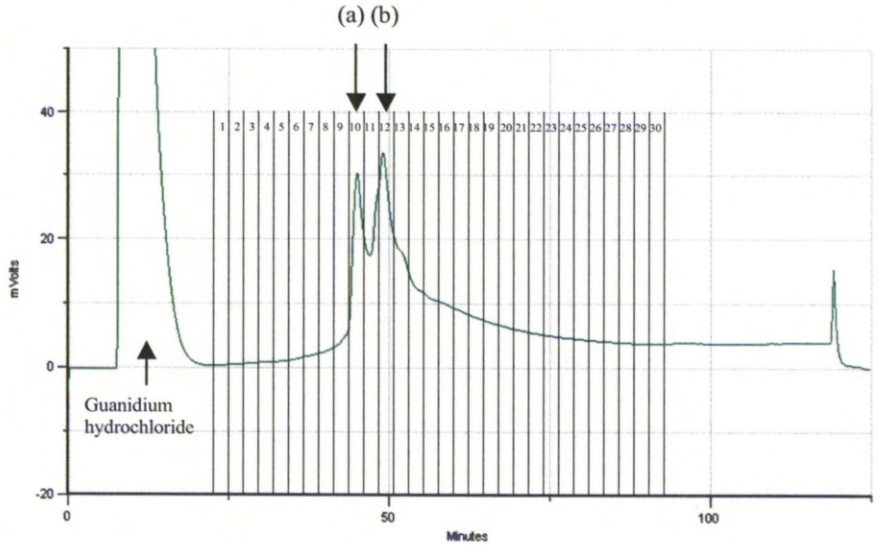

Figure 4.18. HPLC trace of chloroform/methanol precipitated sample. This trace shows different peaks over an acetonitrile gradient (from 5 to 95%). The first peak is truncated due to its high intensity and is due to the guanidine present in the buffer. The second peak is Mat-8 and the third peak has all other impurities including uncleaved fusion protein, MBP, TEV and other unidentified proteins that coeluted from the amylose column with the fusion protein and are found in many fractions. Mat-8 eluted at around 40% acetonitrile.

Fractions were collected from 23 minutes into the run as this is where protein began to be eluted. The first ten fractions were combined and lyophilised which incorporate the first peak (a) shown in Figure 4.18. The yield of Mat-8 per litre of LB expression was determined to be 2.1 mg

according to the microbalance. Figure 4.19. shows these combined lyophilised fractions and subsequent lyophilised fractions on a 15% SDS-PAGE gel. Peak (a) appears to correspond to Mat-8, indicating that the protein has been successfully purified.

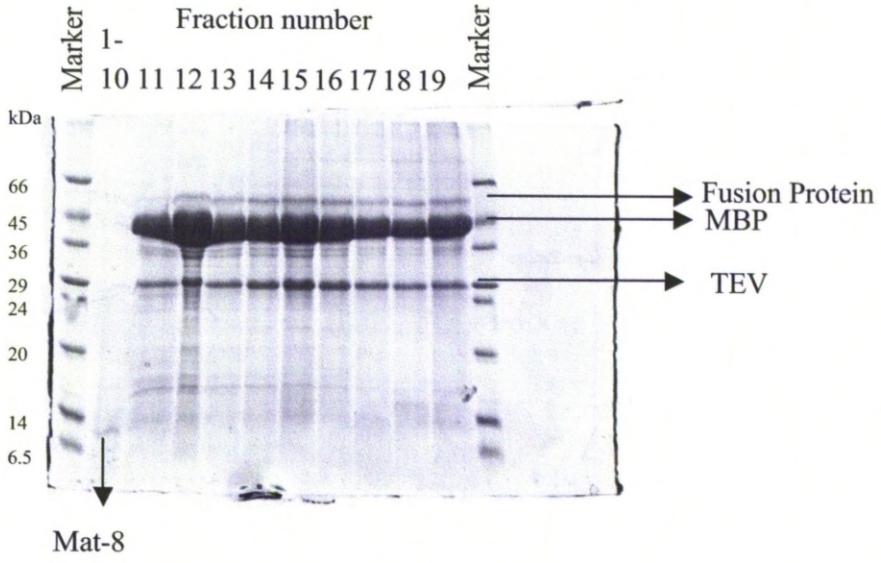

Figure 4.19. SDS-PAGE of HPLC fractions to purify Mat-8. This SDS-PAGE shows how proteins have separated over the acetonitrile gradient. In this run Mat-8 has separated from other impurities. Fraction numbers correspond to the HPLC trace on Figure 4.18. Low range markers (Sigma) are used as shown.

To confirm the identity of Mat-8 a dot blot analysis of each of the HPLC fractions was performed using a specific Mat-8 antibody and fractions from a HPLC run. Figure 4.20 shows the result from fractions 7-13 which incorporates the two main peaks. As indicated by the HPLC trace (Figure 4.19.), fraction 10 gives the most intense dot suggesting this fraction has

the highest concentration of Mat-8. Fraction 9 and 11 contain a lower concentration of Mat-8 indicated by less intense dots. This correlates with the HPLC trace as the height of the peak is lower at these fractions. A positive control using the synthetic peptide Mat-8sf$_{38-68}$ which represents the cytoplasmic region of Mat-8 and a negative control using the synthetic peptide PLM$_{38-72}$ which represents the cytoplasmic region of PLM confirm the antibody is specifically binds to Mat-8.

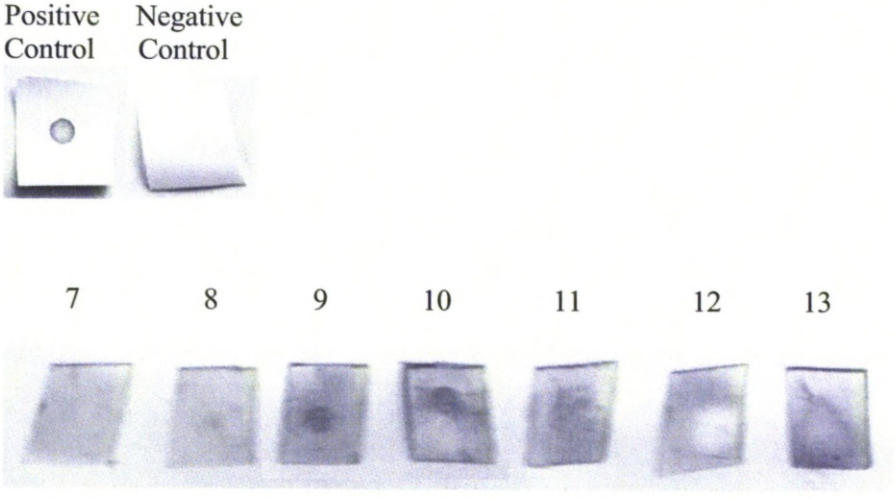

Figure 4.20. Dot Blot of HPLC fractions. Purification was confirmed by performing a dot blot using primary Mat-8 antibody. From left to right the squares represent HPLC fractions incorporating peak (a). (Figure 4.18.) SDS-PAGE of fractions 10-13 is shown in Figure 4.19. The highest concentrations of Mat-8 are in 9th and 10th fraction which suggests peak (a) results from Mat-8 according to the HPLC trace. Positive control using synthetic cytoplasmic Mat-8 peptide and negative control using synthetic cytoplasmic PLM peptide are shown.

4.3.6. Full scale expression/purification of MBP/Mat-8 fusion protein in minimal media

After establishing ideal expression conditions in LB the expression media was then changed to minimal media. Minimal media can be prepared with [^{13}C] glucose and [^{15}N] ammonium chloride, which will uniformly isotopically label proteins suitable for analysis by NMR. The full-scale 1-litre expression conditions used were identical to those for growing in LB until the point of induction where cells were centrifuged (8,000 g, 10 minutes, 4°C) and resuspended in the same volume of minimal media. 15% SDS-PAGE analysis (Figure 4.21.) indicated that there was seemingly no overexpressed protein. A further full-scale experiment was repeated using vitamin and mineral supplements (Buck *et al.*, 2003) to create supplemented minimal media that has been shown to increase protein yield in the same construct with another small transmembrane protein PLB. This did successfully produce an overexpressed band on the gel but it was much less intense than observed in LB (Figure 4.13.). Finally the cell line was changed to C41, which was developed for expressing toxic and membrane proteins (Miroux and Walker, 1996). This bacterial strain gave good levels of overexpression and so Mat-8 was purified in isotopically labelled minimal media using the methods established previously in LB.

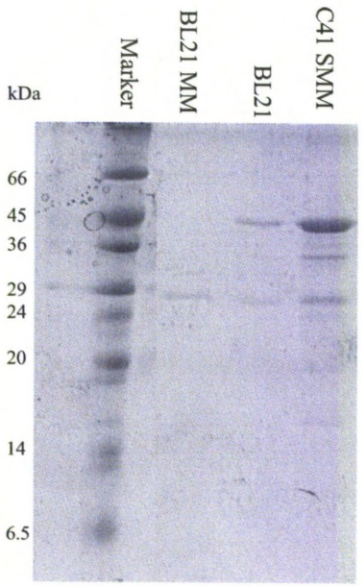

Figure 4.21. Comparison of minimal media expression of MBP/Mat-8 fusion protein in different cell lines. Lanes show protein present bound to the amylose column after overnight binding. MM is expression in minimal media and SMM is in supplemented minimal media. C41 cells are clearly preferable over BL21. Wide range markers (Sigma) are used as shown.

In order to analyse Mat-8 by NMR it must be incorporated into a lipid bilayer to represent its native environment as a membrane protein. This was performed by a process called reconstitution using established methods (Li *et al.*, 1999; Smith *et al.*, 2001). Mat-8 and 2:1 DMPC:DOPG was dissolved in 50:50 chloroform methanol. The chloroform dissolves the lipid whilst the methanol dissolves Mat-8. Whilst the lipid and Mat-8 are in solution bilayers containing Mat-8 are formed. After the reconstituted

samples are dried they can be analysed by NMR. Unfortunately this did not produce a signal on NMR suggesting the yield was not substantial enough. The methods to express and purify Mat-8 are successfully in place however further work needs to be done to improve final yield of fully labelled Mat-8.

4.4. Discussion

Expression and purification of membrane proteins is notoriously difficult and is highlighted by the difficulties presented in this chapter. FXYD proteins have proved particularly difficult to express and purify even in comparison to other membrane proteins (Thai *et al.*, 2005). A successful method for expression and purification of FXYD proteins for analysis by NMR has been established with the pBCL construct (Thai *et al.*, 2005). This involves expressing a fusion protein of a modified BCL protein and the FXYD protein of interest. The modified BCL causes the fusion protein to be expressed as an inclusion body which can be solubilised before cleaving the FXYD protein moiety from the modified BCL by CNBr cleavage. CNBr cleavage is not a desirable method as it has a high risk and a large number of safety precautions must be considered. After attempting to recreate the pBCL method (Figure 4.6.), trials were carried out with a new expression system which expresses and purifies FXYD proteins in a soluble form as a fusion protein with MBP. In this method MBP is cleaved

from the FXYD protein using TEVP that recognises a specific site engineered between the MBP and the FXYD component of the fusion protein. This is a much safer method than CNBr cleavage. Unfortunately, it was not possible to overexpress PLM in significant quantities (Figure 4.7.) despite testing a range of cell strains, including C41 cells which have been developed specifically for the expression of toxic proteins. Indeed, PLM has been reported to be particularly difficult to express (Thai *et al.*, 2005) with the pKSI and pTLE expression systems having poor levels of overexpressed PM fusion proteins. It is possible PLM is too toxic for any cell type in this construct. Expression of Mat-8 with this system produced results which were much more positive (Figure 4.9.). Mat-8 was expressed on a small scale at temperatures of 18, 25 and 37°C and induction times of 3 hours, 5 hours, 7 hours and overnight. Lower temperature usually yields less protein but can often aid solubility. The solubility of Mat-8 is not noticeably affected by temperature so was expressed at 37°C which yields the most protein. Expression was also stopped after only 3 hours as after this time all additional expressed protein was expressed in an insoluble form. Reducing IPTG concentration to 0.25 mM resulted in less total protein but improved solubility further (Figure 4.10.). This suggests that by expressing MBP/Mat-8 fusion protein slowly, the solubility increases. Purification of MBP/Mat-8 fusion protein proved far more difficult than expression. Whilst the amylose column successfully removed the majority of impurities (Figure 4.13.) the problem of separating Mat-8 and MBP

arose. This was made more complex by the requirement of TX-100 (Figure 4.12.) to keep the MBP/Mat-8 fusion protein soluble. Protein can either be eluted from the column as a fusion protein prior to cleavage or cleavage is carried out on the column. An attempt was made to cleave Mat-8 from MBP prior to elution. Theoretically Mat-8 should then elute from the column whilst MBP remains bound to the amylose. This was not successful as MBP apparently co-eluted with Mat-8 (Figure 4.15.). MBP appears to lose affinity for amylose post cleavage, possibly due to a denaturing effect. This appears to occur after cleavage as the MBP/Mat-8 fusion protein has a strong affinity for amylose.

Following the issues of cleaving the fusion protein on-column, the fusion protein was instead eluted with maltose prior to cleavage.Dialysis from buffer with TX-100 to TX-100-free buffer was attempted using dialysis tubing with a 3 kDa cut off to try and remove enough TX-100 monomers. These should pass through the membrane as they have a molecular weight of 647 Da, this causes Mat-8 to precipitate. This did yield a very small pellet with an improved ratio of Mat-8:impurities however Mat-8 still remained in solution even after 3 buffer changes (Figure 4.16.). As a TX-100 concentration of 0.5% (v/v) was used to solubilise MBP/Mat-8 fusion protein, which is above the 0.02% critical micelle concentration (CMC) of TX-100 it is no surprise dialysis proved ineffective as the molecular weight of the micelles is 90 kDa much higher than the 3 kDa cut off.

Chloroform methanol precipitation is a method of precipitating proteins which is particularly effective with TX-100 and membrane proteins (Wessel and Flügge, 1984). In this method proteins are precipitated in an interphase between a lower organic phase (chloroform) and an upper aqueous phase (methanol and water). It was hoped that Mat-8 would remain in the aqueous phase by being solubilised in methanol. However Mat-8 was precipitated at the interphase together with all the impurities (Figure 4.17.). This is probably due to the high percentage of water in the aqueous phase which results in membrane protein insolubility therefore the percentage methanol was not high enough to keep Mat-8 soluble. Despite the failure to separate Mat-8 from other protein impurities this method did result in the removal of the majority of TX-100 allowing the proteins to precipitate. By dissolving the precipitated proteins in guanidium chloride, Mat-8 could be successfully purified via reverse phase HPLC (Figure 4.18.) with a final yield of 2.1 mg per litre of LB expression.

Having established a working method following expression in LB, it was necessary to repeat the work in minimal media in order to produce labelled protein for NMR. Initially this failed to overexpress the MBP/Mat-8 fusion protein. Supplementing the minimal media with vitamins and minerals has improved expression of a similar small transmembrane protein PLB previously (Buck *et al.*, 2003) but in this case it only generated a small

quantity of overexpressed protein (Figure 4.21.). By using the C41 cell strain, overexpression levels were vastly improved (Figure 4.21.). C41 cells have been developed specifically for the expression of toxic proteins and membrane proteins (Miroux and Walker, 1996). Despite the improvement in yield there was still not sufficient protein produced following purification to produce an adequate NMR signal for structural studies.

Despite the insufficient yield in minimal media for NMR experiments, Mat-8 has been successfully expressed and purified in LB. The minimal media yield could be improved if time was available. This opens possibilities of future experiments on full length Mat-8 for example co-reconstituting Mat-8 with the Na^+, K^+-ATPase and observing the effect on activity with Na^+ activation curves. Truncated forms of Mat-8 could be studied where by the cytoplasmic or extracellular regions could be removed in order to see the effect on function. Ultimately, improving this method to produce sufficient labelled protein would be desirable. Possible future experiments could include attempting different cell strains, trying different detergents with a lower CMC that will be better suited for removal by dialysis or finding alternative chloroform methanol precipitation methods without phase separation to purify Mat-8 by precipitation (Hu *et al.*, 2007).

Chapter 5

5.1. Structural and Bioinformatical Studies of FXYD proteins

Chapter 4 highlighted the difficulties of expressing and purifying FXYD proteins suitable for analysis by solid-state NMR. There are many other techniques however, that can provide insights into the structure of proteins. In Chapter 3 synthetic peptides were designed with the same amino acid composition of the cytoplasmic regions of FXYD proteins and used to examine the interactions with lipids and effects on Na^+, K^+-ATPase function. This was possible as the cytoplasmic regions of proteins tend to be soluble as they reside in a fluid environment in the cell. This means synthetic peptides can be studied using routine structural methods such Circular Dichroism spectroscopy (CD) and NMR spectroscopy to give information about secondary structure in the cytoplasmic region without having to overcome the solubility difficulties of the full length protein.

Currently the only FXYD proteins to be solved in complex with the Na^+, K^+-ATPase are the γ-subunit of the Na^+, K^+-ATPase in pig (Morth *et al.*, 2007) and FXYD10 of spiny dogfish, which has no mammalian equivalent (Shinoda *et al.*, 2009). Unfortunately neither the γ-subunit of the Na^+, K^+-ATPase nor FXYD10 have a cytoplasmic region. This means that there are no structural data revealing how the cytoplasmic regions of any FXYD proteins interact with the Na^+, K^+-ATPase. Therefore this chapter will use

a bioinformatic approach to model how the cytoplasmic region of PLM interacts with the Na^+, K^+-ATPase. PLM was selected for this study as it was shown to have the strongest interaction with the Na^+, K^+-ATPase in Chapter 3. This will involve using the structure of the Na^+, K^+-ATPase and using current structural data about PLM solved in the absence of the Na^+, K^+-ATPase which is described below.

The first insight into the structure of the cytoplasmic region of PLM was gained by using CD to estimate α-helical content in the cytoplasmic region of PLM by inducing α helical structure in a synthetic peptide representing the cytoplasmic region with TFE (Clayton *et al.*, 2005). Trifluoroethanol (TFE) is known to induce α-helix in synthetic peptides providing they have a natural propensity to do so (Tamburro *et al.*, 1968). This is because TFE is much more basic than water so intramolecular hydrogen bonding in the peptide is increased due to peptide/solvent hydrogen bonding decreasing (Nelson and Kallenbach, 1986). The CD experiments with TFE performed here revealed the cytoplasmic region of PLM was estimated to contain approximately 15% α-helical content (Figure 5.1.).

Solution NMR of full length FXYD proteins in SDS micelles (Franzin *et al.*, 2007a) revealed the secondary structure of full length PLM, CHIF and short form Mat-8 to contain α-helical and random coil regions but no β-sheet (Figure 5.1.). The levels of α-helical content present in the

cytoplasmic region are approximately double that observed in the CD data. It is unclear if this is due to a loss of structure caused by studying a peptide fragment instead of the full length protein or if the highly negatively charged environment of SDS micelles is inducing additional helical content not observed *in vivo*.

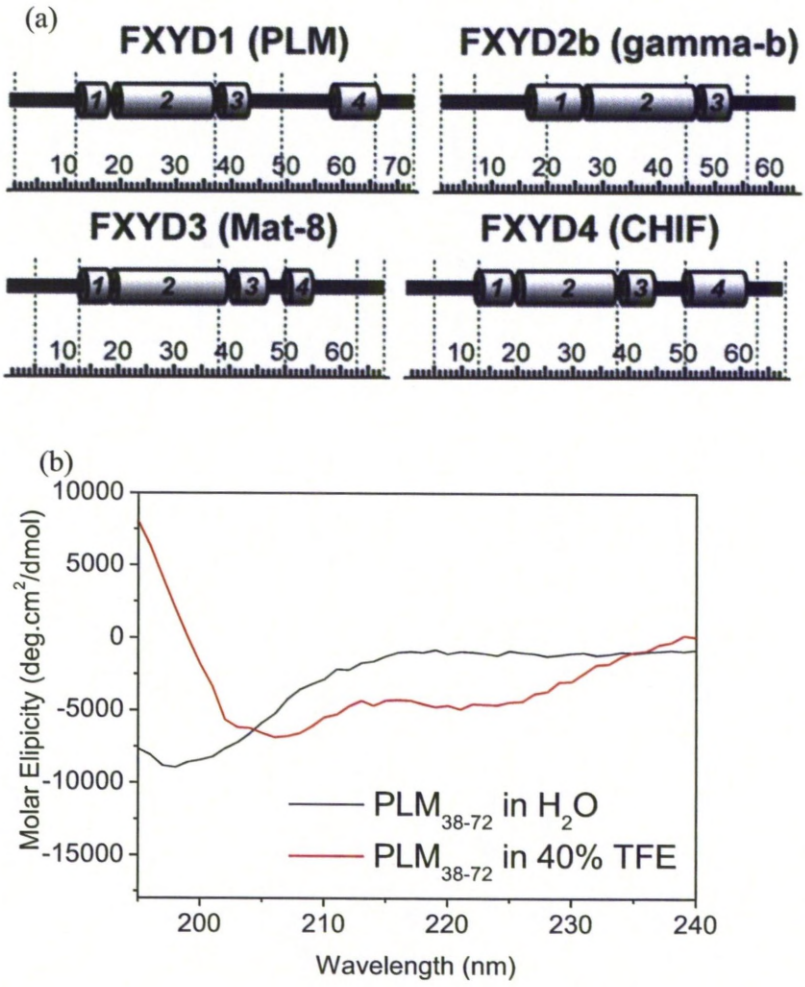

Figure 5.1. α-helical content of FXYD proteins determined by solution state NMR in SDS micelles and CD in H_2O and 40% TFE. Current published data for secondary structure of (a) full-length PLM, Na^+, K^+-ATPase γ-subunit (gamma-b), Mat-8 and CHIF solved by solution-state NMR in SDS micelles (Franzin *et al.*, 2007a) where cylinders indicate α-helix and lines indicate random coil (b) the cytoplasmic region of PLM in water and TFE solved by CD (Clayton *et al.*, 2005).

The 3D structures of human PLM (Teriete *et al.*, 2007) and rat CHIF (Franzin *et al.*, 2007d) have solved by NMR with the proteins solubilised

in SDS micelles in the absence of the Na^+, K^+-ATPase. Due to the homology of the transmembrane region across all FXYD proteins it has been possible to model the Na^+, K^+-ATPase/PLM complex simply by replacing the co-ordinates of the γ-subunit of the Na^+, K^+-ATPase in the pig kidney structure with the co-ordinates of the SDS micelle PLM structure (Teriete *et al.*, 2009). Figure 3.3a. shows this model which suggests the cytoplasmic region of PLM is located in close proximity to both the Na^+, K^+-ATPase cytoplasmic domain and the membrane surface. The same authors paper also showed that phosphorylation of Ser 68 induces significant ^1H and ^{15}N chemical shift changes in helix 4 (Figure 3.3a.) which is located in the cytoplasmic region of PLM, whilst all other chemical shift peaks remain unchanged after phosphorylation. This suggests there is a conformational change of helix 4 induced by phosphorylation of PLM. Figure 3.3b suggests an alternative orientation based on this observation with helix 4 located in close proximity of a negatively charged crevice of the Na^+, K^+-ATPase which leads to the ion binding pocket in the centre of the α-subunit. As the cytoplasmic region of PLM has a net positive charge it could potentially influence a negatively charged crevice which contains conserved acidic residues Asp 813 and Glu 336 that allow the approach of cations but exclude anions through the pump (Reyes and Gadsby, 2006). When just one of these residues has a reversal in charge there is a change from cation to anion selectivity in the whole Na^+, K^+-ATPase channel (Reyes and Gadsby, 2006). This is a

possible explanation for the mechanism of Na^+, K^+-ATPase regulation via phosphorylation of PLM.

This chapter aims to further investigate the limited structural information about the cytoplasmic region of FXYD proteins. CD will be used to determine helical content for the cytoplasmic regions of CHIF and both Mat-8 isoforms to see how they compare to the CD data for PLM. If either of the Mat-8 isoforms are revealed to contain α-helical content by CD they will also be analysed by solution-state NMR in the presence and absence of TFE. CD will also be used to see if lipids induce α-helical content in these due to the binding observed in Chapter 3.

The structure of the cytoplasmic region of PLM will be investigated further. CD experiments in the presence of SDS will be used to determine if SDS induces α-helix to determine the validity of the current structure of PLM (Teriete *et al.*, 2007). Upon this evaluation of the structure of PLM, the possibility of its cytoplasmic region interacting with the Na^+, K^+-ATPase will be further investigated using bioinformatics techniques to identify a putative Na^+, K^+-ATPase –binding motif in the cytoplasmic PLM sequence. The surface of Na^+, K^+-ATPase will also be analysed with bioinformatics to find a conserved and suitable binding region for this motif. These data will be combined to improve the current model of how the cytoplasmic region of PLM might dock into the Na^+, K^+-ATPase in two

different conformations determined by phosphorylation (Teriete *et al.*, 2009).

5.2. Materials and Methods

5.2.1. Materials

Phospholipids were purchased from Avanti® Polar Lipids Inc. Peptides were purchased from Peptide Protein Research Ltd. and were designed to represent the cytoplasmic regions of PLM (Figure 3.1.), short form Mat-8 (Figure 3.2.) and CHIF (Figure 3.5.). Peptides designed to represent the cytoplasmic region of the long form Mat-8 (Figure 3.2.) were purchased from GenicBio Biotechnology Ltd. All other materials were supplied by Sigma.

5.2.2. Preparation of lipid vesicles

See Chapter 3

5.2.3. Circular Dichroism using TFE

Secondary structural measurements with PLM_{38-72} Mat-$8sf_{38-67}$, Mat-$8lf_{38-93}$ or $CHIF_{38-72}$ peptides and the cytoplasmic region of CHIF were carried out by circular dichroism (CD) spectroscopy on a Jasco J-180 spectropolarimeter at 4 °C. Spectra were recorded from 240 to 190 nm using a 0.1 cm cuvette, a scan rate of 20 nm/min, and 4-10 scans per sample. Initial measurements were made on solutions of each of the peptides (100 μM Mat-$8sf_{38-67}$, Mat-$8lf_{38-93}$ or $CHIF_{38-72}$) 10 mM phosphate, pH 7 followed by a stepwise titration with trifluoroethanol

(TFE) to generate measurements at between 10% and 40% (v/v) TFE. The percentage α-helix was calculated using the following equation (Scholtz *et al.*, 1991):

$$\%\, helix = 100\times(\theta_{obs} - \theta_C)/(\theta_H - \theta_C)$$

where $\theta_H = -40000 \times (1 - x/n) + 100T$ and $\theta_C = 640 - 45T$. The quantities θ_H and θ_C represent the molar ellipticity values for 100% α-helix and 100% random coil, respectively, both expressed in deg.cm^2/dmol. The quantity θ_{obs} is the observed molar ellipticity measured at 222 nm, T is the temperature in °C, N is the number of amino acids, and x is a constant set at 2.5, which corrects for non-hydrogen bonded carbonyl groups.

5.2.4. Circular Dichroism in the presence of lipids

In separate experiments the aqueous peptide solutions (100 μM Mat-8sf$_{38-67}$, Mat-8lf$_{38-93}$ or CHIF$_{38-72}$) were measured before and after titrating in SUVs of DMPC and DOPG (in a 2:1 molar ratio) to a final lipid to peptide molar ratio of 100:1. Spectra were recorded from 240 to 190 nm using a 0.1 cm cuvette, a scan rate of 20 nm/min, and 8 scans per sample.

5.2.5. Solution NMR

Two Mat-8lf$_{38-72}$ NMR samples were prepared the first in 5% D_2O and the second in 40% 2,2,2-Trifluoroethanol-d_3 both made to a final volume of 600 µL volume with distilled water. 1D ^{1}H NMR, double-quantum filtered-correlation spectroscopy (DQF-COSY) and nuclear Overhauser effect spectroscopy (NOESY) experiments were performed by Dr. Igor Barsukov. Spectra collected on a 600MHz Bruker spectrometer equipped with TCI cryo probe^{TM}. The number of scans collected for each experiment type were 32 (1D ^{1}H NMR), 16 (DQR-COSY) and 48 (NOESY). All experiments were performed at 20°C and collected with watergate pulse sequence to minimise the intensity of the water peak. The NOESY mixing time was 100 ms.

5.2.6. Bioinformatics

5.2.6.1. Bioinformatic analysis of PLM and long form Mat-8

The potential binding motif was discovered using DiLiMOT (Neduva *et al.*, 2005) which searches several proteins simultaneously for over-represented peptide patterns. Secondary structure was predicted by psipred (Jones, 1999) which analyses the output of a Position-Specific Iterated BLAST (PSIBLAST) (Altschul *et al.*, 1997), with two feed-forward neural networks to predict the secondary structure of the given protein. Disordered regions of PLM and long form Mat-8 were predicted with meta

protein disorder prediction System metaPrDOS (Ishida and Kinoshita, 2008) which uses seven disorder predictors which incorporate several methods to predict disorder including physiochemical properties reflecting amino acid composition such as high-net charge, low hydrophobicity, and/or low sequence complexity.

5.2.6.2. Bioinformatic analysis of the Na^+, K^+-ATPase to determine possible peptide binding sites.

The sequences of the Na^+, K^+-ATPases known to contain FXYD proteins were aligned with MUSCLE (multiple sequence comparison by log-expectation (Edgar, 2004)). The MUSCLE alignment file and the spiny dogfish rectal gland Na^+, K^+-ATPase structure (PDBID: 2ZXE (Shinoda *et al.*, 2009)) was analysed with consurf (Glaser *et al.*, 2003; Landau *et al.*, 2005; Ashkenazy *et al.*, 2010) to determine conserved patches on the surface of the Na^+, K^+-ATPase. Consurf works by using the MUSCLE alignment file to calculate conservation scores and creates a colour coded pdb file to highlight the most and least conserved regions of the protein. Three methods to determine potential peptide binding sites were utilised. The first of these methods is surface triplet propensities (STP) (Mehio *et al.*, 2010) which analyses triplets of adjacent surface atomic groups that can be touched simultaneously by a probe sphere representing a solvent molecule. The second method used was InterProSurf (Negi *et al.*, 2007) which analyses the solvent accessible surface area of amino residues of the

protein of interest (spiny dogfish rectal gland Na^+, K^+-ATPase was used) and uses a propensity scale for interface residues and a clustering algorithm to identify surface regions with residues of high interface propensities which are therefore likely candidates for peptide binding. The final method used was meta-PPSIP (Qin and Zhou, 2007) which combines three methods that utilise sequence conservation in different ways to find consensus residues that are possible peptide docking sites. These methods include solvent accessibilities, secondary structure and sequence conservation.

5.2.6.3. Docking the binding motif of PLM and long form Mat-8 to the Na^+, K^+-ATPase.

Two main methods were employed to predict sites for individual amino acids in the binding motif of PLM and long form Mat-8 produced by DiLiMOT ((Neduva *et al.*, 2005) 5.2.6.1). The first method is Pepsite (Petsalaki *et al.*, 2009) which predicts sites on the protein of interest (i.e. spiny dogfish rectal gland Na^+, K^+-ATPase) by capturing the preferred environment for each selected amino acid in an inputted motif from a database of protein/peptide structure. Pepsite will also try to string together the predicted sites of the amino acids in the motif in sequence with additional distance constraints. The second method utilised Anchorsmap (Ben-Shimon and Eisenstein, 2010) which contains an algorithm which predicts the likelihood of a specified amino acid binding to a specific site. The algorithm has two stages. The first stage is a geometry based stage, in

which sub-pockets which could potentially bind single side chains are detected and amino acid probes are scattered near them. The second stage is an energy based stage in which optimal positions of the probes are calculated through repeated energy minimisation and clustering of nearby calculated orientations after which their ΔG are calculated which gives an idea of the probability of an identified binding site being real.

5.3. Results

5.3.1. Determination of secondary structure of the cytoplasmic region of FXYD proteins.

5.3.1.1. Circular Dichroism

Circular Dichroism (CD) is a technique that detects left and right circular polarised light after being applied to an optically active chiral molecule such as a protein. At any given wavelength of light the absorption of left and right polarised light by the protein will be different. This gives rise to molar ellipticity which is detected over a range of wavelengths in the UV range. Proteins that are predominantly α-helix (Holzwarth and Doty, 1965), β-sheet (Greenfield and Fasman, 1969) or random coil (Venyaminov *et al.*, 1993) all have unique CD spectral signatures as shown in Figure 5.2. Spectra of proteins with unknown secondary structure can be compared to these spectral signatures to understand the structural content present.

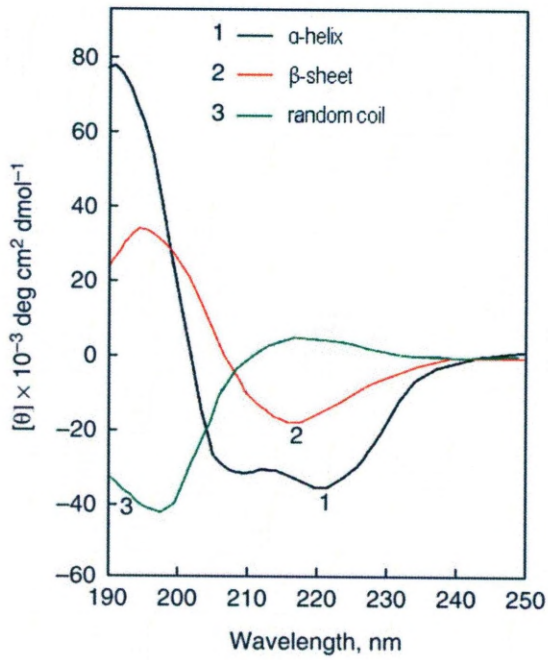

Figure 5.2. Far-UV CD spectral signatures of different secondary structure types. Figure adapted from (Greenfield, 2007). Note the characteristic differences between different states. Random coil exhibits negative CD at ~195 nm, β-sheet exhibits negative CD at 215 nm and α-helix shows a double dip at 205 and 220 nm.

Peptide representing the cytoplasmic region of PLM (PLM_{38-72}) has 15% α-helical content in 40% TFE (Figure 5.1b.) as revealed in CD experiments (Clayton *et al.*, 2005). The secondary structure of the cytoplasmic peptides Mat-$8sf_{38-67}$ (Figure 5.3.), Mat-$8lf_{38-93}$ (Figure 5.4.) and $CHIF_{38-90}$ (Figure 5.5.) were analysed here using CD and the calculated percentage helical content of each at different TFE v/v concentrations of 0%, 10%, 20%, 30% and 40% are shown in Table 5.1. The spectra suggest that the cytoplasmic region of Mat-8sf is disordered in both 0% and 40% TFE whereas the

cytoplasmic region of CHIF has around 7% α-helix induced by 40% TFE which is much lower than reported when full length PLM was solubilised in SDS micelles (Franzin *et al.*, 2007a) in which it has around 50% α-helical content. Although the spectra for Mat-8lf$_{38-93}$ suggests that it undergoes a much larger structural change than CHIF$_{38-69}$ upon addition of 40% TFE this actually only equates to around 8% α-helical content when the number of amino acids are taken into account. For Mat-8lf$_{38-93}$, a 55 amino acid peptide, this equates to approximately 4 amino acids forming an α-helix. It is possible therefore, that the extra amino acids in the cytoplasmic region of long form Mat-8 contain a small helix which could be responsible for the lipid binding and Na^+, K^+-ATPase regulating features of long form Mat-8 presented in Chapter 3 that are not observed in short form Mat-8.

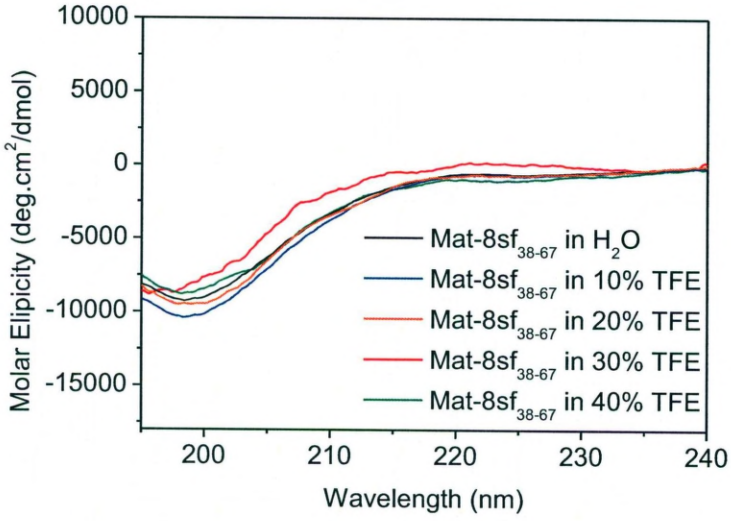

Figure 5.3. Far UV CD measurements of Mat-8sf$_{38-67}$ over a range of TFE concentrations. Spectra are shown for 50 μM Mat-8sf$_{38-67}$ over a 195-240 nm range of wavelengths at 4°C. Data smoothed with adjacent averaging (20 pts).

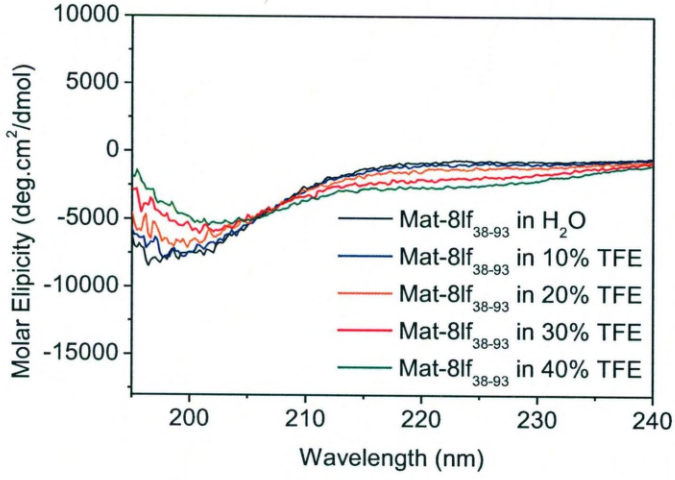

Figure 5.4. Far UV CD measurements of Mat-8lf$_{38-93}$ over a range of TFE concentrations. Spectra are shown for 50 μM Mat-8lf$_{38-93}$ over a 195-240 nm range of wavelengths at 4°C.

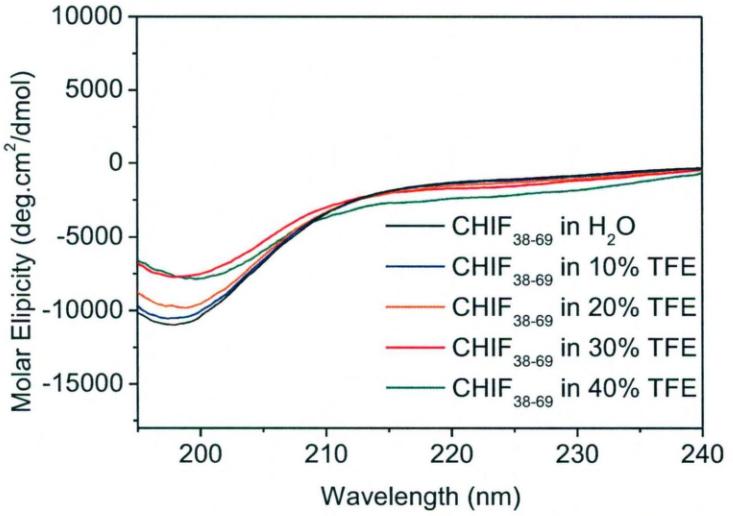

Figure 5.5. Far UV CD measurements of $CHIF_{38-69}$ over a range of TFE concentrations. Spectra are shown for 50 μM $CHIF_{38-69}$ over a 195-240 nm range of wavelengths at 4°C. Data smoothed with adjacent averaging (20 pts).

Table 5.1. Calculated percentage α-helical content in different cytoplasmic peptides at various TFE concentrations.

	Peptide		
% TFE	Mat-8sf$_{38-67}$	Mat-8lf$_{38-90}$	CHIF$_{38-69}$
0	2.2	3.0	4.3
10	2.4	3.6	4.2
20	3.5	4.6	4.7
30	3.6	6.5	6.1
40	0.2	7.7	7.3

5.3.1.2. Solution NMR of Mat-8lf$_{38-93}$

The NMR spectra of PLM_{38-72} in solution has been determined (Hughes *et. al.*, unpublished data). A similar strategy was employed to attempt to gain

further insight into the structure of the cytoplasmic region of the long form Mat-8 given its observed α-helical content in 40% TFE. Initially 1D ^{1}H NMR was performed in both 5% $^{2}H_2O$ and 40% 2,2,2-trifluoroethanol-d_3 to reduce the intensity of solvent signals. Figure 5.6 shows the results of the 1D ^{1}H NMR and an example spectra indicating where each chemical shift type is expected for a protein exhibiting elements of both β-sheet and α-helix secondary structure. In random coil protein spectra the chemical shift dispersion is somewhat reduced by the near-equivalent environments of the various nuclei. Many additional peaks and greater peak dispersion are observed upon addition of TFE from 9-5 ppm where backbone H^N chemical shifts are observed suggesting an induction of secondary structure upon addition of TFE.

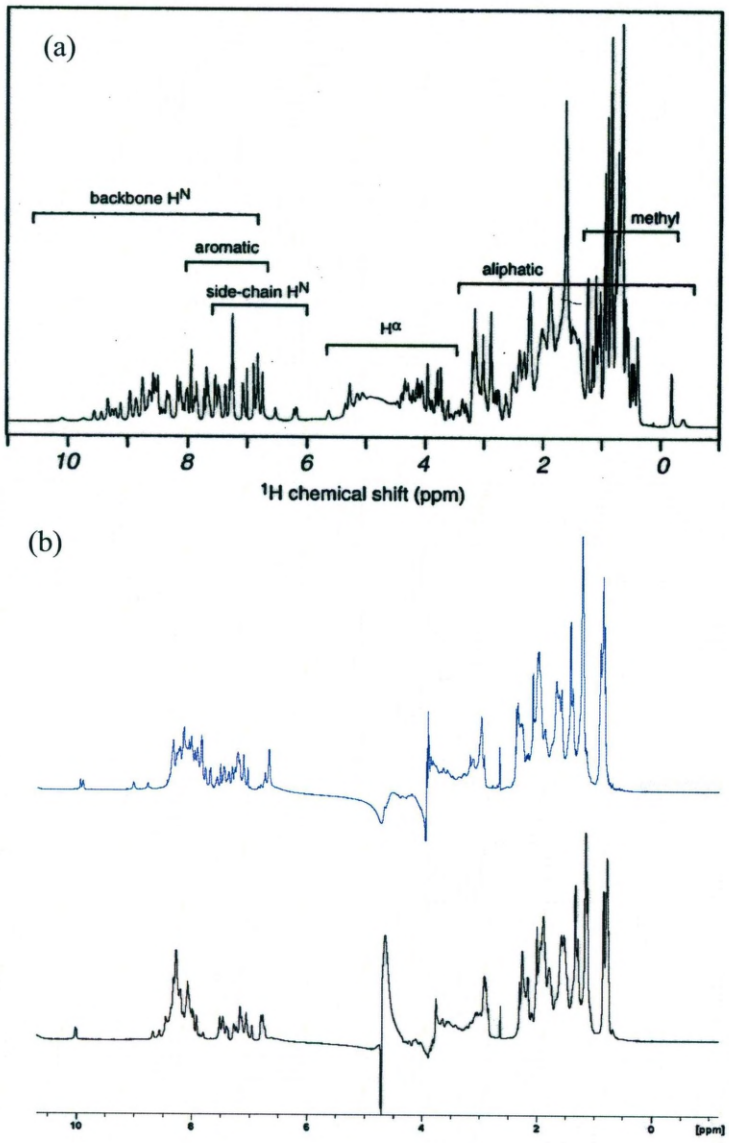

Figure 5.6. Comparison of 1D ^{1}H solution NMR of Mat-8lf$_{38-93}$ with 5% $^{2}H_2O$ and 40% TFE. Example spectra (a) shown to indicate locations of different ^{1}H chemical shifts. (Cavanagh *et al.*, 2007). (b) 5% $^{2}H_2O$ (black) shown below 40% TFE spectra (blue). Spectra are the result of accumulating 32 scans at 20°C.

The 1D NMR spectrum is too complex to assign due to the number of ^{1}H signals observed leading to high levels of overlap between signals. Therefore the two dimensional homonuclear method was attempted (Wuthrich, 1986). ^{1}H ^{1}H COSY NMR is a homonuclear 2D NMR experiment which allows identification of two nuclear spins that are coupled to each other by 3 bonds. There are two types of peak in a COSY spectra. Peaks appearing along the diagonal of the plot and correspond to the peaks on a 1D NMR experiment. Cross peaks off the diagonal result from magnetisation transfer between two coupled nuclei and give rise to two symmetrical peaks above and below the diagonal each of which has two chemical shift components from the two coupled nuclei. The experiments presented here use a DQF which reduces the single quantum transitions and hence width of the diagonal enabling greater resolution. Characteristic of this spectrum is the presence of harlequin shape of the peak comprising two positive and two negative sign contributions. Figure 5.8 shows the results of the DQF-COSY and an example SQF-COSY spectra indicating where each chemical shift type is expected is shown in Figure 5.7. Figure 5.9 shows the NH-αH region where backbone H signals are expected. For a 55 amino acid peptide all non-proline amino acids should give rise to a NH-Hα, unfortunately in the spectra shown this is clearly not the case. Therefore there is potential line broadening of signal due to chemical exchange of labile NH which prevents a full assignment being made.

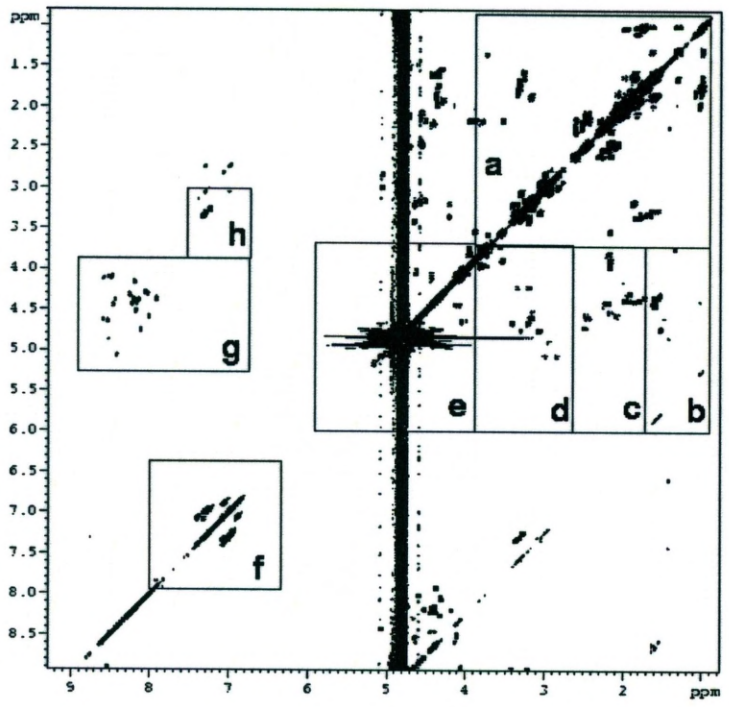

Figure 5.7. Example COSY spectra of neuropeptide Y to indicate locations of different ^{1}H chemical shifts. Figure taken from (Bader *et al.*, 2008). The boxes indicate the following signals:

(a) all non-labile, non-aromatic sidechain protons except those from βH -γCH_3 of Thr, δH-δH of Pro and βH-βH of Ser.

(b) αH-βCH_3 of Ala and βH-γ $CH_3$of Thr.

(c) αH-βH of Val, Ile, Leu, Glu, Gln, Met, Pro, Arg, and Lys.

(d) αH-βH of Cys, Asp, Asn, Phe, Tyr, His and Trp.

(e) αH-αH of Gly,αH-βH of Thr,δH-δH of Pro,αH-βH and βH-βH of Ser.

(f) aromatic ring protons, including 2H-4H of His, as well as sidechain protons from Asn and Gln.

(g) backbone NH-αH.

(h) δ CH_2-εNH of Arg

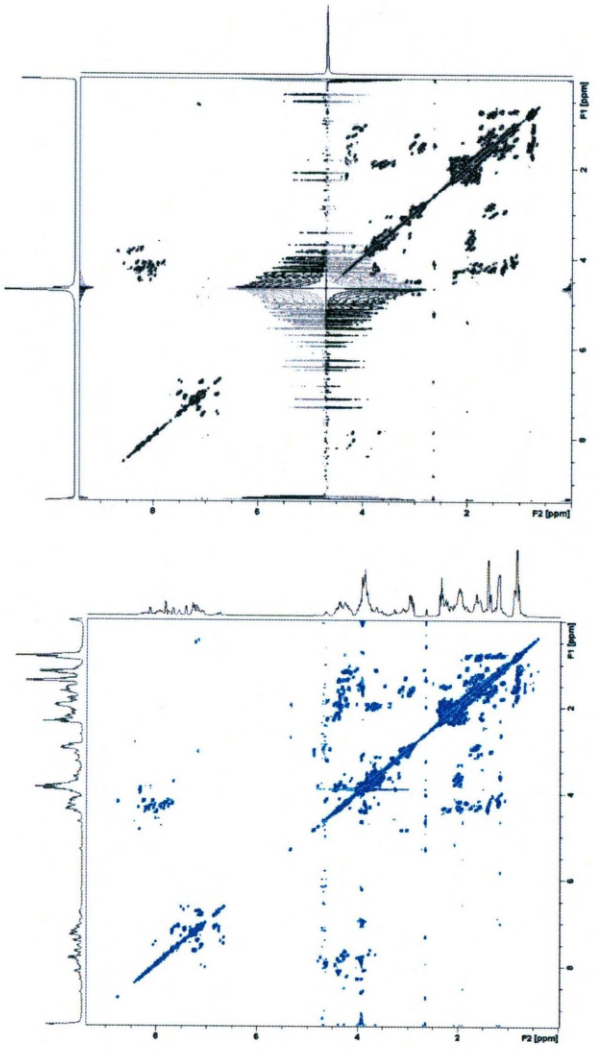

Figure 5.8. Comparison of 2D DQF-COSY solution NMR of Mat-8lf$_{38-93}$ with 5% $^{2}H_2O$ and 40% TFE. 5% $^{2}H_2O$ (black) shown above 40% TFE spectra (blue). Spectra are the result of an accumulation of 16 scans at 20°C. 1D projections of 2D spectra are shown top and left.

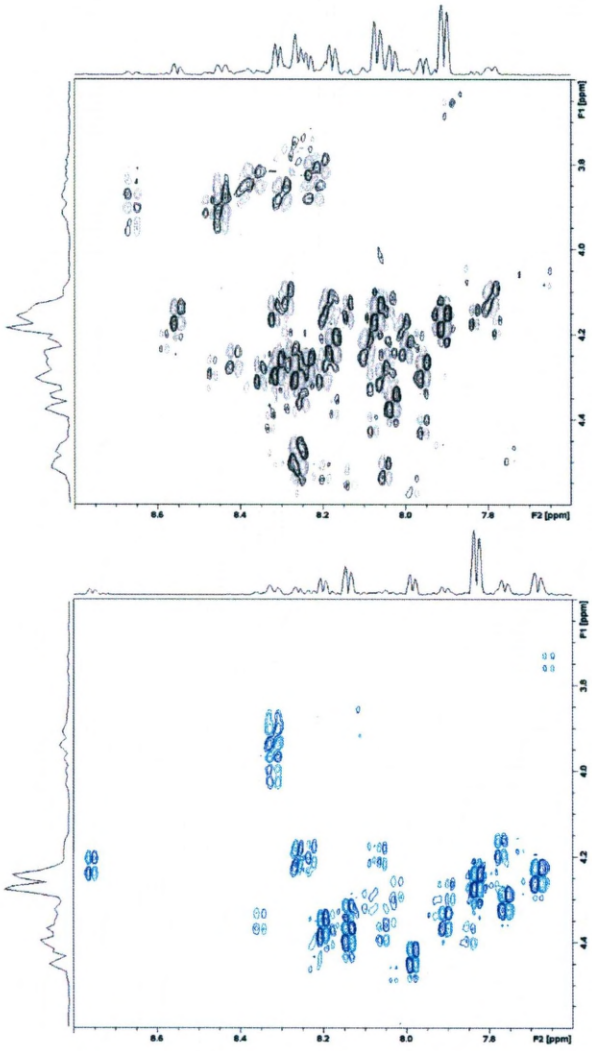

Figure 5.9. Comparison of 2D DQF-COSY of NH-Hα correlation of Mat-8lf$_{38-93}$ with 5% $^{2}H_2O$ and 40% TFE. 5% $^{2}H_2O$ (black) shown alongside 40% TFE spectra (blue). 1D projections of 2D spectra are shown top and left.

Where COSY helps identify chemically bonded nuclei up to 3 bonds, NOESY instead connects nuclear spins that are spatially close in proximity regardless of the number of bonds separating them. Spectra appear similar with diagonal peaks and cross peaks and the technique of sequential

walking combines COSY and NOESY to assign peaks based on their through-bond coupled partner nuclei and spatially coupled partner nuclei respectively. Figure 5.11 shows the ^{1}H ^{1}H NOESY of Mat-8lf$_{38-93}$ and an example spectra indicates (Figure 5.10) where each chemical shift type is expected. This reveals how even with a Watergate pulse sequence the αH region is masked by the signal from water preventing Mat-8lf$_{38-93}$ peaks being observed in this region. Figure 5.12. shows the NH-CH_3 region and although assignment is not possible there is a clear broadening of peaks in this region upon addition of TFE and the quantity of observed NOEs increases. This together with the increased signal dispersion suggests a small but substantial induction of structure.

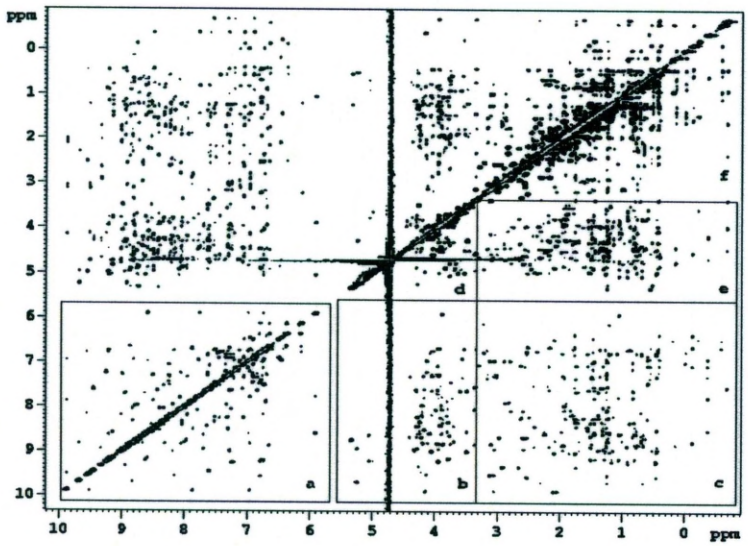

Figure 5.10. Example NOESY spectra of protein D (phage envelope protein) to indicate locations of different ^{1}H chemical shifts. Figure taken from (Bader *et al.*, 2008). The boxes indicate the following signals:

(a) NH; aromatic - NH; aromatic-aromatic.

(b) NH; aromatic - αH; δH of Pro; βH of Ser and Thr.

(c) NH; aromatic - aliphatic sidechains.

(d) αH; δH of Pro; βH of Ser and Thr - αH; δH of Pro; βH of Ser and Thr.

(e) αH; δH of Pro; βH of Ser and Thr - aliphatic sidechains.

(f) Aliphatic sidechains - aliphatic sidechains.

(b) 5% $^{2}H_2O$ (black) shown below 40% TFE spectra (blue). Spectra collected on 600MHz

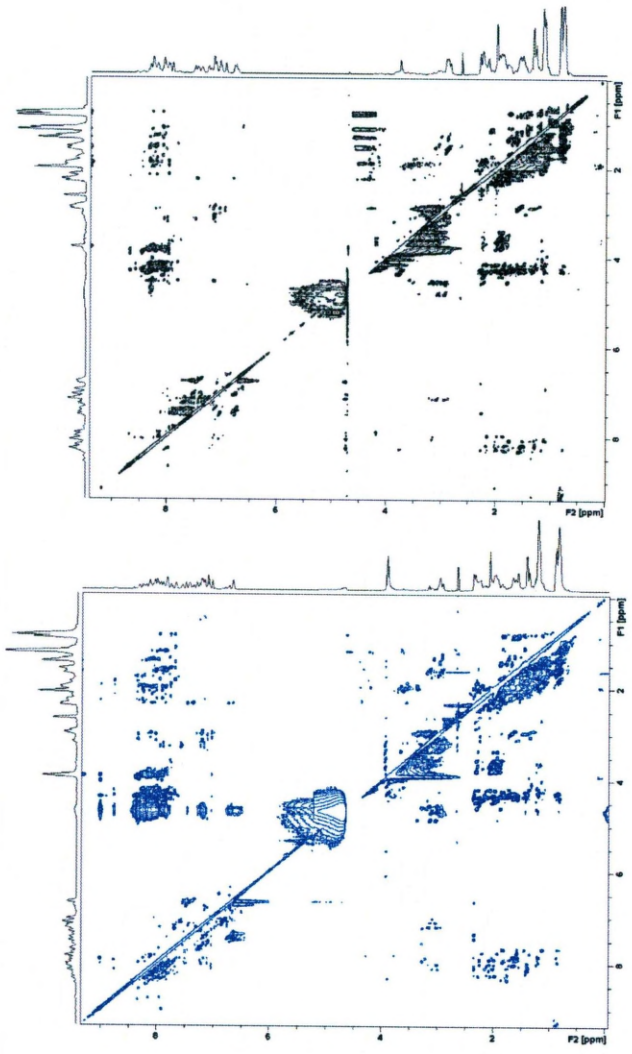

Figure 5.11. Comparison of 2D ^{1}H ^{1}H NOESY solution NMR of Mat-8lf$_{38-93}$ with 5% $^{2}H_2O$ and 40% TFE Spectra are the result of an accumulation of 48 scans at 20°C, 1D projections of 2D spectra are shown top and left.

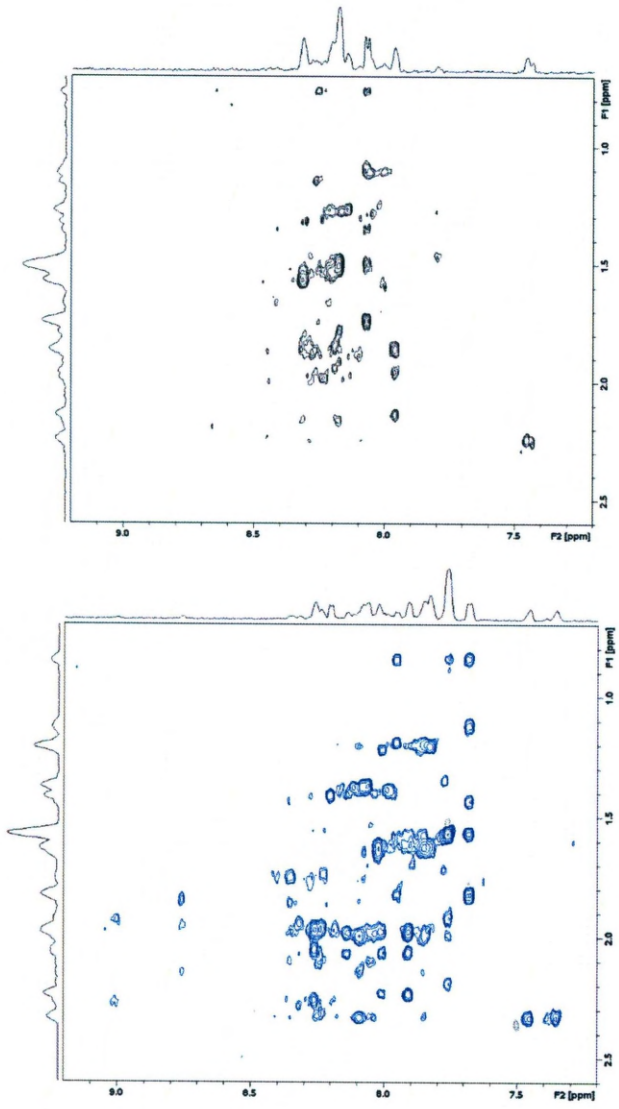

Figure 5.12 Comparison of 2D NOESY of NH-CH_3 NOEs of Mat-8If$_{38-90}$ with 5% ^2H_2O and 40% TFE. 5% ^2H_2O (black) shown alongside 40% TFE spectra (blue). Number and dispersion of peaks increases when TFE has been added. Cross peaks between NH region 7-8.2 ppm and CH_3 region 0.8-2.6 ppm. 1D projections of 2D spectra are shown top and left.

5.2.2. The effect of SDS on the structure of the cytoplasmic region of PLM

The CD data and solution NMR data suggest that the cytoplasmic region long isoform of Mat-8 contains a small quantity of α-helical content not present in the short isoform. This α-helix could be responsible for the inhibition of the Na^+, K^+-ATPase reported in Chapter 3. As PLM and the long form of Mat-8 are the only FXYD proteins known to have a cytoplasmic region that inhibits the Na^+, K^+-ATPase it is possible they share a small α-helical motif that is responsible for this inhibition. As there is no solved structure for long form Mat-8 any modelling studies to investigate this possibility would have to be performed using the structure of PLM (Teriete *et al.*, 2007). The full length structure is limited as it was solved in highly negatively charged SDS micelles which are not indicative of the slightly negatively charged phospholipid bilayer of cell membranes. This highly negatively charged environment may induce additional secondary structure over what is observed *in vivo*. From CD data the percentage of α-helix in the cytoplasmic region of PLM has been calculated as 15% (Clayton *et al.*, 2005) which is double that what is observed in the SDS structure. With this contradiction in mind experiments were undertaken to asses to validity of the PLM structure for use in bioinformatics studies.

To investigate the possibility of SDS inducing α-helical content further CD experiments were performed on PLM_{38-72}. Two sets of experiments were performed. The first was PLM_{38-72} in water with and without SDS at 500 mM; the same concentration used in the full length solved structure (Figure 5.13.). The second was in the presence of 40% TFE again with and without 500 mM SDS (Figure 5.14.). The percentage α-helical content calculated is shown in Table 5.2 calculated by the equation discussed in the methods (5.2.3.). Without SDS, the calculated α-helical content agrees with the published data (Clayton *et al.*, 2005) as there is effectively no α-helix before addition of 40% TFE after which 15% helix is observed. Interestingly, SDS appears to induce around 9% α-helix to a PLM_{38-72} sample in H_2O. When SDS is added to PLM_{38-72} with 40% TFE there is a combined effect as an additional 6% helical content is observed in 40% TFE with SDS over 40% TFE alone. This strongly suggests that the highly negative charge of SDS induces α-helical content that may not be indicative of full length PLM in a cell membrane.

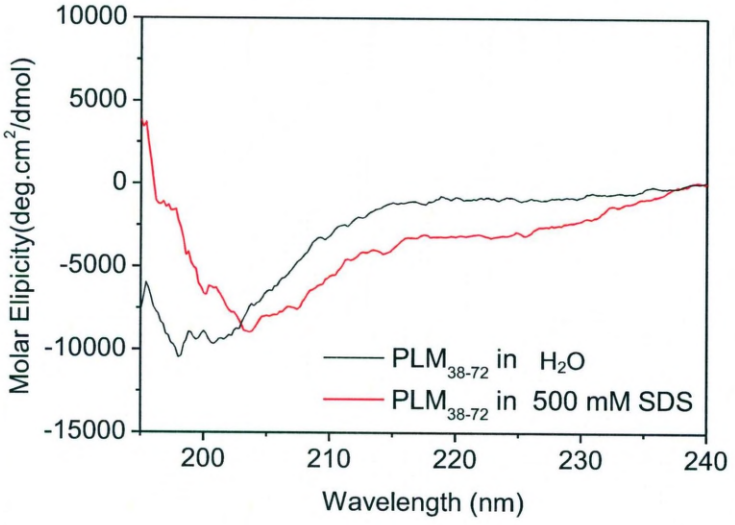

Figure 5.13. Far UV CD measurements of PLM_{38-72} in water with and without SDS. Spectra are shown for 50 μM PLM_{38-72} over a 195-240 nm range of wavelengths at 4°C with and without 500 mM SDS.

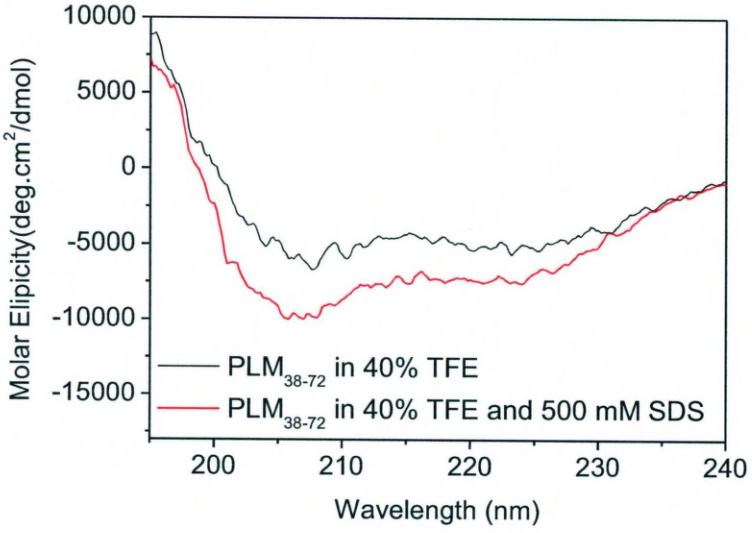

Figure 5.14. Far UV CD measurements of PLM_{38-72} in 40 % TFE with and without SDS. Spectra are shown for 50 μM PLM_{38-72} over a 195-240 nm range of wavelengths at 4°C with and without 500 mM SDS.

Table 5.2. Calculated percentage of α-helical content in PLM_{38-72} at 0 and 40% TFE concentrations with and without SDS.

% TFE	PLM_{38-72}	PLM_{38-72} + SDS
0	3.4	9.3
40	14.8	20.5

The structural data shown so far in this chapter reveal that all of the cytoplasmic FXYD peptides tested, PLM_{38-72} has the largest amount of α-helical content, which is interesting since it also had the greatest effect on Na^+, K^+-ATPase activity (Chapter 3). The current knowledge for the full structure of PLM is limited as it has only been solved in SDS micelles (Teriete *et al.*, 2007). Additionally the CD data shown here reveals that there is an additional 5% α-helix present in PLM_{38-72} that is induced by SDS. However, recent data reveal that α-helical structure can also be induced in PLM_{38-72} by negatively charged phospholipid bilayers (Hughes *et al.*, 2011). This means that the true α-helical content of PLM_{38-72} is most likely higher than observed in CD in the absence of phospholipids but lower than that observed in SDS micelles due to the presence of high negative charge. The differences are relatively small however, therefore the current structure of PLM in SDS micelles is probably similar to its actual structure in cell membranes. This makes it suitable for use in bioinformatic modelling provided the possibility of lower α-helical content is taken into account when interpreting results. Mat-$8lf_{38-93}$ was the only other cytoplasmic FXYD peptide studied that also had an effect on the activity of

the Na^+, K^+-ATPase (Chapter 3). In this chapter CD and solution NMR revealed Mat-8lf$_{38-93}$ contains a small amount of α-helical content that is not present in Mat-8sf$_{38-67}$. This could mean that the additional 26 amino acids of Mat-8lf$_{38-93}$ contribute to the increase in α-helix and that this is responsible for the inhibition of the Na^+, K^+-ATPase. As the cytoplasmic regions of both PLM and the long isoforms of Mat-8 are found in similar locations relative to the Na^+, K^+-ATPase it is possible that they bind to the same site on the protein surface. PLM and long form Mat-8 were therefore further analysed by bioinformatics to test this possibility.

5.3.3. Bioinformatics

5.3.3.1. Determination of possible Na^+, K^+-ATPase binding motif in PLM and long form Mat-8.

In order to determine how the cytoplasmic region of PLM and long form Mat-8 may interact with the Na^+, K^+-ATPase several bioinformatical strategies were employed. Firstly DiLiMOT (Neduva *et al.*, 2005) was used to search for a possible linear binding motif. PLM and long form Mat-8 (Figure 5.15.), were searched for a possible convergently evolved motif that interact with the Na^+, K^+-ATPase with other proteins known to interact with the Na^+, K^+-ATPase which included adducin (Ferrandi *et al.*, 1999), sarcoma (SRC (Tian *et al.*, 2006)), Phosphoinositide-3 kinase (PI3K (Yudowski *et al.*, 2000)) and ankyrin (Ank (Devarajan *et al.*, 1994)).

```
Phospholemman
MASLGHILV FCVGLLTMAK AESPKEHDPF TYDYQSLQIG GLVIAGILFI
          10         20         30         40
LGILIVLSRR CRCKFNQQQR TGEPDEEEGT FRSSIRRLST RRR
50         60         70         80         90

Long form Mat-8
MQKVTLGLL VFLAGFPVLD ANDLEDKNSP FYYDWHSLQV GGLICAGVLC
          10         20         30         40
AMGIIIVMSE WRSSGEQAGR GWGSPPLTTQ LSPTGAKCKC KFGQKSGHHP
50         60         70         80         90
GETPPLITPG SAQS
100        110
```

Figure 5.15. Sequences of PLM and long form Mat-8 used in bioinformatics studies. Colour scheme as follows: signal peptide (red), extracellular domain (green), transmembrane domain (blue) and cytoplasmic domain (purple).

This discovered the motif SxxRxS found in PLM (residues 63-68 SIRRLS) and long form Mat-8 (residues 38-43 SEWRSS) as well as adducin, SRC, PI3K but not Ank (Appendix B). The instances of the motif in these proteins can be seen in the alignment below (Figure 5.16.)

```
PI3K              VYESGPRKSVIP
SRC               KDASQRRRSLEP
Long form Mat-8   IVMSEWRSSGEQ
PLM               FRSSIRRLSTRR
Adducin           GTCSPLRHSFQK
                    *  *  *
```

Figure 5.16. Instances of the SxxRxS motif in proteins studied. Alignment of the amino acids in and around the predicted Na^+, K^+-ATPase motif in the proteins studied by DiLiMOT. Box indicates location of SxxRxS motif.

DiLiMOT calculated an S_{cons} value (which is the product of all binomial probabilities from the genomes considered) of $5.94e^{-08}$ and a P value of $1.03e^{-06}$. The P value is much below 0.001 suggesting the occurrence of the motif is statistically significant. However the S_{cons} value is above the $7.0x10^{-38}$ cut off value quoted by DiLiMOT for humans. This is due to the limited number of proteins used in the experiment but it can still be considered a hypothetical motif. For all the proteins used in this instance there is experimental evidence confirming that they interact with the Na^+, K^+-ATPase.

Interestingly, the SxxRxS motif this incorporates Ser 68 of PLM which, as discussed in Chapter 3 is a phosphorylation site which reduces the inhibitory effect on the Na^+, K^+-ATPase when phosphorylated. Chapter 3 also discussed how the corresponding serine in long form Mat-8 could possibly be phosphorylated. Long form Mat-8 has so far only been discovered in humans however PLM has been characterised in cow, dog, human, mouse, rat, western clawed frog and African clawed frog (Crambert *et al.*, 2002). The instance of the motif SIRRLS is identical in all these species with the exception of the western clawed frog which has the leucine substituted for a methionine. Crucially the SxxRxS is conserved through all species as conservation is described as a key feature of short linear motifs (Davey *et al.*, 2012).

Secondary structure data are available for PLM (Teriete *et al.*, 2007) as it has had its full structure solved in SDS micelles. No residue-specific secondary structure information is available for long form Mat-8. Therefore secondary structure was predicted for both PLM (Figure 5.17. to use in parallel with the experimental data) and long form Mat-8 (Figure 5.18.) using psipred (Jones, 1999). In both cases the SxxRxS motif is predicted to occur at the end of an α-helix. The α-helical content of the cytoplasmic region of PLM is predicted to be approximately 30% which would agree with the SDS micelle structure of PLM (Teriete *et al.*, 2007). The disorder predictor metaPrDOS predicts that the instance of the SxxRxS motif in PLM is disordered (Figure 5.19.) whilst it is predicted to be ordered in long form Mat-8 (Figure 5.20.). This may suggest that in solution the motif in PLM is disordered but in the native environment of the membrane surface and the Na^+, K^+-ATPase could form ordered secondary structure.

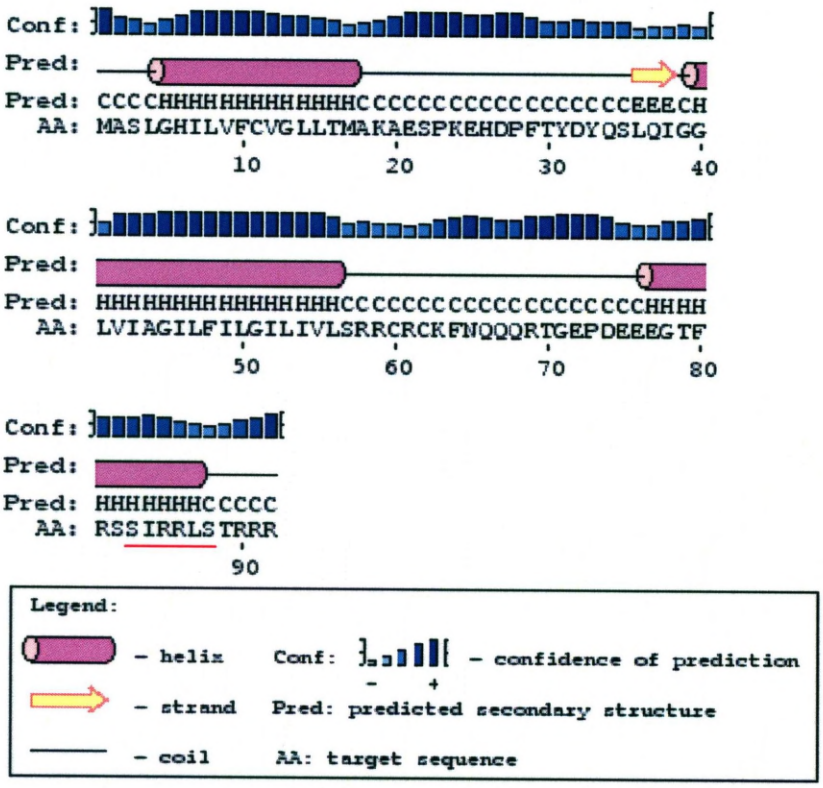

Figure 5.17. Predicted secondary structure of PLM. Figure produced using psipred. Location of SxxRxS motif is underlined in red.

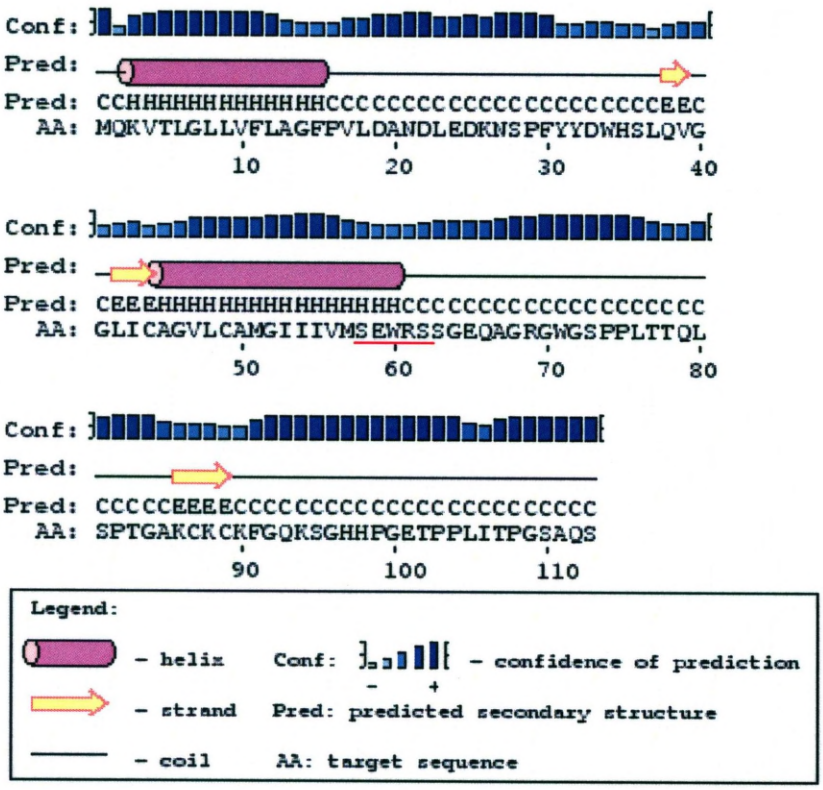

Figure 5.18. Predicted secondary structure of long form Mat-8. Figure produced using psipred. Location of SxxRxS motif is underlined in red.

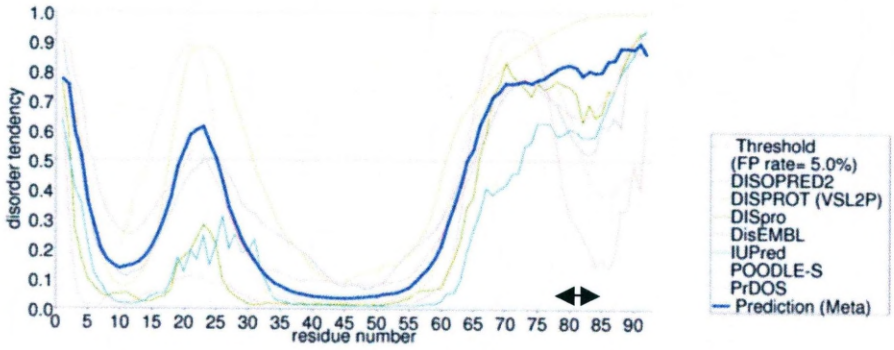

Figure 5.19. metaPrDOS prediction of disorder in PLM. metaPrDOS predicts disorder by determining the mean values of disorder tendency predicted by several methods. It predicts SxxRxS to be disordered. Location of motif indicated by arrow.

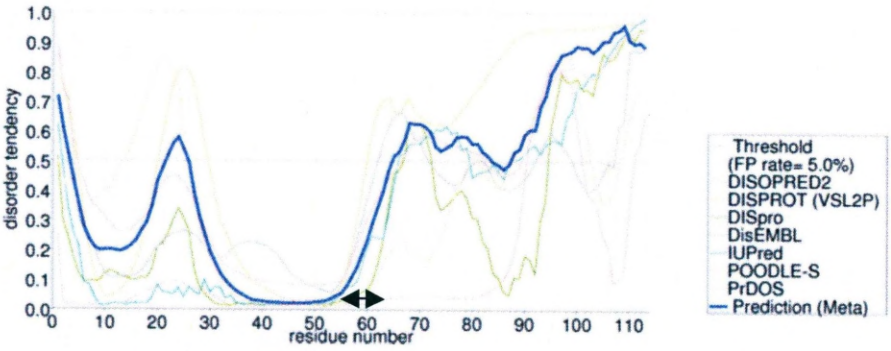

Figure 5.20. metaPrDOS prediction of disorder in long form Mat-8. metaPrDOS predicts disorder by determining the mean values of disorder tendency predicted by several methods. It predicts SxxRxS to be ordered. Location of motif indicated by arrow.

5.3.3.2. Determination of possible peptide binding sites on the surface of the Na^+, K^+-ATPase

After identifying a possible Na^+, K^+-ATPase binding motif in PLM and long form Mat-8, the Na^+, K^+-ATPase structure was analysed to try and

find potential binding sites for the motif. When considering these methods it is important to consider the position of the membrane in respect to the Na^+, K^+-ATPase as the cytoplasmic region of both PLM and long form Mat-8 can only viably interact with the cytoplasmic region of the Na^+, K^+-ATPase. Figure 5.21. shows the position of the cell membrane as predicted by the orientations of proteins in membranes (OPM) database (Lomize *et al.*, 2006) which has been verified with experimental data with several membrane proteins. This and all subsequent data in this chapter is produced using spiny dogfish rectal gland Na^+, K^+-ATPase ((Shinoda *et al.*, 2009) PDBID:2ZXE).

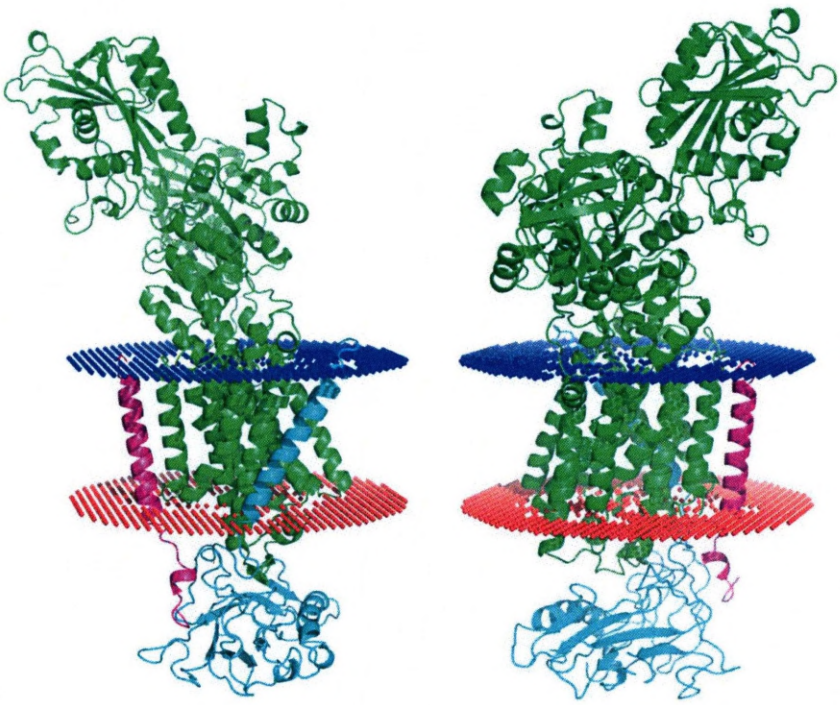

Figure 5.21. Membrane location relative to the Na^+, K^+-ATPase. The location of the membrane relative to the Na^+, K^+-ATPase as calculated by OPM is shown above in two different views where the orientation on the right is rotated 180° about the y axis from the structure on the left. The cytoplasmic membrane surface is in blue whilst the extracellular membrane surface is in red.

Initially, the Na^+, K^+-ATPase was analysed for sequence conservation. The likelihood of a potential binding site being real is increased when it is conserved through many species. The α-subunit sequence of spiny dogfish rectal gland Na^+, K^+-ATPase was aligned using MUSCLE to all other instances of the Na^+, K^+-ATPase that were from species which are known to express FXYD proteins. ConSurf was used to calculate a conservation measure which it mapped to the structure of the Na^+, K^+-as shown in Figure 5.22. Due to the relatively small number of species that are known to express FXYD proteins high conservation is observed in the majority of the Na^+, K^+-ATPase which means it is not particularly useful for finding peptide binding sites.

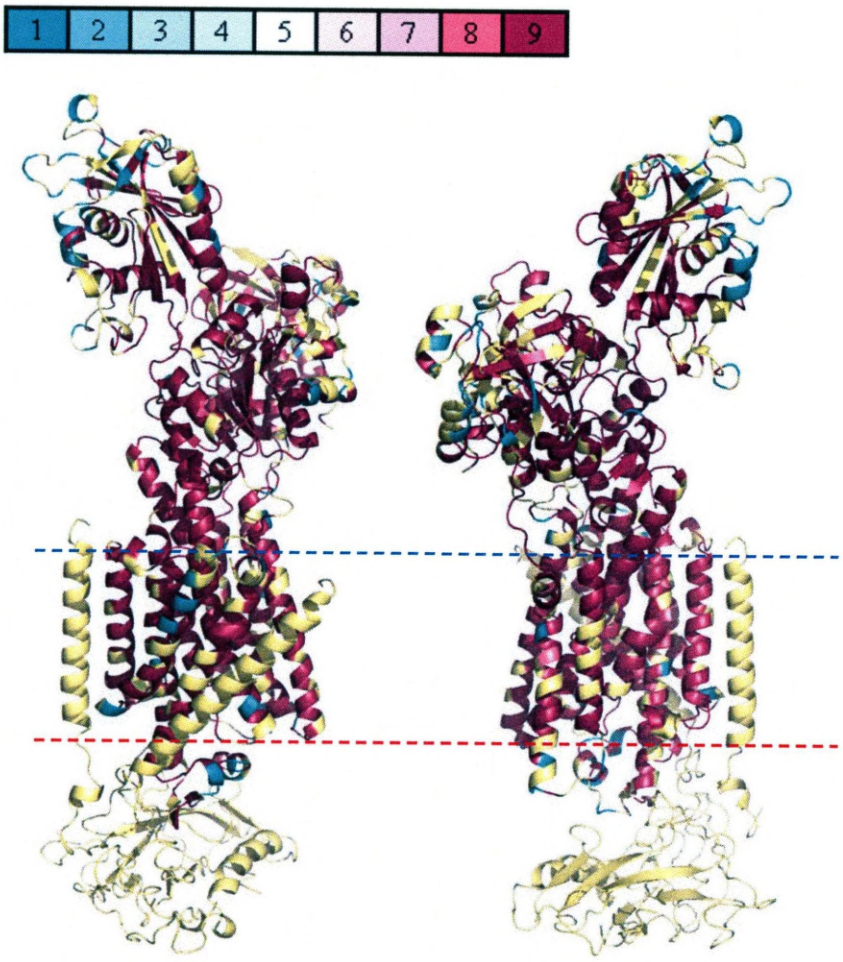

Figure 5.22. Conservation analysis of the Na^+, K^+-ATPase using Consurf. All instances of the Na^+, K^+-ATPase in species which are known to express FXYD proteins were aligned and analysed using Consurf. The Consurf colour scheme is shown with a score of 1 being least conserved and a score of 9 being most conserved. The cytoplasmic membrane surface is indicated by a dotted blue line whilst the extracellular membrane surface is indicated by a dotted red line.

Three servers were used to try and determine possible binding sites for peptides on the surface of the Na^+, K^+-ATPase. Prosurf (Figure 5.23.) only identified sites within the transmembrane region of the Na^+, K^+-ATPase which is inaccessible to the motif which lies in the cytoplasmic region of PLM and long form Mat-8. It appears the majority of sites identified are in the regions where the α-subunit of the Na^+, K^+-ATPase is in close proximity of FXYD 10 and the β-subunit of the Na^+, K^+-ATPase suggesting their interactions are preventing other potential sites being discovered by this method. PPISP (Figure 5.24.) has predicted the majority of its sites in the negatively charged cavity (Reyes and Gadsby, 2006) located within the transmembrane domain. There are some predicted sites above this cavity which lie above the membrane surface. Finally STP (Figure 5.25.) was also used and predicts the majority of sites throughout the transmembrane region most likely due to its hydrophobicity. It does predict certain sites in the cytoplasmic region of the Na^+, K^+-ATPase to be more likely binding sites for peptides than others which may become significant when combined with other methodologies.

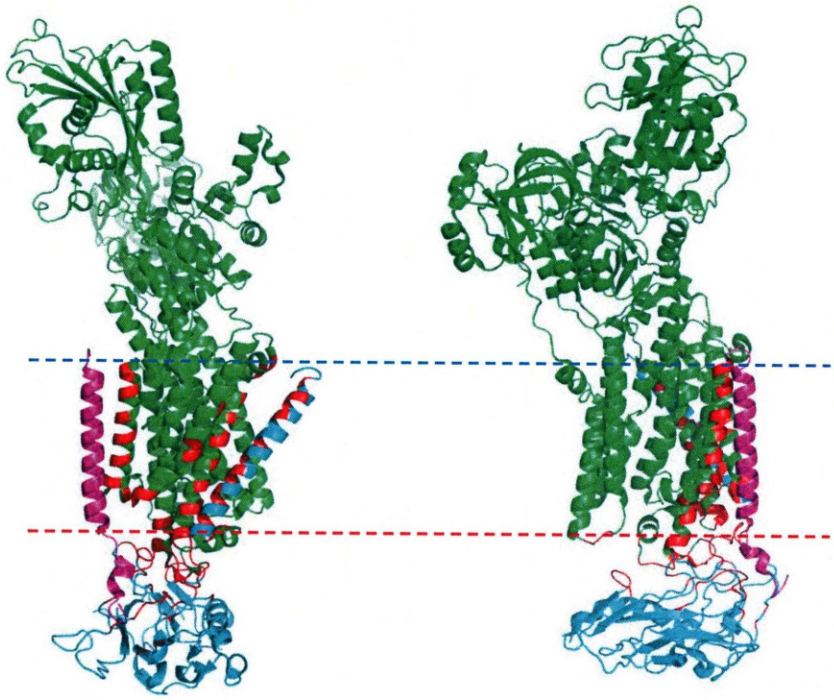

Figure 5.23. Analysis of the Na^+, K^+-ATPase for potential non-specific peptide binding sites by Prosurf. The residues determined by Prosurf to be potential peptide binding sites are coloured in red. The α-subunit of the Na^+, K^+-ATPase is in green, the β-subunit is in cyan and FXYD10 is in magenta. The cytoplasmic membrane surface is indicated by a dotted blue line whilst the extracellular membrane surface is indicated by a dotted red line.

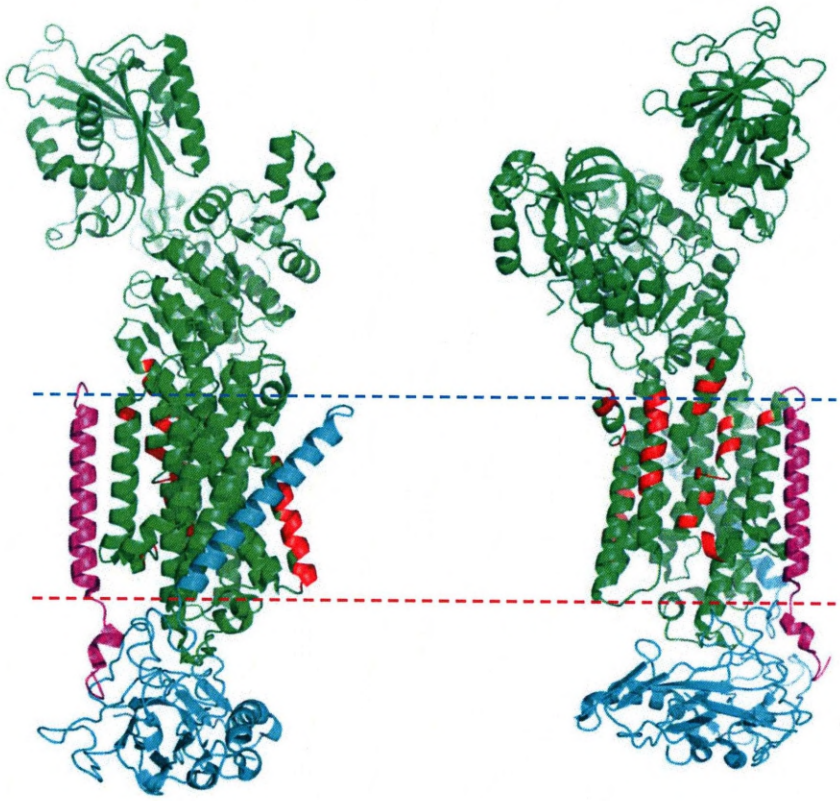

Figure 5.24. Analysis of the Na^+, K^+-ATPase for potential non-specific peptide binding sites by metaPPISP. The residues determined by metaPPISP to be potential peptide binding sites are coloured in red. The α-subunit of the Na^+, K^+-ATPase is in green, the β-subunit is in cyan and FXYD10 is in magenta. The cytoplasmic membrane surface is indicated by a dotted blue line whilst the extracellular membrane surface is indicated by a dotted red line.

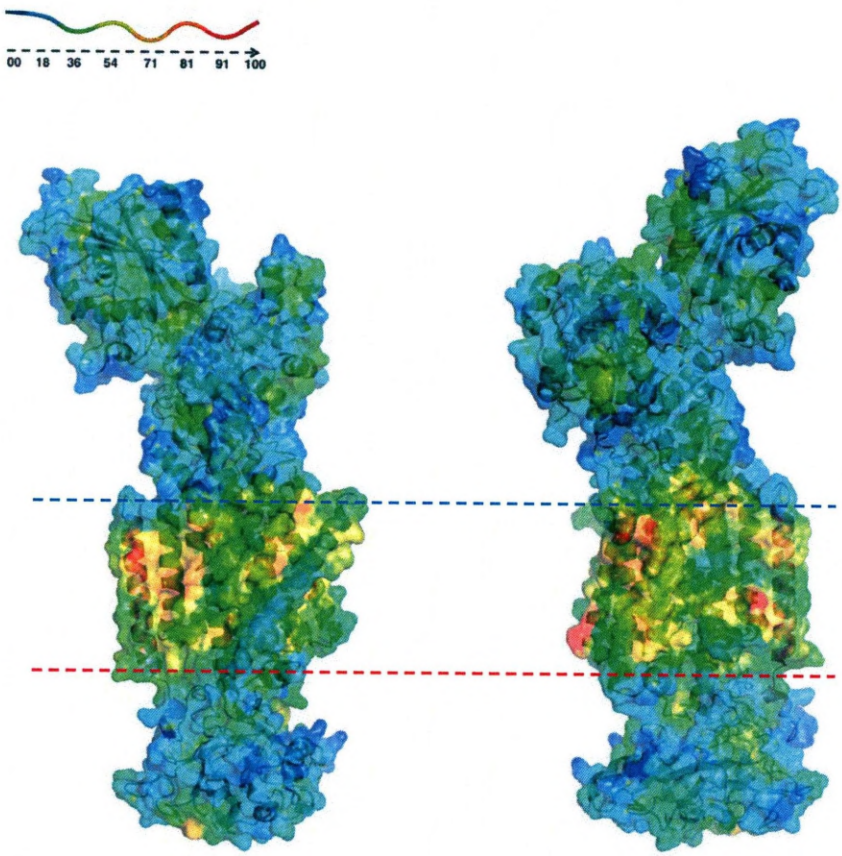

Figure 5.25. Analysis of the Na^+, K^+-ATPase for potential non-specificpeptide binding sites by STP. STP was used to analyse the surface of the Na^+, K^+-ATPase for potential binding sites. The colour scheme is indicated on a scale of 0-100 where 100 is the most likely. Surface is shown semi transparent to show locations of all subunits of the Na^+, K^+-ATPase. The cytoplasmic membrane surface is indicated by a dotted blue line whilst the extracellular membrane surface is indicated by a dotted red line.

5.3.3.3. Determination of specific motif binding locations in the Na^+, K^+-ATPase.

Two methods were employed to try to find more specific binding locations for the SxxRxS motif on the Na^+, K^+-ATPase. As these methods are more specific the size of the input file is limited. For this reason, and to reduce the number of false positives the PDB structure of the Na^+, K^+-ATPase had portions of amino acids removed from the structure. These included the entire FXYD10 and β-subunit of the Na^+, K^+-ATPase and regions of the α-subunit of the Na^+, K^+-ATPase inaccessible to the cytoplasmic region of PLM which included the extracellular region, part of the transmembrane region towards the extracellular side of the membrane and parts of the cytoplasmic region furthest from the cell membrane. The first software utilised on this new structure was PepSite. This software finds binding pockets and attempts to string together a given sequence of amino acids in the binding pocket ensuring each amino acid lies in a suitable environment and the sites lie spaced with separations compatible with the inputted motif sequence. However, it can often lead to unrealistic results. For example it can string together two sites that are close in space but are located at opposite sides of the protein. PepSite often erroneously uses the same potential amino acid binding site twice when there are two instances of the same amino acid in an inputted motif. Figure 5.26 reveals all the potential amino acid binding sites uncovered on the Na^+, K^+-ATPase for the SxxRxS motif in PLM and long form Mat-8. For PLM all potential amino acid

binding sites were in the transmembrane region, therefore inaccessible to the cytoplasmic region of PLM. In long form Mat-8 all but one sites calculated are also in the transmembrane region. The one site that is in the cytoplasmic region is for an arginine residue and is located above the negative cavity suggested as a possible alternative orientation (Teriete *et al.*, 2009). Many of the sites in both cases are at the base of the structure where regions of the original structure have been removed. This suggests that by using a structure altered in this way creates false binding sites.

PLM potential binding sites Long form Mat-8 potential binding sites

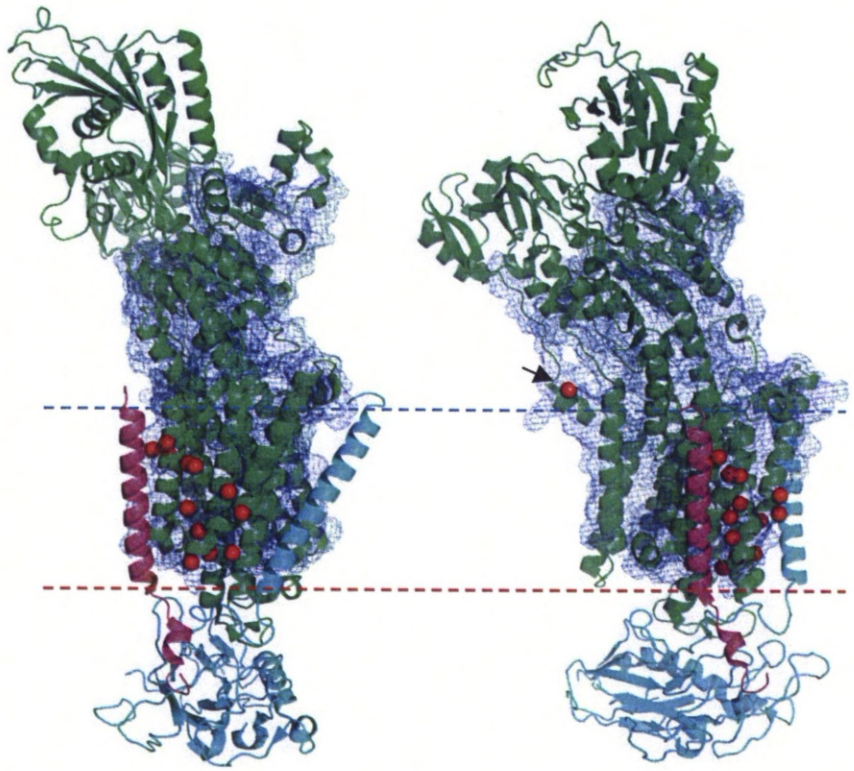

Figure 5.26. PepSite results for altered Na^+, K^+-ATPase structure. PepSite was used to find binding sites for the amino acid residues in the motifs discovered in PLM (SIRRLS) and long form Mat-8 (SEWRSS). The region of the protein analysed is indicated by the blue mesh. All predicted binding sites are indicated by red spheres. The cytoplasmic membrane surface is indicated by a dotted blue line whilst the extracellular membrane surface is indicated by a dotted red line. This means only one site (indicated by arrow) is above the membrane surface.

Anchorsmap was used on the same edited Na^+, K^+-ATPase structure. Anchorsmap finds surface only sites for given amino acids. Unfortunately serine is not compatible with this method due to its small sidechain. Isoleucine also did not work with Anchorsmap due to technical problems with the presently distributed version of the software. Therefore arginine (present in both SIRRLS of PLM and SEWRSS of long form Mat-8), leucine (present in SIRRLS of PLM) and glutamate and tryptophan (both in SEWRSS of long form Mat-8) were inputted into Anchorsmap. Figure 5.27. and 5.28 show the top 200 sites calculated by this method. As serine could not be used with this method the arginine data is most important, as it is the only residue present in all instances of the SxxRxS motif that can be detected by Anchorsmap. PLM also has an additional arginine site in the motif over long form Mat-8 which could explain its increased effect on Na^+, K^+-ATPase activity due to a higher charge affinity. Interestingly there are two major clusters of arginine sites that are circled in all figures. With the exception of glutamate in one of these sites there are possible sites for all other amino acids in these clusters. They are two possible candidates of docking locations that agree with the current model (Teriete *et al.*, 2009).

Leucine

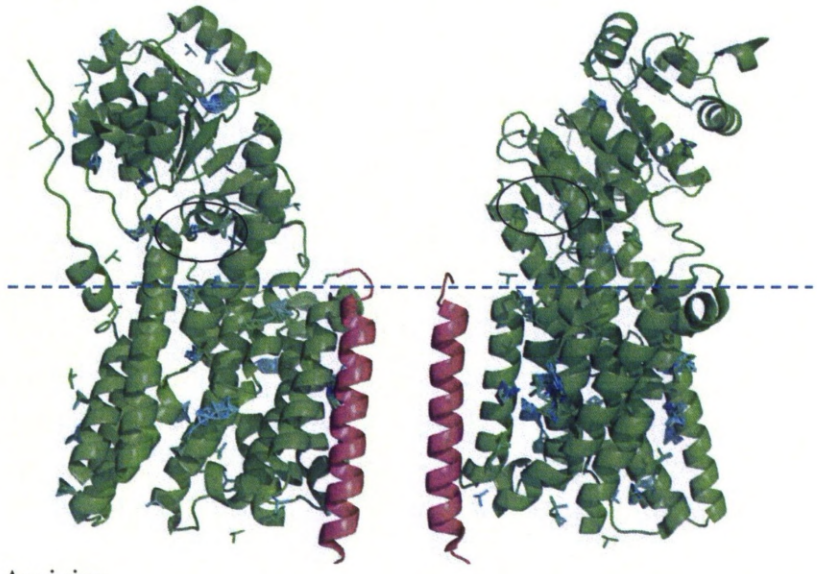

Arginine

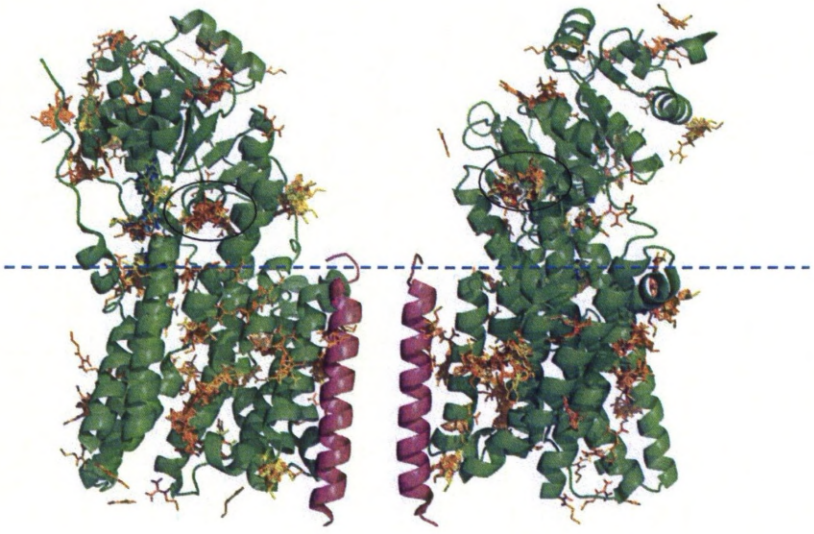

Figure 5.27. Predicted sites for leucine and arginine determined by Anchorsmap. In both cases the top 200 predicted sites are shown with a spectral colour scheme indicating probability with blue being the most likely and red being the least likely. Blue dotted lines indicate the cytoplasmic membrane surface.

Glutamate

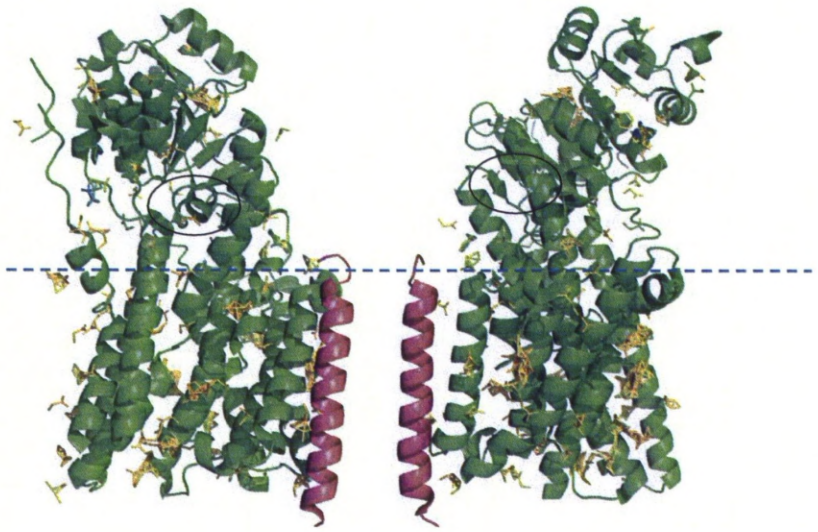

Tryptophan

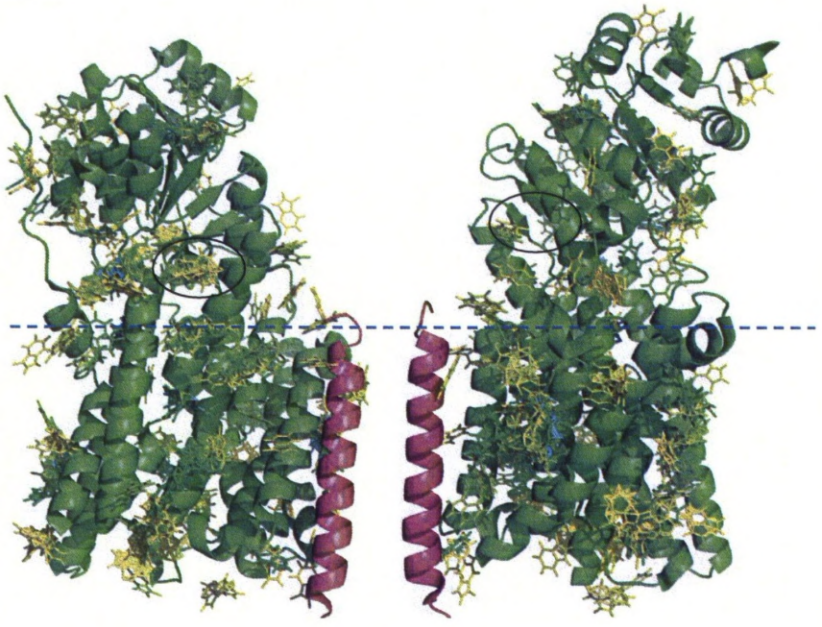

Figure 5.28. Predicted sites for glutamate and tryptophan determined by Anchorsmap. In both cases the top 200 predicted sites are shown with a spectral colour scheme indicating probability with blue being the most likely and red being the least likely. Blue dotted lines indicate the cytoplasmic membrane surface.

5.3.3.4. Determining possible orientations of the motif within the Na^+, K^+-ATPase.

Not only are the two clusters of arginine sites in close proximity of other amino acid sites in the Mat-8 and PLM motif but they are also conserved (Figure 5.22.). One cluster is also in close proximity of the arginine site in the cytoplasmic region of the Na^+, K^+-ATPase determined by PepSite (Figure 5.26.) and several cytoplasmic sites determined by metaPPISP (Figure 5.24.). Using these data the helix solved in the cytoplasmic region of PLM by NMR in SDS micelles (Teriete *et al.*, 2007) and the unstructured amino acids at the C-terminus was successfully docked into one of these sites using PyMol (Figure 5.29). This reveals potential interactions of the positive sidechains of arginine residues in PLM with negative sidechains of glutamate and aspartate residues located at the N-terminus of helix M5 of the Na^+, K^+-ATPase. The sidechains of the arginines required no manipulation for this interaction with the exception of Arg 66 for which a very small adjustment of one of the most common arginine sidechain rotamers from the backbone-dependent rotamer library in PyMol. These interactions could feasibly be weakened upon phosphorylation of Ser 63 and/or Ser 68 due to the removal of positive charges. It also reveals the surfaces of both PLM and the Na^+, K^+-ATPase are sterically compatible at this site. Finally the positively charged sidechains of the unstructured arginine residues can also simultaneously interact with negatively charged cell membranes in this conformation.

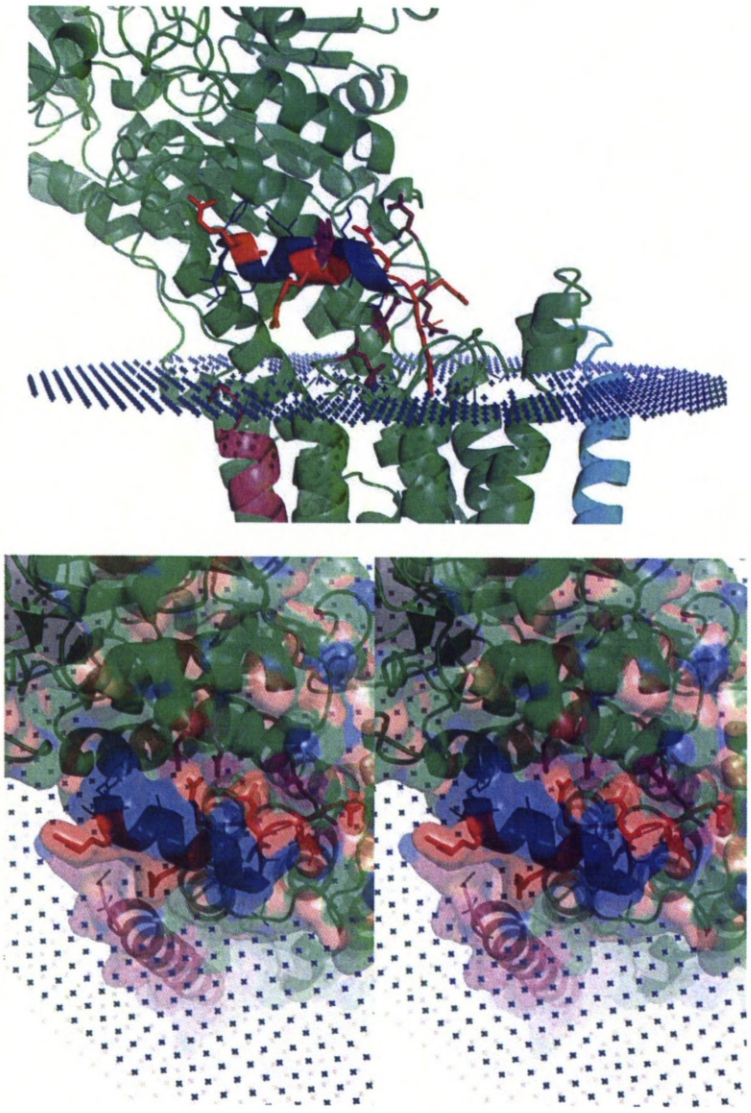

Figure 5.29. Proposed orientation of the α-helix in the cytoplasmic region of PLM

The helix of PLM is shown in blue with its arginine residues highlighted in red. Negatively charged residues in the Na^+, K^+-ATPase are shown in purple with side chains represented by sticks. Blue dots indicate membrane surface. 3D image shown in cross-eyed stereo.

The surface of the other possible site is shown in Figure 5.30. The arginine binding site is located in a very small pocket which is therefore incompatible with an α-helix. This is also true in the recently solved structure in a different conformation also shown on this figure (Yatime *et al.*, 2011) where the pocket is even smaller. It therefore seems unlikely that the alternative orientation due to Ser 68 phosphorylation of PLM corresponds to what is proposed in the model.

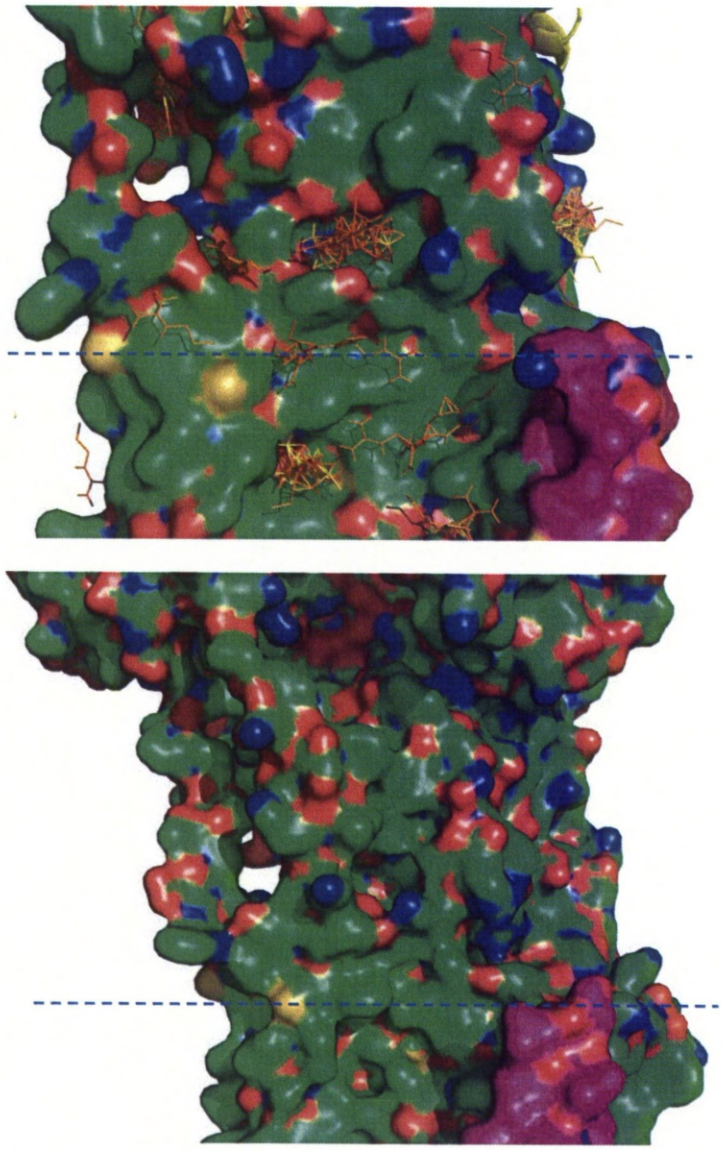

Figure 5.30. Predicted arginine binding sites on the surface of the Na^+, K^+-ATPase Although several sites are predicted in a pocket which lies above the membrane surface in a location similar to the proposed alternative orientation after phosphorylation of Ser 68 (top image) this pocket is sterically incompatible with an α-helix. An alternative Na^+, K^+-ATPase conformation (Yatime *et al.*, 2011) has an even smaller pocket (bottom image) making the interaction less likely. Cytoplasmic membrane surface indicated by dotted blue line.

5.4. Discussion

In this chapter several practical and bioinformatics methods have been employed to gain further insights of structural details of the cytoplasmic region FXYD proteins in the absence of any solved structures in either lipid bilayers or native cell membranes.

Currently, the γ-subunit of the Na^+, K^+-ATPase in pig (Morth *et al.*, 2007) and FXYD10 in shark (Shinoda *et al.*, 2009) are the only FXYD proteins to have a full structure solved in native membranes whilst in complex with the Na^+, K^+-ATPase. As both of these FXYD proteins have no cytoplasmic region it is difficult to determine how the cytoplasmic regions of other FXYD proteins may function in the absence of a structure of the Na^+, K^+-ATPase in complex with a FXYD protein such as PLM which does have a cytoplasmic region. PLM (Teriete *et al.*, 2007) and CHIF (Franzin *et al.*, 2007d) do have full structures solved and short form Mat-8 has secondary structure solved (Franzin *et al.*, 2007a) in SDS micelles in the absence of the Na^+, K^+-ATPase. SDS micelles are not representative of a cell membrane as they form a monolayer rather than a bilayer. This chapter also reveals that SDS micelles induce additional α-helical content in the cytoplasmic region of FXYD proteins (Figure 5.11. and Figure 5.12.). This is likely due to the highly negative charge present in SDS. As phospholipid membranes with a 33% negative charge have been revealed to induce α-helix in PLM_{38-72} (Hughes *et al.*, 2011) it is feasible that native membranes

that have around an overall 12.5% negative charge (Akio, 1971) will also induce α-helical content in PLM_{38-72}. This suggests the true helical content is only probably slightly lower than observed in the full length PLM NMR-structure solved in the presence of SDS micelles. This means the structural data are suitable for modelling discussed later.

TFE induces helical content in synthetic peptides only when they have the natural propensity to do so (Tamburro *et al.*, 1968). This was observed to be approximately 15% in PLM_{38-72} (Clayton *et al.*, 2005), 0% in short form Mat-8_{38-67}, 8% in Mat-$8lf_{38-93}$ and 8% in $CHIF_{38-69}$ (Table 5.1.). This suggests that the binding to negatively charged lipids and inhibition of the Na^+, K^+-ATPase by cytoplasmic peptides observed in Chapter 3 is dependent on structure, as PLM_{38-72} binds more strongly to negatively charged membranes and inhibits the Na^+, K^+-ATPase more than any of the other peptides tested and has the highest helical content. Mat-$8lf_{38-93}$ also binds to negatively charged membranes and inhibits the Na^+, K^+-ATPase but to a lesser extent than PLM_{38-72} and has lower helical content. Mat-$8sf_{38-67}$, which has no helical content, exhibits only very weak binding to negatively charged membranes and also has no effect on Na^+, K^+-ATPase activity. As Mat-$8sf_{38-67}$ and Mat-$8lf_{38-93}$ are identical apart from the insertion of an additional 26 amino acids in Mat-$8lf_{38-93}$ it can be hypothesised that the helical content in Mat-$8lf_{38-93}$ lies somewhere within this 26 amino acid insert. Mat-$8lf_{38-93}$ has also been analysed by solution

NMR experiments to try and assign the apparent helical content and confirm this hypothesis (Figure 5.7.-Figure 5.10.). However, the number of peaks observed is clearly below the number of amino acids present in the peptide. The spectra do reveal an increased dispersion of signal upon addition of TFE and an increase of quantity of NOEs. Although this does not help determine which amino acids form the helical content it does support the CD data that measured a small amount of secondary structure content in Mat-8lf$_{38\text{-}93}$. It is possible that the structure is unstable in solution and the cytoplasmic region of long form Mat-8 needs to be in a native environment in close proximity of lipid headgroups and the cytoplasmic region of the Na^+, K^+-ATPase.

Although the structure of PLM can be used to model the interaction of the cytoplasmic region of PLM with the Na^+, K^+-ATPase by replacing the co-ordinates of a FXYD protein in a Na^+, K^+-ATPase solved structure like has been done with γ-subunit of the Na^+, K^+-ATPase in pig kidney (Teriete *et al.*, 2009), this assumes the structure of PLM will not be at all affected by the Na^+, K^+-ATPase. It is even more difficult to determine how the cytoplasmic region for long form Mat-8 as the only structural data available for it are the limited data presented in this chapter. Therefore a bioinformatic approach was taken to try to understand how the cytoplasmic region of both PLM and long form Mat-8 might interact with the Na^+, K^+-ATPase. As they are both FXYD proteins and have homologous

transmembrane domains (Geering, 2006) it can be assumed they occupy the same relative location whilst in complex with the Na^+, K^+-ATPase as FXYD10 in spiny dogfish rectal gland Na^+, K^+-ATPase (Shinoda *et al.*, 2009). This also increases the chance that the cytoplasmic region of both PLM and long form Mat-8 bind to the Na^+, K^+-ATPase at a similar site. With this hypothesis, DiLiMOT was used to discover a potential motif present in the cytoplasmic region of PLM, long form Mat-8 and several other proteins known to interact with the Na^+, K^+-ATPase. The sequence of this motif is SxxRxS and its occurrence are the residues SIRRLS in PLM and SEWRSS in long form Mat-8. In PLM the motif is predicted to be at the end of a helix as predicted by psipred (Figure 5.17.) and solved by solution NMR in SDS micelles (Teriete *et al.*, 2007). It is also predicted to be disordered by metaPrDOS (Figure 5.19.) but this could suggest it forms a stable helix upon binding cell membranes and/or the Na^+, K^+-ATPase. Indeed the frequency of short linear motifs in predicted disorder regions is reported to be over 70% and it appears they have a propensity to form secondary structure upon interaction with an ordered protein (Fuxreiter *et al.*, 2007). The motif in long form Mat-8 is also predicted to be at the end of a helix (Figure 5.18.) but is predicted to be ordered (Figure 5.20.). Due to the potential functionality of this motif it is possible these residues are responsible for the helical content of long form Mat-8.

Several methods were employed to find potential binding sites for the motif on the surface of the Na^+, K^+-ATPase. Consurf revealed that the majority of the Na^+, K^+-ATPase is conserved in species which are known to express FXYD proteins. Although this is expected as relatively few species are known to express FXYD proteins it does limit the studies as finding conserved patches on protein surfaces is extremely helpful when finding binding sites (Figure 5.22.). Other methods to find potential peptide binding sites appeared to be limited due to the hydrophobic content of the transmembrane region skewing the data in the case of PPISP (Figure 5.24.) and STP (Figure 5.25.) whereas Prosurf (Figure 5.26.) only calculates sites that are involved in the interaction of the α-subunit of the Na^+, K^+-ATPase with the β-subunit and FXYD10. Prosurf did reveal certain sites close to the membrane surface in the cytoplasm.

The specific amino acids found in the instances of the motif in PLM and long form Mat-8 were run locally on PepSite using a structure of the Na^+, K^+-ATPase with large regions removed as they are inaccessible to the cytoplasmic region of the Na^+, K^+-ATPase (Figure 5.26.). Unfortunately these data were again skewed by the transmembrane region. The Na^+, K^+-ATPase structure inputted into PepSite had portions removed from the filed deemed inaccessible to the cytoplasmic region of PLM. This meant many potential binding sites were found in one region of the structure where part of the protein had been removed. This suggests these are false

positives as PepSite treated it as the surface of the protein when in reality it is not. PepSite did reveal one potential arginine binding site near the membrane surface in the cytoplasm in a similar location to the sites determined by Prosurf. The altered Na^+, K^+-ATPase was also used with Anchorsmap with amino acids in the instances of the motif of SIRRLS in PLM and SEWRSS in long form Mat-8 (Figure 5.27-Figure 5.28.), with the exception of serine and isoleucine are incompatible with Anchorsmap. This revealed two potential locations for the docking of the motif to SIRRLS in PLM and SEWRSS in long form Mat-8. One orientation (Figure 5.29) puts the cytoplasmic helix in a site both sterically and electrostatically compatible with the Na^+, K^+-ATPase and would only require a small change in orientation of the cytoplasmic region compared to the SDS micelle solved structure (Teriete *et al.*, 2007). NMR studies revealed that Ser 68 phosphorylation of PLM causes a conformational change in the cytoplasmic helix (Teriete *et al.*, 2009). It was proposed that the cytoplasmic region either adapts a conformation identical to the structure in SDS micelles or an alternative conformation where it binds to an alternative site on the Na^+, K^+-ATPase in close proximity of the negatively charged crevice located in the transmembrane region (Figure 3.3.). It is unlikely that PLM adopts a conformation identical to the SDS micelle structure as it is solved in both a lipid-free, and a Na^+, K^+-ATPase-free environment. The surface of the Na^+, K^+- proposed alternative PLM conformation induced by Ser 68 phosphorylation also seems unlikely as

despite there being potential arginine sites found by Anchorsmap in this region, the surface in is not compatible with an α-helix in either the E2P.($2K^+$) or the E2P conformations (Figure 5.30). The true change in the cytoplasmic region of PLM due to phosphorylation could be far more simple with the proposed interaction (Figure 5.29.) being weakened and thus causing movement of the helix due to the negative charge added by the phosphate group. This would explain the smaller effect on Na^+, K^+-ATPase function observed in phosphorylated PLM_{38-72} over unphosphorylated PLM_{38-72}.

As the proposed interaction occurs at the N-terminus of helix M5 of the Na^+, K^+-ATPase it could feasibly cause the whole helix to move towards the cytoplasmic region for PLM. As described in the introduction (Chapter 1.1.3.), the third Na^+ binding site is located at the C-terminus of helix M5, M6 and M9 (Morth *et al.*, 2007) so a movement of helix M5 is likely to have an effect on the affinity for Na^+ of the third binding site which could explain the reduction of ATPase activity caused by the cytoplasmic region of PLM.

The true nature of the interaction of the cytoplasmic region of PLM and long form Mat-8 with the Na^+, K^+-ATPase will only be definitively understood if a structure for both in complex with the Na^+, K^+-ATPase is solved. However this provides some possibilities of how the interactions

may occur. Further bioinformatics could also be used to model full length FXYD proteins with the Na^+, K^+-ATPase to see how the entire cytoplasmic region of PLM and long form Mat-8 could orientate whilst in the proposed conformations.

Chapter 6

6.1. NMR studies of ouabain analogues

The previous three chapters concentrated on structural and biophysical studies of FXYD proteins, physiological regulators of the Na^+, K^+-ATPase. This chapter concentrates on structural studies of cardiac glycosides which are pharmacological regulators of the Na^+, K^+-ATPase and possibly have an additional physiological role. The cardiac glycosides such as ouabain have been used as drugs for cardiac arrhythmia and congestive heart failure over 200 years (Withering, 1785). The cardiac glycosides are potent and very specific inhibitors of the Na^+, K^+-ATPase (Hansen, 1984). As the cardiac glycosides inhibit the Na^+, K^+-ATPase there is an increase of Na^+ ions in the cytoplasm with a loss of intracellular K^+ to the extracellular space. The increased Na^+ concentration inside the cell lowers the activity of the Na^+/Ca^{2+} exchanger that usually exchanges extracellular Na^+ for intracellular Ca^{2+} (Tanaka *et al.*, 2007). With the Na^+/Ca^{2+} exchanger not functioning intracellular Ca^{2+} concentration also increases. Cardiac glycosides are described as positive inotropic agents as by increasing intracellular Na^+ and Ca^{2+} ion concentration they increase the strength of heart muscle contraction.

There are still uncertainties about the recognition site for cardiac glycosides and the structure and orientation of drugs within the site of

action. Ouabain binds to the K^+ sensitive Na^+, K^+-ATPase in the E2 conformation (Yoda and Yoda, 1982). Before K^+ binds the Na^+, K^+-ATPase is in a high affinity ouabain binding state (E_2P) and after K^+ binds it is in a low affinity ouabain binding state ($E_2P(2K^+)$). Before the Na^+, K^+-ATPase had been successfully crystallized and subsequently analysed by X-ray crystallography in 2007 (Morth *et al.*, 2007) there were few structural insights into how the Na^+, K^+-ATPase/ouabain reaction might occur. In the absence of a crystal structure, solid-state NMR provided initial indicators of the structure of cardiac glycosides in the site of action. (Middleton *et al.*, 2000). To achieve this ouabain was modified with acetonide bridges at two locations to allow isotope labels to be incorporated for NMR studies. Figure 6.1 shows the chemical structures of ouabain and the derivatives used. Diacetylated ouabain (ODA Figure 6.1.) was produced with [$^2H_6$]acetone which gave deuterated methyl groups. This made it suitable for analysis by ^2H NMR to probe the local dynamics of the interaction between ouabain and the Na^+, K^+-ATPase. All modified ouabain derivatives were inhibitors albeit with a lower potency than ouabain.

Ouabain

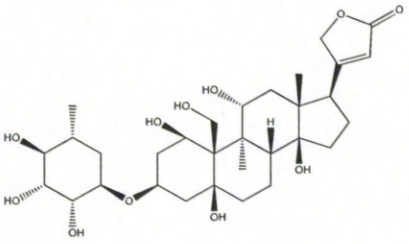

Monoacetonide (OMA)

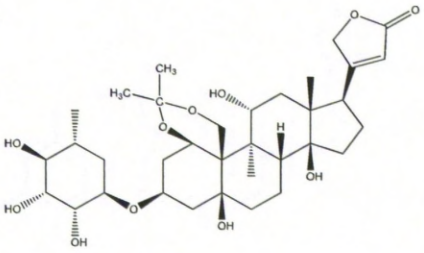

Diacetonide (ODA)

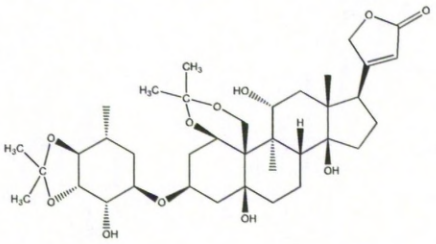

steroid-Flurodiacetonide (OFDA)

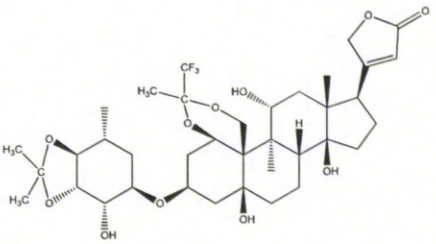

Figure 6.1. Ouabain and acetonide derivatives. The chemical structures of ouabain and the chemical derivatives are shown. OMA has one acetyl bridge at the steroid group whereas ODA has an acetyl bridge at both the steroid and rhamnose group. OFDA is produced by monoacetylating ouabain with fluroacetone then transferring to acetone or ^{13}C acetone to form the rhamnose acetyl bridge. ODA can be produced with [$^{2}H_6$]acetone which gives deuterated acetyl groups i.e. CH_3 groups would instead be CD_3 groups. OFDA can also be produced with a CH_2F group in place of CF_3 (Middleton *et al.*, 2000).

^{2}H NMR revealed the rhamnose was only loosely associated with the binding site on the Na^+, K^+-ATPase whereas the steroid group was more constrained. CP-MAS ^{13}C-NMR on ODA revealed the acetyl bridge of the rhamnose group had a chemical shift change upon binding to the Na^+, K^+-ATPase, which is possibly due to the rhamnose being situated close to aromatic side groups. OFDA was used in double resonance experiments

(^{19}F, ^{13}C) to determine the structure of OFDA whilst bound to the Na^+, K^+-ATPase. These data was used to model the interaction of ODA within the Na^+, K^+-ATPase binding site, using the recently determined crystal structure of the homologous protein SERCA (Toyoshima *et al.*, 2000). The model showed just one possibility of the interaction with ODA bound to the Na^+, K^+-ATPase whilst lying across the membrane surface obeying all the constraints determined by NMR. The absolute orientation of the ouabain ligand within the Na^+, K^+-ATPase could not be determined.

More recently crystal structures of the Na^+, K^+-ATPase including a structure from spiny dogfish with bound ouabain (Ogawa *et al.*, 2009) have shed more light on the digitalis site. This Na^+, K^+-ATPase was stabilised in a form analogous to the E_2P ($2K^+$) conformation by using MgF_4^{2-} before crystallising. This is the low ouabain affinity conformation. Ouabain was soaked into the crystal and then the structure of the complex was solved by x-ray crystallography. Ouabain was found to be intercalated into the membrane and agrees with the constraints revealed in the NMR studies (Middleton *et al.*, 2000). Figure 6.2. compares the possible model from the NMR studies and the crystal structure of the Na^+, K^+-ATPase with bound ouabain.

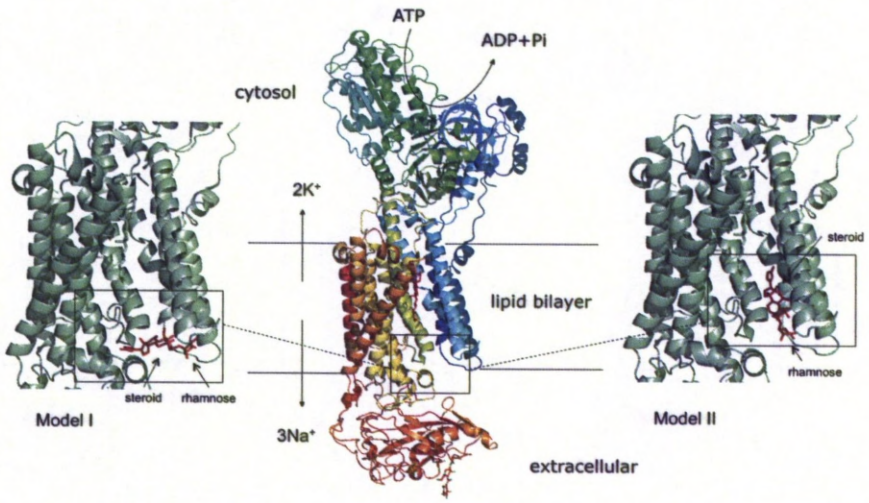

Figure 6.2. Possible models of Na^+, K^+-ATPase/ouabain interaction. Following dynamics and solid state NMR studies model I was created as a possible interaction that obeyed the constraints determined. Model II which also obeys these constraints comes from a structure of Na^+, K^+-ATPase in a low ouabain affinity conformation that had ouabain soaked into the crystal.

Questions still remain on the orientation of ouabain in membrane embedded Na^+, K^+-ATPase, largely because the crystal structure was limited in that it was solved in a low ouabain affinity conformation of Na^+, K^+-ATPase. This may not even be observed in nature as the high affinity form of Na^+, K^+-ATPase preceded the low affinity form in the cycle so upon binding ouabain it stops the cycle from continuing. The Na^+, K^+-ATPase was also crystallised before ouabain was added which means ouabain was binding to an inactive protein, which may affect the interaction.

This chapter aims to characterise the Na^+, K^+-ATPase/cardiac glycoside interaction in a non-crystalline, membrane environment using *in silico* and solid-state NMR methods. The aims of this work provided an opportunity to evaluate a new solid-state NMR approach for studying ligand binding using paramagnetic broadening relaxation agents.

6.2. Materials and Methods

6.2.1. Materials

Preparative and analytical thin-layer chromatography (TLC) plates, ouabain octahydrate and fluoroacetone provided by Sigma-Aldrich. Acetone was purchased from Fisher Scientific. ^{13}C acetone was purchased from Goss Scientific. Na^+, K^+-ATPase was prepared as described in chapter 3.2.2.

6.2.2.1. Na^+, K^+-ATPase/ouabain docking (GOLD)

Bioinformatics studies were performed with Genetic Optimisation for Ligand Docking (GOLD) (Jason *et al.*, 2005). Experimental parameters were given to Dr. Jaclyn Bibby who ran the experiments. This software relies on a genetic algorithm (GA) that incorporates many features. The GA allows for full ligand flexibility or fixed ligand and partial selected active site flexibility (Jones *et al.*, 1997). Crucially the GA ensures each docking would cause loosely bound water to displace on binding which is

fundamental to any ligand/protein binding. Experimentally determined interactions deposited on the Protein Data Bank have been compared to interactions determined by GOLD and have 71% agreement (Jones *et al.*, 1997). Various Na^+, K^+-ATPase structures from the PDB (PDBID: 3KDP (Morth *et al.*, 2007), PDBID: 2ZXE (Shinoda *et al.*, 2009) and PDBID: 3A3Y (Ogawa *et al.*, 2009)) were selected as protein files. A SERCA structure also from the PDB was selected due to its homology with the α-subunit of the Na^+, K^+-ATPase as a negative control (PDBID: 1SU4 (Toyoshima *et al.*, 2000)). The ouabain ligand was extracted from the Na^+, K^+-ATPase PDB file with bound ouabain (3A3Y). OMA and ODA ligands were made using the chemid database. The search point centres were selected based on the cluster of amino acids showed to be involved in ouabain binding in mutagenesis studies (Price and Lingrel, 1988; Price *et al.*, 1989; Lingrel *et al.*, 1991; Canessa *et al.*, 1992; Burns and Price, 1993; Canessa *et al.*, 1993; Schultheis and Lingrel, 1993; Schultheis *et al.*, 1993; Palasis *et al.*, 1996; Croyle *et al.*, 1997b). The top 100 ranked orientations were selected with ChemScore (Baxter *et al.*, 1998) The positions and angles defining the orientation of ouabain in the output files were calculated using a C program developed by Dr. David Middleton and visualised using Origin.

6.2.2.2. Modeller

Sali Lab Modeller 9v8 (Sali and Blundell, 1993) was used to produce a homology model of the high-ouabain affinity E_2P conformation of the Na^+, K^+-ATPase using the E_2P conformation of SERCA deposited in the PDB (PDBID:3B9B) as a template (Toyoshima *et al.*, 2000). Methods follow the basic modelling tutorial on the Sali Lab website (http://salilab.org/modeller/tutorial). The spiny dogfish rectal gland was selected and its sequence was aligned using the align2d() command in modeller which takes into account structural information of the template as well as sequence. After the models were built the best model was selected with the lowest discrete optimized protein energy (DOPE) assessment score which is a statistical potential which assesses homology models based on the finite size compared to the template structure.

6.2.3. Synthesis of ouabain derivatives

Ouabain monoacetonide (OMA) and ouabain diacetonide (ODA) were prepared following a procedure described earlier (Middleton *et al.*, 2000). Ouabain octahydrate (50 mg) was dissolved in acetone (1 g). Copper sulphate (200 mg) was added and mixture was stirred at room temperature in darkness for 48 hr. The product solution was separated from insoluble copper sulfate by vacuum filtration. The remaining product was analysed by analytical TLC to confirm that the reaction had occurred to produce OMA and ODA (Figure 6.1). To prepare ^{13}C-labelled OMA and ODA [2-^{13}C]acetone was used as the solvent.

6.2.4. OMA and ODA purification

6.2.4.1 Analytical thin layer chromatography

After ouabain was incubated in acetone for 2 days the product solution was spotted onto analytical TLC plates and placed in a mobile phase of 3:1 ethyl acetate: methanol and the solvent front allowed to run ~10 cm before being dried and sprayed with 50% H_2SO_4. Plates were placed on a heat block until development.

6.2.4.2 Silica chromatography

Silica slurry was produced by mixing silica with 3:1 ethyl acetate: methanol. The slurry was then poured into the gravity column and packed under vacuum. The column was then closed before slowly adding the sample to the silica and loading onto the column with additional solvent. 1mL samples were taken as solvent was continuously added to the top. Samples checked via analytical TLC to find which fractions contained ouabain derivatives.

6.2.4.3. Preparative Thin Layer Chromatography

Samples were streaked onto the base of preparative TLC plates with a glass pasteur pipette and placed in solvent (3:1 ethyl acetate: methanol) and the solvent line was allowed to run close to the edge of the plate before being dried and sprayed with 50% H_2SO_4. A narrow preparative TLC plate was run alongside this before being dried and sprayed with 50% H_2SO_4. This plate was developed on a heat block and used as a guide for the other plate

to determine where to scrape off silica that contains OMA or ODA. Silica was collected in test tubes and OMA or ODA was eluted by adding methanol and vortexing. Samples were then filtered to remove silica, dried to a film under nitrogen and fully dried on the vac pump overnight.

6.2.5. Testing inhibitory potencies of ouabain derivatives

The inhibitory potencies of ouabain, OMA and ODA and were calculated as the IC_{50} (the inhibitor concentration causing 50% enzyme inactivation) for ATP hydrolysis using the Baginski method as has been shown previously (Middleton *et al.*, 2000).

Na^+, K^+-ATPase 0.5 mg protein ml^{-1}) was preincubated in incubation medium (3 mM $MgCl_2$, 3 mM Pi, 40 mM Tris, pH 7.3) and 0–100 mM of ouabain, OMA or ODA. This was incubated at 20°C for 60 min, an aliquot was subsequently transferred to hydrolytic assay medium (30 mM Histidine, 3 mM Na-ATP, 20 mM KCl, 4 mM $MgCl_2$, 0.33 mg mL^{-1} albumin), whereby the enzyme and glycoside was diluted 40-fold and incubated for a further 10 min before determining the liberated Pi by a colorimetric assay. The selectivity and binding affinity of the ouabain derivatives were determined from competition experiments using [^{3}H]ouabain. Na^+, K^+-ATPase membranes (0.25 mg protein ml^{-1}) were added to incubation medium containing 5–280 nM ouabain with 3,000 B

ml^{-1} [^{3}H]ouabain and either OMA or ODA to a final concentration of 0–5 mM. The mixture was incubated at 37°C for 3 h and filtered to determine the amount of free ouabain left in the solution. The amount of bound ouabain was calculated as the difference between the radioactivity of the initial incubation medium and the filtrate. Displacement of [^{3}H]ouabain by OMA and ODA was followed by incubating Na^+, K^+-ATPase (0.23 mg protein ml^{-1}) in incubation medium containing 30 nM [^{3}H]ouabain for 60 min at 37°C. Ouabain, OMA, or ODA was added to a final concentration of 50 mM, and the release of bound [^{3}H]ouabain was followed for up to 25 hr by filtration as described above (Middleton *et al.*, 2000).

6.2.6. ^{13}C NMR of ouabain derivatives

Samples were transferred to a 4 mm diameter magic-angle spinning rotor. The rotor held 100 µL of membrane sample containing Na^+, K^+-ATPase (13 nmoles) complexed with ouabain or derivatives (16 µmoles) and concentrations of Mn^{2+} of 0-5 mM. Experiments are based on previous solid-state NMR studies of the Na^+, K^+-ATPase (Middleton *et al.*, 2011). Spectra were obtained by using a Bruker Avance 400 instrument operating at a frequency of 100.13 MHz for ^{13}C. Membrane samples were spun at a MAS rate of 5.0-8.0 kHz for one-dimensional (1D) experiments. 1D spectra were obtained by averaging no more than 170 000 transients. Conditions common to all experiments were a 4.0 µs ^{1}H excitation pulse,

two-pulse phase modulated (TPPM) proton decoupling at a field of 85 kHz during signal acquisition and a 1 s recycle delay pulse. For CP-MAS experiments cross-polarisation was achieved with a 2 ms contact time at a proton field of 65 kHz. Each spectrum was the result of accumulating 102,400 transients in 5 blocks of 20,480 transients at temperatures of -25°C, -10°C and 4°C.

6.3. Results

6.3.1. Investigation of the Na^+, K^+-ATPase/ouabain interaction using GOLD

In order to gain further insight into the interaction of cardiac glycosides with the Na^+, K^+-ATPase after the low ouabain affinity Na^+, K^+-ATPase structure was published (Ogawa *et al.*, 2009) GOLD was selected as a software package to dock the ouabain ligand into the Na^+, K^+-ATPase structures deposited into the PDB (PDBIDs: 3KDP, 2ZXE, 3A3Y). GOLD requires a central residue to be selected and calculates docking sites within a 20 Å from this residue. The central residue was selected by highlighting residues on the Na^+, K^+-ATPase shown to effect ouabain binding (Figure 1.9 and Table 6.1.) and picking a central point in the main cluster of residues (central start point). After experimental parameters were defined, all GOLD experiments were run by Dr. Jacyln Bibby.

Table 6.1. Amino acids shown to affect ouabain sensitivity of the Na^+, K^+-ATPase in site directed mutagenesis experiments. The decrease in apparent $K_{0.5}$ is given to allow comparison between different species and different studies of the Na^+, K^+-ATPase. The fold increase is therefore relative to the wild type Na^+, K^+-ATPase used in the cited studies.

Original Amino Acid	*Decrease in apparent $K_{0.5}$ (-fold)*	*Reference*
C104F	23	(Canessa *et al.*, 1992)
Y108A	9.1	(Canessa *et al.*, 1992)
Q111R	12.5	(Price and Lingrel, 1988)
D121N	65	(Price *et al.*, 1989)
N122D	3.9	(Lingrel *et al.*, 1991)
P118K	3.9	(Schultheis and Lingrel, 1993)
Y308C	2.7	(Canessa *et al.*, 1993)
L330Q	7.9	(Croyle *et al.*, 1997b)
A331G	3.1	(Croyle *et al.*, 1997b)
T338N	3.3	(Croyle *et al.*, 1997b)
F786N	19	(Palasis *et al.*, 1996)
L793P	24	(Palasis *et al.*, 1996)
T797N	80	(Burns and Price, 1993)
F863L	5.7	(Palasis *et al.*, 1996)
R880P	7.9	(Schultheis *et al.*, 1993)
F982S	6.3	(Croyle *et al.*, 1997b)

6.3.1.1. Validation of GOLD

Although GOLD has successfully produced publishable protein/ligand data in other membrane proteins (Horsefield *et al.*, 2006; Klepsch *et al.*, 2011) experiments needed to be performed to ensure the suitability of GOLD to docking ouabain into the Na^+, K^+-ATPase. The low ouabain affinity Na^+, K^+-ATPase (PDBID:3KDP) structure was used to test the reliability of the GOLD prediction algorithm. The ouabain ligand was removed from 3KDP in PyMol then redocked back into it using GOLD (Figure 6.3.). The active site centre was selected in the middle of the main cluster of amino acids that affect ouabain binding (Table 6.1.) and ouabain was docked within a 20 Å range of this active site centre. The top 100 ranked orientations all only deviate slightly from the x-ray crystallography structure (Figure 6.3.) To test the GOLD software further a new start point was selected away from the main cluster of residues at the protein surface (Leu 791) in close proximity of the previous active site centre. This results in a more varied distribution of orientations (Figure 6.4.) and it does not pick up the actual ouabain bound in the original structure. This shows the software is most accurate when a specific active site location is selected.

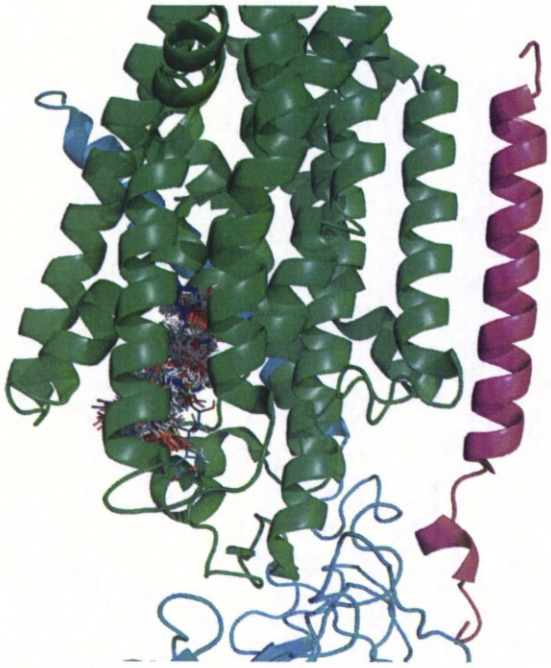

Figure 6.3. Evaluating the reliability of GOLD for prediction of Na^+, K^+-ATPase/ouabain interactions. The Na^+, K^+-ATPase structure with bound ouabain (PDBID:3A3Y) had its ligand removed and then redocked using ouabain. The active site centre was picked in the middle of the main cluster of amino acids that affect ouabain binding (Table 6.1.) and ouabain was docked within a 20 Å radius of this. The ouabain bound in the original structure is shown in navy blue.

Figure 6.4. Evaluating the reliability of GOLD for prediction of Na^+, K^+-ATPase/ouabain interactions. The Na^+, K^+-ATPase structure with bound ouabain (PDBID:3A3Y) had its ligand removed and then redocked using ouabain. The active site centre was picked at the surface of the protein in close proximity of the previous centre used (Figure 6.4.). Ouabain was docked within a 20 Å radius of this active site centre. The ouabain bound in the original structure is shown in navy blue.

The reliability of using GOLD to predict Na^+, K^+-ATPase/ouabain interactions was tested by using SERCA as a negative control. SERCA is homologous to the α-subunit of the Na^+, K^+-ATPase which ouabain binds to. Despite this homology, ouabain does not bind to SERCA so GOLD should give a relatively random distribution of orientations of docked ouabain. A non-occluded E2 conformation structure of SERCA was used with PDBID: 3B9B (Toyoshima *et al.*, 2000) as the corresponding E2

conformation in the Na^+, K^+-ATPase is the high ouabain affinity state. The active site centre selected corresponds to the location of the active site centre used in the Na^+, K^+-ATPase in the middle of the main cluster of amino acids that affect ouabain binding. Figure 6.5. shows there are two major clusters of dockings that are both very broad in distribution and orientation.

Figure 6.5. Evaluating the reliability of GOLD for prediction of Na^+, K^+-ATPase/ouabain interactions using SERCA as a negative control. The E2 SERCA structure (PDBID: 3B9B) is homologous to the α-subunit of the Na^+, K^+-ATPase but does not bind ouabain. The active site centre was picked in the middle of the main cluster of amino acids that affect ouabain binding (Table 6.1.) and ouabain was docked within a 20 Å radius of this.

6.3.1.2. Application of GOLD to the ouabain free structures of the Na^+, K^+-ATPase

Ouabain was next docked using GOLD on the two originally deposited ouabain-free structures of the Na^+, K^+-ATPase (Morth *et al.*, 2007; Shinoda *et al.*, 2009) that are from pig kidney (PDBID:3KDP) and spiny dogfish rectal gland (PDBID:2ZXE). This was designed to determine if there were any potential differences in the interaction of the Na^+, K^+-ATPase and ouabain between species. Both pig kidney (Figure 6.6.) and spiny dogfish rectal gland (Figure 6.7.) appear similar with two major clusters of dockings.

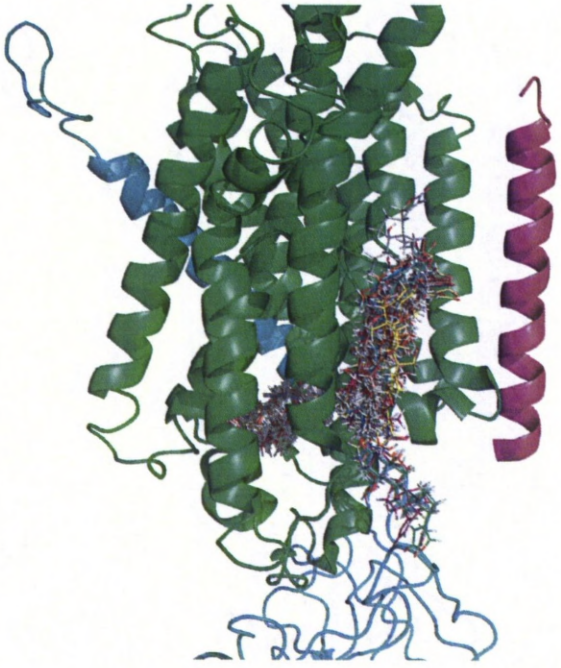

Figure 6.6. GOLD docking distribution of ouabain into Na^+, K^+-ATPase in pig kidney. GOLD was used to dock ouabain into the Na^+, K^+-ATPase from pig kidney (PDBID: 3KDP) in the E_2P ($2K^+$) conformation. The active site centre was picked in the middle of the main cluster of amino acids that affect ouabain binding (Table 6.1.) and ouabain was docked within a 20 Å radius of this.

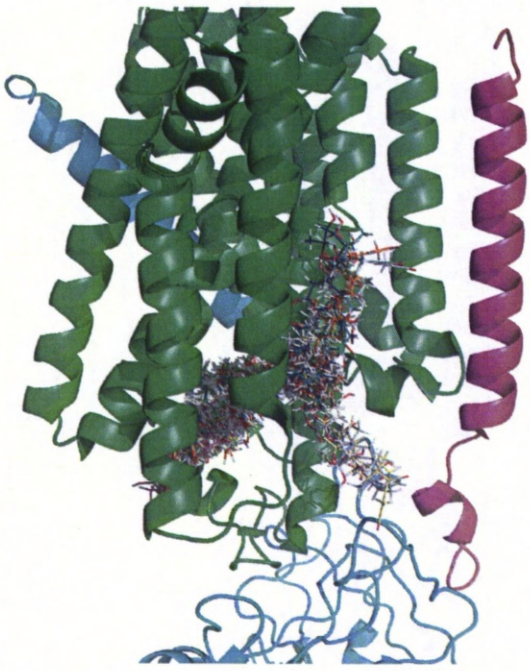

Figure 6.7. GOLD docking distribution of ouabain into Na^+, K^+-ATPase in spiny dogfish rectal gland. GOLD was used to dock ouabain into the Na^+, K^+-ATPase spiny dogfish rectal gland (PDBID: 2ZXE) in the E_2P ($2K^+$) conformation. The active site centre was picked in the middle of the main cluster of amino acids that affect ouabain binding (Table 6.1.) and ouabain was docked within a 20 Å radius of this.

6.3.1.3. Statistical analysis of GOLD results

Although the orientations of ouabain docked in the Na^+, K^+-ATPase appear similar in both species as would be expected, there are noticeable differences between them. To visualise this data statistically a C program was written and run by Dr. David Middleton to determine three variables. The first is the distance (r) from the centre of mass of each docked ouabain ligand to the centre of mass of the Na^+, K^+-ATPase. The two other variables are a pair of angles (θ and ψ). These angles are calculated relative

to the principal axes of inertia of the Na^+, K^+-ATPase (Figure 6.8a.). A straight line is drawn between two points on ouabain (Figure 6.8b.). These sites were selected as they are at opposite ends of the most rigid part of the ouabain structure. The angles produced with this line in the principal axes of inertia of the Na^+, K^+-ATPase are calculated on both the xy and yz planes (Figure 6.8c.). These angles define the orientation of the inhibitor in within the Na^+, K^+-ATPase.

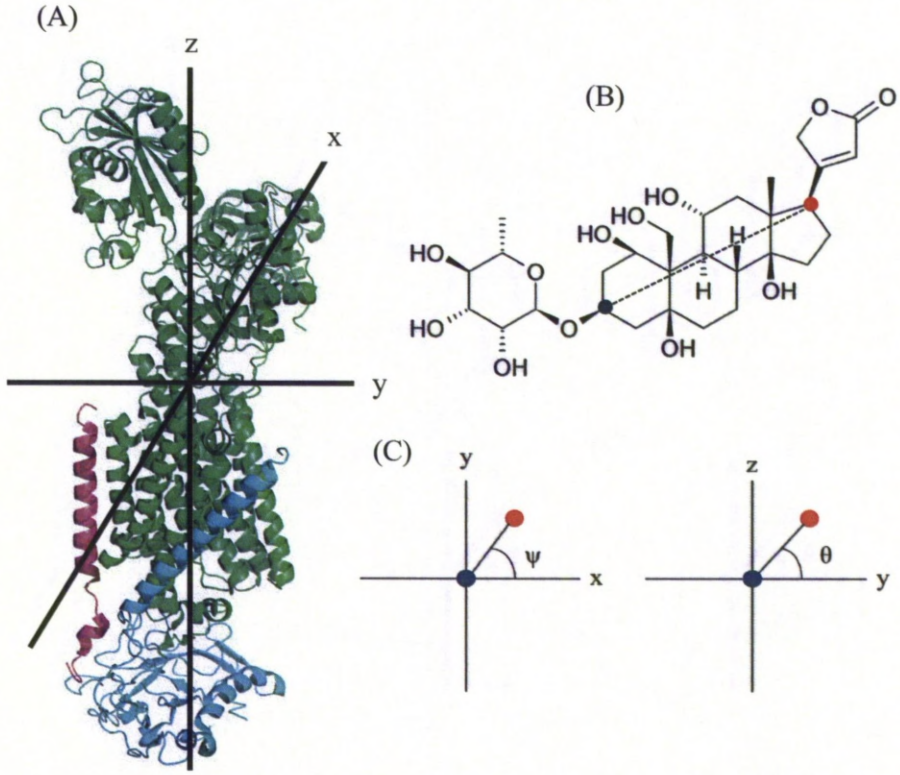

Figure 6.8. Definition of the angles defining the orientation of ouabain docked into Na^+, K^+-ATPase. Angles of docked ouabain ligands relative to the Na^+, K^+-ATPase were calculated to represent orientations. This was performed by first rotating the Na^+, K^+-ATPase into its principal axes of inertia (A) and selecting two sites on the ouabain ligand in a rigid part of the molecule labelled in red and blue (B). With this data the angles θ and ψ were calculated (B)

The distance (r) was calculated for both pig kidney and spiny dogfish rectal gland (Figure 6.9.) In pig kidney the majority of r values are 46-48 Å whereas in spiny dogfish rectal gland the majority of r values are 50-52 Å. A small change like this could be explained by the small differences in structure between the two species.

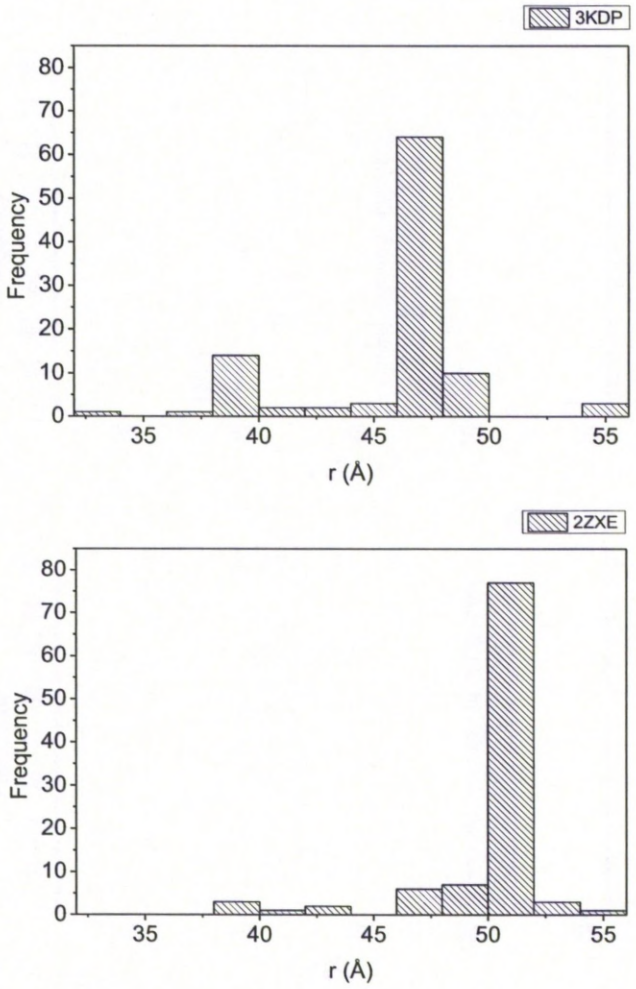

Figure 6.9. Histograms representing the distribution of distances from the centre of mass of the Na^+, K^+-ATPase to the centre of mass of the top 100 ranked ouabain dockings in pig kidney and spiny dogfish rectal gland. The distances from each of the top 100 ranked ouabain dockings obtained from GOLD in pig kidney (PDBID: 3KDP) and spiny dogfish rectal gland (PDBID: 2ZXE) were calculated and are presented here as histograms

The angles θ and ψ that define the orientation of a docked ouabain ligand in the Na^+, K^+-ATPase site are plotted as a scattergram for both pig kidney

and spiny dogfish rectal gland (Figure 6.10.). These reveal the majority of orientations have a similar ψ angle of approximately -45°. There is a greater spread of distributions of angle θ in both species. Also there are two separate clusters between species of angle θ at around 50° for spiny dogfish rectal gland and 135° for pig kidney which again is likely due to the differences in structure and sequence between the Na^+, K^+-ATPase in pig kidney and spiny dogfish rectal gland. Crucially there are no dockings at 90°, i.e. parallel to the membrane surface which was arbitrarily defined in the earlier solid-state NMR study (Middleton *et al.*, 2000) which suggests the x-ray crystallography data showing ouabain parallel with the transmembrane helices of the Na^+, K^+-ATPase (Shinoda *et al.*, 2009) is a more accurate representation of the interaction.

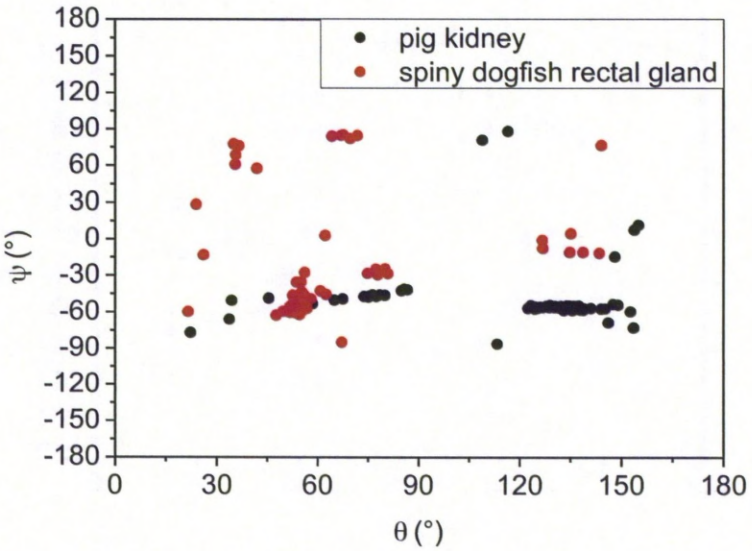

Figure 6.10. Scattergram representing spread of orientations of the top 100 ranked ouabain dockings in the principal axes of inertia of the Na^+, K^+-ATPase from pig kidney and spiny dogfish rectal gland. The angles Ψ and θ were calculated (explained in Figure 6.9.) for the top 100 ranked ouabain dockings and plotted against each other in a scattergram to give an idea of the spread and of orientations obtained from GOLD experiments.

The structure of the Na^+, K^+-ATPase in the ouabain-sensitive E_2P conformation is not known. A homology model of the Na^+, K^+-ATPase in the E_2P conformation was therefore produced using modeller by taking the spiny dogfish rectal gland sequence and modelling it to the E_2P structure of SERCA (Toyoshima *et al.*, 2000). SERCA is homologous to the α-subunit of the Na^+, K^+-ATPase and no E_2P structure of the Na^+, K^+-ATPase had been published at the time of writing. The E_2P conformation is the high

ouabain affinity conformation so is more ideal for these studies. Figure 6.11. shows that in this model there is a far less random distribution of orientations. This suggests the high ouabain affinity Na^+, K^+-ATPase may bind ouabain in a very different way to the low ouabain affinity Na^+, K^+-ATPase.

Figure 6.11. GOLD analysis of ouabain docking to the E_2P model of the Na^+, K^+-ATPase. The E_2P conformation of the Na^+, K^+-ATPase is the high ouabain affinity conformation whereas the two structures studied so far are the low ouabain affinity E_2P ($2K^+$) conformation. An E_2P structure was produced in Modeller (modelled to the E_2P SERCA structure) and the GOLD experiments were run as before.

6.3.2. NMR Analysis

Based on GOLD, ouabain is predicted to have a higher propensity to dock into the protein roughly parallel with the long axis rather than sitting on the

membrane surface. The E2P model however revealed there are potential differences between how ouabain binds to the low-ouabain affinity and high-ouabain affinity conformations of the Na^+, K^+-ATPase. Therefore, a novel approach using solid-state NMR combined with paramagnetic broadening was used to analyse the orientation of ouabain in the high-affinity Na^+, K^+-ATPase state. For NMR analysis ^{13}C must be incorporated into ouabain without losing affinity for the digitalis site. This was achieved previously by forming the acetonides (OMA and ODA) with ^{13}C labels at the quaternary carbon sites (Middleton *et al.*, 2000). The solid-state NMR ^{13}C spectrum of ODA bound to the Na^+, K^+-ATPase has two signature peaks at ~100 ppm and ~110 ppm from the steroid and rhamnose acetonides respectively (Middleton *et al.*, 2000). The identity of ^{13}C labelled OMA and ODA was confirmed by mass spectrometry (Figure 6.12.) with masses of 650.6 and 690.6 expected respectively (this includes sodium adducts).

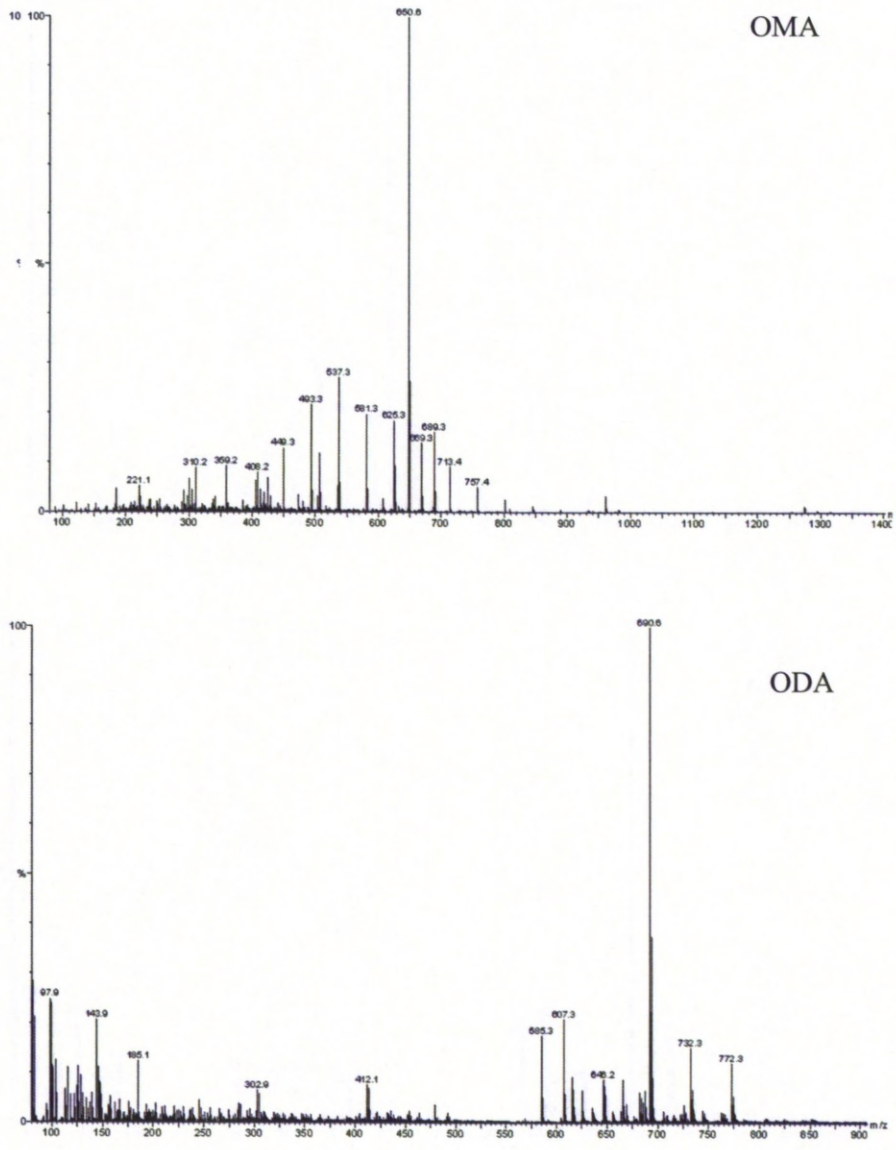

Figure 6.12 Mass Spectrometry of OMA and ODA with ^{13}C acetonide bridges.

6.3.2.1. Testing suitability of OMA and ODA using GOLD

To ensure OMA and ODA would bind to the Na^+, K^+-ATPase in a similar way to ouabain GOLD was used to dock the OMA (Figure 6.14.) and

ODA (Figure 6.14.) ligands to spiny dog rectal gland as had been done previously with ouabain (Figure 6.7). Statistical analysis shows a very similar distribution of distances from the centre of mass of the Na^+, K^+-ATPase to the centre of mass of ligand (ouabain/OMA) as shown in Figure 6.15. The distribution of orientations of ligand is also similar as shown in Figure 6.16 although the main cluster of orientations has become more widespread.

Figure 6.13. GOLD docking distribution of OMA into Na^+, K^+-ATPase in spiny dogfish rectal gland. GOLD was used to dock OMA into the Na^+, K^+-ATPase spiny dogfish rectal gland (PDBID: 2ZXE) in the E_2P ($2K^+$) conformation. The active site centre was picked in the middle of the main cluster of amino acids that affect ouabain binding (Table 6.1.) and ouabain was docked within a 20 Å radius of this.

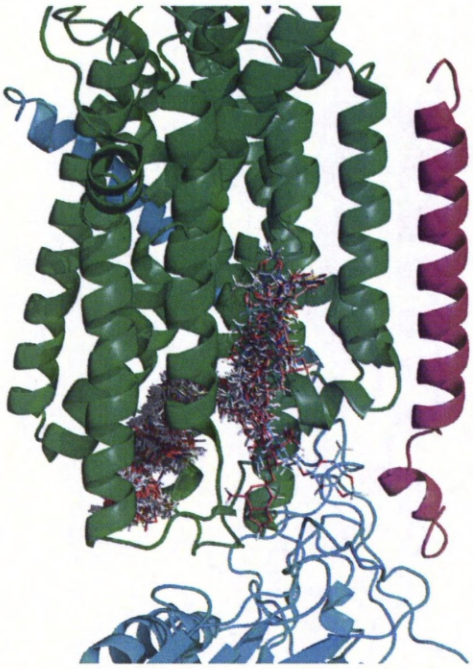

Figure 6.14. GOLD docking distribution of ODA into Na^+, K^+-ATPase in spiny dogfish rectal gland GOLD was used to dock ODA into the Na^+, K^+-ATPase spiny dogfish rectal gland (PDBID: 2ZXE) in the E_2P ($2K^+$) conformation. The active site centre was picked in the middle of the main cluster of amino acids that affect ouabain binding (Table 6.1.) and ouabain was docked within a 20 Å radius of this.

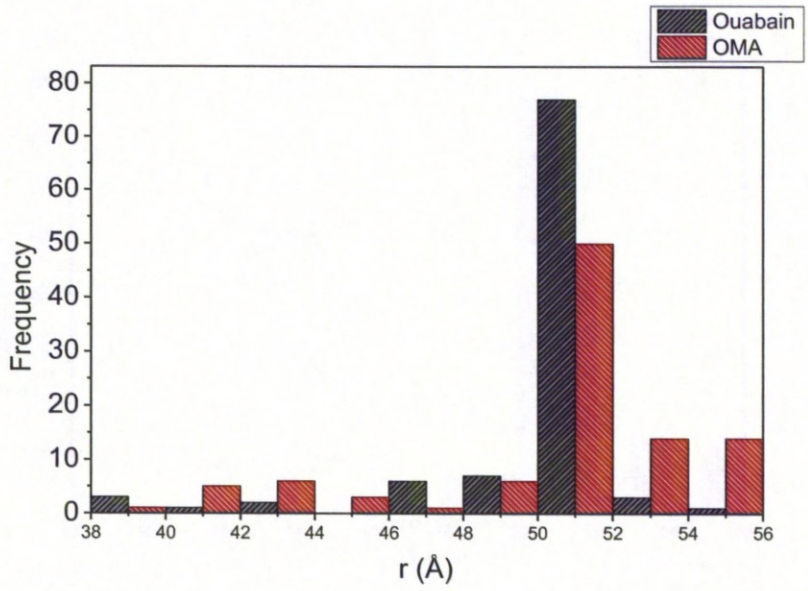

Figure 6.15. Histogram representing the comparison of distribution of distances from the centre of mass of the Na^+, K^+-ATPase to the centre of mass of the top 100 ranked dockings in spiny dogfish rectal gland between ouabain and OMA. The distances from each of the top 100 ranked ouabain and OMA dockings obtained from GOLD in spiny dogfish rectal gland (PDBID: 2ZXE) were calculated and are presented here as a histogram

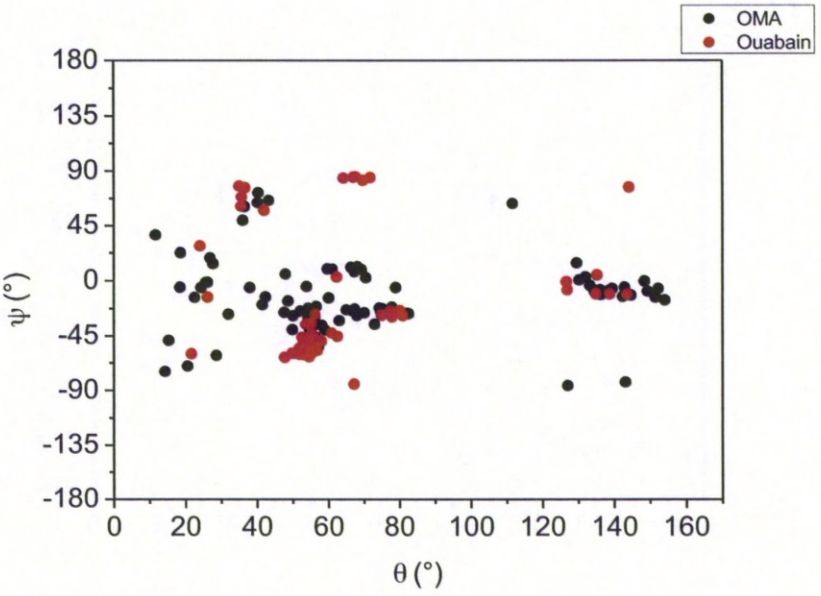

Figure 6.16. Scattergram representing the comparison of the spread of orientations of the top 100 ranked dockings between ouabain and OMA in the principal axes of inertia of the Na^+, K^+-ATPase from spiny dogfish rectal gland. The angles Ψ and θ were calculated (explained in Figure 6.9.) for the top 100 ranked ouabain and OMA dockings and plotted against each other in a scattergram to give an idea of the spread and of orientations obtained from GOLD studies.

6.3.2.2. Testing the potencies of OMA and ODA compared to ouabain.

To ensure the ouabain derivatives produced had similar inhibitory effects on the Na^+, K^+-ATPase to what had been observed previously (Middleton *et al.*, 2000), the effects of the synthesised ODA on the Na^+, K^+-ATPase was analysed by ATPase assays. A $K_{0.5}$ of around 6 μM for ODA compared to around 0.5 μM for ouabain was observed (Figure 6.18.) which makes ODA much less potent than ouabain (as had been observed

previously where OMA and ODA exhibited IC_{50} values of between 5 and 15 μM compared to <0.08μM for ouabain). The published data also show how ODA displaces [^{3}H]ouabain in a similar manner to unlabelled ouabain suggesting ODA binds at the same site albeit with lower potency.

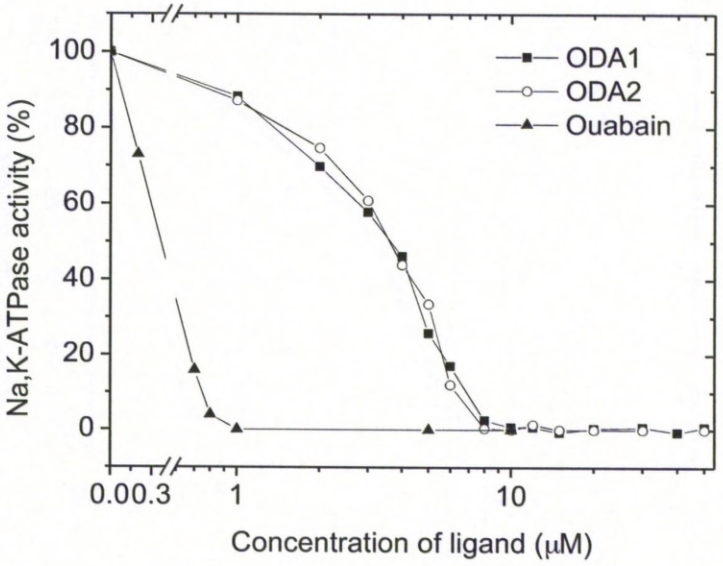

Figure 6.17. Inhibition curves of ouabain and ODA. In two ODA samples tested the potency of ODA was much lower than that of ouabain.

6.3.2.3. CP-MAS ^{13}C NMR

NMR samples of the Na^+, K^+-ATPase were prepared by Prof. Mikael Esmann of the University of Aarhus. These all contained spiny dogfish Na^+, K^+-ATPase and included samples with OMA or ODA and a range of manganese concentrations. Magic angle spinning was combined with cross-polarisation to allow the transfer of magnetisation from ^{1}H to ^{13}C and

improve signal to noise (this is described in more detail in Chapter 2). Cross polarisation is only effective when ^{13}C nuclei are in a restrained state. Whilst in solution, molecules undergo isotropic tumbling preventing cross-polarisation occurring. Ligands can be restrained and allow cross-polarisation to occur by being frozen or binding to a restrained molecule such as a membrane protein embedded in a membrane. Although cross-polarisation will occur on ^{13}C nuclei in a ligand bound to a membrane protein at non-freezing temperatures, the molecular motions will scale down non-polar interactions reducing cross-polarisation efficiency. In a frozen membrane these dynamics are reduced which improves cross-polarisation efficiency giving better signal. This does mean that both free and bound ligand will produce signal due to the freezing temperatures so when selecting experimental temperatures there is a trade off between having a high enough temperature so free ligand is undetected and a low enough temperature for efficient cross-polarisation (Spooner *et al.*, 1994). This work studies ouabain derivatives both at frozen and unfrozen states.

Samples were also treated with various concentrations of manganese. Manganese is a paramagnetic broadening agent which means it shortens the T2 time (relaxation time). With a shorter relaxation time the sensitivity reduces causing peaks to broaden. Previous paramagnetic broadening studies have probed the depths of peptides (Gröbner *et al.*, 1999; Buffy *et al.*, 2003) and drugs (Boland and Middleton, 2008) in lipid bilayers, by

comparing the broadening of peaks from the lipids which locations are known to peaks of the ligand which locations are unknown. The effect of manganese is proportional to distance so if a low concentration of manganese was added to a sample of the Na^+, K^+-ATPase in a cell membrane the manganese would bind to the membrane surface and the most accessible parts of the protein surface. Experiments run at higher manganese concentration would have manganese bind to less accessible regions of the protein surface causing peaks on the spectra to broaden further and would also bring manganese into closer proximity of the less accessible nuclei and will also broaden their chemical shift peaks. By using ODA and analysing the broadening of both chemical shift peaks separately their individual accessibility can be determined and will help understand the orientation of ouabain in the Na^+, K^+-ATPase further. A typical ^{13}C CP-MAS NMR spectra of the Na^+, K^+-ATPase is shown in Figure 6.18 with added OMA at 4°C. The OMA peak can be seen at 100 ppm and is displaced by ouabain showing it binds to the same site. The signal can be assigned exclusively to OMA in the high affinity site.

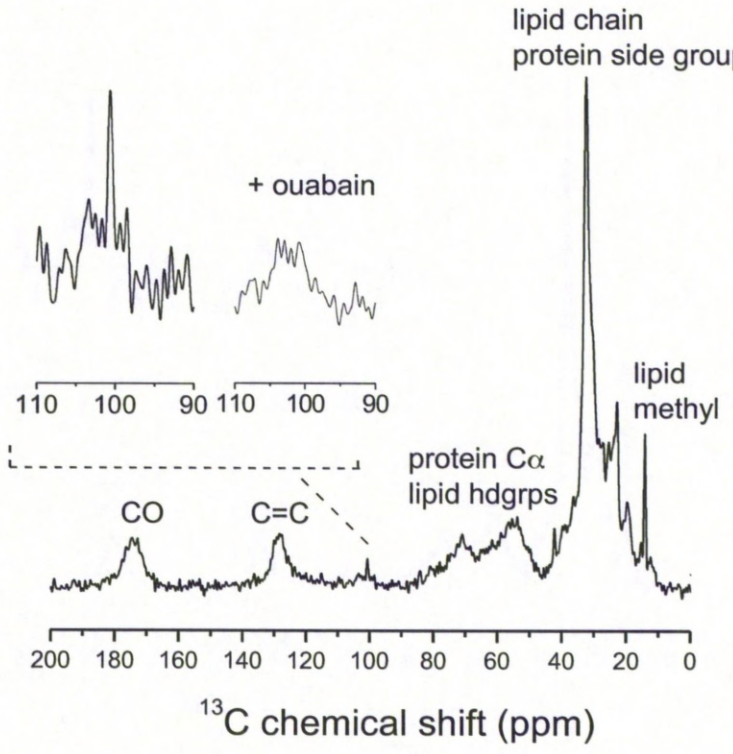

Figure 6.18. Example of a ^{13}C spectrum of Na^+, K^+-ATPase with OMA at 4°C. The signal of OMA is found around 100 ppm and is shown enlarged. This also shows a sample to which ouabain was added before OMA and displaces it from the binding site of the Na^+, K^+-ATPase causing a signal loss at 100 ppm. There are many other peaks between 0 and 200 ppm that are caused by natural abundance ^{13}C nuclei each of which is labelled with its source.

Initial experiments were performed on Na^+, K^+-ATPase with OMA as it could be produced in a higher yield compared to ODA and could be used to determine starting conditions for ODA experiments. Two temperatures were attempted (4°C and -25°C) and were both performed at 4000 Hz

spinning rate. The natural abundance ^{13}C were observed as follows; lipid chain and protein side groups at 50-0 ppm (Figure 6.19), Cα and lipid headgroups at 80-50 ppm (Figure 6.20), C=C at 140-115 (Figure 6.21) and CO at 185-160 ppm (Figure 6.22.). Spectra are shown at -25°C with similar results at 4°C. Spectra are normalised to the lipid methyl peak as it should not be significantly affected by manganese due to its inaccessibility caused by its location at the centre of the phospholipid bilayer. These are all affected to different degrees by manganese which is due to their accessibility. Lipid headgroups are affected the most by manganese as they are particularly accessible.

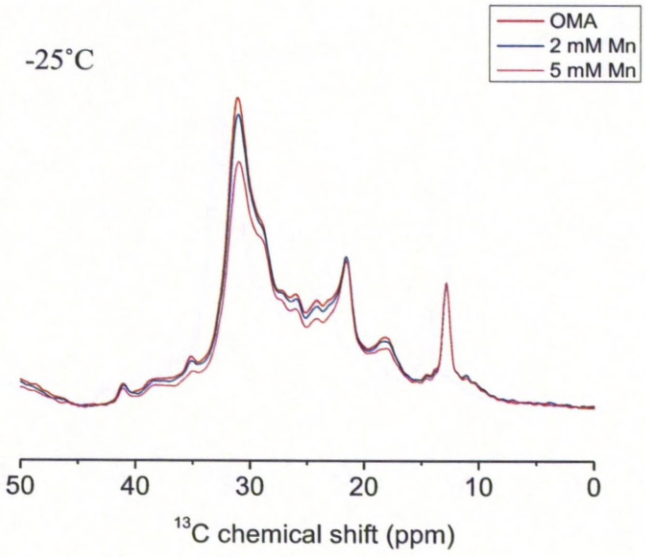

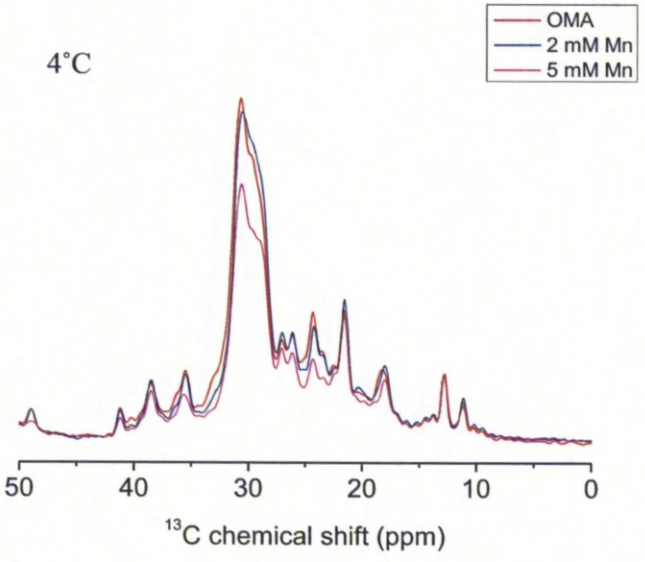

Figure 6.19 ^{13}C Spectra of Na^+, K^+-ATPase samples with OMA at various manganese concentrations at -25°C and 4°C in the 50-0 ppm range where lipid chain and protein side groups occur. Spectra are the result of accumulating 102,400 transients in 5 blocks of 20,480 transients with a spinning rate of 4000 Hz. Spectra are normalised to the lipid methyl peak.

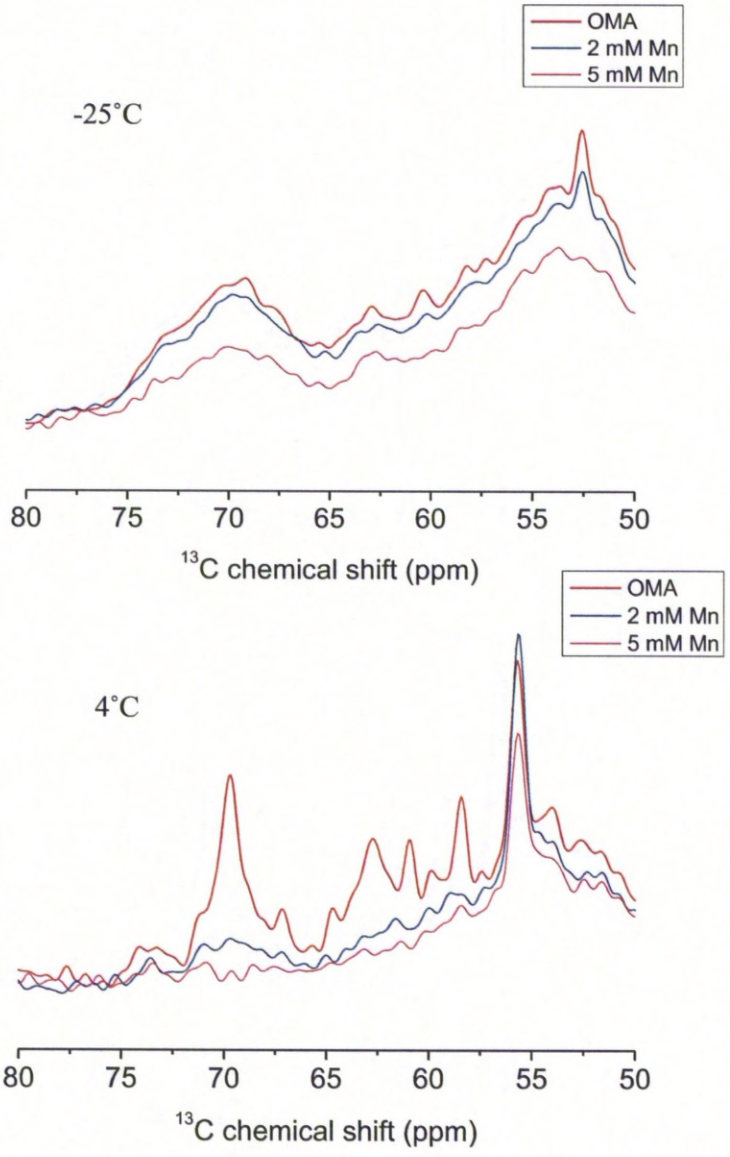

Figure 6.20 ^{13}C Spectra of Na^+, K^+-ATPase samples with OMA at various manganese concentrations at -25°C and 4°C in the 80-50 ppm range where protein Cα and lipid headgroups occur. Spectra are the result of accumulating 102,400 transients in 5 blocks of 20,480 transients with a spinning rate of 4000 Hz. Spectra are normalised to the lipid methyl peak.

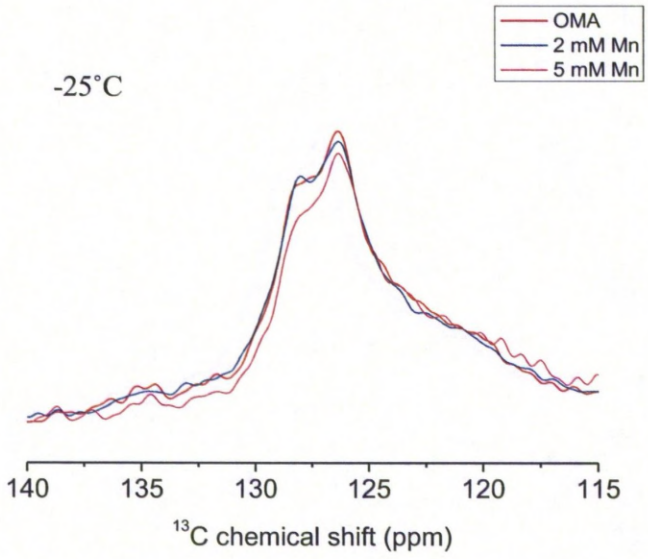

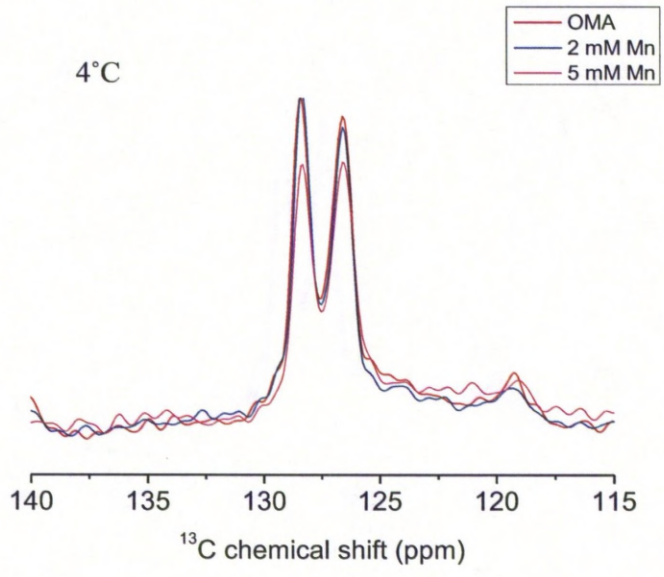

Figure 6.21 ^{13}C Spectra of Na^+, K^+-ATPase samples with OMA at various manganese concentrations at -25°C and 4°C in the 140-115 ppm range where C=C occur. Spectra are the result of accumulating 102,400 transients in 5 blocks of 20,480 transients with a spinning rate of 4000 Hz. Spectra are normalised to the lipid methyl peak.

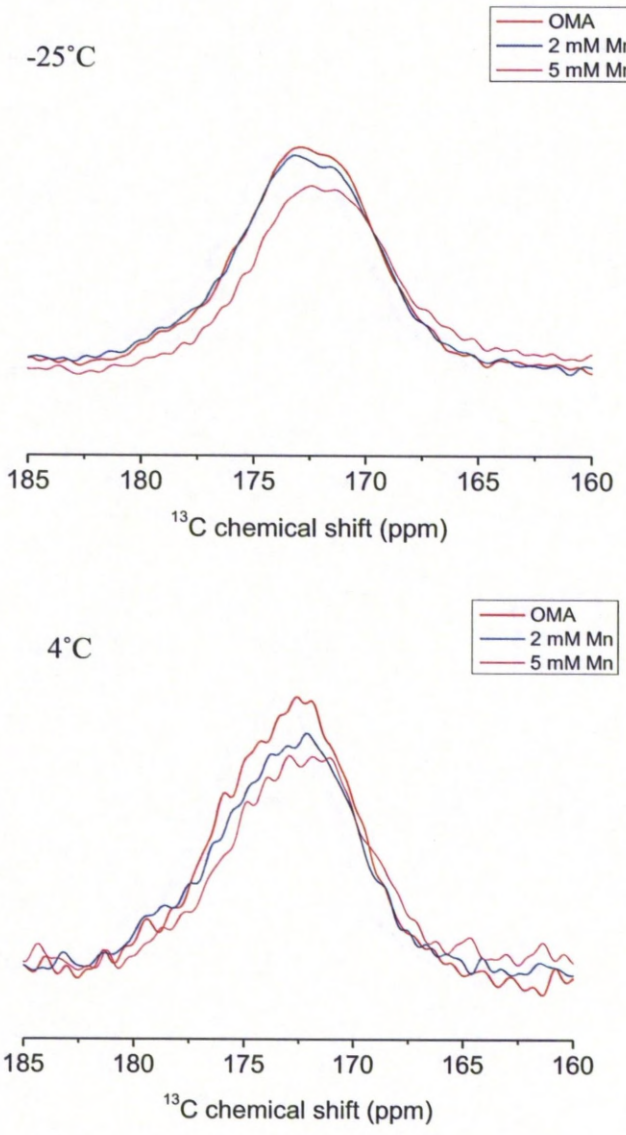

Figure 6.22 ^{13}C Spectra of Na^+, K^+-ATPase samples with OMA at various manganese concentrations at -25°C and 4°C in the 185-160 ppm range where CO occur. Spectra are the result of accumulating 102,400 transients in 5 blocks of 20,480 transients with a spinning rate of 4000 Hz. Spectra are normalised to the lipid methyl peak.

A Na^+, K^+-ATPase spectrum without OMA (labelled background) is shown with a Na^+, K^+-ATPase spectrum with OMA (labelled OMA) to highlight the peak derived from OMA at both -25°C (Figure 6.23.) and 4°C (Figure 6.24.).

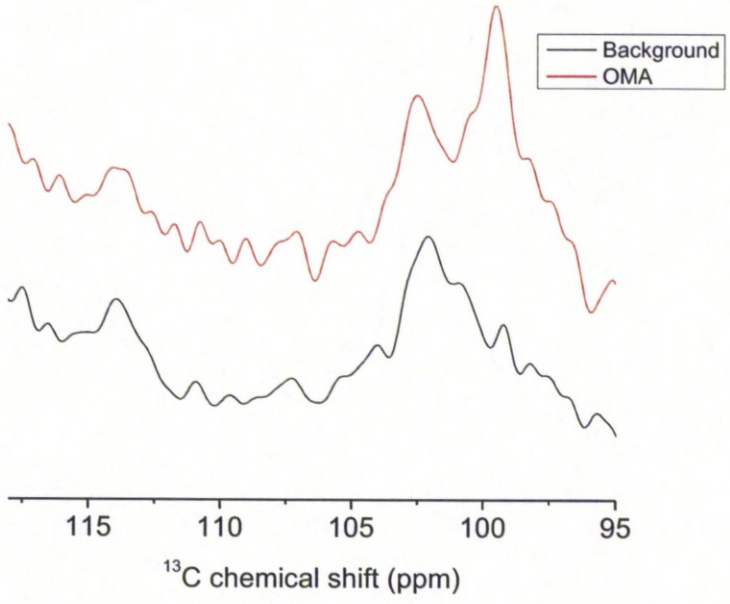

Figure 6.23. ^{13}C Spectra of Na^+, K^+-ATPase samples with OMA at 118-95 ppm of Na^+, K^+-ATPase with and without OMA at -25°C. The OMA peak is expected at 100 ppm. Black spectrum shows Na^+, K^+-ATPase alone (background). Red spectrum shows Na^+, K^+-ATPase with OMA.

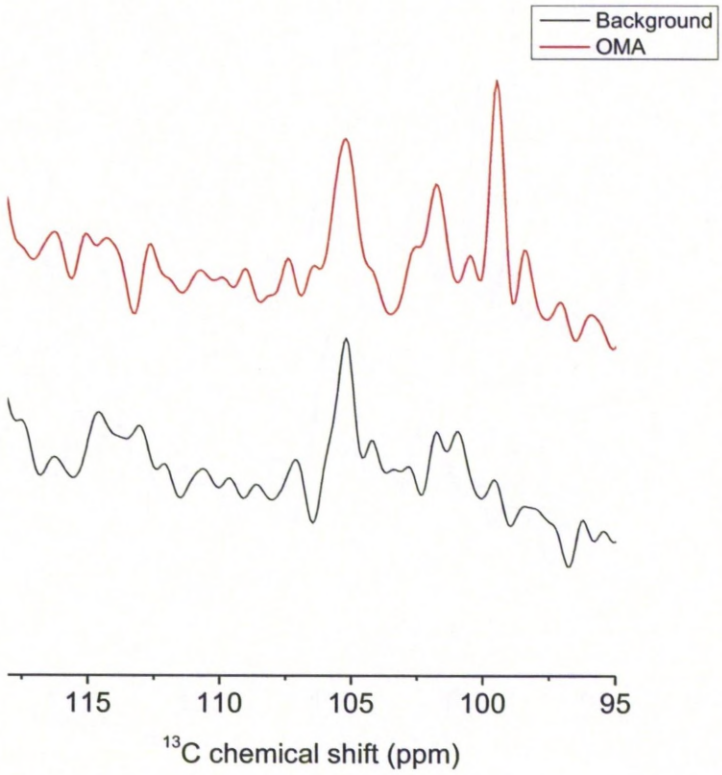

Figure 6.24. ^{13}C Spectra of Na^+, K^+-ATPase samples with OMA at 118-95 ppm of Na^+, K^+-ATPase with and without OMA at 4°C. The OMA peak is expected at 100 ppm. Black spectrum shows Na^+, K^+-ATPase alone (background). Red spectrum shows Na^+, K^+-ATPase with OMA.

In another control ouabain was added to Na^+, K^+-ATPase before adding OMA. Ouabain should displace OMA and reduce total OMA binding. At -25°C as the sample is frozen and both bound and unbound OMA will be observed in the spectra. Figure 6.25 reveals little change between the Na^+, K^+-ATPase samples with OMA alone and Na^+, K^+-ATPase with ouabain and OMA as a result of this. This was repeated with Na^+, K^+-ATPase

samples with no phosphate which should reduce binding. Slightly less intense peaks are observed for both OMA (blue) and Ouabain/OMA (pink) with no phosphate; again a large change would not be expected at this temperature as unbound OMA will still be observed. Figure 6.26. shows the same set of four Na^+, K^+-ATPase samples with OMA or Ouabain and OMA both in the presence and absence of phosphate at 4°C. At this temperature unbound OMA will not be observed in the NMR spectra. Indeed the OMA peak is observed in the Na^+, K^+-ATPase with OMA spectrum but not in the spectrum where ouabain is also present suggesting ouabain is displaces the OMA. This confirms OMA is binding at the same site as ouabain as expected. Interestingly OMA still binds albeit slightly less so in the absence of phosphate. This binding can also be prevented by the binding of ouabain.

.

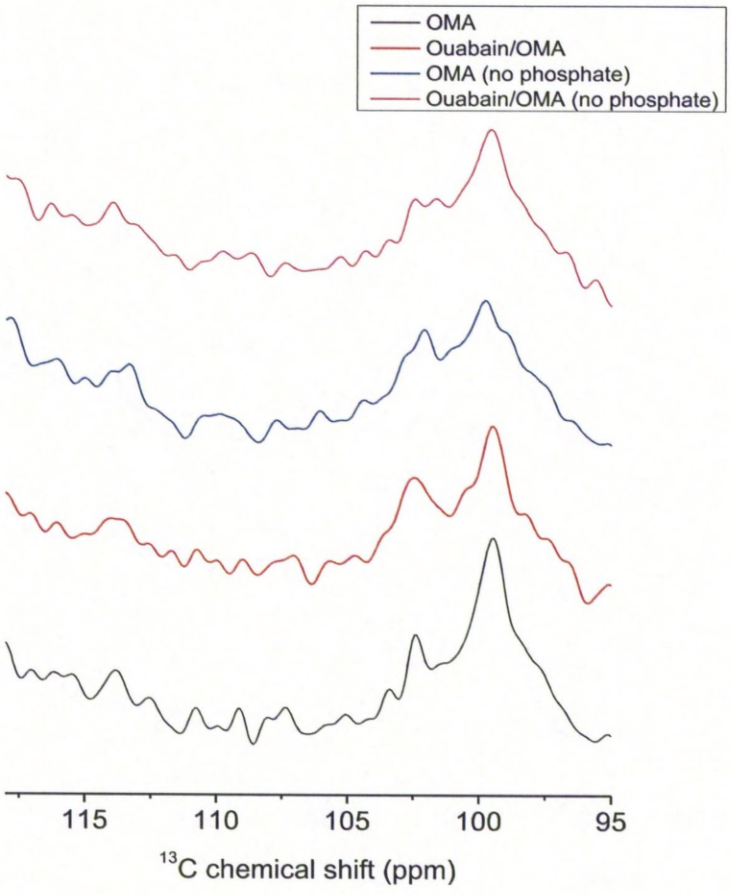

Figure 6.25. ^{13}C Spectra of Na^+, K^+-ATPase samples with OMA at 118-95 ppm of Na^+, K^+-ATPase with and without OMA at -25°C. The OMA peak is expected at 100 ppm. Black spectrum shows Na^+, K^+-ATPase with OMA. Red spectrum shows Na^+, K^+-ATPase with ouabain and OMA. Blue and Pink spectra are identical to Black and Red respectively with no phosphate added.

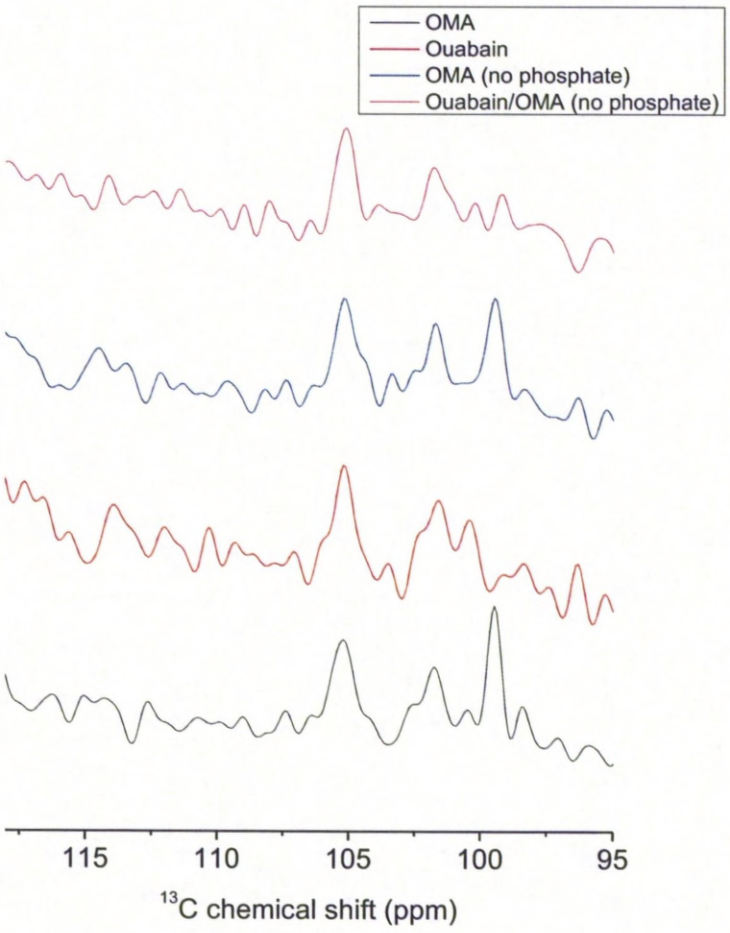

Figure 6.26. ^{13}C Spectra of Na^+, K^+-ATPase samples with OMA at 118-95 ppm of Na^+, K^+-ATPase with and without OMA at 4°C. The OMA peak is expected at 100 ppm. Black spectrum shows Na^+, K^+-ATPase with OMA. Red spectrum shows Na^+, K^+-ATPase with ouabain and OMA. Blue and Pink spectra are identical to Black and Red respectively with no phosphate added shows Spectra are the result of accumulating 102,400 transients in 5 blocks of 20,480 transients with a spinning rate of 4000 Hz. Spectra are normalised to the lipid methyl peak.

Figure 6.27. and Figure 6.28 (-25°C and 4°C respectively) show the effect of manganese on the OMA peak which reduces with increased manganese concentrations as expected. This meant a system was in place to obtain distance data for both ODA peaks separately with similar experiments.

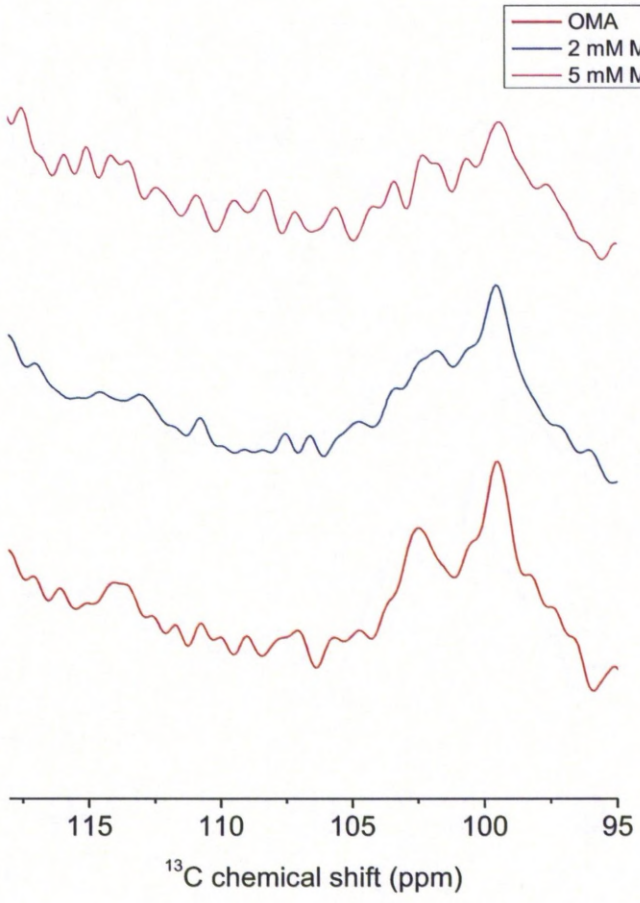

Figure 6.27 ^{13}C Spectra of Na^+, K^+-ATPase samples at 118-95 ppm at -25°C. The OMA peak is expected at 100 ppm. Spectra indicate the effect of various manganese concentrations on the OMA peak.

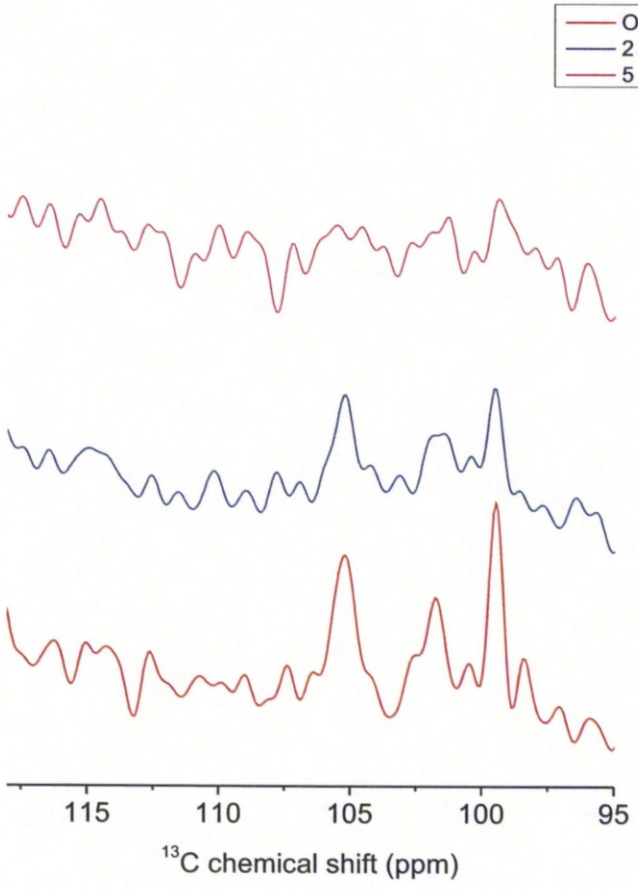

Figure 6.28 ^{13}C Spectra of Na^+, K^+-ATPase samples at 118-95 ppm at 4°C. Spectra indicate the effect of various manganese concentrations on the OMA peak.

Similar experiments were next attempted with ODA. Figure 6.29 shows the region where the ODA signal is expected at -25°C. Unlike OMA at this temperature the resolution is poor in this region and no peaks can be assigned. This suggests there could be a range of orientations of ODA that give rise to a distribution of frequencies that cause the signal to broaden.

The effect of manganese on other regions of the spectrum was similar to what had been observed previously in OMA and is discussed later.

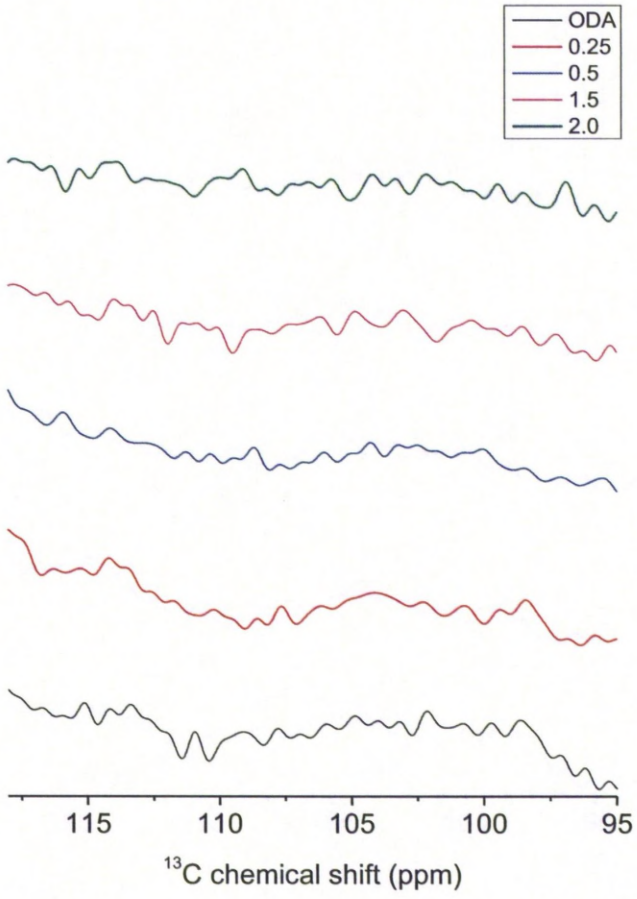

Figure 6.29 The effect of manganese on ^{13}C Spectra of Na^+, K^+-ATPase samples with ODA at 118-95 ppm at -25°C. The ODA peaks are expected at 100 and 110ppm. Resolution is too poor to see either peak and therefore determine the effects of manganese.

To improve resolution and signal to noise whilst keeping the sample below freezing for preservation the temperature was raised to -10°C. It appears at -25°C both bound and unbound ODA is being observed so the

experimental temperature needed to be increased. The spinning frequency was increased to 8000 Hz as increased spinning rate will remove more of the effects of chemical shift anisotropy and improve signal strength. This improved resolution can be seen in Figure 6.30 where a Na^+, K^+-ATPase spectrum without ODA (labelled background) is compared to a spectrum of Na^+, K^+-ATPase with ODA (labelled ODA) to highlight the peaks derived from ODA The steroid peak is as expected like in OMA at 100 ppm however the steroid peak expected at 110 ppm is hard to distinguish unlike previous observations (Middleton *et al.*, 2000). This is either due to ODA degrading during or after the Na^+, K^+-ATPase sample preparation or ODA binding in a different location to ouabain and OMA. The spectra of Na^+, K^+-ATPase and ODA with 0, 0.25, 0.5 and 1.0 mM manganese are shown in Figure 6.31. The steroid peak is completely lost at 0.25 mM Mn whereas the effects on the rhamnose peak are difficult to determine. In OMA the steroid peak was still present at 5 mM Mn. This suggests ODA is binding at the surface of the protein as the steroid peak is lost at such low Mn concentrations.

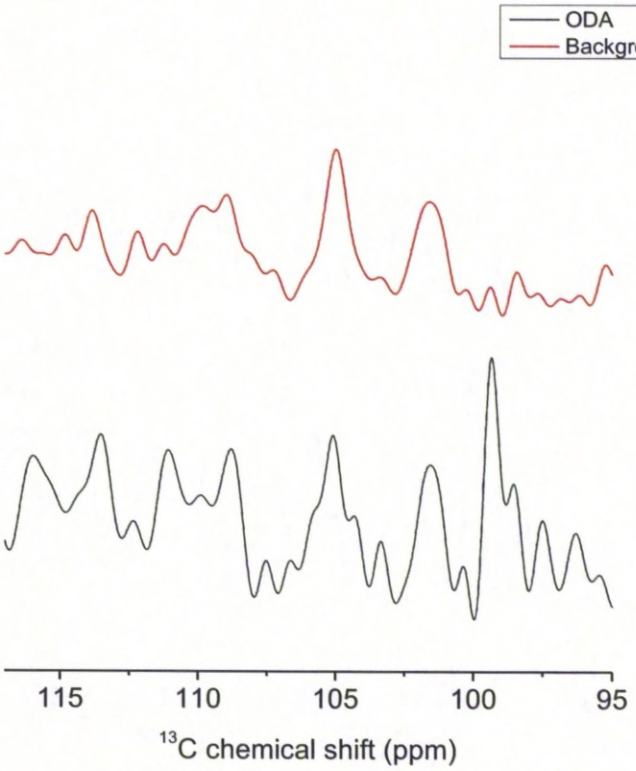

Figure 6.30. ^{13}C Spectra of Na^+, K^+-ATPase samples with ODA at 118-95 ppm of Na^+, K^+-ATPase with and without OMA at -10°C. The ODA peaks is expected at 100 and 110 ppm. Black spectrum shows Na^+, K^+-ATPase alone (background). Red spectrum shows Na^+, K^+-ATPase with OMA.

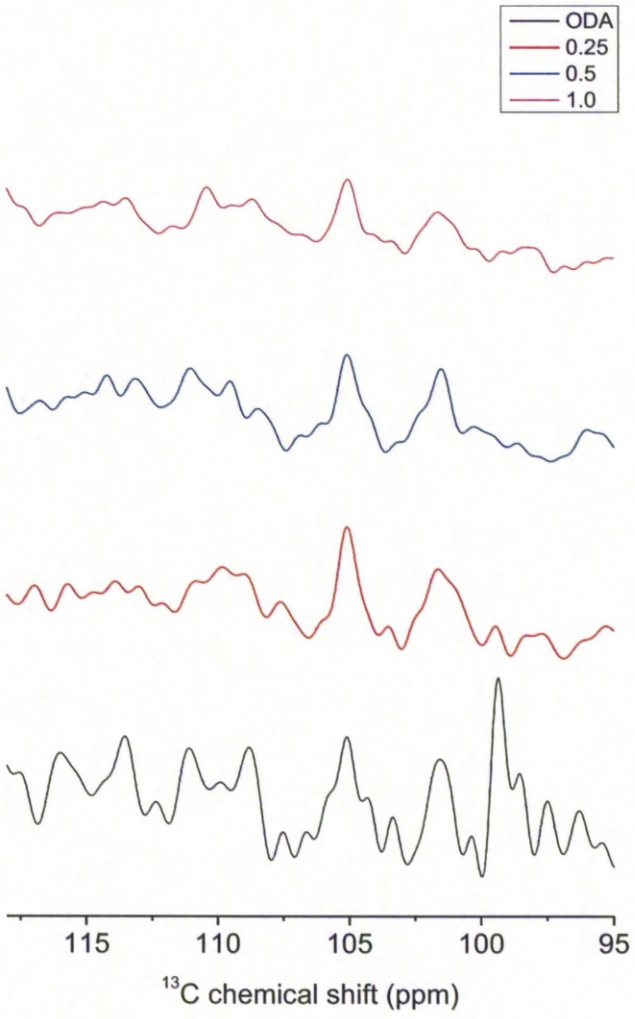

Figure 6.31. ^{13}C Spectra of Na^+, K^+-ATPase samples with ODA at various manganese concentrations at -10°C. The ODA peaks are expected at 100 and 110 ppm. Spectra indicate the effect of various manganese concentrations on the OMA peaks.

For this system to be successful, similar effects by manganese on the natural abundance ^{13}C peaks from lipid and the Na^{+}, K^{+}-ATPase must be observed. The OMA spectra of the key regions that represent the different carbon types observed are shown in Figure 6.19-22 at both -25°C and 4°C. Figure 6.32-35 show the ODA spectra in the same region at -25°C and -10°C. The peak intensities of the peaks indicated by the arrows on these spectra were calculated as percentages relative to the manganese free spectra (i.e. OMA or ODA alone) and plotted against manganese concentration to see the reproducibility of the effects of manganese on natural abundance ^{13}C. Figure 6.36 and Figure 6.37 show these plots and reveal similar effects of manganese to peak intensities in each case with the exception of the peak at 69 ppm which is very different at -25°C. This is in the lipid headgroup region and may be due to the different properties of the membrane at particularly cold temperatures. This does show that there is consistency above -10°C making the system reproducible.

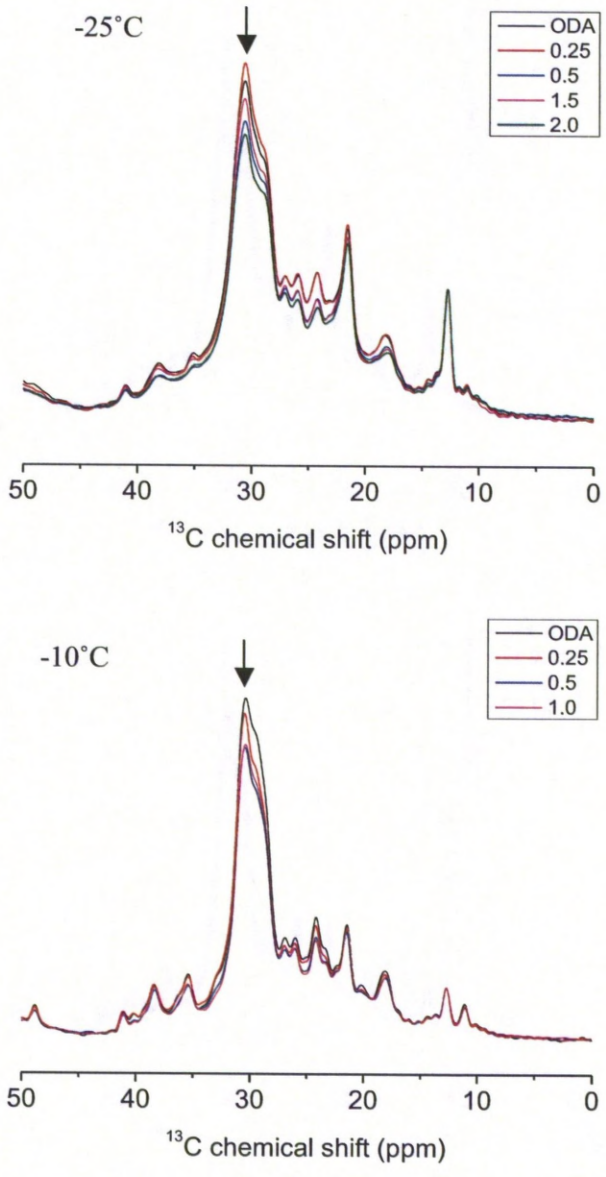

Figure 6.32 ^{13}C Spectra of Na^+, K^+-ATPase samples with ODA at various manganese concentrations at -25°C and -10°C in the 50-0 ppm range where lipid chain and protein side groups occur. Spectra are the result of accumulating 102,400 transients in 5 blocks of 20,480 transients with a spinning rate of 4000 Hz at -25°C and 8000 Hz at -10°C. Spectra are normalised to the lipid methyl peak.

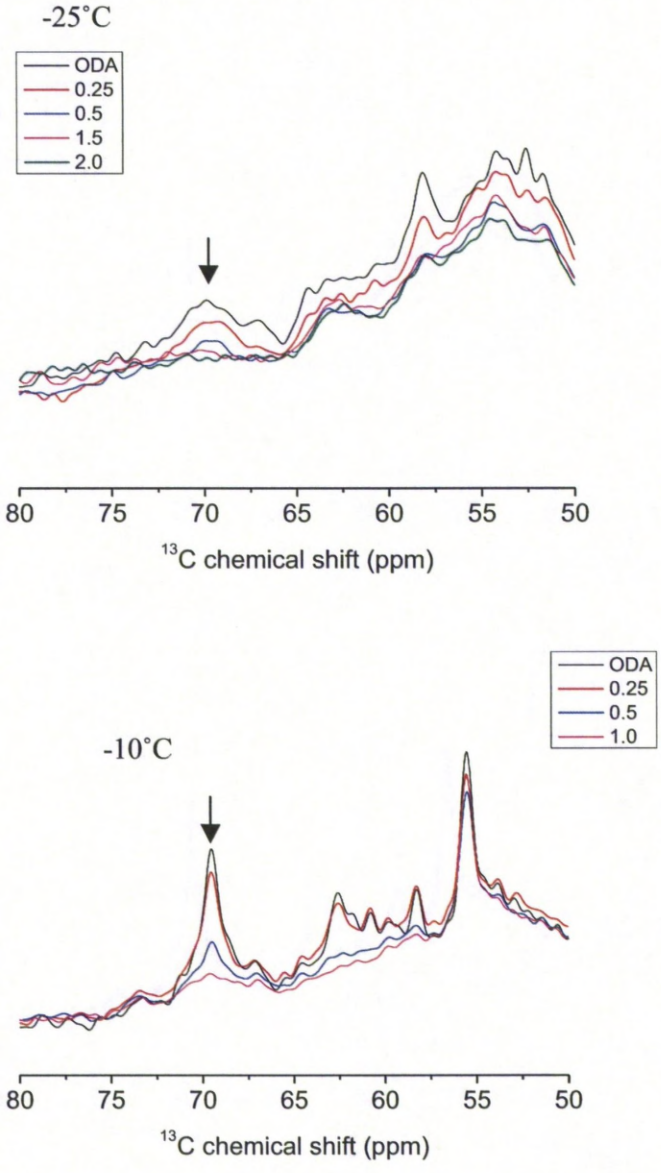

Figure 6.33 ^{13}C Spectra of Na^+, K^+-ATPase samples with ODA at various manganese concentrations at -25°C and -10°C in the 80-50 ppm range where protein Cα and lipid headgroups occur. Spectra are the result of accumulating 102,400 transients in 5 blocks of 20,480 transients with a spinning rate of 4000 Hz at -25°C and 8000 Hz at -10°C. Spectra are normalised to the lipid methyl peak.

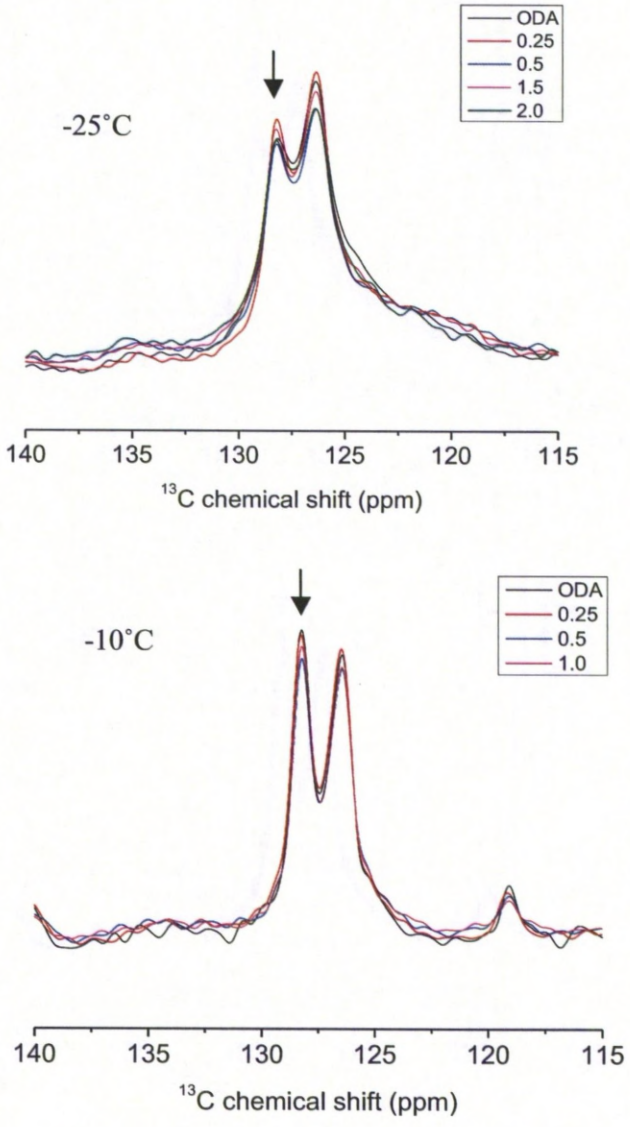

Figure 6.34 ^{13}C Spectra of Na^+, K^+-ATPase samples with OMA at various manganese concentrations at -25°C and -10°C in the 140-115 ppm range where C=C occur. Spectra are the result of accumulating 102,400 transients in 5 blocks of 20,480 transients with a spinning rate of 4000 Hz at -25°C and 8000 Hz at -10°C. Spectra are normalised to the lipid methyl peak.

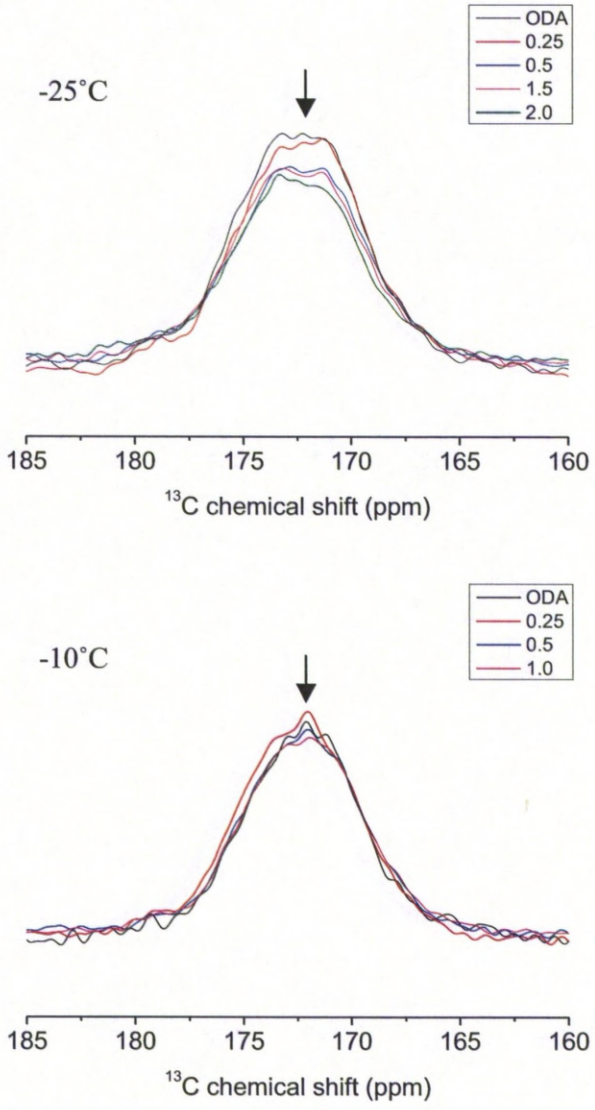

Figure 6.35 ^{13}C Spectra of Na^+, K^+-ATPase samples with ODA at various manganese concentrations at -25°C and -10°C in the 185-160 ppm range where CO occur. Spectra are the result of accumulating 102,400 transients in 5 blocks of 20,480 transients with a spinning rate of 4000 Hz at -25°C and 8000 Hz at -10°C. Spectra are normalised to the lipid methyl peak.

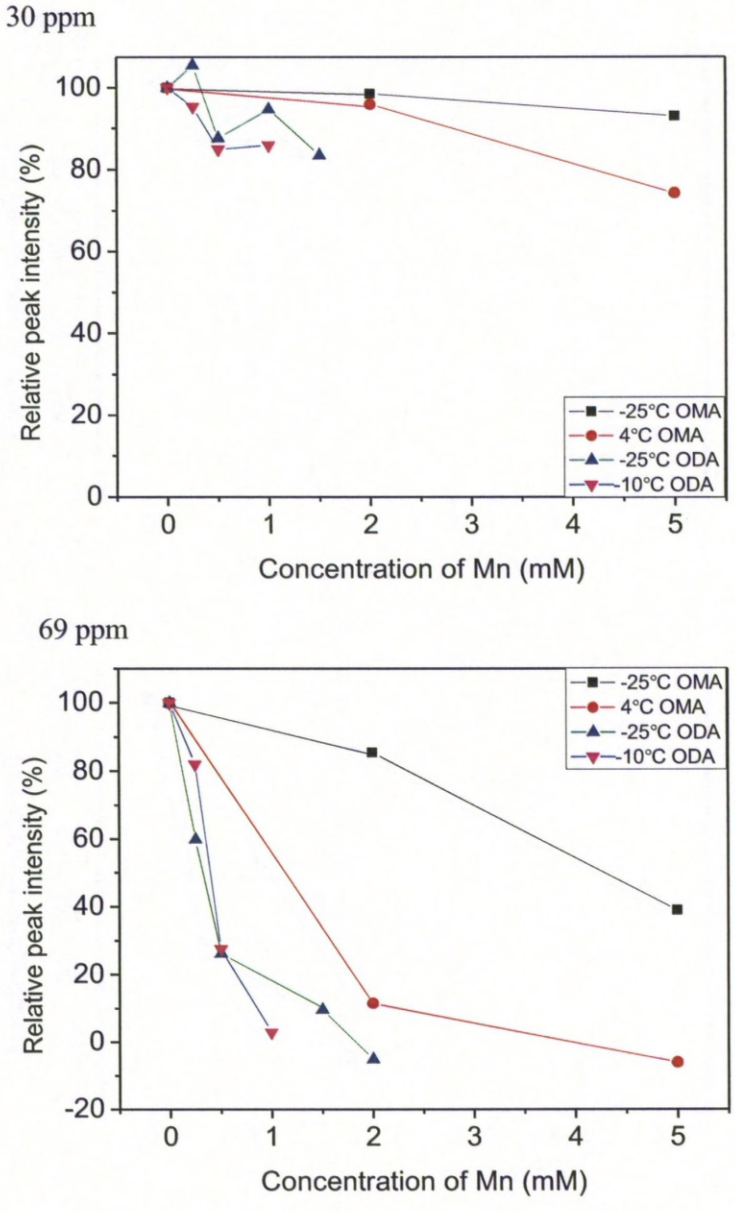

Figure 6.36 Scattergraphs to show relative peak intensities at 30 and 69 ppm against manganese concentration for all experiments performed. Experiments were performed at a range of manganese concentrations (0-5 mM) with both OMA and ODA at various temperatures indicated on the graphs.

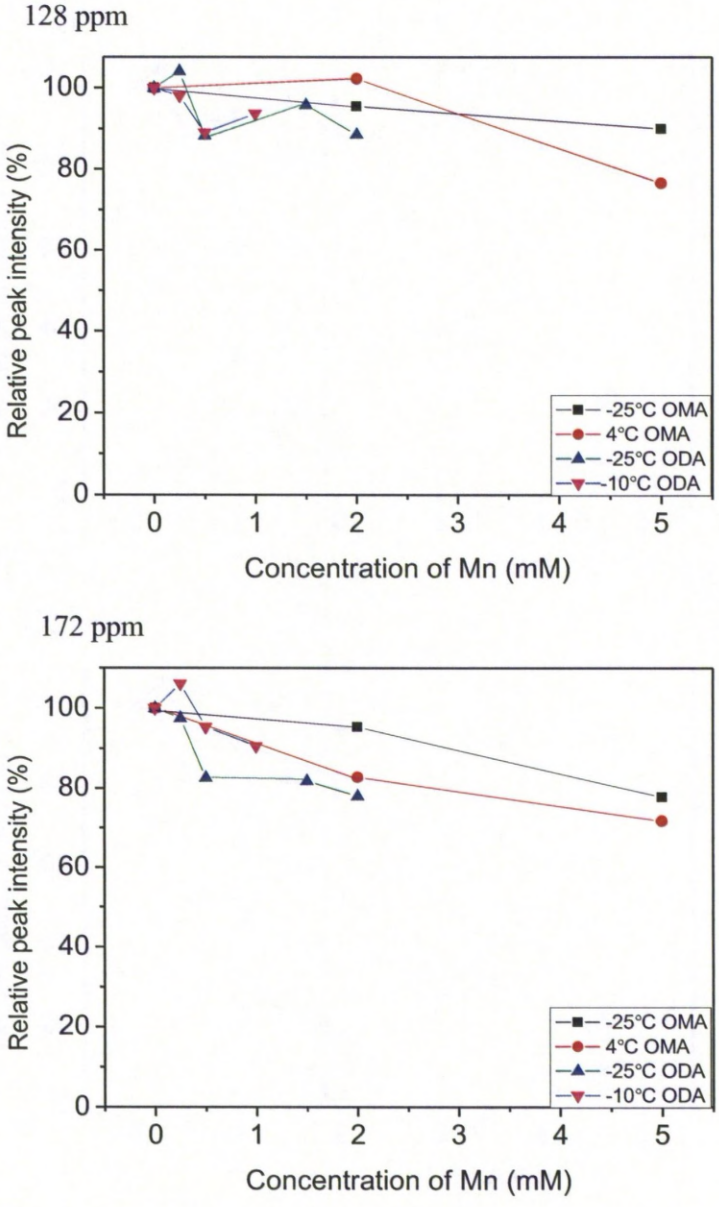

Figure 6.37 Scattergraphs to show relative peak intensities at 172 and 128 ppm against manganese concentration for all experiments performed. Experiments were performed at a range of manganese concentrations (0-5 mM) with both OMA and ODA at various temperatures indicated on the graphs.

6.4. Discussion

This final chapter shifts focus from the physiological inhibitors, the FXYD proteins to the pharmacological inhibitors the cardiac glycosides. Although all experiments shown here are on just one member of the cardiac glycosides known as ouabain, their identical steroid backbones indicate their mechanism is likely very similar. Although the work presented here fails to give a real insight into how cardiac glycosides bind to the Na^+, K^+-ATPase the aim to develop a novel method of probing the location of ligands within transmembrane regions of proteins was successful. ODA gave unusual results in that previously it gave rise to a signature pair of peaks in the NMR spectra (Middleton *et al.*, 2000) whereas in the data presented here it either appeared as one broad peak (Figure 6.29.) in the case of -25°C experiments or only the steroid peak appeared as expected whereas the rhamnose peak was hard to distinguish in the case of -10°C experiments (Figure 6.30.). Although the steroid peak appears at -10°C it diminishes in manganese concentrations as low as 0.25 mM (Figure 6.31.) at which only a small effect is observed on lipid headgroups (Figure 6.33.). In OMA experiments this peak has not fully diminished in manganese concentrations as high as 5 mM (Figure 6.25-26.). This suggests OMA and ODA are binding in different locations within the Na^+, K^+-ATPase with OMA binding within the protein near the surface whereas ODA binds on the surface itself leaving the ^{13}C nuclei very prone to the effects of manganese on T2 relaxation times. It is unclear why ODA is acting in this

way when it has not done previously. Fresh ODA would need to be produced to see if ODA possibly degraded during or after the preparation of Na^+, K^+-ATPase samples for NMR which could explain its unusual binding. There is a possibility ODA binds to a surface site as it is shown as a possibility in GOLD experiments (Figure 6.14.). If these problems can be overcome the system is in place to determine the accessibility of both ODA peaks. As shown in Figures 6.36-37 the peak intensities of natural abundance ^{13}C reduce as a result of increased manganese concentration in a similar manner in all cases apart from -25°C lipid headgroups. Slight deviations have to be expected due to the methods of purification of the Na^+, K^+-ATPase samples it is impossible to have the same quantity of protein between samples.

Since these experiments were performed a high ouabain affinity Na^+, K^+-ATPase structure with bound ouabain has been solved (Yatime *et al.*, 2011). Unlike the low ouabain affinity structure (Ogawa *et al.*, 2009) where the Na^+, K^+-ATPase was crystallised before soaking ouabain into the crystal this structure stabilised the Na^+, K^+-ATPase with ouabain itself before crystallisation. This meant that ouabain bound to the Na^+, K^+-ATPase whilst still active. This structure reveals two key things. Firstly it reveals the homology model (Figure 6.11) is unrepresentative of the true E_2P conformation as revealed by the alignment of the homology model with the high ouabain affinity structure in Figure 6.38. For any further

homology models to be used with Na^+, K^+-ATPase better strategies will have to be developed.

Figure 6.38. Alignment of high ouabain affinity Na^+, K^+-ATPase with E_2P homology model. This alignment highlights the clear differences between the E_2P homology model of the α-subunit (red) presented in this work (using SERCA as a template) and the high ouabain affinity E_2P Na^+, K^+-ATPase (green, cyan and magenta PDBID: 3N23).

Secondly it reveals the differences between the high and low ouabain affinity structures of the Na^+, K^+-ATPase. Figure 6.39. is an alignment of both Na^+, K^+-ATPase structures with bound ouabain. Although very similar there is a clear difference between the two. It is unclear if this difference is due to the different affinities or the different species used as

the low ouabain affinity structure is from spiny dogfish rectal gland and the high ouabain affinity structure is from pig kidney. The possibility of differences between species is also brought into question by the GOLD Na^+, K^+-ATPase/ouabain docking presented here. Whilst the distance from the centre of mass of the Na^+, K^+-ATPase to the centre of mass of ouabain modelled by GOLD is similar between species (Figure 6.9) the orientation of ouabain within the Na^+, K^+-ATPase is noticeably different (Figure 6.10). By solving high ouabain affinity spiny dogfish rectal gland and low ouabain affinity pig kidney Na^+, K^+-ATPase it could be confirmed if there really are differences between species. Additionally by overcoming the problems with ODA the NMR experiments presented here could provide more evidence and hold the advantage over x-ray crystallography of being performed on active protein.

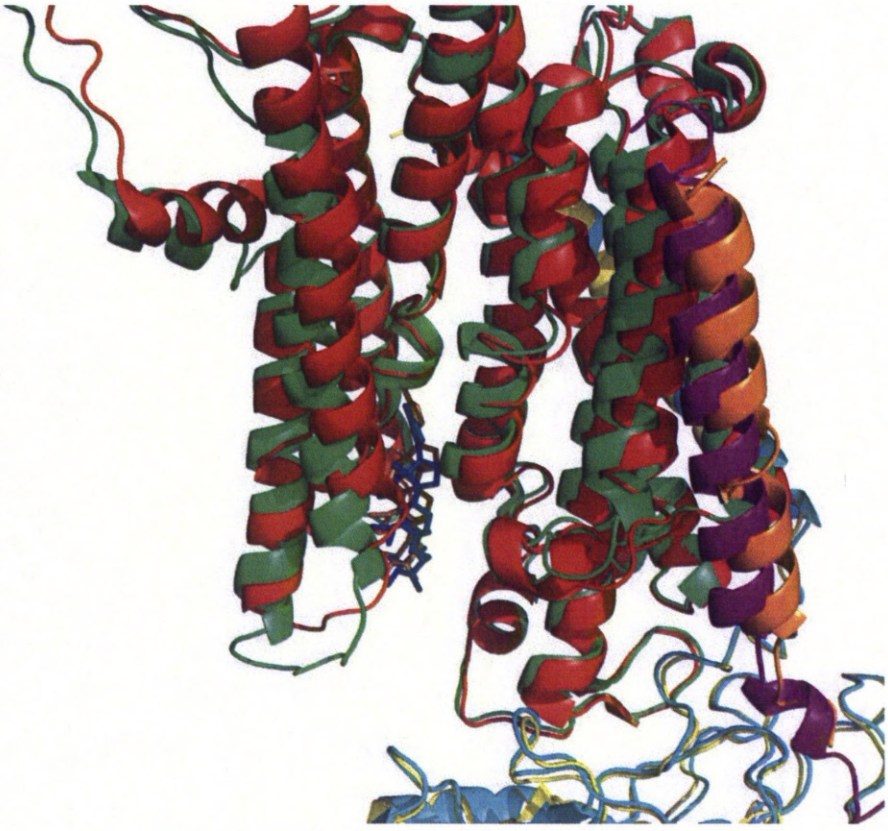

Figure 6.39. Alignment of Na^+, K^+-ATPase bound to ouabain in low and high affinity conformations. Low ouabain affinity Na^+, K^+-ATPase from spiny dogfish (green α-subunit, cyan β-subunit, magenta FXYD protein (FXYD10) with brown ouabain PDBID: 3A3Y) is shown aligned to high ouabain affinity Na^+, K^+-ATPase (red α-subunit, yellow β-subunit, orange FXYD protein (FXYD10) with blue ouabain PDBID: 3N23).

Chapter 7

7.1. General Discussion

The general aim of this project was to gain a better understanding of two classes of regulators of the Na^+, K^+-ATPase, one physiological and one pharmacological, using a range of biophysical and biochemical techniques. The first class of regulators are the FXYD proteins which are a family of small transmembrane proteins that are expressed tissue specifically and form a complex with the Na^+, K^+-ATPase (Garty and Karlish, 2005). The second class of regulators are the cardiac glycosides, which are very potent pharmacological inhibitors of the Na^+, K^+-ATPase and have been administered as drugs for over 200 years.

This was a timely project for analysis of regulators of Na^+, K^+-ATPase as four different structures of the protein (Morth *et al.*, 2007; Ogawa *et al.*, 2009; Shinoda *et al.*, 2009; Yatime *et al.*, 2011) were solved and published during the course of the work. The results presented in this thesis have provided new insights into the how the cytoplasmic region of both PLM and the long isoform of Mat-8 interact with the Na^+, K^+-ATPase and cell membranes. For cardiac glycosides additional insights into the orientation of ouabain within the Na^+, K^+-ATPase have been made. Moreover, the methodology developed in this thesis will enable further examination of FXYD proteins and cardiac glycosides. For FXYD proteins, the short

isoform of Mat-8 was successfully expressed and purified and a new solid-state NMR based method has been developed to probe the depths of ligands within the binding pockets of transmembrane proteins.

7.2. Conclusions

7.2.1. FXYD Proteins

At the outset of the project the aim was to develop an expression and purification system for the production of milligram quantities of ^{15}N and ^{13}C labelled FXYD proteins for NMR. Although this has yet to be achieved much progress has been made toward this goal. Membrane proteins are notoriously difficult to express and purify (Grisshammer and Tateu, 1995). Indeed, another group has reported specific problems in expressing and purifying FXYD proteins, which was addressed by designing the pBCL vector which requires the mutation of methionine residues to leucine residues to facilitate CNBr cleavage (Thai *et al.*, 2005). As Mat-8 contains two methionine residues in its transmembrane region this construct is not ideal and attempts to recreate the system were unsuccessful. By developing a new system in the pMAL plasmid (Riggs, 2001), Mat-8 was successfully expressed and purified in LB. This system produces Mat-8 as a fusion protein with MBP. The procedure incurred many problems as the purification procedure required soluble protein. The insolubility of Mat-8 caused by its hydrophobic transmembrane region meant that detergent was

required as an aid to solubility. This meant many methods had to be attempted to remove the detergent after purification of Mat-8 and cleavage from its fusion partner MBP. A successful method was reached by purifying the Mat-8/MBP fusion protein in the amylose column, cleaving with TEVP, precipitating protein with chloroform methanol precipitation and purifying by HPLC after dissolving the protein in guanidium chloride. This large number of purification steps may be why when the process was repeated in labelled minimal media, not enough protein was present to produce an NMR signal. Nevertheless a system is now in place to produce Mat-8 and with appropriate optimisation may yield enough labelled protein for NMR.

Although the lack of labelled protein prevented structural analysis of full-length FXYD proteins by NMR, several other methods were employed to gain structural insights into the soluble cytoplasmic regions of FXYD proteins. CD revealed the α-helical content of PLM_{38-72} (Clayton *et al.*, 2005), Mat-$8sf_{38-67}$, Mat-$8lf_{38-90}$ and $CHIF_{38-69}$ to be approximately 15%, 0%, 8% and 7% respectively. This shows that the diversity of amino acid sequence between FXYD proteins in the cytoplasmic region is also reflected in the structure of the cytoplasmic region of FXYD proteins providing further evidence they confer the tissue specific features of FXYD proteins. The level of α-helical content of PLM_{38-72} estimated by CD is around half the level of α-helical content solved by solution NMR in

SDS micelles. Further CD presented here shows that SDS induces additional α-helical content in PLM_{38-72}. This is most likely because SDS is a highly negative detergent which is not a suitable proxy for a cell membrane which is a bilayer with a much lower surface charge.

As the cytoplasmic region is the most varied part of the FXYD proteins work was undertaken to understand the function and interactions of this region within PLM and Mat-8. One of the questions addressed in this thesis is whether the cytoplasmic domains of FXYD proteins interact directly with Na^+,K^+-ATPase, or are stabilised by interactions with the phospholipid membrane surface, or whether both interactions occur in dynamic equilibrium. PLM is particularly interesting in the cytoplasmic region as it has two PKA/PKC phosphorylation sites at Ser 63 and Ser 68 (Palmer *et al.*, 1991; Mounsey *et al.*, 2000). The PLM cytoplasmic domain alone partially inhibits Na^+, K^+-ATPase but when Ser 68 is phosphorylated in PLM_{54-72} the Na^+, K^+-ATPase activity is stimulated to a level above that in the absence of the peptide (Pavlovic *et al.*, 2007). It would also appear that phosphorylation reduces the affinity of the cytoplasmic region of PLM for negatively charged membranes as shown here by ITC and also reduces the potency of the PLM cytoplasmic region as an inhibitor of the Na^+, K^+-ATPase. This suggests that phosphorylation regulates the function of the cytoplasmic region as an inhibitor of the Na^+, K^+-ATPase as it reduces the affinity of PLM_{38-72} for both the Na^+, K^+-ATPase and phospholipids which

is supported by the fact that the cytoplasmic region of the short isoform of Mat-8 and CHIF have no effect on Na^+, K^+-ATPase function and are not phosphorylated by PKA or PKC. By testing the binding of PLM_{38-72} in the presence of the Na^+, K^+-ATPase it would appear that the interaction with cell membranes is much weaker than previously reported (Clayton *et al.*, 2005). This suggests that the role of PLM phosphorylation in regulating the Na^+, K^+-ATPase is largely caused by reducing its affinity for the binding site on the protein and the reduction of binding to negatively charged cell membranes observed in $pPLM_{38-72}$ over PLM_{38-72} is insubstantial especially since native membranes have a much lower surface charge (Akio, 1971) than the 2:1 DMPC DOPG membranes which were used in these NMR experiments. This interaction could still be crucial to the stability of the cytoplasmic region of PLM. An interesting finding of this work is that the cytoplasmic region of the long isoform of Mat-8 is a weak inhibitor of the Na^+, K^+-ATPase, albeit to a smaller degree than PLM. This isoform is a relatively new discovery and thus poorly understood (Bibert *et al.*, 2006), it is not known if it is physiologically phosphorylated. It does have three predicted phosphorylation sites not present in the short isoform of Mat-8 which may mean phosphorylation plays a role in its regulation like in PLM.

Bioinformatics was also used to gain insights into how the cytoplasmic region of PLM and long form Mat-8 might interact with the Na^+, K^+-

ATPase with the spiny dogfish rectal gland structure (Shinoda *et al.*, 2009) being used in the studies. This led to the discovery of the motif SxxRxS using DiLiMOT which is present in the cytoplasmic region of PLM and long form Mat-8 but no other FXYD proteins. It is also present in several other proteins that interact with the Na^+, K^+-ATPase. Whilst the motif is predicted to be at the end of a helix in both PLM and long form Mat-8 it is only predicted to be disordered in PLM. Disorder has proved to be a common feature in small linear motifs with the premise of becoming ordered upon binding (Davey *et al.*, 2012). Another common feature of short linear motif is conservation. The long isoform of Mat-8 has currently only been discovered in humans so its conservation is unclear. However the motif is preserved in all known instances of PLM, which include mammals and amphibians. Finding a potential location for this motif on the surface of the Na^+, K^+-ATPase proved more difficult. This is because a major method of predicting binding locations is to analyse the surface of a target protein for conservation. Unfortunately the number of species known to express FXYD proteins is relatively small and thus the majority of the Na^+, K^+-ATPase surface is conserved across these species. Other methods were limited by the fact the Na^+, K^+-ATPase is a membrane protein and the hydrophobic membrane region is calculated as potential binding sites for peptides which is inaccessible to the cytoplasmic region of a FXYD protein. Anchorsmap is a more motif specific method for analysing protein surfaces for binding sites in that it finds locations for specific amino acid

residues. This revealed a potential binding site for the SxxRxS motif which is located on the surface of the Na^+, K^+-ATPase in close proximity of the cytoplasmic cell membrane surface. This binding site is in a similar location to where is appears in the proposed model within helix 4 of PLM (Teriete *et al.*, 2007; Teriete *et al.*, 2009). By modelling the cytoplasmic helix of PLM from the solved structure into this site it reveals it is both sterically and electrostatically compatible. Furthermore the side chain of an arginine residue in the random coil structure at the C-terminus of this helix is able to interact with the membrane surface which provides a possible explanation for how the cytoplasmic region of PLM may interact with both the Na^+, K^+-ATPase and the membrane surface.

This interaction would occur at the N-terminus of helix M5 of the Na^+, K^+-ATPase. It would therefore appear when the cytoplasmic region of PLM binds to the Na^+, K^+-ATPase it causes a movement of helix M5. This movement causes the C-terminus of helix M5 to move away from the third Na^+ binding site which located at the C-terminus of helix M5, M6 and M9 (Morth *et al.*, 2007). This would surely have an effect on the affinity for Na^+ of the third binding site which would explain the inhibitory effects of the cytoplasmic region of PLM on Na^+, K^+-ATPase activity.

Anchorsmap calculated another binding site that would place the α-helix in a similar location to the one proposed in a recent model as an alternative PLM orientation induced by phosphorylation (Teriete *et al.*, 2009). However analysis of the protein surface at this location reveals it is unlikely to be a real site as the pocket appears too small to accommodate an α-helix.

There appears to be a direct relationship between the structural and functional studies of FXYD cytoplasmic domains carried out in this thesis. PLM_{38-72} has the greatest effect on the function of the Na^+, K^+-ATPase and has the highest affinity for cell membranes of all the FXYD proteins tested, and also has the largest α-helical content. Mat-$8lf_{38-93}$ also has an effect on the function of the Na^+, K^+-ATPase and has an affinity for phospholipid membranes but Mat-$8sf_{38-67}$ has no significant effect on Na^+, K^+-ATPase or affinity for membranes. Interestingly Mat-$8sf_{38-67}$ is essentially unstructured whereas Mat-$8lf_{38-93}$ has approximately 8% α-helical content suggesting that the inhibitory function of the long isoform of Mat-8 and inactivity of the short isoform of Mat-8 could be related to structure. The proposed interaction between the SxxRxS motif in PLM and Na^+, K^+-ATPase also shows how the cytoplasmic region of PLM can interact with both the Na^+, K^+-ATPase and cell membranes simultaneously which supports the observation of PLM_{38-72} binding to cell membranes in the presence of the Na^+, K^+-ATPase.

7.2.2. Cardiac Glycosides

Further understanding of the interaction of cardiac glycosides with the Na^+, K^+-ATPase has been gained with both solid-state NMR and computer prediction methods. By analysing the low-ouabain affinity Na^+, K^+-ATPase structures with GOLD, the possibility of ouabain occupying slightly different orientations in different species was revealed. This was surprising given the high specificity of ouabain to the Na^+, K^+-ATPase (Jewell *et al.*, 1992). Work has begun to confirm this observation experimentally by developing a novel solid-state NMR method for determining the depth of ligands within its binding site. By using cross-polarisation, ^{13}C signals from a ^{13}C labelled derivative of ouabain bound to Na^+,K^+-ATPase can be detected. These signals along with peaks from specific locations in the membrane and Na^+, K^+-ATPase such as lipid headgroups and C=C are reduced by the paramagnetic broadening agent manganese. Manganese will bind to membrane and protein surfaces and reduce the relaxation times of the nuclear spins in its local proximity. The effect on each spin is dependent on the distance from the manganese in that the closer it is the larger the effect on broadening. This means each ^{13}C peak of the Na^+, K^+-ATPase is diminished based on accessibility to Mn^{2+}, so whilst lipid headgroup signals will diminish at low quantities of manganese due to their ease of accessibility, less accessible signals like the

lipid methyl which is found in the middle of the lipid bilayer will not be significantly affected by manganese. By adding a ligand such as ouabain labelled with ^{13}C at two chemically and magnetically distinct sites, the relative effects of Mn^{2+} on these two peaks can be analysed to give information about the ligand orientation in the binding site. By comparing the broadening of the two ^{13}C peaks on ouabain to the broadening of the natural abundance peaks in the Na^+, K^+-ATPase membranes, the accessibility of the two ^{13}C label sites on ouabain can be estimated separately. This means if one site is closer to the protein surface than the other and therefore more exposed, its NMR peak will be more affected by manganese. The labelling method used in these experiments involved forming acetonide bridges at two locations on ouabain at the steroid moiety and rhamnose moiety. This produced OMA (steroid moiety label only) and ODA (steroid and rhamnose moiety labelled). Experiments with OMA proved very successful and appeared to show that ouabain was bound to the Na^+, K^+-ATPase and close to the protein surface. To understand the orientation of ouabain ODA needs to be used as it has two distinguishable sites that can be analysed. Unfortunately, ODA behaved very differently to OMA as the steroid ^{13}C peak was completely diminished at a very low manganese concentration suggesting it was binding to a different site on the surface. The rhamnose peak appeared very differently to what had been observed previously (Middleton *et al.*, 2000) suggesting it was occupying a range of orientations. Experiments run on ODA before the NMR

experiments showed it binds competitively with ouabain which suggests it was binding to the same site. This suggests an issue arose during sample preparation and the ODA possibly degraded preventing it from binding to the cardiac glycoside binding site in the Na^+, K^+-ATPase. Nevertheless the system is in place to repeat the method with fresh sample.

7.3. Future Work

7.3.1. Further Development of the pMAL expression system for FXYD proteins

The work presented here lays the foundations for many other experimental possibilities. With the successful expression and purification of Mat-8 its role in regulation of the Na^+, K^+-ATPase can be further investigated. Initially the Na^+, K^+-ATPase could be reconstituted with Mat-8 in synthetic membranes. The ATPase activity could be then measured and compared to activity of the Na^+, K^+-ATPase reconstituted without Mat-8 to gain further insights into the effect of full length Mat-8 as a regulator of the Na^+, K^+-ATPase (Crambert *et al.*, 2005). As preparations of the Na^+, K^+-ATPase contain γ-subunit or FXYD10 this will not be ideal as they will bind to the Na^+, K^+-ATPase in the same location. If a method to purify FXYD-protein free native Na^+, K^+-ATPase or a method to express and purify the Na^+, K^+-ATPase could be developed this could solve this problem. However the expression, and purification of a heterodimeric membrane protein would be

extremely difficult. SERCA has been successfully expressed in yeast and purified (Jidenko *et al.*, 2006) which is promising due to its homology with the α-subunit of the Na^+, K^+-ATPase. The β-subunit is likely to cause many additional problems as it will need to be co-expressed and form a complex with the α-subunit which is not an issue in SERCA.

There were several purification steps involved in the production of Mat-8 which meant insufficient quantities of labelled protein were produced for NMR. By reducing the number of steps the yield may be improved enough to produce an NMR signal. In addition alternative detergents with higher critical micellar concentrations could be used to solubilise the fusion protein, facilitating full removal of the detergent by dialysis and possibly allowing precipitation of pure Mat-8. Alternatively this could also be achieved by using a different chloroform precipitation method that has successfully removed small transmembrane proteins from detergents and impurities (Hu *et al.*, 2007). An alternative expression construct with a different fusion partner may also be investigated to improve the solubility of the fusion protein and eliminate the requirement for detergents. Upon successful expression and purification of $^{13}C/^{15}N$ labelled short form Mat-8 it could then be possible to reconstitute it into synthetic lipid bilayers with a similar composition to native membranes and solve the structure by NMR as has been done for the small membrane protein kaliotoxin (Lange *et al.*, 2005). This would be a superior method to what has been employed

for PLM (Teriete *et al.*, 2007) and CHIF (Franzin *et al.*, 2007d) which were solved in SDS micelles which are a highly negatively charged monolayer unlike the slightly negatively charged bilayer observed in cell membranes. With a successful system in place for Mat-8 work could then be done to apply it to other FXYD proteins, particularly the long isoform of Mat-8 so the structural differences between the two isoforms could be compared.

7.3.2. The cytoplasmic regions of PLM and long form Mat-8 as Na^+, K^+-ATPase inhibitors

As the ATPase assays of PLM_{38-72} on Na^+, K^+-ATPase reconstituted into 2:1 DMPC:DOPG at 100 mM Na^+ showed much less inhibition than in native membranes, a full Na^+ titration curve needs to be produced to see if there is a reduction on $K_{0.5}$ or V_{max}. If there is a reduction in these parameters then it would suggest that PLM_{38-72} does not immobilise DOPG as previously reported (Clayton *et al.*, 2005) and rather binds to lipid membrane surfaces. It would also be interesting to perform experiments in DMPC DOPS membranes as PLM_{38-72} binds more strongly to DOPS which is a eukaryotic lipid than DOPG which is a prokaryotic lipid. It is possible that the nature of the experiments that show PLM_{38-72} immobilised DOPG are flawed as they are performed in LMVs which could mean a high local concentration of peptide in the interbilayer space could increase the effect of PLM_{38-72} on DOPG. However it is possible that the stronger

interaction between PLM_{38-72} and DOPS could be significant as if it immobilised DOPS in Na^+, K^+-ATPase reconstituted in DMPC:DOPS it would increase the local concentration of DMPC around the Na^+, K^+-ATPase which would not support function.

7.3.3. Further Bioinformatics

The Na^+ activation curve of the Na^+, K^+-ATPase in the presence of the long isoform of Mat-8 revealed an increase in $K_{0.5}$. It also failed to reach maximal activity but Hill curve fitting suggested there was no effect on V_{max}. To confirm this additional experiments would need to be performed at higher Na^+ concentrations to produce a full curve where V_{max} is reached.

Although the cytoplasmic helix of PLM was modelled onto the surface of the Na^+, K^+-ATPase this hypothesis could be strengthened by modelling the full length protein. This could be achieved using Modeller which can model loops using a satisfaction of spatial restraints method. (Fiser *et al.*, 2000). If the structure of long form Mat-8 could be solved then similar methods could be employed to model the interaction of its cytoplasmic region with the Na^+, K^+-ATPase

7.3.4. The orientation of ouabain bound to the Na^+, K^+-ATPase

Finally, with the system in place to analyse the depths of acetonide bridges on ouabain by solid-state NMR, the ODA experiments need to be repeated to determine the orientation of ouabain in the Na^+, K^+-ATPase. By doing this in both pig kidney and spiny dogfish rectal gland Na^+, K^+-ATPase membranes it can be determined if there really are differences between species in the orientation of ouabain bound to the Na^+, K^+-ATPase as ouabain is a very potent and specific inhibitor of the Na^+, K^+-ATPase if there is a variations of orientations between species the interaction may not be as specific as first thought. It would also be advantageous to perform solution-state NMR on both OMA and ODA to confirm how they are observed on an NMR spectrum when not constrained by being bound to the Na^+, K^+-ATPase.

In conclusion, this work has not only provided insights into the mechanism of the cytoplasmic regions of FXYD proteins it has also developed several novel methods for the analysis of both FXYD proteins and cardiac glycosides; inhibitors of the Na^+, K^+-ATPase and opens up many possibilities for further study.

APPENDIX A

```
CLUSTAL 2.1 multiple sequence alignment


alpha-1
MGKGVGRDKYEPAAVSEQGDKKGKKGKKDRDMDELKKEVSMDDHKLSLDELHRKYGTDL
S 60
alpha-3          MG-----DKKD-----
DKDSPKKNKGKERRDLDDLKKEVAMTEHKMSVEEVCRKYNTDCV 50
alpha-2          MGRGAGREYSPAATTAENGGGKKKQ--
KEKELDELKKEVAMDDHKLSLDELGRKYQVDLS 58
SERCA1           ----------------------------------------
MEAAHAKTTEECLAYFGVSET 21
SERCA2           ----------------------------------------
MENAHTKTVEEVLGHFGVNES 21
SERCA3           ----------------------------------------
MEAAHLLPAADVLRHFSVTAE 21

*  .  :    : .

alpha-1
RGLTSARAAEILARDGPNALTPPPTTPEWIKFCRQLFGGFSMLLWIGAILCFLAYSIQA
A 120
alpha-3
QGLTHSKAQEILARDGPNALTPPPTTPEWVKFCRQLFGGFSILLWIGAILCFLAYGIQA
G 110
alpha-2
KGLTNQRAQDVLARDGPNALTPPPTTPEWVKFCRQLFGGFSILLWIGAILCFLAYGIQA
A 118
SERCA1
TGLTPDQVKRNLEKYGLNELPAEEGKTLWELVIEQFEDLLVRILLLAACISFVLAWFEE
G 81
SERCA2
TGLSLEQVKKLKERWGSNELPAEEGKTLLELVIEQFEDLLVRILLLAACISFVLAWFEE
G 81
SERCA3
GGLSPAQVTGARERYGPNELPSEEGKSLWELVLEQFEDLLVRILLLAALVSFVLAWFEE
G 81
                 **:  :.     : * * *..   ..    . .*: . :
:* :.* :.*:   :: .

alpha-1
TEEEPQNDNLYLGVVLSAVVIITGCFSYYQEAKSSKIMESFKNMVPQQALVIRNGEK--
M 178
alpha-3
TEDDPSGDNLYLGIVLAAVVIITGCFSYYQEAKSSKIMESFKNMVPQQALVIREGEK--
M 168
```

```
alpha-2
MEDEPSNDNLYLGVVLAAVVIVTGCFSYYQEAKSSKIMDSFKNMVPQQALVIREGEK--
M 176
SERCA1          EE---
TITAFVEPFVILLILIANAIVGVWQERNAENAIEALKEYEPEMGKVYRADRKSVQ 138
SERCA2          EE---
TITAFVEPFVILLILVANAIVGVWQERNAENAIEALKEYEPEMGKVYRQDRKSVQ 138
SERCA3          EE---
TTTAFVEPLVIMLILVANAIVGVWQERNAESAIEALKEYEPEMGKVIRSDRKGVQ 138
                 *       :   .*:  ::: .. .. :** ::.. ::::*:
*: . * * ..*

alpha-1         SINAEEVVVGDLVEVKGGDRIPADLRIISANG--
CKVDNSSLTGESEPQTRSPDFTNEN- 235
alpha-3         QVNAEEVVVGDLVEIKGGDRVPADLRIISAHG--
CKVDNSSLTGESEPQTRSPDCTHDN- 225
alpha-2         QINAEEVVVGDLVEVKGGDRVPADLRIISSHG--
CKVDNSSLTGESEPQTRSPEFTHEN- 233
SERCA1
RIKARDIVPGDIVEVAVGDKVPADIRILAIKSTTLRVDQSILTGESVSVIKHTEPVPDP
R 198
SERCA2
RIKAKDIVPGDIVEIAVGDKVPADIRLTSIKSTTLRVDQSILTGESVSVIKHTDPVPDP
R 198
SERCA3
RIRARDIVPGDIVEVAVGDKVPADLRLIEIKSTTLRVDQSILTGESVSVTKHTEAIPDP
R 198
                 :.*.::* **:**:  **::***:*:   :.   :**:*
***** .  : .:   :

alpha-1         --
PLETRNIAFFSTNCVEGTARGIVVYTGDRTVMGRIATLASGLEGGQTPIAAEIEHFIH
293
alpha-3         --
PLETRNITFFSTNCVEGTARGVVVATGDRTVMGRIATLASGLEVGKTPIAIEIEHFIQ
283
alpha-2         --
PLETRNICFFSTNCVEGTARGIVIATGDRTVMGRIATLASGLEVGRTPIAMEIEHFIQ
291
SERCA1
AVNQDKKNMLFSGTNIAAGKALGIVATTGVGTEIGKIRDQMAATEQDKTPLQQKLDEFG
E 258
SERCA2
AVNQDKKNMLFSGTNIAAGKAMGVVVATGVNTEIGKIRDEMVATEQERTPLQQKLDEFG
E 258
SERCA3
AVNQDKKNMLFSGTNITSGKAVGVAVATGLHTELGKIRSQMAAVEPERTPLQRKLDEFG
R 258
                   :.:*: * .** . *.* *:.  **  * :*:*     .
*  :**:  :::.* .

alpha-1         IITGVAVFLGVSFFILSL------
ILEYTWLEAVIFLIGIIVAN----VPEGLLATVTVC 343
alpha-3         LITGVAVFLGVSFFILSL------
ILGYTWLEAVIFLIGIIVAN----VPEGLLATVTVC 333
```

```
alpha-2          LITGVAVFLGVSFFVLSL------
ILGYSWLEAVIFLIGIIVAN----VPEGLLATVTVC 341
SERCA1
QLSKVISLICVAVWLINIGHFNDPVHGGSWFRGAIYYFKIAVALAVAAIPEGLPAVITT
C 318
SERCA2
QLSKVISLICIAVWIINIGHFNDPVHGGSWIRGAIYYFKIAVALAVAAIPEGLPAVITT
C 318
SERCA3
QLSHAISVICVAVWVINIGHFADPAHGGSWLRGAVYYFKIAVALAVAAIPEGLPAVITT
C 318
                  :: .  .: ::.:::.:          :*:...:: : * **
:**** *.:*.*

alpha-1
LTLTAKRMARKNCLVKNLEAVETLGSTSTICSDKTGTLTQNRMTVAHMWFDNQIHEADT
T 403
alpha-3
LTLTAKRMARKNCLVKNLEAVETLGSTSTICSDKTGTLTQNRMTVAHMWFDNQIHEADT
T 393
alpha-2
LTLTAKRMARKNCLVKNLEAVETLGSTSTICSDKTGTLTQNRMTVAHMWFDNQIHEADT
T 401
SERCA1
LALGTRRMAKKNAIVRSLPSVETLGCTSVICSDKTGTLTTNQMSVCKMFIIDKVDGDIC
L 378
SERCA2
LALGTRRMAKKNAIVRSLPSVETLGCTSVICSDKTGTLTTNQMSVCRMFILDRVEGDTC
S 378
SERCA3
LALGTRRMARKNAIVRSLPSVETLGCTSVICSDKTGTLTTNQMSVCRMFVVAEADAGSC
L 378
                  *:* ::***:**.:*:.* :*****.**.**********
*:*:*.:*:.  . .

alpha-1          ENQSGVSFDKTSA-----------------
TWLALSRIAGLCNRAVFQANQENLPILKRA 446
alpha-3          EDQSGTSFDKSSH-----------------
TWVALSHIAGLCNRAVFKGGQDNIPVLKRD 436
alpha-2          EDQSGATFDKRSP-----------------
TWTALSRIAGLCNRAVFKAGQENISVSKRD 444
SERCA1
LNEFSITGSTYAPEGEVLKNDKPVRPGQYDGLVELATICALCNDSSLDFNEAKGVYEKV
G 438
SERCA2
LNEFTITGSTYAPIGEVHKDDKPVNCHQYDGLVELATICALCNDSALDYNEAKGVYEKV
G 438
SERCA3
LHEFTISGTTYTPEGEVRQGDQPVRCGQFDGLVELATICALCNDSALDYNEAKGVYEKV
G 438
                  .:   :  . :                    *: *..***
: :. .: :    *

alpha-1          VAGDASESALLKCIELC---------------
CGSVKEMRERYAKIVEIPFNSTNKYQLS 491
```

```
alpha-3         VAGDASESALLKCIELS---------------
SGSVKLMRERNKKVAEIPFNSTNKYQLS 481
alpha-2         TAGDASESALLKCIELS---------------
CGSVRKMRDRNPKVAEIPFNSTNKYQLS 489
SERCA1
EATETALTTLVEKMNVFNTDVRSLSKVERANACNSVIRQLMKKEFTLEFSRDRKSMSVY
C 498
SERCA2
EATETALTCLVEKMNVFDTELKGLSKIERANACNSVIKQLMKKEFTLEFSRDRKSMSVY
C 498
SERCA3
EATETALTCLVEKMNVFDTDLQALSRVERAGACNTVIKQLMRKEFTLEFSRDRKSMSVY
C 498
                 * ::: : *:: :::                 ..:*     :
*:. : ..    .

alpha-1
IHKNPNTSEPQHLLVMKGAPERILDRCSSILLHGKEQPLDEELKDAFQNAYLELGGLGE
R 551
alpha-3
IHETEDPNDNRYLLVMKGAPERILDRCSTILLQGKEQPLDEEMKEAFQNAYLELGGLGE
R 541
alpha-2         IHEREDSPQS-
HVLVMKGAPERILDRCSTILVQGKEIPLDKEMQDAFQNAYMELGGLGER 548
SERCA1
SPAKSSRAAVGNKMFVKGAPEGVIDRCNYVRVGTTRVPLTGPVKEKIMAVIKEWGTGRD
T 558
SERCA2          TPNKPSRTSMS-
KMFVKGAPEGVIDRCTHIRVGSTKVPMTSGVKQKIMSVIREWGSGSDT 557
SERCA3
TPTRPHPTGQGSKMFVKGAPESVIERCSSVRVGSRTAPLTPTSREQILAKIRDWGSGSD
T 558
                              :.:***** :::**. : :     *:
:: :     : *   :

alpha-1         VLGFCHLFLPDEQFPEGFQFDTDDVNFPIDN-
LCFVGLISMIDPPRAAVPDAVGKCRSAG 610
alpha-3         VLGFCHYYLPEEQFPKGFAFDCDDVNFTTDN-
LCFVGLMSMIDPPRAAVPDAVGKCRSAG 600
alpha-2         VLGFCQLNLPSGKFPRGFKFDTDELNFPTEK-
LCFVGLMSMIDPPRAAVPDAVGKCRSAG 607
SERCA1
LRCLALATRDTPPKREEMVLDDSARFLEYETDLTFVGVVGMLDPPRKEVTGSIQLCRDA
G 618
SERCA2
LRCLALATHDNPLRREEMHLEDSANFIKYETNLTFVGCVGMLDPPRIEVASSVKLCRQA
G 617
SERCA3
LRCLALATRDAPPRKEDMELDDCSKFVQYETDLTFVGCVGMLDPPRPEVAACITRCYQA
G 618
                 :  :.          . : ::     .  :. * ***
:.*:****  *. .:  * .**
```

```
alpha-1
IKVIMVTGDHPITAKAIAKGVGIISEGNETVEDIAARLNIPVSQVNPRDAKACVVHGSD
L 670
alpha-3
IKVIMVTGDHPITAKAIAKGVGIISEGNETVEDIAARLNIPVSQVNPRDAKACVIHGTD
L 660
alpha-2
IKVIMVTGDHPITAKAIAKGVGIISEGNETVEDIAARLNIPMSQVNPREAKACVVHGSD
L 667
SERCA1          IRVIMITGDNKGTAIAICRRIGIFGENE---------------
-----EVADRAYTGREF 658
SERCA2          IRVIMITGDNKGTAVAICRRIGIFGQDE---------------
-----DVTSKAFTGREF 657
SERCA3          IRVVMITGDNKGTAVAICRRLGIFGDTE---------------
-----DVAGKAYTGREF 658
                *:*:*:***:  ** **.: :**:.: :
:.   .  * ::

alpha-1
KDMTSEQLDDILKYHTEIVFARTSPQQKLIIVEGCQRQGAIVAVTGDGVNDSPALKKAD
I 730
alpha-3
KDFTSEQIDEILQNHTEIVFARTSPQQKLIIVEGCQRQGAIVAVTGDGVNDSPALKKAD
I 720
alpha-2
KDMTSEQLDEILKNHTEIVFARTSPQQKLIIVEGCQRQGAIVAVTGDGVNDSPALKKAD
I 727
SERCA1          DDLPLAEQREACR--
RACCFARVEPSHKSKIVEYLQSYDEITAMTGDGVNDAPALKKAEI 716
SERCA2          DELNPSAQRDACL--
NARCFARVEPSHKSKIVEFLQSFDEITAMTGDGVNDAPALKKAEI 715
SERCA3          DDLSPEQQRQACR--
TARCFARVEPAHKSRIVENLQSFNEITAMTGDGVNDAPALKKAEI 716
                .::      :         ***..* :*  ***  *  .
*.*:*******:******:*

alpha-1
GVAMGIAGSDVSKQAADMILLDDNFASIVTGVEEGRLIFDNLKKSIAYTLTSNIPEITP
F 790
alpha-3
GVAMGIAGSDVSKQAADMILLDDNFASIVTGVEEGRLIFDNLKKSIAYTLTSNIPEITP
F 780
alpha-2
GIAMGISGSDVSKQAADMILLDDNFASIVTGVEEGRLIFDNLKKSIAYTLTSNIPEITP
F 787
SERCA1          GIAMGS-
GTAVAKTASEMVLADDNFSTIVAAVEEGRAIYNNMKQFIRYLISSNVGEVVCI 775
SERCA2          GIAMGS-
GTAVAKTASEMVLADDNFSTIVAAVEEGRAIYNNMKQFIRYLISSNVGEVVCI 774
SERCA3          GIAMGS-
GTAVAKSAAEMVLSDDNFASIVAAVEEGRAIYSNMKQFIRYLISSNVGEVVCI 775
                *:***  *: *:* *::*:* ****::**:.*****
*:.*:*: * * ::**: *:. :
```

```
alpha-1
LIFIIANIPLPLGTVTILCIDLGTDMVPAISLAYEQAESDIMKRQPRNPKTDKLVNERL
I 850
alpha-3
LLFIMANIPLPLGTITILCIDLGTDMVPAISLAYEAAESDIMKRQPRNPRTDKLVNERL
I 840
alpha-2
LLFIIANIPLPLGTVTILCIDLGTDMVPAISLAYEAAESDIMKRQPRNSQTDKLVNERL
I 847
SERCA1
FLTAALGLPEALIPVQLLWVNLVTDGLPATALGFNPPDLDIMDRPPRSPKEPLISGWLF
F 835
SERCA2
FLTAALGFPEALIPVQLLWVNLVTDGLPATALGFNPPDLDIMNKPPRNPKEPLISGWLF
F 834
SERCA3
FLTAILGLPEALIPVQLLWVNLVTDGLPATALGFNPPDLDIMEKLPRSPREALISGWLF
F 835
                  ::    .:* .* .: :* ::* ** :** :*.:: .:
***.: **..:   : .  ::

alpha-1
SMAYGQIGMIQALGGFFTYFVILAENGFLPIHLLGLRVDWDDRWINDVEDSYGQQWTYE
Q 910
alpha-3
SMAYGQIGMIQALGGFFSYFVILAENGFLPGNLVGIRLNWDDRTVNDLEDSYGQQWTYE
Q 900
alpha-2
SMAYGQIGMIQALGGFFTYFVILAENGFLPSRLLGIRLDWDDRTMNDLEDSYGQEWTYE
Q 907
SERCA1          RYMAIGGYVGAATVGAAAWWFLYAEDGPH------
VNYSQLTHFMQCTEDNTHFEGIDCE 889
SERCA2          RYLAIGCYVGAATVGAAAWWFIAADGGPR------
VSFYQLSHFLQCKEDNPDFEGVDCA 888
SERCA3          RYLAIGVYVGLATVAAATWWFVYDAEGPH------
INFYQLRNFLKCSEDNPLFAGIDCE 889
                         :  *  .  :::.:    *        :      .
::  **.

alpha-1
RKIVEFTCHTAFFVSIVVVQWADLVICKTRRNSVFQQGMKNKILIFGLFEETALAAFLS
Y 970
alpha-3
RKVVEFTCHTAFFVSIVVVQWADLIICKTRRNSVFQQGMKNKILIFGLFEETALAAFLS
Y 960
alpha-2
RKVVEFTCHTAFFASIVVVQWADLIICKTRRNSVFQQGMKNKILIFGLLEETALAAFLS
Y 967
SERCA1
VFEAPEPMTMALSVLVTIEMCNALNSLSENQSLLRMPPWVNIWLLGSICLSMSLHFLIL
Y 949
SERCA2
IFESPYPMTMALSVLVTIEMCNALNSLSENQSLLRMPPWENIWLVGSICLSMSLHFLIL
Y 948
```

```
SERCA3
VFESRFPTTMALSVLVTIEMCNALNSVSENQSLLRMPPWMNPWLLVAVAMSMALHFLIL
L 949
                      .   *: . :.:     *   . .:. :      *
*: .:   . :*  ::

alpha-1
CPGMGVALRMYPLKPTWWFCAFPYSLLIFVYDEVRKLIIRRRPGGWVEKETYY------
- 1023
alpha-3
CPGMDVALRMYPLKPSWWFCAFPYSFLIFVYDEIRKLILRRNPGGWVEKETYY------
- 1013
alpha-2
CPGMGVALRMYPLKVTWWFCAFPYSLLIFIYDEVRKLILRRYPGGWVEKETYY------
- 1020
SERCA1
VDPLPMIFKLRALDLTQWLMVLKISLPVIGLDEILKFVARNYLEDPEDE--RRK-----
- 1001
SERCA2
VEPLPLIFQITPLNVTQWLMVLKISLPVILMDETLKFVARNYLEPGKEC--
VQPATKSCS 1006
SERCA3
VPPLPLIFQVTPLSGRQWVVVLQISLPVILLDEALKYLSRNHMHACLYPGLLRTVSQAW
S 1009
                  : : ::: .*.   *. .:  *: ::  **  * : *.

alpha-1          ------------------------------------
alpha-3          ------------------------------------
alpha-2          ------------------------------------
SERCA1           ------------------------------------
SERCA2           FSACTDGISWPFVLLIMPLVIWVYSTDTNFSDMFWS 1042
SERCA3           RQPLTTSWTPDHTGRNEPEVSAGNRVESPVCTSD-- 1043
```

APPENDIX B

DiLiMoT

Below we show all motifs, including those that appear in regions or proteins not used for the P-/Scons calculation (i.e. in filtered domains, or duplicate homologous regions). Filtered regions appear in a lower case letters. An asterix in the alignment indicates that the motif is present in that species, in addition to the original sequence (ORG) (help)
You can download sequences below in fasta format (download).

The proteins below contain the SxxRxS motif.

>Adducin
MNGDSRAAVVTSPPPTTAPHKERYFDRVDENNPEYLRERNMAPDLRQDFNMMEQKKRVS
MILQSPAFCEELESMIQEQFKKGKNPTGLLALQQIADFMTTNVPNVYPAAPQGGMAALN
MSLGMVTPVNDLRGSDSIAYDKGEKLLRCklaafyrladlfgwsqliynhittrvnseq
ehflivpfgllysevtasslvkinlqgdivdrgstnlgvnqagftlhsaiyaarpdvkc
vvhihtpagaavsamkcgllpispealslgevayhdyhgilvdeeekvliqknlgpksk
vlilrnhglvsvgesveeafyyihnlvvaceiqvrtlasaggpdnlvllnpEKYKAKSR
SPGSPVGEGTGSPPKWQIGEQEFEALMRMLDNLGYRTGYPYRYPALREKSKKYSDVEVP
ASVTGYSFASDGDSGTCSPLRHSFQKQQREKTRWLNSGRGDEASEEGQNGSSPKSKTKW
TKEDGHRTSTSAVPNLFVPLNTNPKEVQEMRNKIREQNLQDIKTAGPQSQVLCGVVMDR
SLVQGELVTASKAIIEKEYQPHVIVSTTGPNPFTTLTdreleeyrreverkqkgseenl
deareqkeksPPDQPAVPHPPPSTPIKLEEDLVPEPTTGDDSDAATFKPTLPDLSPDEP
SEALGFPMLEKEEEAHRPPSPTEAPTEASPEPAPDPAPVAEEAAPSAVEEGAAADPGSD
GSPGKSPSKKKKKFRTPSFLKKSKKKSDS

>Mat8
MQKVTLGLLVFLAGFPVLDANDLEDKNSPFYYDWhslqvgglicagvlcamgiiivMSE
WRSSGEQAGRGWGSPPLTTQLSPTGAKCKCKFGQKSGHHPGETPPLITPGSAQS

>PI3K
MAASGVPRGCDILIVYSPDAEEWCQYLQTLFLSSRQVRSQKILTHRLGPEASFSAEDLS
LFLSTRCVVVLLSAELVQHFHKPALLPLLQRAFHPPHRVVRLLCGVRDSEEFLDFFPDW
AHWQELTCDDEPETYVAAVKKAISEDSGCDSVTDTEPEDEKVVSYSKQQNLPTVTSPGN
LMVVQPDRIRCGAETTVYVIVRCKLDDRVATEAEFSPEDSPSVRMEAKVENEYTISVKA
PNLSSGNVSLKIYSGDLVVCETVISYYTDMEEIGNLLSNAANPVEFMCQAFKIVPYNTE
TLDKLLTESLKNNIPASGLHLFGINQLEEEDMMTNQRDEELPTLLHFAAKYGLKNLTAL
LLTCPGALQAYSVANKHGHYPNTIAEKHGFRDLRQFIDEYVETVDMLKSHIKEELMHGE
EADAVYESMAHLSTDLLMKCSLNPGCDEDLYESMAAFVPAATEDLYVEMLQASTSNPIP
GDGFSRATKDSMIRKFLEGNSMGMTNLERDQCHLGQEEDVYHTVDDDEAFSVDLASRPP
VPVPRPETTAPGAHQLPDNEPYIFKVFAEKSQERPGNFYVSSESIRKGPPVRPWRDRPQ
SSIYDPFAGMKTPGQRQLITLQEQVKLGIVNVDEAVLHFKEWQLNQKKRSESFRFQQEN
LKRLRDSITRRQREKQKSGKQTDLEITVPIRHSQHLPAKVEFGVYESGPRKSVIPPRTE
LRRGDWKTDSTSSTASSTSNRSSTRSLLSVSSGMEGDNEDNEVPEVTRSRSPGPPQVDG
TPTMSLERPPRVPPRAASQRPPTRETFHPPPPVPPRGR

>PLM
Maslghilvfcvglltmakaespkehdpftydyqslqigglviagilfilgilivlsrr
crckfnqqqrtgepdEEEGTFRSSIRRLSTRRR

>SRC
MGSNKSKPKDASQRRRSLEPAENVHGAGGGAFPASQTPSKPASADGHRGPSAAFAPAAA
EPKLFGGFNSSDTVTSPQRAGPLAGGVTtfvalydyesrtetdlsfkkgerlqivnnte
gdwwlahslstgqtgyipsnyvapsdSIQAEewyfgkitrreserlllnaenprgtflv
resettkgayclsvsdfdnakglnvkhykirkldsggfyitsrtqfnslqqlvayyskh
adgLCHRLTTVCPTSKPQTQGLAKDAWEIPRESLrlevklgqgcfgevwmgtwngttrv
aiktlkpgtmspeaflqeaqvmkklrheklvqlyavvseepiyivteymskgslldflk
getgkylrlpqlvdmaaqiasgmayvermnyvhrdlraanilvgenlvckvadfglarl
iedneytarqgakfpikwtapeaalygrftiksdvwsfgilltelttkgrvpypgmvnr
evldqvergyrmpcppecpeslhdlmcqcwrkepeerptfeylqaflEDYFTSTEPQYQ
PGENL

The proteins below do not contain the SxxRxS motif.

>Ank
MPYSVGFREADaatsflraarsgnldkaldhlrngvdintCNQNglnglhlaskeghvkm
vvellhkeiiletttkKgntalhiaalagqdevvrelvnyganvnaqsqKgftplymaaq
enhlevvkfllenganqnvateDgftplavalqqghenvvahlinygtkgkvrlpalhia
arnddtrtaavllqndpnpdvlskTgftplhiaahyenlnvaqlllnrgasvnftpqNgi
tplhiasrrgnvimvrllldrgaqietktkDeltplhcaarnghvriseilldhgapiqa
ktkNglspihmaaqgdhldcvrlllqydaeidditlDhltplhvaahcghhrvakvlldk
gakpnsralNgftplhiackknhvrvmelllktgasidavteSgltplhvasfmghlpiv
knllqrgaspnvsnvKvetplhmaaraghtevakyllqnkakvnakakDdqtplhcaari
ghtnmvkllennanpnlattAghtplhiaareghvetvlallekeasqacmtkKgftpl
hvaakygkvrvaelllerdahpnaagkNgltplhvavhhnnldivkllprggsphspaw
NgytplhiaakqnqvevarsllqyggsanaesvQgvtplhlaaqeghaemvalllskqan
gnlgnkSgltplhlvaqeghvpvadvlikhgvmvdattrMgytplhvashygniklvkfl
lqhqadvnaktkLgysplhqaaqqghtdivtlllkngaspnevssDGTTPLAIAKRLGYI
SVTDVLKVVTDETSFVLVSDKHRMSFPETVDEILDVSEDEGEELISFKAERRDSRDVDEE
KELLDFVPKLDQVVESPAIPRIPCAMPETVVIRSEEQEQASKEYDEDSLIPSSPATETSD
NISPVASPVHTgflvsfmvdarggsmrgsrhnglrvvipprtcaaptritcrlvkpqkls
tppplaeeeglasriialgptgaqflspviveiphfashgrgdrelvvlrsengsVWKEH
RSRYGESYLDQILNGMDEELGSLEELEKKRVCRIITTDFPLYFVIMSRLCQDYDTIGPEG
GSLKSKLVPLVQATFPENAVTKRVKLALQAQPVPDELVTKLLGNQATFSPIVTVEPRRRK
FHRPIGLRIPLPPSWTDNPRDSGEGDTTSLRLLCSVIGGTDQAQWEDITGTTKLVYANEC
ANFTTNVSARFWLSDCPRTAEAVNFATLLYKELTAVPYMAKFVIFAKMNDPREGRLRCYC
MTDDKVDKTLEQHENFVEVARSRDIEVLEGMSLFAELSGNLVPVKKAAQQRSFHFQSFRE
NRLAMPVKVRDSSREPGGSLSFLRKAMKYEDTQHILCHLNITMPPCAKGSGAEDRRRTPT
PLALRYSILSESTpgslsgteqaemkmavisehlglswaelarelqfsvedinrirvenp
nslleqsvallnlwviregqnanmenlytalqsidrgeivnmlegsgRQSRNLKPDRRHT
DRDYSLSPSQMNGYSSLQDELLSPASLGCALSSPLRADQYWNEVAVLDAIPLAATEHDTM
LEMSDMQVWSAGLTPSLVTAEDSSLECSKAEDSDATGHEWKLEGALSEEPRGPELGSLEL
VEDDTVDSDATNGLIDLLEQEEGQRSEEKLPGSKRQDDATGAGQDSENEVSLVSGHQRGQ
ARITHSPTVSQVTERSQDRLQDWDADGSIVSYLQDAAQGSWQEEVTQGPHSFQGTSTMTE
GLEPGGSQEYEKVLVSVSEHTWTEQPEAESSQADRDRRQQGQEEQVQEAKNTFTQVVQGN
EFQNIPGEQVTEEQFTDEQGNIVTKKIIRKVVRQIDLSSADAAQEHEEVTVEGPLEDPSE
LEVDIDYFMKHSKDHTSTPNP

REFERENCES

Abraham, T., R. N. A. H. Lewis, et al. (2005). "Isothermal Titration Calorimetry Studies of the Binding of a Rationally Designed Analogue of the Antimicrobial Peptide Gramicidin S to Phospholipid Bilayer Membranes†." Biochemistry **44**(6): 2103-2112.

Akio, T. (1971). "Lipid comosition of sarcoplasmic reticulum of human skeletal muscle." Biochimica et Biophysica Acta (BBA) - Lipids and Lipid Metabolism **248**(1): 12-20.

Alpes, H., H. J. Apell, et al. (1988). "Reconstitution of Na+/K+-ATPase into phosphatidylcholine vesicles by dialysis of nonionic alkyl maltoside detergents." Biochimica et Biophysica Acta (BBA) - Biomembranes **946**(2): 379-388.

Altschul, S. F., T. L. Madden, et al. (1997). "Gapped BLAST and PSI-BLAST: a new generation of protein database search programs." Nucleic Acids Research **25**(17): 3389-3402.

Arêas, J. A. G., G. Gröbner, et al. (1998). "Interaction of a type II myosin with biological membranes studied by 2H solid state NMR." Biochemistry **37**(16): 5582-5588.

Arêas, J. A. G., G. J. Gröbner, et al. (1997). "Use of solid-state 2H NMR for studying protein-lipid interactions at emulsion interfaces." Magnetic Resonance in Chemistry **35**: S119-S124.

Arimochi, J., A. Kobayashi, et al. (2005). "Stable expression and visualization of Mat-8 (FXYD-3) tagged with a fluorescent protein in Chinese Hamster Ovary (CHO)-K1 cells." Biotechnology Letters **27**(14): 1017-1024.

Arimochi, J., A. Ohashi-Kobayashi, et al. (2007). "Interaction of mat-8 (FXYD-3) with Na+/K+-ATPase in colorectal cancer cells." Biological and Pharmaceutical Bulletin **30**(4): 648-654.

Asano, Y., U. A. Liberman, et al. (1976). "Thyroid thermogenesis. Relationships between Na+-dependent respiration and Na+ + K+-adenosine triphosphatase activity in rat skeletal muscle." The Journal of clinical investigation **57**(2): 368-379.

Ashkenazy, H., E. Erez, et al. (2010). "ConSurf 2010: calculating evolutionary conservation in sequence and structure of proteins and nucleic acids." Nucleic Acids Research **38**(suppl 2): W529-W533.

Bader, R., M. Lerch, et al. (2008). NMR of Membrane-Associated Peptides and Proteins. Protein Science Encyclopedia, Wiley-VCH Verlag GmbH & Co. KGaA.

Baginski, E. S., P. P. Foa, et al. (1967). "Microdetermination of Inorganic Phosphate, Phospholipids, and Total Phosphate in Biologic Materials." Clin Chem **13**(4): 326-332.

Bagrov, A. Y., O. V. Fedorova, et al. (1998). "Characterization of a Urinary Bufodienolide Na+,K+-ATPase Inhibitor in Patients After Acute Myocardial Infarction." Hypertension **31**(5): 1097-1103.

Bartlett, G. R. (1959). "Phosphorus Assay in Column Chromatography." Journal of Biological Chemistry **234**(3): 466-468.

Baxter, C. A., C. W. Murray, et al. (1998). "Flexible docking using Tabu search and an empirical estimate of binding affinity." Proteins **33**(3): 367-382.

Beguin, P., G. Crambert, et al. (2001). "CHIF, a member of the FXYD protein family, is a regulator of Na,K-ATPase distinct from the [gamma]-subunit." EMBO J **20**(15): 3993-4002.

Beguin, P., G. Crambert, et al. (2002). "FXYD7 is a brain-specific regulator of Na,K-ATPase [alpha]1-[beta] isozymes." EMBO J **21**(13): 3264-3273.

Beguin, P., X. Wang, et al. (1997). "The [gamma] subunit is a specific component of the Na,K-ATPase and modulates its transport function." EMBO J **16**(14): 4250-4260.

Ben-Shimon, A. and M. Eisenstein (2010). "Computational Mapping of Anchoring Spots on Protein Surfaces." Journal of Molecular Biology **402**(1): 259-277.

Bibert, S., D. Aebischer, et al. (2009). "A Link between FXYD3 (Mat-8)-mediated Na,K-ATPase Regulation and Differentiation of Caco-2 Intestinal Epithelial Cells." Mol. Biol. Cell **20**(4): 1132-1140.

Bibert, S., S. Roy, et al. (2006). "Structural and functional properties of two human FXYD3 (Mat-8) isoforms." Journal of Biological Chemistry **281**(51): 39142-39151.

Blanco, G. and R. W. Mercer (1998). "Isozymes of the Na-K-ATPase: heterogeneity in structure, diversity in function." American Journal of Physiology - Renal Physiology **275**(5): F633-F650.

Blom, N., S. Gammeltoft, et al. (1999). "Sequence and structure-based prediction of eukaryotic protein phosphorylation sites." Journal of Molecular Biology **294**(5): 1351-1362.

Boland, M. P. and D. A. Middleton (2008). "The dynamics and orientation of a lipophilic drug within model membranes determined by 13C solid-state NMR." Physical Chemistry Chemical Physics **10**(1): 178-185.

Buck, B., J. Zamoon, et al. (2003). "Overexpression, purification, and characterization of recombinant Ca-ATPase regulators for high-resolution solution and solid-state NMR studies." Protein Expression and Purification **30**(2): 253-261.

Buffy, J. J., T. Hong, et al. (2003). "Solid-State NMR Investigation of the Depth of Insertion of Protegrin-1 in Lipid Bilayers Using Paramagnetic Mn2+." Biophysical Journal **85**(4): 2363-2373.

Burns, E. L. and E. M. Price (1993). "Random mutagenesis of the sheep Na,K-ATPase alpha-1 subunit generates a novel T797N mutation

that results in a ouabain-resistant enzyme." Journal of Biological Chemistry **268**(34): 25632-25635.

Canessa, C. M., J. D. Horisberger, et al. (1992). "Mutation of a cysteine in the first transmembrane segment of Na,K-ATPase α subunit confers ouabain resistance." EMBO Journal **11**(5): 1681-1687.

Canessa, C. M., J. D. Horisberger, et al. (1993). "Mutation of a tyrosine in the H3-H4 ectodomain of Na,K-ATPase alpha subunit confers ouabain resistance." J. Biol. Chem. **268**(24): 17722-17726.

Cavanagh, J., W. J. Fairbrother, et al. (2007). Chapter 3 - Experimental aspects of NMR spectroscopy. Protein NMR Spectroscopy (Second Edition). Burlington, Academic Press: 114-270.

Champeil, P., T. Menguy, et al. (1998). "Characterization of a Protease-resistant Domain of the Cytosolic Portion of Sarcoplasmic Reticulum Ca2+-ATPase." Journal of Biological Chemistry **273**(12): 6619-6631.

Chan, H., V. Babayan, et al. (2010). "The P-Type ATPase Superfamily." Journal of Molecular Microbiology and Biotechnology **19**(1-2): 5-104.

Clayton, J. C., E. Hughes, et al. (2005). "The cytoplasmic domains of phospholamban and phospholemman associate with phospholipid membrane surfaces." Biochemistry **44**(51): 17016-17026.

Crambert, G., M. Füzesi, et al. (2002). "Phospholemman (FXYD1) associates with Na,K-ATPase and regulates its transport properties." Proceedings of the National Academy of Sciences **99**(17): 11476-11481.

Crambert, G. and K. Geering (2003). "FXYD Proteins: New Tissue-Specific Regulators of the Ubiquitous Na,K-ATPase." Sci. STKE **2003**(166): re1-.

Crambert, G., C. Li, et al. (2005). "FXYD3 (Mat-8), a new regulator of Na,K-ATPase." Molecular Biology of the Cell **16**(5): 2363-2371.

Crambert, G., C. Li, et al. (2004). "FXYD7, Mapping of Functional Sites Involved in Endoplasmic Reticulum Export, Association With and Regulation of Na,K-ATPase." Journal of Biological Chemistry **279**(29): 30888-30895.

Crowell, K. J., C. M. Franzin, et al. (2003). "Expression and characterization of the FXYD ion transport regulators for NMR structural studies in lipid micelles and lipid bilayers." Biochimica et Biophysica Acta (BBA) - Proteins & Proteomics **1645**(1): 15-21.

Croyle, M. L., A. L. Woo, et al. (1997a). "Extensive random mutagenesis analysis of the Na+/K+-ATPase α subunit identifies known and previously unidentified amino acid residues that alter ouabain sensitivity." European Journal of Biochemistry **248**(2): 488-495.

Croyle, M. L., A. L. Woo, et al. (1997b). "Extensive Random Mutagenesis Analysis of the Na+/K+-ATPase α Subunit Identifies Known and

Previously Unidentified Amino Acid Residues that Alter Ouabain Sensitivity Implications for Ouabain Binding." European Journal of Biochemistry **248**(2): 488-495.

Davey, N. E., K. Van Roey, et al. (2012). "Attributes of short linear motifs." Molecular BioSystems.

Davis, J. H., K. R. Jeffrey, et al. (1976). "Quadrupolar echo deuteron magnetic resonance spectroscopy in ordered hydrocarbon chains." Chemical Physics Letters **42**(2): 390-394.

Dean, R. B. (1941). "Theories of electrolyte equilibrium in muscle." Biol. Symp **3**: 331-348.

Delprat, B., D. Schaer, et al. (2007). "FXYD6 Is a Novel Regulator of Na,K-ATPase Expressed in the Inner Ear." Journal of Biological Chemistry **282**(10): 7450-7456.

Devarajan, P., D. A. Scaramuzzino, et al. (1994). "Ankyrin binds to two distinct cytoplasmic domains of Na,K-ATPase alpha subunit." Proceedings of the National Academy of Sciences **91**(8): 2965-2969.

Dixon, I. M. C., T. Hata, et al. (1992). "Sarcolemmal calcium transport in congestive heart failure due to myocardial infarction in rats." American Journal of Physiology - Heart and Circulatory Physiology **262**(5 31-5): H1387-H1394.

Dostanic, I., J. E. J. Schultz, et al. (2004). "The α1 Isoform of Na,K-ATPase Regulates Cardiac Contractility and Functionally Interacts and Co-localizes with the Na/Ca Exchanger in Heart." Journal of Biological Chemistry **279**(52): 54053-54061.

Duer, M. J. (2004). Solid-State NMR Spectroscopy, Blackwell Publishing Ltd.

Edgar, R. C. (2004). "MUSCLE: multiple sequence alignment with high accuracy and high throughput." Nucleic Acids Research **32**(5): 1792-1797.

Esmann, M. (1988). "ATPase and phosphatase activity of Na+,K+-ATPase: Molar and specific activity, protein determination." Methods in Enzymology **156**: 105-115.

Esmann, M., J. C. Skou, et al. (1979). "Solubilization and molecular weight determination of the (Na+ + K+)-ATPase from rectal glands of Squalus acanthias." Biochimica et Biophysica Acta (BBA) - Enzymology **567**(2): 410-420.

Evans, J. N. S. (1995). Biomolecular NMR Spectroscopy, Oxford University Press.

Ferrandi, M., S. Salardi, et al. (1999). "Evidence for an interaction between adducin and Na+-K+-ATPase: relation to genetic hypertension." American Journal of Physiology - Heart and Circulatory Physiology **277**(4): H1338-H1349.

Fiser, A., R. Kinh Gian Do, et al. (2000). "Modeling of loops in protein structures." Protein Science **9**(9): 1753-1773.

Franzin, C. M., X. M. Gong, et al. (2007a). "Structures of the FXYD regulatory proteins in lipid micelles and membranes." Journal of Bioenergetics and Biomembranes **39**(5-6): 379-383.

Franzin, C. M., X. M. Gong, et al. (2007b). "NMR of membrane proteins in micelles and bilayers: The FXYD family proteins." Methods **41**(4): 398-408.

Franzin, C. M. and P. M. Macdonald (2001). "Polylysine-Induced 2H NMR-Observable Domains in Phosphatidylserine/Phosphatidylcholine Lipid Bilayers." Biophysical Journal **81**(6): 3346-3362.

Franzin, C. M., P. Teriete, et al. (2007c). "Membrane orientation of the Na,K-ATPaSe regulatory membrane protein CHIF determined by solid-state NMR." Magnetic Resonance in Chemistry **45**(SUPPL.): S192-S197.

Franzin, C. M., P. Teriete, et al. (2007d). "Structural similarity of a membrane protein in micelles and membranes." Journal of the American Chemical Society **129**(26): 8078-8079.

Fuller, W., J. Howie, et al. (2009). "FXYD1 phosphorylation in vitro and in adult rat cardiac myocytes: threonine 69 is a novel substrate for protein kinase C." American Journal of Physiology - Cell Physiology **296**(6): C1346-C1355.

Fuxreiter, M., P. Tompa, et al. (2007). "Local structural disorder imparts plasticity on linear motifs." Bioinformatics **23**(8): 950-956.

Garty, H. and S. J. D. Karlish (2005). "FXYD proteins: Tissue-specific regulators of the Na,K-ATPase." Seminars in Nephrology **25**(5): 304-311.

Garty, H., M. Lindzen, et al. (2002). "A functional interaction between CHIF and Na-K-ATPase: implication for regulation by FXYD proteins." American Journal of Physiology - Renal Physiology **283**(4): F607-F615.

Geering, K. (2001). "The Functional Role of β Subunits in Oligomeric P-Type ATPases." Journal of Bioenergetics and Biomembranes **33**(5): 425-438.

Geering, K. (2006). "FXYD proteins: New regulators of Na-K-ATPase." American Journal of Physiology - Renal Physiology **290**(2): F241-F250.

Glaser, F., T. Pupko, et al. (2003). "ConSurf: Identification of Functional Regions in Proteins by Surface-Mapping of Phylogenetic Information." Bioinformatics **19**(1): 163-164.

Glynn, I. M. and D. E. Richards (1982). "Occlusion of rubidium ions by the sodium-potassium pump: its implications for the mechanism of potassium transport." The Journal of Physiology **330**(1): 17-43.

Godfraind, T. (1984). "Mechanism of action of cardiac glycosides." European Heart Journal **5**(suppl F): 303-308.

Greenfield, N. J. (2007). "Using circular dichroism collected as a function of temperature to determine the thermodynamics of protein unfolding and binding interactions." Nat. Protocols **1**(6): 2527-2535.

Greenfield, N. J. and G. D. Fasman (1969). "Computed circular dichroism spectra for the evaluation of protein conformation." Biochemistry **8**(10): 4108-4116.

Grisshammer, R. and C. G. Tateu (1995). "Overexpression of integral membrane proteins for structural studies." Quarterly Reviews of Biophysics **28**(03): 315-422.

Gröbner, G., C. Glaubitz, et al. (1999). "Probing Membrane Surfaces and the Location of Membrane-Embedded Peptides by 13C MAS NMR Using Lanthanide Ions." Journal of Magnetic Resonance **141**(2): 335-339.

Grzmil, M., S. Voigt, et al. (2004). "Up-regulated expression of the MAT-8 gene in prostate cancer and its siRNA-mediated inhibition of expression induces a decrease in proliferation of human prostate carcinoma cells." International journal of oncology **24**(1): 97-105.

Hamlyn, J. M., M. P. Blaustein, et al. (1991). "Identification and characterization of a ouabain-like compound from human plasma." Proceedings of the National Academy of Sciences **88**(14): 6259-6263.

Han, F., J. Bossuyt, et al. (2006). "Phospholemman Phosphorylation Mediates the Protein Kinase C-Dependent Effects on Na+/K+ Pump Function in Cardiac Myocytes." Circ Res **99**(12): 1376-1383.

Hansen, A. S., K. L. Kraglund, et al. (2011). "Bulk properties of the lipid bilayer are not essential for the thermal stability of Na,K-ATPase from shark rectal gland or pig kidney." Biochemical and Biophysical Research Communications **406**(4): 580-583.

Hansen, O. (1984). "Interaction of cardiac glycosides with (Na+ + K+)-activated ATPase. A biochemical link to digitalis-induced inotropy." Pharmacological Reviews **36**(3): 143-163.

Hatou, S., M. Yamada, et al. (2010). "Role of Insulin in Regulation of Na+-/K+-Dependent ATPase Activity and Pump Function in Corneal Endothelial Cells." Investigative Ophthalmology & Visual Science **51**(8): 3935-3942.

Heppel, L. A. (1939). "The electrolytes of muscle and liver in potassium-depleted rats." Am. J. Physiol. **127**: 385-391.

Heppel, L. A. and C. L. A. Schmidt (1938). "Studies on the potassium metabolism of the rat during pregnancy, lactation, and growth." Univ. Calif. Publ. Physiol. **8**: 189-196.

Herse, P. and L. Adams (1995). "EFFECT OF HYPERGLYCEMIA DURATION ON RABBIT CORNEAL THICKNESS AND ENDOTHELIAL ATPASE ACTIVITY." Acta Ophthalmologica Scandinavica **73**(2): 158-161.

Herse, P. R. (1990). "Corneal hydration control in normal and alloxan-induced diabetic rabbits." Investigative Ophthalmology & Visual Science **31**(11): 2205-2213.

Hevesy, G. (1938). "The application of isotopic indicators in biological research." Enzymologia **5**: 138-157.

Hilgemann, D. W. (1994). "Channel-like function of the Na,K pump probed at microsecond resolution in giant membrane patches." Science **263**(5152): 1429-1432.

Hobbs, A. S. and P. B. Dunham (1978). "Interaction of external alkali metal ions with the Na-K pump of human erythrocytes: a comparison of their effects on activation of the pump and on the rate of ouabain binding." The Journal of General Physiology **72**(3): 381-402.

Holmgren, M., J. Wagg, et al. (2000). "Three distinct and sequential steps in the release of sodium ions by the Na+/K+-ATPase." Nature **403**(6772): 898-901.

Holzwarth, G. and P. Doty (1965). "The Ultraviolet Circular Dichroism of Polypeptides1." Journal of the American Chemical Society **87**(2): 218-228.

Hornack, J. P. (2011). "Basics of NMR." Retrieved 15/08, 2011, from **http://www.cis.rit.edu/htbooks/nmr/**.

Horsefield, R., V. Yankovskaya, et al. (2006). "Structural and Computational Analysis of the Quinone-binding Site of Complex II (Succinate-Ubiquinone Oxidoreductase)." Journal of Biological Chemistry **281**(11): 7309-7316.

Hu, J., H. Qin, et al. (2007). "Structural biology of transmembrane domains: efficient production and characterization of transmembrane peptides by NMR." Protein science : a publication of the Protein Society **16**(10): 2153-2165.

Hughes, E., C. A. P. Whittaker, et al. (2011). "A study of the membrane association and regulatory effect of the phospholemman cytoplasmic domain." Biochimica et Biophysica Acta (BBA) - Biomembranes **1808**(4): 1021-1031.

Inoue, K., S. Kato, et al. (2002). "The corneal endothelium and thickness in type II diabetes mellitus." Japanese Journal of Ophthalmology **46**(1): 65-69.

Ishida, T. and K. Kinoshita (2008). "Prediction of disordered regions in proteins based on the meta approach." Bioinformatics **24**(11): 1344-1348.

Jason, C., J. W. M. Nissink, et al. (2005). Protein-Ligand Docking Virtual Screening with GOLD. Virtual Screening in Drug Discovery, CRC Press: 379-415.

Jewell, E. A., O. I. Shamraj, et al. (1992). "Isoforms of the α subunit of Na,K-ATPase and their significance." Acta Physiologica Scandinavica, Supplement **146**(607): 161-169.

Jia, L.-G., C. Donnet, et al. (2005). "Hypertrophy, increased ejection fraction, and reduced Na-K-ATPase activity in phospholemman-deficient mice." American Journal of Physiology - Heart and Circulatory Physiology **288**(4): H1982-H1988.

Jidenko, M., G. Lenoir, et al. (2006). "Expression in yeast and purification of a membrane protein, SERCA1a, using a biotinylated acceptor domain." Protein Expression and Purification **48**(1): 32-42.

Joachim, S. (1997). "Titration calorimetry of lipid–peptide interactions." Biochimica et Biophysica Acta (BBA) - Reviews on Biomembranes **1331**(1): 103-116.

Jones, D. T. (1999). "Protein secondary structure prediction based on position-specific scoring matrices." Journal of Molecular Biology **292**(2): 195-202.

Jones, G., P. Willett, et al. (1997). "Development and validation of a genetic algorithm for flexible docking." Journal of Molecular Biology **267**(3): 727-748.

Jørgensen, P. L. (1974). "Purification and characterization of (Na+ + K+)-ATPase III. Purification from the outer medulla of mammalian kidney after selective removal of membrane components by sodium dodecylsulphate." Biochimica et Biophysica Acta (BBA) - Biomembranes **356**(1): 36-52.

Jorgensen, P. L., K. O. Håkansson, et al. (2003). Structure and Mechanism of Na,K-ATPase: Functional Sites and Their Interactions. **65:** 817-849.

Kapust, R. B., J. Tözsér, et al. (2002). "The P1′ specificity of tobacco etch virus protease." Biochemical and Biophysical Research Communications **294**(5): 949-955.

Kawamura, A., J. Guo, et al. (1999). "On the structure of endogenous ouabain." Proceedings of the National Academy of Sciences **96**(12): 6654-6659.

Kayed, H., J. Kleeff, et al. (2006). "FXYD3 is overexpressed in pancreatic ductal adenocarcinoma and influences pancreatic cancer cell growth." International Journal of Cancer **118**(1): 43-54.

Klepsch, F., P. Chiba, et al. (2011). "Exhaustive Sampling of Docking Poses Reveals Binding Hypotheses for Propafenone Type Inhibitors of P-Glycoprotein." PLoS Comput Biol **7**(5): e1002036.

Landau, M., I. Mayrose, et al. (2005). "ConSurf 2005: the projection of evolutionary conservation scores of residues on protein structures." Nucleic Acids Research **33**(suppl 2): W299-W302.

Lange, A., S. Becker, et al. (2005). "A Concept for Rapid Protein-Structure Determination by Solid-State NMR Spectroscopy." Angewandte Chemie International Edition **44**(14): 2089-2092.

Li, C., O. Capendeguy, et al. (2005). "A third Na+-binding site in the sodium pump." Proceedings of the National Academy of Sciences of the United States of America **102**(36): 12706-12711.

Li, M., L. G. Reddy, et al. (1999). "A Fluorescence Energy Transfer Method for Analyzing Protein Oligomeric Structure: Application to Phospholamban." Biophysical Journal **76**(5): 2587-2599.

Lian, L.-Y. and D. A. Middleton (2001). "Labelling approaches for protein structural studies by solution-state and solid-state NMR." Progress in Nuclear Magnetic Resonance Spectroscopy **39**(3): 171-190.

Libet, B. (1948). "Adenosinetriphosphatase in nerve." Federation Proceedings **7**(1): 72.

Lin, M. H. and T. Akera (1978). "Increased (Na+,K+)-ATPase concentrations in various tissues of rats caused by thyroid hormone treatment." Journal of Biological Chemistry **253**(3): 723-726.

Lingrel, J. B., J. Orlowski, et al. (1991). "Regulation of the alpha-subunit genes of the Na,K-ATPase and determinants of cardiac glycoside sensitivity." Society of General Physiologists series **46**: 1-16.

Lomize, M. A., A. L. Lomize, et al. (2006). "OPM: Orientations of Proteins in Membranes database." Bioinformatics **22**(5): 623-625.

Lowry, O. H., N. J. Rosebrough, et al. (1951). "PROTEIN MEASUREMENT WITH THE FOLIN PHENOL REAGENT." Journal of Biological Chemistry **193**(1): 265-275.

Lubarski, I., K. Pihakaski-Maunsbach, et al. (2005). "Interaction with the Na,K-ATPase and Tissue Distribution of FXYD5 (Related to Ion Channel)." Journal of Biological Chemistry **280**(45): 37717-37724.

Mathews, W. R., D. W. DuCharme, et al. (1991). "Mass spectral characterization of an endogenous digitalislike factor from human plasma." Hypertension **17**(6): 930-935.

Mehio, W., G. J. L. Kemp, et al. (2010). "Identification of protein binding surfaces using surface triplet propensities." Bioinformatics **26**(20): 2549-2555.

Melero, C., M. Medarde, et al. (2000). "A Short Review on Cardiotonic Steroids and Their Aminoguanidine Analogues." Molecules **5**(1): 51-81.

Middleton, D. A., E. Hughes, et al. (2011). "The Conformation of ATP within the Na,K-ATPase Nucleotide Site: A Statistically Constrained Analysis of REDOR Solid-State NMR Data." Angewandte Chemie International Edition **50**(31): 7041-7044.

Middleton, D. A., S. Rankin, et al. (2000). "Structural insights into the binding of cardiac glycosides to the digitalis receptor revealed by solid-state NMR." Proceedings of the National Academy of Sciences **97**(25): 13602-13607.

Miroux, B. and J. E. Walker (1996). "Over-production of Proteins inEscherichia coli: Mutant Hosts that Allow Synthesis of some Membrane Proteins and Globular Proteins at High Levels." Journal of Molecular Biology **260**(3): 289-298.

Morrison, B. W. and P. Leder (1994). "neu and ras initiate murine mammary tumors that share genetic markers generally absent in c-myc and int-2-initiated tumors." Oncogene **9**(12): 3417-3426.

Morrison, B. W., J. Randall Moorman, et al. (1995). "Mat-8, a novel phospholemman-like protein expressed in human breast tumors, induces a chloride conductance in Xenopus oocytes." Journal of Biological Chemistry **270**(5): 2176-2182.

Morth, J. P., B. P. Pedersen, et al. (2007). "Crystal structure of the sodium-potassium pump." Nature **450**(7172): 1043-1049.

Mounsey, J. P., J. E. John, III, et al. (2000). "Phospholemman Is a Substrate for Myotonic Dystrophy Protein Kinase." J. Biol. Chem. **275**(30): 23362-23367.

Muchmore, S. W., M. Sattler, et al. (1996). "X-ray and NMR structure of human Bcl-xL, an inhibitor of programmed cell death." Nature **381**(6580): 335-341.

Nakamoto, R. K. and G. Inesi (1984). "Studies of the interactions of 2',3'-O-(2,4,6-trinitrocyclohexyldienylidine)adenosine nucleotides with the sarcoplasmic reticulum (Ca2+ + Mg2+)-ATPase active site." Journal of Biological Chemistry **259**(5): 2961-2970.

Neduva, V., R. Linding, et al. (2005). "Systematic Discovery of New Recognition Peptides Mediating Protein Interaction Networks." PLoS Biol **3**(12): e405.

Negi, S. S., C. H. Schein, et al. (2007). "InterProSurf: a web server for predicting interacting sites on protein surfaces." Bioinformatics **23**(24): 3397-3399.

Nelson, J. W. and N. R. Kallenbach (1986). "Stabilization of the ribonuclease S-peptide α-helix by trifluoroethanol." Proteins: Structure, Function, and Bioinformatics **1**(3): 211-217.

Ogawa, H., T. Shinoda, et al. (2009). "Crystal structure of the sodium-potassium pump (Na+,K+-ATPase) with bound potassium and ouabain." Proceedings of the National Academy of Sciences **106**(33): 13742-13747.

Oldenburg, K. R., R. F. Epand, et al. (1996). "Conformational studies on analogs of recombinant parathyroid hormone and their interactions with phospholipids." Journal of Biological Chemistry **271**(29): 17582-17591.

Olsen, T. and N. Busted (1981). "Corneal thickness in eyes with diabetic and nondiabetic neovascularisation." British Journal of Ophthalmology **65**(10): 691-693.

Orkin, S. (1990). "MOLECULAR-CLONING - A LABORATORY MANUAL, 2ND EDITION - SAMBROOK,J, FRITSCH,EF, MANIATIS,T." Nature **343**(6259): 604-605.

Palasis, M., T. A. Kuntzweiler, et al. (1996). "Ouabain Interactions with the H5-H6 Hairpin of the Na,K-ATPase Reveal a Possible

Inhibition Mechanism via the Cation Binding Domain." Journal of Biological Chemistry **271**(24): 14176-14182.

Palmer, C. J., B. T. Scott, et al. (1991). "Purification and complete sequence determination of the major plasma membrane substrate for cAMP-dependent protein kinase and protein kinase C in myocardium." Journal of Biological Chemistry **266**(17): 11126-11130.

Pavlovic, D., W. Fuller, et al. (2007). "The intracellular region of FXYD1 is sufficient to regulate cardiac Na/K ATPase." The FASEB Journal **21**(7): 1539-1546.

Petsalaki, E., A. Stark, et al. (2009). "Accurate Prediction of Peptide Binding Sites on Protein Surfaces." PLoS Comput Biol **5**(3): e1000335.

Pieter, S. and R. Fanie (1998). "Bufadienolides of plant and animal origin." Natural Product Reports **15**(4): 397-413.

Prassas, I. and E. P. Diamandis (2008). "Novel therapeutic applications of cardiac glycosides." Nat Rev Drug Discov 7(11): 926-935.

Price, E. M. and J. B. Lingrel (1988). "Structure-function relationships in the sodium-potassium ATPase .alpha. subunit: site-directed mutagenesis of glutamine-111 to arginine and asparagine-122 to aspartic acid generates a ouabain-resistant enzyme." Biochemistry **27**(22): 8400-8408.

Price, E. M., D. A. Rice, et al. (1989). "Site-directed mutagenesis of a conserved, extracellular aspartic acid residue affects the ouabain sensitivity of sheep Na,K-ATPase." Journal of Biological Chemistry **264**(36): 21902-21906.

Pu, H. X., F. Cluzeaud, et al. (2001). "Functional Role and Immunocytochemical Localization of the γa and γb Forms of the Na,K-ATPase γ Subunit." Journal of Biological Chemistry **276**(23): 20370-20378.

Qin, S. and H.-X. Zhou (2007). "meta-PPISP: a meta web server for protein-protein interaction site prediction." Bioinformatics **23**(24): 3386-3387.

Reusch, W. (2000). "Nuclear Magnetic Resonance Spectroscopy." Retrieved 15/08, 2011, from **http://www2.chemistry.msu.edu/faculty/reusch/VirtTxtJml/Spectrpy/nmr/nmr1.htm#nmr1**.

Reyes, N. and D. C. Gadsby (2006). "Ion permeation through the Na+,K+-ATPase." Nature **443**(7110): 470-474.

Riggs, P. (2001). Expression and Purification of Maltose-Binding Protein Fusions. Current Protocols in Molecular Biology, John Wiley & Sons, Inc.

Roszkowska, A. M., C. G. Tringali, et al. (1999). "Corneal Endothelium Evaluation in Type I and Type II Diabetes mellitus." Ophthalmologica **213**(4): 258-261.

Sachs, J. R. (1974). "Interaction of External K, Na, and Cardioactive Steroids with the Na-K Pump of the Human Red Blood Cell." The Journal of General Physiology **63**(2): 123-143.

Sali, A. and T. L. Blundell (1993). "Comparative protein modelling by satisfaction of spatial restraints." Journal of Molecular Biology **234**(3): 779-815.

Santos, H. d. L., M. L. Lopes, et al. (2005). "Na,K-ATPase reconstituted in liposomes: effects of lipid composition on hydrolytic activity and enzyme orientation." Colloids and Surfaces B: Biointerfaces **41**(4): 239-248.

Sasaki, T., M. Inui, et al. (1992). "Molecular mechanism of regulation of Ca2+ pump ATPase by phospholamban in cardiac sarcoplasmic reticulum. Effects of synthetic phospholamban peptides on Ca2+ pump ATPase." Journal of Biological Chemistry **267**(3): 1674-1679.

Schatzmann HJ, R. B. (1965). "Inhibition of the active Na-K-transport and Na-K-activated membrane ATP-ase of erythrocyte stroma by ouabain." Helv Physiol Pharmacol Acta. **65**(1): C47-49.

Schneider, R., V. Wray, et al. (1998). "Bovine Adrenals Contain, in Addition to Ouabain, a Second Inhibitor of the Sodium Pump." Journal of Biological Chemistry **273**(2): 784-792.

Scholtz, J. M., H. Qian, et al. (1991). "Parameters of helix–coil transition theory for alanine-based peptides of varying chain lengths in water." Biopolymers **31**(13): 1463-1470.

Schultheis, P. J. and J. B. Lingrel (1993). "Substitution of transmembrane residues with hydrogen-bonding potential in the .alpha. subunit of sodium-potassium ATPase reveals alterations in ouabain sensitivity." Biochemistry **32**(2): 544-550.

Schultheis, P. J., E. T. Wallick, et al. (1993). "Kinetic analysis of ouabain binding to native and mutated forms of Na,K-ATPase and identification of a new region involved in cardiac glycoside interactions." J. Biol. Chem. **268**(30): 22686-22694.

Seelig, J. and P. M. Macdonald (1987). "Phospholipids and proteins in biological membranes. Deuterium NMR as a method to study structure, dynamics, and interactions." Accounts of Chemical Research **20**(6): 221-228.

Shattock, M. J. (2009). "Phospholemman: its role in normal cardiac physiology and potential as a drugable target in disease." Current Opinion in Pharmacology **9**(2): 160-166.

Shinoda, T., H. Ogawa, et al. (2009). "Crystal structure of the sodium-potassium pump at 2.4A resolution." Nature **459**(7245): 446-450.

Shull, G. E., A. Schwartz, et al. (1985). "Amino-acid sequence of the catalytic subunit of the (Na+ + K+)ATPase deduced from a complementary DNA." Nature **316**(6030): 691-695.

Silverman, B. d. Z., W. Fuller, et al. (2005). "Serine 68 phosphorylation of phospholemman: acute isoform-specific activation of cardiac Na/K ATPase." Cardiovascular Research **65**(1): 93-103.

Skou, J. C. (1957). "THE INFLUENCE OF SOME CATIONS ON AN ADENOSINE TRIPHOSPHATASE FROM PERIPHERAL NERVES." Biochimica Et Biophysica Acta **23**(2): 394-401.

Skou, J. C. (1965). "ENZYMATIC BASIS FOR ACTIVE TRANSPORT OF NA+ AND K+ ACROSS CELL MEMBRANE." Physiological Reviews **45**(3): 596-&.

Skou, J. C. and M. Esmann (1983). "The effects of Na+ and K+ on the conformational transitions of (Na+ + K+)-ATPase." Biochimica et Biophysica Acta (BBA) - Protein Structure and Molecular Enzymology **746**(1-2): 101-113.

Smith, S. O., T. Kawakami, et al. (2001). "Helical structure of phospholamban in membrane bilayers." Journal of Molecular Biology **313**(5): 1139-1148.

Spooner, P. J., N. G. Rutherford, et al. (1994). "NMR observation of substrate in the binding site of an active sugar-H+ symport protein in native membranes." Proceedings of the National Academy of Sciences **91**(9): 3877-3881.

Steinbach, H. B. (1940). "Chemical and concentration potentials in the giant fibers of squid nerves." Journal of Cellular and Comparative Physiology **15**(3): 373-386.

Sweadner, K. J. and C. Donnet (2001). "Structural similarities of Na,K-ATPase and SERCA, the Ca(2+)-ATPase of the sarcoplasmic reticulum." The Biochemical journal **356**(Pt 3): 685-704.

Sweadner, K. J. and E. Rael (2000). "The FXYD gene family of small ion transport regulators or channels: cDNA sequence, protein signature sequence, and expression." Genomics **68**(1): 41-56.

Tamburro, A. M., A. Scatturin, et al. (1968). "Conformational-transitions of bovine pancreatic ribonuclease S-peptide." FEBS Letters **1**(5): 298-300.

Tanaka, H., H. Shimada, et al. (2007). "Involvement of the Na+/Ca2+ Exchanger in Ouabain-Induced Inotropy and Arrhythmogenesis in Guinea-Pig Myocardium as Revealed by SEA0400." Journal of Pharmacological Sciences **103**(2): 241-246.

Teriete, P., C. M. Franzin, et al. (2007). "Structure of the Na,K-ATPase regulatory protein FXYD1 in micelles." Biochemistry **46**(23): 6774-6783.

Teriete, P., K. Thai, et al. (2009). "Effects of PKA phosphorylation on the conformation of the Na,K-ATPase regulatory protein FXYD1." Biochimica et Biophysica Acta (BBA) - Biomembranes **1788**(11): 2462-2470.

Thai, K., J. Choi, et al. (2005). "Bcl-XL as a fusion protein for the high-level expression of membrane-associated proteins." Protein Science **14**(4): 948-955.

Tian, J., T. Cai, et al. (2006). "Binding of Src to Na+/K+-ATPase Forms a Functional Signaling Complex." Molecular Biology of the Cell **17**(1): 317-326.

Tipsmark, C. K. (2008). "Identification of FXYD protein genes in a teleost: tissue-specific expression and response to salinity change." American Journal of Physiology - Regulatory, Integrative and Comparative Physiology **294**(4): R1367-R1378.

Toyoshima, C., M. Nakasako, et al. (2000). "Crystal structure of the calcium pump of sarcoplasmic reticulum at 2.6 [angst] resolution." Nature **405**(6787): 647-655.

Venyaminov, S. Y., I. A. Baikalov, et al. (1993). "Circular Dichroic Analysis of Denatured Proteins: Inclusion of Denatured Proteins in the Reference Set." Analytical Biochemistry **214**(1): 17-24.

Vilsen, B. (1995). "Mutant Glu781 .fwdarw. Ala of the rat kidney Na+,K+-ATPase displays low cation affinity and catalyzes ATP hydrolysis at a high rate in the absence of potassium ions." Biochemistry **34**(4): 1455-1463.

Vilsen, B., D. Ramlov, et al. (1997). "Functional Consequences of Mutations in the Transmembrane Core Region for Cation Translocation and Energy Transduction in the Na+, K+-ATPase and the SR Ca2+-ATPasea." Annals of the New York Academy of Sciences **834**(1): 297-309.

Walaas, S. I., A. J. Czernik, et al. (1994). "Protein kinase C and cyclic AMP-dependent protein kinase phosphorylate phospholemman, an insulin and adrenaline-regulated membrane phosphoprotein, at specific sites in the the carboxy terminal domain." Biochemical Journal **304**(2): 635-640.

Wessel, D. and U. I. Flügge (1984). "A method for the quantitative recovery of protein in dilute solution in the presence of detergents and lipids." Analytical Biochemistry **138**(1): 141-143.

Withering, W. (1785). An account of the foxglove and some of its medical uses; with practical remarks on the dropsy, and some other diseases. Birmingham, Swinney.

Wuthrich, K. (1986). NMR of Proteins and Nucleic Acids. New York, Wiley.

Yalcin, Y., D. Carman, et al. (1999). "Regulation of Na/K-ATPase gene expression by thyroid hormone and hyperkalemia in the heart." Thyroid **9**(1): 53-59.

Yamamoto, H., K. Okumura, et al. (2009). "FXYD3 protein involved in tumor cell proliferation is overproduced in human breast cancer tissues." Biological and Pharmaceutical Bulletin **32**(7): 1148-1154.

Yatime, L., M. Laursen, et al. (2011). "Structural insights into the high affinity binding of cardiotonic steroids to the Na+,K+-ATPase." Journal of Structural Biology **174**(2): 296-306.

Yoda, A. and S. Yoda (1982). "Interaction between ouabain and the phosphorylated intermediate of Na,K-ATPase." Molecular Pharmacology **22**(3): 700-705.

Yudowski, G. A., R. Efendiev, et al. (2000). "Phosphoinositide-3 kinase binds to a proline-rich motif in the Na+,K+-ATPase α subunit and regulates its trafficking." Proceedings of the National Academy of Sciences **97**(12): 6556-6561.

Zhang, X.-Q., J. R. Moorman, et al. (2006). "Phospholemman overexpression inhibits Na+-K+-ATPase in adult rat cardiac myocytes: relevance to decreased Na+ pump activity in postinfarction myocytes." Journal of Applied Physiology **100**(1): 212-220.

Zhu, M., J. Li, et al. (2003). "The Association of α-Synuclein with Membranes Affects Bilayer Structure, Stability, and Fibril Formation." Journal of Biological Chemistry **278**(41): 40186-40197.